Royal Institute of Technology

On Satellite Gravity Gradiometry

Mehdi Eshagh

Doctoral Dissertation in Geodesy

Royal Institute of Technology (KTH)
Division of Geodesy

10044 Stockholm
Sweden

June 2009

Mehdi Eshagh: On Satellite Gravity Gradiometry

Supervisor:

Professor Lars E. Sjöberg

Faculty Opponent:

Professor Zdenek Martinec

GFZ German Research Centre for Geosciences, Helmholtz Centre Potsdam, Germany

Evaluation committee:

Professor Pavel Novak

Department of Mathematics, University of West Bohemia, Czech Republic

Professor Axel Ruhe

Department of Numerical Analysis, Royal Institute of Technology (KTH), Stockholm, Sweden

Professor Artu Ellmann

Department of Civil Engineering, Tallinn University of Technology, Tallinn, Estonia

To:

My wife Mahsa and our little daughter Venus

Abstract

Satellite gravity gradiometry measures the second-order partial derivatives of the Earth's gravitational potential based on differential accelerometry. Measuring the gravitational gradients at satellite level opens a new way to compute a precise and high resolution geopotential model from space. The upcoming satellite mission gravity field and steady-state ocean circulation (GOCE) is dedicated to provide precise gradiometric data in this respect. It is claimed to achieve geoid and gravity anomaly with 1 cm and 1 mGal accuracies, respectively with $1^\circ \times 1^\circ$ resolution using the delivered Earth gravitational model from GOCE data.

In this thesis new expressions for the gravitational gradients are developed. A new expression for tensor spherical harmonics are presented and used to solve the gradiometric boundary value problems and to compute a geopotential model. It is found that the vertical-horizontal gradients are more suited than the other gradients in geopotential modeling. Topographic and atmospheric effects on the satellite gravity gradiometry data are formulated in spherical harmonics, and numerically investigations in Fennoscandia and Iran show that the topographic effect is in the 1 and 2 E level in these areas. A new atmospheric density model is proposed, and the atmospheric effect based on this model is within 5 mE. Second-order partial derivatives of the extended Stokes' formula are modified in a least-squares sense to validate the satellite gravity gradiometry data. Downward continuation of each element of the gravitational tensor is studied using the Tikhonov regularization. The gravitational gradients T_{zz}, T_{xx}, T_{yy}, T_{xz}, T_{yz} and T_{xy} are suited for determining gravity anomaly at sea level. Combination of the satellite data to recover the global and local gravity field is investigated. It is shown that the combination of integral solutions of the gradiometric boundary value problems using variance component estimation, is beneficial in geopotential modeling. In local gravity field determination, it is concluded that a grid of $1^\circ \times 1^\circ$ gravity anomalies with 1 mGal accuracy is achievable from directly combined continuation of the satellite gradiometric data. The polar gaps due to an inclined orbit are studied, and it is shown that T_{xy} and T_{yz} are better than the other gradients for estimating the gravity anomaly in the polar gaps. The combined inversion of the satellite gradiometric data (after biased-correction step) can determine $1^\circ \times 1^\circ$ gravity anomalies with 1 and 3 mGal accuracy in the north and south polar gaps, respectively.

Keywords: satellite orbit, atmospheric density model, lateral density variation, validation, downward continuation, joint inversion, ring modification

Acknowledgments

I cannot find any word to appreciate my supportive supervisor professor Lars E. Sjöberg. Actually the words are not eligible enough to express how I am impressed by this great man. I learnt many things from this good pattern of my life in the last 5 years. Without his helps this thesis never came to the end. I would like to express my gratitude and indebtness to him although writing thousands of similar sentences of appreciation neither is sufficient. Lars! You never be forgotten during my life and I am with you every where that I am.

Docent M. Horemuz and Dr. H. Fan are also appreciated for reading the draft version of thesis and controlling its quality and commenting on that.

There are several persons that they had a big contribution during this thesis work that must be appreciated. Professor M.S. Petrovskaya is cordially acknowledged for stimulating discussion about different expressions for the gravitational gradients. Professor Z. Martinec is also appreciated for his guidance and introducing one of his papers which played a key role in my thesis. Professor P. Novak is appreciated for his help about his analytical atmospheric density model; Dr. P. Ditmar is also appreciated for his great help for correcting that part of the thesis about atmospheric density model. Dr. P. Xu is also acknowledged for his great help about downward continuation and inversion of gradiometric data and variance-components estimation in ill-posed problem. Professor P. C. Hansen is also appreciated because of his kind guidance about regularization and proving me his regularization software. Professor C. Hwang is acknowledged for his helps about average acceleration power. Professor E. Grafarend is appreciated for the nice scientific discussion and guidance during his residence in KTH. I am thankful to Professor R. Rummel for his help.

I would like to appreciate the friends who helped me. Drs. A. Shabanloui for providing some materials, R. Kiamehr, A. Ellmann, J. Ågren and P. Ulotu for their discussions and guidance. Dr. J. V. Andersson is appreciated for his great helps during my illness period. My close friend Mr. M. Bagherbandi is appreciated as he proved that he is a real friend of mine during may residence in Sweden. Mr. E. Asenjo and Mrs. U. Danila are cordially acknowledged for their kind helps. Mr. M. Abdollahzadeh is appreciated for his helps in numerical algorithms.

I appreciate two encouraging persons that motivated me to continue my studies to PhD level, Dr. M. Najafi-Alamdari and Dr. V. E. Ardestani. Their supports never are forgotten.

The Swedish National Space Board is cordially acknowledged for the financial support to project no. 63/07:1.

A heartfelt word of thanks goes to my wife Mahsa for her understanding and patience during my PhD studies and the great helps. I owe a considerable debt to her. My little daughter Venus opened a new life for me during our residence abroad, which was the sweetest period of my life, those times are not forgettable.

My parents are appreciated for their encouragements and motivations to continue my studies more and more.

Contents

Chapter 1

Introduction

1.1 Background…….....1
1.2 The author's investigations…….3

Chapter 2

Alternative expressions in global synthesis and analysis

2.1 Introduction…….....4
2.2 Gravitational potential…….....6
2.3 Gravitational gradients in a geocentric frame…….....6
2.3.1 Alternative expressions for gravitational gradients in a geocentric frame……8
2.3.2 New expressions for gravitational vector and tensor in geocentric frame…….....14
2.4 Gravitational gradients in LNOF…….....16
2.4.1 Alternative expressions for gravitational gradients in the LNOF…….....17
2.5 Gravitational gradients in ORF…….....23
2.5.1 Equations of motion of a satellite ……...25
2.5.2 Simplification of the geopotential perturbing force acting on a satellite… …….....26
2.6 The GBVPs……..32
2.6.1 Traditional expressions for the TSHs …….....35
2.6.2 Alternative expressions for the TSHs…….....36
2.7 Numerical studies……..41
2.8 Error propagation……..43
2.9 Average power of gravitational gradients…….44

Chapter 3

Topographic and atmospheric effects

3.1 Introduction……...47
3.2 Topographic and atmospheric potentials in spherical harmonics…….49
3.3 External and internal topographic potentials in spherical harmonics…...50
3.3.1 TE on the SGG data in LNOF…….52

3.3.2 Numerical studies on TE on the SGG data over Fennoscandia and Iran……52
3.3.1 LDVE of topography on the SGG data……...55
3.4 External and internal atmospheric potentials in spherical harmonics.....58
3.4.1 The ADMs……..……58
3.4.1.1 The standard ADM (USSA76)……...59
3.4.1.2 Exponential ADM……..……60
3.4.1.3 Sjöberg's ADM (KTHA)……60
3.4.1.4 Novak's ADM (NADM) ……...61
3.4.1.5 New KTH ADM (NKTHA) …….....61
3.4.2 External and internal atmospheric potentials based on NADM and USSA76……61
3.4. 2.1 Numerical studies on AE on the SGG data over Iran and Fennoscandia……..65
3.4.3 Atmospheric potential based on KTHA……...67
3.4.3.1 AE on the SGG data in ORF……71
3.4.4 Reformulation of the SHCs of atmospheric potentials based on KTHA……...……73
3.4.5 External and internal atmospheric potentials based on exponential ADM……75
3.4.6 Atmospheric potential based on the NKTHA……...83
3.4.7 Summary of AEs……..87
3.5 Remote-Compute-Restore scheme ……...88
3.6 Topographic and atmospheric biases in spherical harmonics on the SGG data……90

Chapter 4

Least-squares modification

4.1 Introduction……...93
4.2 LSM and MM of the extended Stokes formula……..95
4.2.1 Numerical studies on modification of the extended Stokes formula……98
4.3 LSM and VV gravitational gradient……..……101
4.3.1 Modification of the SOD of ESF ……102
4.3.2 Numerical studies on modification of the SOD of ESF……105
4.4 LSM and VH gravitational gradients ……107
4.4.1 Truncation error for the VH gravitational gradients……..108
4.4.2 Error of terrestrial data in VH derivatives of the extended Stokes formula……...109
4.4.3 LSM of the VH derivatives of the extended Stokes formula…...109
4.5 LSM and HH gravitational gradients……...113
4.5.1 Truncation errors for the HH gravitational gradients……114
4.5.2 Error of terrestrial data of HH derivatives of the extended Stokes formula……...116
4.5.3 LSM of the HH derivative of the extended Stokes formula……..117
4.6 Modification with data in a spherical ring……...119
4.7 Derivations of $e_{nk}^{0}\left(\psi_0\right)$, $e_{nk}^{1}\left(\psi_0\right)$ and $e_{nk}^{2}\left(\psi_0\right)$ ……..123

4.8 A simple numerical study on modification with a spherical ring……125

Chapter 5

Local gravity field determination

5.1 Introduction……130
5.2 Inversion by second-order derivatives of the extended Stokes formula……132
5.3 Singularity investigations on isotropic kernels……...133
5.4 Regularization……136
5.4.1 Tikhonov regularization……136
5.5 Numerical studies on downward continuation of the SGG data…….137
5.5.1 Recovery of $1^\circ \times 1^\circ$ gravity anomaly from $0.5^\circ \times 0.5^\circ$ SGG data……138
5.5.2 Recovery of $0.5^\circ \times 0.5^\circ$ gravity anomaly from $0.25^\circ \times 0.25^\circ$ SGG data……141
5.5.3 Recovery of $1^\circ \times 1^\circ$ gravity anomaly from $0.25^\circ \times 0.25^\circ$ SGG data……144
5.6 Inversion of Eötvös type gradients……..146
5.7 Estimated errors……..……147
5.8 Biased-corrected estimation of the gravity anomalies……153
5.9 Truncation errors of the integral formulas……...156

Chapter 6

Combinations of SGG data

6.1 Introduction……159
6.2 The Gauss-Helmert adjustment model……160
6.3 The BQUE of a VC……161
6.4 The BQUNE of a VC……161
6.5 The MBQUNE of a VC……..162
6.6 Optimal combination of integral solution of GBVPs……..163
6.6.1 Simple mean versus weighted mean……164
6.6.2 Adjustment by condition model……164
6.6.3 VCE and re-weighting solution……167
6.6.4 Numerical investigation in VCE and re-weighting process……..172
6.7 Combination of the gravitational gradients in local gravity field determination……176
6.7.1 Simple joint inversion of the SGG data by least-squares…….176
6.7.2 Joint inversion of SGG data and VCE……..179
6.7.2.1 VCE in ill-posed problems……179
6.7.2.2 Bias analysis of the BQUE. ……..……180
6.7.2.3 Biased-corrected VCE……...181
6.7.2.4 Numerical studies on VCE in ill-posed problems…….183
6.7.3 Bias analysis of Sjöberg's VC estimator in an

ill-posed problem……..187
6.7.4 Biased-corrected Sjöberg's VC estimator……188

Chapter 7

The polar gaps

7.1 Introduction……189
7.2 Loss of power of gravitational signal due to polar gaps in SGG……190
7.3 The gravitational gradients around polar gaps……...192
7.4 Gravity field recovery in the polar gaps……...194
7.5 Joint inversion of SGG data for recovering gravity anomaly in polar gaps……196

Chapter 8

Conclusions and future works

8.1 Conclusions……198
8.2 Future works……...202

References……204

List of tables

Table 2.1. Statistics of second-order gradients of disturbing potential in geocentric frame. Unit: 1 E……23
Table 2.2. Statistics of second-order gradients of disturbing potential in LNOF. Unit: 1 E…….....23
Table 2.3. Statistics of effect of orbital perturbations on SGG data. Unit: 1 E …….....31
Table 2.4. Statistics of effect of perturbed satellite track azimuth on SGG data in ORF. Unit: 1 E…….32
Table 2.5. Maximum degree of the geopotential coefficients determined from SGG data at 250 km level within 1% (0.1%) relative errors of degree variances……43
Table 2.6. Maximum degree of the geopotential coefficients determined from SGG data at 250 km level until 1% relative errors degree variances between true and estimated coefficients as well as degree of resolution…….....44
Table 2.7. Cut-off degrees of the gradients based on different criteria…….....46

Table 3.1. Statistics of TE on SGG data in Fennoscandia and Iran in LNOF. Unit: 1 E…….....55
Table 3.2. Statistics of LDVE of topography in Fennoscandia and Iran in LNOF. Unit: 1 mE…….....58
Table 3.3. Molecular temperature gradients, Novák (2000)…….....59
Table 3.4. Values of the atmospheric mass density based on the USSA61 and USSA76. Unit: 1 kg/m^3 …….....60
Table 3.5. Statistics of AE on SGG data in Fennoscandia and Iran in LNOF. Unit: 1 mE…….66
Table 3.6. Correlation coefficients between topographic height, and TE and AE in Fennoscandia and Iran……...67
Table 3.7. AE on the SGG data at 250km level based on NADM and KTHA up to 10 km in ORF. Unit: 1 mE……...72
Table 3.8. Statistics of AE on SGG data at 250 km level over Fennoscandia based on exponential ADM and KTHA in ORF. Unit: 1 mE…….....81
Table 3.9. Statistics of AE on SGG data at 250 km level based on KTHA and modified KTHA in ORF. Unit: 1 mE……86
Table 3.10. Statistics of AE on SGG data at 250 km level based on NKTHA in ORF. Unit: 1 mE…….86

Table 4.1. Estimated disturbing potential using modified estimators by LSM divided by 9.8 at 250 km level with 1 mGal error for terrestrial data. Unit: 1 m……100
Table 4.2. Different estimates of disturbing potential divided by 9.8 m/s^2 at 250 km with 5 mGal error of terrestrial data. Unit: 1 m……...100
Table 4.3. Different estimates for $\tilde{T}_{zz}(P)$ at 250 km using modified estimators with capsize of $\psi_0 = 3^0$. Unit: 1 cE …….106
Table 5.1. Maxima and minima of singular values of different system of equations and their corresponding condition numbers κ for recovering $1^\circ \times 1^\circ$ gravity anomaly from $0.5^\circ \times 0.5^\circ$ SGG data……..139
Table 5.2. Statistics of errors of $1^\circ \times 1^\circ$ recovered gravity anomalies from $0.5^\circ \times 0.5^\circ$ SGG data using Tikhonov regularization (based on L-curve and GCV) with Gaussian noise of 1 mE. Unit: 1 mGal…….....140

Table 5.3. Statistics of errors of $1^\circ \times 1^\circ$ recovered gravity anomalies from $0.5^\circ \times 0.5^\circ$ SGG data using Tikhonov regularization (based on L-curve and GCV) with Gaussian noise of 1 cE. Unit: 1 mGal……140
Table 5.4. Values of regularization parameter of the coefficient matrices for recovering $1^\circ \times 1^\circ$ gravity anomaly from $0.5^\circ \times 0.5^\circ$ SGG data derived for Tikhonov regularization using L-curve and GCV, for 1 mE and 1 cE noise on SGG data……141
Table 5.5. Maxima and minima of singular values of different system of equations and their corresponding condition numbers κ for recovering $0.5^\circ \times 0.5^\circ$ gravity anomaly from $0.25^\circ \times 0.25^\circ$ SGG data…….....142
Table 5.6. Statistics of errors of $0.5^\circ \times 0.5^\circ$ recovered gravity anomalies from $0.25^\circ \times 0.25^\circ$ SGG data using Tikhonov regularization (based on L-curve and GCV) with Gaussian noise of 1 mE. Unit: 1 mGal……..143
Table 5.7. Statistics of errors of $0.5^\circ \times 0.5^\circ$ recovered gravity anomalies from $0.25^\circ \times 0.25^\circ$ SGG data using Tikhonov regularization (based on L-curve and GCV) with Gaussian noise of 1 cE. Unit: 1 mGal……143
Table 5.8. Values of regularization parameter of the coefficient matrices for recovering $0.5^\circ \times 0.5^\circ$ gravity anomaly from $0.25^\circ \times 0.25^\circ$ SGG data derived for Tikhonov regularization using L-curve and GCV, for 1 mE and 1 cE noise on SGG data……143
Table 5.9. Maxima and minima of singular values of different system of equations and their corresponding condition numbers κ for recovering $1^\circ \times 1^\circ$ gravity anomaly from $0.25^\circ \times 0.25^\circ$ SGG data……..145
Table 5.10. Statistics of errors of $1^\circ \times 1^\circ$ recovered gravity anomalies from $0.25^\circ \times 0.25^\circ$ SGG data using Tikhonov regularization (based on L-curve and GCV) with Gaussian noise of 1 mE. Unit: 1 mGal……145
Table 5.11. Statistics of errors of $1^\circ \times 1^\circ$ recovered gravity anomalies from $0.25^\circ \times 0.25^\circ$ SGG data using Tikhonov regularization (based on L-curve and GCV) with Gaussian noise of 1 cE. Unit: 1 mGal…….....145
Table 5.12. Values of regularization parameter of the coefficient matrices for recovering $1^\circ \times 1^\circ$ gravity anomaly from $0.25^\circ \times 0.25^\circ$ SGG data derived for Tikhonov regularization using L-curve and GCV, for 1 mE and 1 cE noise on SGG data……...146
Table 5.13. Statistics of errors of $1^\circ \times 1^\circ$ recovered gravity anomalies obtained from inversion of $0.5^\circ \times 0.5^\circ$ and $0.25^\circ \times 0.25^\circ$ Eötvös type gradients. Unit: 1 mGal.147
Table 5.14. Statistics of estimated error of $1^\circ \times 1^\circ$ recovered gravity anomalies from $0.5^\circ \times 0.5^\circ$ SGG data (with 1 mE and 1 cE Gaussian noise). Unit: 1 mGal……...149
Table 5.15. Statistics of estimated error of $1^\circ \times 1^\circ$ recovered gravity anomalies from $0.5^\circ \times 0.5^\circ$ SGG data (with 1 mE and 1 cE Gaussian noise). Unit: 1 mGal……...150
Table 5.16. Statistics of estimated error of $1^\circ \times 1^\circ$ recovered gravity anomalies from $0.25^\circ \times 0.25^\circ$ SGG data (with 1 mE and 1 cE Gaussian noise). Unit: 1 mGal…...151
Table 5.17. A-posteriori variance factors and biases due to regularization in recovering $1^\circ \times 1^\circ$ gravity anomalies from $0.5^\circ \times 0.5^\circ$ and $0.25^\circ \times 0.25^\circ$ SGG data……...152
Table 5.18. A-posteriori variance factors in recovering $0.5^\circ \times 0.5^\circ$ gravity anomalies from $0.25^\circ \times 0.25^\circ$ SGG data……152
Table 5.19. Statistics of errors of biased-corrected $1^\circ \times 1^\circ$ recovered gravity anomalies from $0.5^\circ \times 0.5^\circ$ SGG data (with 1 mE and 1 cE Gaussian noise). Unit: 1 mGal……..154
Table 5.20. Statistics of errors of biased-corrected recovered $1^\circ \times 1^\circ$ gravity

anomalies from $0.25^\circ \times 0.25^\circ$ SGG data (with 1 mE and 1 cE Gaussian noise). Unit: 1 mGal……..156
Table 5.21. Statistics of errors of biased-corrected recovered $0.5^\circ \times 0.5^\circ$ gravity anomalies from $0.25^\circ \times 0.25^\circ$ SGG data (with 1 mE and 1 cE Gaussian noise). Unit: 1 mGal……..156
Table 5.22. Statistics of truncation error of estimated $0.5^\circ \times 0.5^\circ$ gravitational gradients from $1^\circ \times 1^\circ$ gravity anomalies using Eq. (5.14). Unit: 1 E……..158
Table 5.23. Statistics of truncation error of estimated $0.25^\circ \times 0.25^\circ$ gravitational gradients from $0.5^\circ \times 0.5^\circ$ gravity anomalies using Eq. (5.14). Unit: 1 E……158
Table 6.1. DOVCs of VV, HH and VH solution for *n*=200 and *m*=2……..174
Table 6.2. DOVC ratios for VV, HH and VH solutions based on stochastic model 1 for *n*=200, *m*=2, *n*=230, *m*=5, *n*=245, *m*=8……..174
Table 6.3. DOVCs of $T_{zz}, T_{xx}, T_{yy}, T_{xy}, T_{xz}$ and T_{yz} for *n*=200 and *m*=2…….176
Table 6.4. DOVC ratios of $T_{zz}, T_{xx}, T_{yy}, T_{xy}, T_{xz}$ and T_{yz} based on stochastic model 2 for *n*=200, *m*=2, *n*=230, *m*=5, *n*=245, *m*=8…….176
Table 6.5. Statistics of errors of recovered gravity anomalies from SGG data with 1 mE and 1 cE noise levels. Unit: 1 mGal……..179
Table 6.6. Statistics of errors of bias-corrected recovered gravity anomalies from SGG data with 1 mE and 1 cE noise levels. Unit: 1 mGal…….179
Table 6.7. VCs, biases due to regularization and biased-corrected VCs……..184
Table 6.8. Statistics of errors of recovered gravity anomalies considering VCE and biased-corrected VCE. Unit: 1 mGal……...185
Table 6.9. VCs, biases due to regularization and biased-corrected VCs……..186
Table 6.10. Statistics of errors of recovered gravity anomalies. Unit: 1 mGal……187

Table 7.1. Statistics of total errors of recovered gravity anomalies in polar gaps. Unit: 1 mGal…….195
Table 7.2. Statistics of total errors of biased-corrected recovered gravity anomalies in polar gaps. Unit: 1 mGal……196
Table 7.3. Statistics of errors of joint recovered and biased-corrected joint recovered gravity anomalies from SGG data in polar gaps. Unit: 1 mGal……..197
Table 7.4. Estimated errors of recovered gravity anomalies from joint inversion of SGG data. Unit: 1 mGal……..197

List of figures

Figure 2.1. Gravitational gradients in geocentric frame. (a) $T_{\theta\theta}$, (b) $T_{\lambda\lambda}$, (c) T_{rr}, (d) $T_{\theta\lambda}$, (e) $T_{r\theta}$ and (f) $T_{r\lambda}$. Unit: 1 E……16

Figure 2.2. Geocentric frame (x_{geo}, y_{geo}, z_{geo}) and LNOF (x, y, z)……16

Figure 2.3. ORF (u, v, w) and inertial frame (x_{int}, y_{int}, z_{int})……16

Figure 2.4. Gravitational gradients in LNOF. (a) T_{xx}, (b) T_{yy}, (c) T_{zz}, (d) T_{xy}, (e) T_{xz} and (f) T_{yz}. Unit: 1 E……22

Figure 2.5. Orbital perturbations of GOCE in one day revolution. (a) semi-major axis of orbital ellipse, (b) inclination, (c) eccentricity, (d) perigee argument, (e) right ascension of ascending node and (f) mean motion ……...30

Figure 2.6. Effect of orbital perturbations on (a) T_{xx}, (b) T_{yy}, (c) T_{zz}, (d) T_{xy}, (e) T_{xz} and (f) T_{yz}. Unit : 1 E……..31

Figure 2.7. Effect of satellite track azimuth perturbations in ORF on (a) T_{uu}, (b) T_{vv}, (c) T_{uv}, (d) T_{uw} and (e) T_{vw}. Unit: 1 E……32

Figure 2.8. Relative errors between true and estimated degree variances of geopotential field in percent……..41

Figure 2.9. (a), (b) and (c) are the percentage relative error degree variances of true and computed EGM with $15' \times 15'$ resolution……...42

Figure 2.10. Degree variances of geopotential model determined from SGG data at 250 km level with different resolutions. (a), (b) and (c) are the solutions of the first, second and third integrals in Eqs. (2.67a)-(2.67c), respectively……42

Figure 3.1. Long-wavelength topographic height of Fennoscandia and Iran obtained by SHCs of JGP95e global model to degree and order 360. Unit: 1 m……..53

Figure 3.2. TE on SGG data in Fennoscandia in LNOF. Unit: 1 E……54

Figure 3.3. TE on SGG data in Iran in LNOF. Unit: 1 E……54

Figure 3.4 General schematic structure of crust in CRUST2……..56

Figure 3.5. Long-wavelength LDV of upper crust in (a) Fennoscandia and (b) Iran. Unit: 1 g/cm^3 ……..56

Figure 3.6. LDVE of topography in Fennoscandia in LNOF on (a) $V_{xx}(P)$, (b) $V_{yy}(P)$, (c) $V_{zz}(P)$, (d) $V_{xy}(P)$, (e) $V_{xz}(P)$ and (f) $V_{yz}(P)$, respectively. Unit: 1 E……...57

Figure 3.7. LDVE of topography in Iran in LNOF on (a) $V_{xx}(P)$, (b) $V_{yy}(P)$, (c) $V_{zz}(P)$, (d) $V_{xy}(P)$, (e) $V_{xz}(P)$ and (f) $V_{yz}(P)$, respectively. Unit: 1 E……57

Figure 3.8. AE on SGG data in Fennoscandia in LNOF. Unit: 1 mE……65

Figure 3.9. AE on SGG data in Iran in LNOF. Unit: 1 mE……66

Figure 3.10. (a) NADM in green, KTHA in red and USSA76 in blue versus elevation (vertical axis is in logarithmic scale), (b) deference between NADM and USSA76 in blue, KTHA and USSA76 in red, respectively to 10 km elevation……70

Figure 3.11. Behaviour of unitless zero-degree harmonic of the atmospheric potential versus various Z. (a) Z=0 to 50 km and (b) Z=0 to 250 km……72
Figure 3.12. AE on SGG data at 250 km elevation, based on the exponential ADM in Fennoscandia in ORF, (a) V_{uu}^{a}, (b) V_{vv}^{a}, (c) V_{ww}^{a}, (d), V_{uv}^{a}, (e) V_{uw}^{a} and (f) V_{vw}^{a}. Unit: 1 mE……..81
Figure 3.13. (a) and (b) difference between the indirect AEs due to the exponential ADM and KTHA, on the gravity anomaly and geoid, respectively…….82
Figure 3.14. (a) Modified KTHA in red (vertical axis is in logarithmic scale), (b) NKTHA based on the USSA76 in red (vertical axis is in logarithmic scale), (c) differences between approximating models of KTHA, modified KTHA New KTHA and USSA76. (d) fitting of the exponential ADM and KTHA to the atmospheric density of the standard model……85
Figure 3.15. AE on the SGG data at 250 km based on the NKTHA, (a) V_{uu}, (b) V_{vv}, (c) V_{ww}, (d) V_{uv}, (e) V_{uw} and (f) V_{vw}. Unit: 1 mE……..87
Figure 4.1. (a) Behaviour of ESF before and after different LSM methods. (b) Behaviour of ESF before and after MM and BLSM with errorless data……....99
Figure 4.2. (a) Global RMSE of disturbing potential estimators based on different LSM methods. (b) Global RMSE of disturbing potential estimator based on MM and BLSM with errorless data. Unit: 1 m……..99
Figure 4.3. Topographic height of Fennoscandia and test area. Unit: 1 m……100
Figure 4.4. (a) Behaviour of original and modified SOD of ESF, (b) behaviour of original and modified SOD of ESF using MM and BLSM with errorless data……105
Figure 4.5. (a) Global RMSE of $\tilde{T}_{zz}(P)$ estimators based on different LSM methods. (b) Global RMSE of $\tilde{T}_{zz}(P)$ estimator based on MM and BLSM with errorless data. Unit: 1 E……..106
Figure 4.6. Truncation area of restricted data to a ring……120
Figure 4.7. (a) MM of ESF for a ring between ψ_0=1° and ψ_1=5° and, (b) ψ_0=5° and ψ_1=20° ……126
Figure 4.8. (a) BLSM of ESF for a ring between $\psi_0 = 1^\circ$ and $\psi_1 = 5^\circ$ and, (b) $\psi_0 = 5^\circ$ and $\psi_1 = 20^\circ$ with errorless data…….....126
Figure 4.9. (a) BLSM of ESF for a ring between $\psi_0 = 1^\circ$ and $\psi_1 = 5^\circ$ and, (b) ψ_0=5° and ψ_1=20° with erroneous data……127
Figure 4.10. (a) MM of SOD of ESF for a ring between ψ_0=2° and ψ_1=8° and, (b) ψ_0=8° and ψ_1=20° ……...128
Figure 4.11. (a) BLSM of SOD of ESF for a ring between ψ_0=2° and ψ_1=8° and, (b) ψ_0=8° and ψ_1=20° with errorless data……128
Figure 4.12. (a) BLSM of SOD of ESF for a ring between ψ_0=2° and ψ_1=8° and, (b) ψ_0=8° and ψ_1=20° with errorless data…….129
Figure 5.1. Gravity anomalies generated by EGM96 with $1^\circ \times 1^\circ$ resolution in Fennoscandia. Unit: 1 mGal……137
Figure 5.2. Singular values of $\mathbf{A}_{zz}$, $\mathbf{A}_{xx}$, $\mathbf{A}_{yy}$, $\mathbf{A}_{xy}$, $\mathbf{A}_{xz}$ and $\mathbf{A}_{yz}$ matrices, for recovering $1^\circ \times 1^\circ$ gravity anomaly from $0.5^\circ \times 0.5^\circ$ SGG data……138
Figure 5.3. Generated Gaussian noise of (a) 1 mE and (b) 1 cE on gravitational gradients……139
Figure 5.4. Singular values of $\mathbf{A}_{zz}$, $\mathbf{A}_{xx}$, $\mathbf{A}_{yy}$, $\mathbf{A}_{xy}$, $\mathbf{A}_{xz}$ and $\mathbf{A}_{yz}$ matrices, for recovering

$0.5^\circ \times 0.5^\circ$ gravity anomaly from $0.25^\circ \times 0.25^\circ$ SGG data……..141
Figure 5.5. Generated Gaussian noise of (a) 1 mE and (b) 1 cE on gravitational gradients……142
Figure 5.6. Singular values of $\mathbf{A}_{zz}$, $\mathbf{A}_{xx}$, $\mathbf{A}_{yy}$, $\mathbf{A}_{xy}$, $\mathbf{A}_{xz}$ and $\mathbf{A}_{yz}$ matrices, for recovering $1^\circ \times 1^\circ$ gravity anomaly from $0.25^\circ \times 0.25^\circ$ SGG data……...144
Figure 5.7. Singular values of $\mathbf{A}_{xx}$ - $\mathbf{A}_{yy}$, $2\,\mathbf{A}_{xy}$, $\mathbf{A}_{xz}$ and $\mathbf{A}_{yz}$ for recovering $1^\circ \times 1^\circ$ gravity anomalies from (a) $0.25^\circ \times 0.25^\circ$ and, (b) $0.5^\circ \times 0.5^\circ$ SGG data ……..146
Figure 5.8. Estimated error of $1^\circ \times 1^\circ$ recovered gravity anomalies from $0.5^\circ \times 0.5^\circ$ (a) T_{xx} , (b) T_{yy} , (c) T_{zz} , (d) T_{xy} , (e) T_{xz} and (f) T_{yz} with 1 mE Gaussian noise. Unit: 1 mGal……..148
Figure 5.9. Estimated error of $0.5^\circ \times 0.5^\circ$ recovered gravity anomalies from $0.25^\circ \times 0.25^\circ$ (a) T_{xx} , (b) T_{yy} , (c) T_{zz} , (d) T_{xy} , (e) T_{xz} and (f) T_{yz} with 1 mE Gaussian noise. Unit: 1 mGal…….....149
Figure 5.10. Estimated error of $1^\circ \times 1^\circ$ recovered gravity anomalies from $0.25^\circ \times 0.25^\circ$ (a) T_{xx} , (b) T_{yy} , (c) T_{zz} , (d) T_{xy} , (e) T_{xz} and (f) T_{yz} with 1 mE Gaussian noise. Unit: 1 mGal……150
Figure 5.11. Estimated biases of $1^\circ \times 1^\circ$ recovered gravity anomalies from $0.5^\circ \times 0.5^\circ$ (a) T_{xx} , (b) T_{yy} , (c) T_{zz} , (d) T_{xy} , (e) T_{xz} and (f) T_{yz} with 1 mE Gaussian noise. Unit: 1 mGal……153
Figure 5.12. Estimated biases of $1^\circ \times 1^\circ$ recovered gravity anomalies from $0.25^\circ \times 0.25^\circ$ (a) T_{xx} , (b) T_{yy} , (c) T_{zz} , (d) T_{xy} , (e) T_{xz} and (f) T_{yz} with 1 mE Gaussian noise. Unit: 1 mGal……..154
Figure 5.13. Estimated biases of $0.5^\circ \times 0.5^\circ$ recovered gravity anomalies from $0.25^\circ \times 0.25^\circ$ (a) T_{xx} , (b) T_{yy} , (c) T_{zz} , (d) T_{xy} , (e) T_{xz} and (f) T_{yz} with 1 mE Gaussian noise. Unit: 1 mGal……..155
Figure 5.14. Truncation error of $0.5^\circ \times 0.5^\circ$ estimated gravitational gradients (a) δT_{xx} , (b) δT_{yy} , (c) δT_{zz} , (d) δT_{xy} , (e) δT_{xz} and (f) δT_{yz} from $1^\circ \times 1^\circ$ gravity anomalies. Unit: 1 E……..157
Figure 5.15. Truncation error of $0.25^\circ \times 0.25^\circ$ estimated gravitational gradients (a) δT_{xx} , (b) δT_{yy} , (c) δT_{zz} , (d) δT_{xy} , (e) δT_{xz} and (f) δT_{yz} from $0.5^\circ \times 0.5^\circ$ gravity anomalies. Unit: 1 E…….158
Figure 6.1. (a) Simple mean, (b) weighted mean, (c) error degree variance of simple and weighted mean…….....164
Figure 6.2. (a) Condition adjustment solution. (b) Difference between condition adjustment solution and simple mean……...167
Figure 6.3. True, simple mean and combined solution 1……..172
Figure 6.4. VC ratios for (a) VV solution, (b) HH solution and (c) VH solution for n=200 and m=2……173
Figure 6.5. True, simple mean, combined solution 1 and 2…….174
Figure 6.6. Difference between true and simple mean, combined solution 1 and 2…….174
Figure 6.7. VC ratios for T_{zz} ,T_{xx} ,T_{yy} ,T_{xy} ,T_{xz} and T_{yz} ……175
Figure 6.8. Singular values of the coefficients matrix of joint inversion problem Eq. (6.38), when resolution of SGG data is $0.5^\circ \times 0.5^\circ$ and required gravity anomalies is $1^\circ \times 1^\circ$ ……...177

Figure 6.9. Recovered gravity anomalies from joint inversion of SGG data with 1 mE noise. Unit: 1 mGal……...177
Figure 6.10. Estimated error of recovered gravity anomalies in joint inversion of SGG data with (a) 1 mE and (b) 1 cE noise. Unit: 1 mGal……...178
Figure 6.11. Biases of recovered gravity anomalies from SGG data with (a) 1 mE and (b) 1 cE noise. Unit: 1 mGal……...178
Figure 6.12. VC ratios during VCE process when noise level is (a) 1 mE and (b) 1 cE……...183
Figure 6.13. VC ratios during biased-corrected VCE process when noise level is (a) 1 mE and (b) 1 cE……184
Figure 6.14. Regularization parameter variations during VCE process when noise level is (a) 1 mE and (b) 1 cE……...184
Figure 6.15. VC ratios during VCE process when noise level is (a) 1 mE and (b) 1 cE……..185
Figure 6.16. Biased-corrected VC ratios during VCE process when noise level is (a) 1 mE and (b) 1 cE……...186
Figure 6.17. Regularization parameter variations during VCE process when noise level is (a) 1 mE and (b) 1 cE……...186
Figure 7.1. Polar gaps……190
Figure 7. 2. Relative error of geopotential coefficients (a) VV, (b) VH and (c) HH GBVPs……...191
Figure 7.3. Generated gravity anomalies in (a) NPG and (b) SPG. Unit: 1 mGal……192
Figure 7.4. Generated gravitational gradients (a) T_{xx}, (b) T_{yy}, (c) T_{zz}, (d) T_{xy}, (e) T_{xz} and (f) T_{yz} at 250 km level from gravity anomalies in NPG. Unit: 1 E……...193
Figure 7.5. Generated gravitational gradients (a) T_{xx}, (b) T_{yy}, (c) T_{zz}, (d) T_{xy}, (e) T_{xz} and (f) T_{yz} at 250 km level from gravity anomalies in SPG. Unit: 1 E……193
Figure 7.6. Generated Gaussian noise of 1 mE. Unit: 1 E……194
Figure 7.7. Errors of recovered gravity anomalies in (a) NPG and (b) SPG. Unit: 1 mGal……..194
Figure 7.8. Estimated error of recovered gravity anomalies in (a) NPG and (b) SPG. Unit. 1 mGal……195
Figure 7.9. Errors of biased-corrected recovered gravity anomalies in (a) NPG and (b) SPG. Unit: 1 mGal……196
Figure 7.10. Errors of recovered gravity anomalies by joint inversion and biased-corrected joint inversion (a) NPG and (b) SPG. Unit: 1 mGal……..197

List of abbreviations

ADM	atmospheric density model
AE	atmospheric effect
ALF	associated Legendre function
BQUE	best quadratic unbiased estimator
BQUNE	best quadratic unbiased non-negative estimator
BLSM	biased least-squares modification
CHAMP	challenging minisatellite payload
DOVC	degree-order variance component
EGM	Earth's gravitational model
ESF	extended Stokes' function
GBVP	gradiometric boundary value problem
GCV	generalized cross validation
GOCE	gravity field and steady-state ocean circulation explorer
GPS	global positioning system
GRACE	gravity recovery and climate experiment
HH	horizontal-horizontal
IAG	International association of Geodesy
KTHA	Kungliga Tekniska Högskolan atmospheric density model
LC	lower crust
LDV	lateral density variation
LDVE	lateral density variation effect
LNOF	local north oriented frame
LSM	least-squares modification
MM	Mododensky's modification
MBQUNE	modified best quadratic unbiased non-negative estimator
MC	middle crust
NADM	Novak atmospheric density model
NPG	north polar gap
OLSM	optimum least squares modification
ORF	orbital frame
RMSE	root mean square error
SGG	satellite gravity gradiometry
SHC	spherical harmonic coefficient
SOD	second-order radial derivative
SPG	South polar gap
TE	topographic effect
TSH	tensor spherical harmonic

UC	upper crust
ULSM	unbiased least-squares modification
USSA	United States standard atmosphere
VH	vertical-horizontal
VV	vertical-vertical
VC	variance component
VCE	variance component estimation

Chapter 1

Introduction

1.1 Background

The gravitational field determination from space is an old story. The perturbation analysis and applications of dynamic satellite geodesy is one of the most famous approaches in this subject. In the classical method of geopotential modeling, orbital perturbations of satellites (which were designed for other geodetic purposes) were analyzed. Such satellites are not low orbiters and therefore not suitable for gravitational field determination. The Earth gravitational model (EGM) obtained from analyzing these orbits cannot include higher degrees and orders than 70. In order to obtain a higher degree EGM, the solution must be either combined with terrestrial data or subject to some constraints. In the former method the solution would not be a satellite-only EGM and in the latter case the higher degree harmonics than, say, 70 will be fiction as the solution is subjected to a constraint which is not clear where it is realistic. In order to obtain a high resolution satellite-only EGM, some special satellite missions must be designed. The last three dedicated satellite missions for gravity field determination are the Challenging Minisatellite Payload (CHAMP) (Reigber et al. 2004) and the Gravity Recovery and Climate Experiment (GRACE) (Tapely et al. 2005). These missions were only designed for using the new satellite technology and the developed perturbation theory to recover the gravitational field. In CHAMP high-low satellite-to-satellite tracking data (between the Global Positioning System (GPS) satellites and the CHAMP satellite) is used to determine a precise orbit for the satellite. The orbit is analyzed to determine geopotential coefficients to degree and order 119. GRACE mission consists of a twin satellite, and the range rate between these two satellites is measured by low-low satellite-to-satellite tracking technique. The low-low and high-low satellite-to-satellite tracking data (with the GPS satellites) are used together to precisely determine the satellites orbit. The low-low technique gives another idea to gradiometry by measurements of the satellite pair; see e.g Keller and Sharifi (2005) or Sharifi (2006). This method of gradiometry and the information of the precise orbit has been analyzed to determine a precise EGM to degree and order 150. The Gravity field and steady-state Ocean Circulation Explore

(GOCE) mission (see e.g. Balmino et al. 1998 and 2001, ESA 1999, Albertella et al. 2002), was launched on 17th of March in 2009. In this mission differential acceleometry, or satellite gravity gradiometry (SGG) technique is directly used. In this case the gravitational gradients as well as the satellite orbit are used to recover a high-resolution precise EGM. It is expected to determine an EGM to degree and order 200. Such an EGM will have good precision in long and short wavelengths of the gravitational signal. The EGM will yield 1 cm and 1 mGal accuracy for geoid and gravity anomaly, respectively with $1^\circ \times 1^\circ$ resolution.

In SGG, the geopotential coefficients are determined in two different ways: time-wise approach, and space-wise approach. In the former the satellite observations are considered as a time series, and the series is related to the geopotential coefficients using the second-order derivatives of the well-known expression of the potential in terms of orbital parameters. The latter approach considers the observations as functions of position instead of time. The space-wise approach can also be preformed in two different ways: one can use either the least-squares method or quadrature formulas. In this dissertation emphasis is on the quadrature integral formulas, which are solutions of gradiometric boundary value problems (GBVPs) to compute the geopotential coefficients. Furthermore the thesis will answer the following questions:

1. Is there a simpler expression for the gravitational gradients than the traditional ones? Is it possible to avoid differentiating the ALFs for the gradients? Can we remove singular terms in the expressions when the latitude is 90° or -90°? How are the geopotential coefficients derived from the solution of GBVPs using tensor spherical harmonics (TSHs)? What is the relation between the resolution of SGG data and the maximum achievable degree of the EGM to be recovered?
2. How big are the topographic effect (TE) and the lateral density variation effect (LDVE) of topography on the SGG data? Is it possible to find a better atmospheric density model (ADM) than the existing ADMs? How big is the atmospheric effect (AE) based on this ADM?
3. Is it possible to use the least-squares modification (LSM) method to modify the second-order partial derivatives of the extended Stokes formula to generate the gravitational gradients at satellite level?
4. Which is the most suitable gravitational gradient to be continued downward to sea level? How is the truncation errors of the integral with non-isotropic kernels estimated? Is it possible to obtain the gravity anomaly with 1 mGal accuracy from direct inversion of the SGG data?
5. How can the gravitational gradients be combined to obtain a better gravitational field solution than that obtained from a single gradient?
6. Which is the suitable gradient for gravitational recovery in polar gaps? How does the joint inversion of gradients improve the solution of the gravitational field in these areas?

1.2 The Author's contributions

The author's investigations are summarized in six parts:

1. We have presented new expressions for the gravitational gradients in a geocentric frame, local north-oriented frame (LNOF) and orbital frame (ORF). Also we have proposed new formulas for geopotential force acting on a satellite and the TSHs. The new expressions for the TSHs are used in the solution of the GBVPs to recover an EGM from the SGG data at the 250 km level.

2. We have investigated the TE and LDVE of topographic masses on the SGG data in Fennoscandia and Iran. We have formulated and investigated the AE based on some ADMs, such as USSA76, Novak (NADM), Sjöberg (KTHA), and exponential ADMs for the direct and indirect AEs. We have proposed a new ADM and formulated the AE based on this model.

3. We have developed the biased LSM (BLSM), unbiased LSM (ULSM) and optimum LSM (OLSM) to SGG, to modify the second-order partial derivatives of the extended Stokes formula and generating the gradients at satellite level. We have proposed a strategy to modify the vertical-horizontal (VH) gradients and the horizontal-horizontal (HH) gradients integral formulas.

4. We have investigated the downward continuation of each gradient from satellite level to gravity anomaly at sea level, as well as their combinations.

5. We have used VCE to obtain optimal solution for determining the geopotential coefficients. It is also used for determining the gravity anomaly and downward continuation of the SGG data.

6. The estimation of gravity anomaly from the SGG data is numerically investigated in the north polar gap (NPG) and the south polar gap (SPG).

Chapter 2

Alternative expressions in global synthesis and analysis

2.1 Introduction

The gravitational gradients can be expressed in terms of spherical harmonics. The spherical harmonic coefficients (SHCs) of the gravitational field can easily be inserted to these expressions for synthesizing the gravitational gradients. There are different frames to express these gradients such as geocentric frame, local north-oriented frame (LNOF) and orbital frame (ORF); see e.g. Koop (1993). The synthesis is time consuming for a huge number of gradients. In such a case, vectorization algorithms are beneficial. Rizos (1979) proposed an efficient computer technique for the evaluation of the geopotential from spherical harmonic models and Bettadpur et al. (1992) presented a vectorization algorithm in this matter. This algorithm could be more efficient if the Clenshaw method is considered as well (Clenshaw 1955, Tscherning and Poder 1982). Some algorithms were presented by Holmes and Featherstone (2002a) and (2002b) to synthesize the spherical harmonic summation and stabilize the generation of the ALFs and their first- and second-order derivatives. Their goal seems to be to construct a synthetic EGM (Baran et al. 2006). Bethencourt et al. (2005) presented an algorithm for high-degree synthesis using a personal computer by Clenshaw technique. Eshagh (2009a) used the fully-vectorized technique for synthesis and analysis in gradiometry. Eshagh and Abdollahzadeh (2009a) used a semi-vectorization technique, which is more efficient than fully-vectorization to speed up the computations in gradiometric synthesis and analysis.

The traditional expression of the gravitational gradients has complicated forms, involving first- and second-order derivatives of the ALFs and singular terms at the poles. Balmino et al. (1990) and (1991) presented some formulas for these gradients in a geocentric frame based on Cartesian coordinates and compared the gradients based on different software. Petrovskaya and Vershkov (2006) with reference to Ilk (1983) presented other formulas in the LNOF and the ORF. Ilk (1983) presented some useful relations among the ALFs, which were used by Petrovskaya and

Vershkov (2006). Claessen (2005) derived new relations for the ALFs which are useful as well. Petrovskaya and Vershkov (2007) expressed the gravitational gradients in terms of the satellite Cartesian coordinates. Some geophysical interpretations for the gravitational gradients in LNOF are given by Kiamehr et al. (2008).

The geopotential coefficients can be derived using least-squares or quadrature formulas. The least-squares approach can be used in two different ways: time-wise and space-wise approaches. Rummel and Colombo (1985) studied the gravity field determination from SGG numerically, and they concluded that the geopotential coefficients obtained from SGG are more or less the same as those obtained form orbital analysis after two iteration. Rummel et al. (1993) considered both time-wise and space-wise approaches and compared these methods. Rummel and van Gelderen (1995) investigated the relation between the spectral characteristics of gravity field and the Meissl scheme. Rummel (1997) discussed the spectral analysis of SGG. Klees et al. (2000) presented an efficient method for recovering the gravity field in time-wise mode. Sneeuw (1994) presented a historical perspective of global spherical harmonic analysis and synthesis in least-squares and numerical quadrature formula. Sneeuw (2003) considered time-wise and space-wise approaches and presented an efficient algorithm of geopotential modeling. Ditmar et al. (2003a) and (2003b) presented a fast technique for computing the geopotential coefficients using conjugate gradients and pre-conditioning in space-wise approach and used the Tikhonov regularization method and three different methods of selecting the regularization parameter. Another possible way of geopotential modeling is to use least-squares collocation; see e.g. Tscherning (2001a) and (2002) and Arabelos and Tscherning (2007). The numerical quadrature formulas are of interest for Petrovskaya (1996), Petrovskaya and Zielinski (1997), Petrovskaya et al. (2001) and Petrovskaya and Vershkov (2002) and (2008). The geopotential coefficients can be determined from spectral solution of the GBVPs. In solving these GBVPs, combinations of the gravitational gradients are considered. The VV, VH and HH gradients are considered separately so that the orthogonality of the TSHs hold; for more details about the TSHs; see e.g. Freeden et al. (1994), Rummel (1997), Gelderen and Rummel (2001) and (2002), Martinec (2003), Toth (2003) and Bölling and Grafarend (2005). This property opens a way to use integral formulas to determine the coefficients.

In this chapter we will present new expressions for the gravitational gradients in geocentric frame, LNOF and ORF. The advantages of these expressions are their simplicity to use, as they do not include derivatives of the ALFs and they contain no singular terms at the poles. Also a new expression for the geopotential perturbing force is presented, which has the same benefits as the expressions for the gravitational gradients. These formulas are applied to express the magnitudes of the gravitational gradients at satellite level, or, in other words, the SGG data. Also, some investigations are made on the orbital perturbations of an imaginary satellite at 250 km level to consider their effects on the SGG data. The spectral solutions of the GBVPs, which are involved with the TSHs, are used to determine an EGM from the SGG data in the LNOF. A new expression is also provided for the TSHs, which is simpler than the traditional one.

2.2 Gravitational potential

Let the Earth's gravitational potential be represented by a truncated series of spherical harmonics. The truncated spherical harmonic expression for the disturbing potential can be written:

$$T\left(P\right)=\frac{GM}{R}\sum_{n=2}^{N_{\max}}\sum_{m=-n}^{n}\left(\frac{R}{r}\right)^{n+1}t_{nm}Y_{nm}\left(P\right), \tag{2.1}$$

where, $Y_{nm}\left(P\right)$ is the fully-normalized spherical harmonics at point P with the following orthogonality property:

$$\iint_{\sigma}Y_{nm}\left(P\right)Y_{n'm'}\left(P\right)d\sigma=4\pi\delta_{nn'}\delta_{mm'}, \tag{2.2}$$

δ stands for the Kronecker delta, r is the geocentric radius and σ is the unit sphere. The fully-normalized spherical harmonics can also be written:

$$Y_{nm}\left(P\right)=Q_{m}\left(\lambda\right)\bar{P}_{n|m|}\left(\theta\right), \tag{2.3}$$

where

$$Q_{m}\left(\lambda\right)=\begin{cases}\cos m\lambda & m\leq 0\\ \sin m\lambda & m>0\end{cases}. \tag{2.4}$$

θ is the co-latitude and λ is the longitude. In Eq. (2.1), GM is the geocentric gravitational constant and R radius of the sphere equal to semi-major axis of the reference ellipsoid. In Eq. (2.3) $\bar{P}_{n|m|}\left(\theta\right)$ is the fully-normalized ALF of degree n and order m, $N_{\max}$ is the maximum degree of truncation of the expansion, t_{nm} are the harmonic coefficients of the disturbing potential, with $t_{nm}=\bar{S}_{nm}$, if $m>0$ and $t_{nm}=\bar{C}_{nm}$, if $m\leq 0$, $\bar{C}_{nm}$ and $\bar{S}_{nm}$ being the fully-normalized cosine and sine SHCs of the disturbing potential. By the above representation for the disturbing potential we will continue our discussion by introducing different frames in expressing the gravitational gradients in Section 2.3.

2.3 Gravitational gradients in a geocentric frame

Before starting any discussion, we should explain our definition for a geocentric frame. This frame is defined in such a way that its z-axis points to the mean Earth poles of rotation, the x- and y- axes are in the mean equatorial plane with the x-axis towards the Greenwich meridian on the equator and the frame holds right handed. This frame is illustrated in Figure 2.1. Any point P can be expressed in either spherical (r,θ,λ) or Cartesian (x, y, z) coordinates. The gradient of the disturbing potential in the spherical coordinates becomes:

$$\nabla T\left(P\right)=\left[\frac{\partial}{\partial r}\quad\frac{\partial}{\partial\theta}\quad\frac{\partial}{\partial\lambda}\right]T\left(P\right),\tag{2.5}$$

with the scale factors of respective coordinates

$$h_r=1,\ h_\theta=r,\ h_\lambda=r\sin\theta\,.\tag{2.6}$$

Here the gravitational vector components can be expressed as (Novak and Grafarend 2006, Eqs. 50-52, p. 578):

$$T_r\left(P\right)=h_r^{-1}\frac{\partial T\left(P\right)}{\partial r}=-\frac{GM}{R^2}\sum_{n=2}^{N_{\max}}\sum_{m=-n}^{n}\left(n+1\right)\left(\frac{R}{r}\right)^{n+2}t_{nm}Q_m\left(\lambda\right)\bar{P}_{n|m|}\left(\theta\right)\ ,\tag{2.7a}$$

$$T_\theta\left(P\right)=h_\theta^{-1}\frac{\partial T\left(P\right)}{\partial\theta}=\frac{GM}{R^2}\sum_{n=2}^{N_{\max}}\sum_{m=-n}^{n}\left(\frac{R}{r}\right)^{n+2}t_{nm}Q_m\left(\lambda\right)\frac{\partial\bar{P}_{n|m|}\left(\theta\right)}{\partial\theta},\tag{2.7b}$$

$$T_\lambda\left(P\right)=h_\lambda^{-1}\frac{\partial T\left(P\right)}{\partial\lambda}=\frac{GM}{R^2\sin\theta}\sum_{n=2}^{N_{\max}}\sum_{m=-n}^{n}\left(\frac{R}{r}\right)^{n+2}m\,t_{nm}Q_{-m}\left(\lambda\right)\bar{P}_{n|m|}\left(\theta\right)\ .\tag{2.7c}$$

In Eq. (2.7a) the ALFs can be written in a recursive form, and the Clenshaw algorithm (Clenshaw 1955) can easily be employed to sum up the relation; see e.g. Tscherning and Poder (1982). Equations (2.7a)-(2.7c) can be modified using the Holmes and Featherstone (2002a) scheme to obtain a stable solution even for very high degrees and orders of the ALFs. The gravitational tensor at point P, $\mathbf{T}_{r\theta\lambda}\left(P\right)$, can be expressed by:

$$\mathbf{T}_{r\theta\lambda}\left(P\right)=\nabla\otimes\nabla T\left(P\right)=\begin{bmatrix}\frac{\partial^2T\left(P\right)}{\partial r^2} & \frac{\partial^2T\left(P\right)}{\partial r\partial\theta} & \frac{\partial^2T\left(P\right)}{\partial r\partial\lambda}\\ \frac{\partial^2T\left(P\right)}{\partial\theta\partial r} & \frac{\partial^2T\left(P\right)}{\partial\theta^2} & \frac{\partial^2T\left(P\right)}{\partial\theta\partial\lambda}\\ \frac{\partial^2T\left(P\right)}{\partial\lambda\partial r} & \frac{\partial^2T\left(P\right)}{\partial\lambda\partial\theta} & \frac{\partial^2T\left(P\right)}{\partial\lambda^2}\end{bmatrix},\tag{2.8}$$

where $\otimes$ is the tensor product of two gradient vectors (the symbol stands for the matrix product of two general vectors, and in this particular case, the vectors are presented by the gradients of the disturbing potential). The gravitational tensor, having the above form, is a symmetric tensor of rank two (Novak and Grafarend 2006). The entries of this tensor in terms of spherical harmonics are (Novak and Grafarend 2006, Eqs. 53-58, p. 579):

$$T_{rr}(P) = h_r^{-2}\frac{\partial^2 T(P)}{\partial r^2} = \frac{GM}{R^3}\sum_{n=2}^{N_{\max}}\sum_{m=-n}^{n}(n+1)(n+2)\left(\frac{R}{r}\right)^{n+3} t_{nm}Q_m(\lambda)\bar{P}_{n|m|}(\theta), \quad (2.9a)$$

$$T_{\theta\theta}(P) = h_\theta^{-2}\frac{\partial^2 T(P)}{\partial \theta^2} = \frac{GM}{R^3}\sum_{n=2}^{N_{\max}}\sum_{m=-n}^{n}\left(\frac{R}{r}\right)^{n+3} t_{nm}Q_m(\lambda)\frac{\partial^2 \bar{P}_{n|m|}(\theta)}{\partial \theta^2}, \quad (2.9b)$$

$$T_{\lambda\lambda}(P) = h_\lambda^{-2}\frac{\partial^2 T(P)}{\partial \lambda^2} = -\frac{GM}{R^3\sin^2\theta}\sum_{n=2}^{N_{\max}}\sum_{m=-n}^{n}\left(\frac{R}{r}\right)^{n+3} m^2 t_{nm}Q_m(\lambda)\bar{P}_{n|m|}(\theta), \quad (2.9c)$$

$$T_{r\theta}(P) = h_r^{-1}h_\theta^{-1}\frac{\partial^2 T(P)}{\partial r\partial \theta} = -\frac{GM}{R^3}\sum_{n=2}^{N_{\max}}\sum_{m=-n}^{n}(n+1)\left(\frac{R}{r}\right)^{n+3} t_{nm}Q_m(\lambda)\frac{\partial \bar{P}_{n|m|}(\theta)}{\partial \theta}, \quad (2.9d)$$

$$T_{r\lambda}(P) = h_r^{-1}h_\lambda^{-1}\frac{\partial^2 T(P)}{\partial r\partial \lambda} = \frac{GM}{R^3\sin\theta}\sum_{n=2}^{N_{\max}}\sum_{m=-n}^{n}(n+1)\left(\frac{R}{r}\right)^{n+3} m\, t_{nm}Q_{-m}(\lambda)\bar{P}_{n|m|}(\theta), \quad (2.9e)$$

$$T_{\theta\lambda}(P) = h_\theta^{-1}h_\lambda^{-1}\frac{\partial^2 T(P)}{\partial \theta\partial \lambda} = -\frac{GM}{R^3\sin\theta}\sum_{n=2}^{N_{\max}}\sum_{m=-n}^{n}\left(\frac{R}{r}\right)^{n+3} m\, t_{nm}Q_{-m}(\lambda)\frac{\partial \bar{P}_{n|m|}(\theta)}{\partial \theta}. \quad (2.9f)$$

As one can see, some relations are related to the first- or second-order derivatives of the ALFs, and also, some of the relations contain the terms $1/\sin\theta$ or $1/\sin^2\theta$. Equation (2.9a) has the simplest form among these relations, and it can easily be summed up using Clenshaw or Horner approach; e.g., Holmes and Featherstone (2002a). Holmes and Featherstone (2002b) have also presented a recursive relation for the second-order derivative for very high degree and order of the ALFs, so that the Clenshaw or Horner algorithms can easily be used in Eq. (2.9b). Equation (2.9c) contains the term $1/\sin^2\theta$, and Eqs. (2.9e) and (2.9f) include the term $1/\sin\theta$ and the first-order derivatives of the ALFs.

2.3.1. Alternative expressions for gravitational gradients in geocentric frame

We start our mathematical derivations of some alternative expressions from Eq. (2.7b) containing the first-order derivative of the ALF with respect to co-latitude. For simplicity we will use the abbreviated notation $P_{n|m|} = P_{n|m|}(\theta)$ through this chapter. Let us first introduce the following lemma.

Lemma 2.1 (Ilk 1983, Z.1.44):

$$\frac{\partial P_{n|m|}}{\partial \theta} = \frac{1}{2}\left[(n+|m|)(n-|m|+1)P_{n,|m|-1} - P_{n,|m|+1}\right].$$

Based on Lemma 2.1, Proposition 2.1 follows.

Proposition 2.1:

$$\frac{\partial \bar{P}_{n|m|}}{\partial \theta} = a^1_{nm} \bar{P}_{n,|m|-1} + a^2_{nm} \bar{P}_{n,|m|+1},$$

where

$$a^1_{nm} = \frac{1}{2}\sqrt{n+|m|}\sqrt{n-|m|+1}\sqrt{\left(2-\delta_{|m|0}\right)\Big/\left(2-\delta_{|m|-1,0}\right)},$$

and

$$a^2_{nm} = -\frac{1}{2}\sqrt{n-|m|}\sqrt{n+|m|+1}\sqrt{\left(2-\delta_{|m|0}\right)\Big/\left(2-\delta_{|m|+1,0}\right)}.$$

Here δ is the Kronecker delta.

Proof. By considering the normalization using

$$\bar{P}_{n|m|} = \sqrt{\frac{\left(n+|m|\right)!}{\left(2-\delta_{|m|0}\right)\left(2n+1\right)\left(n-|m|\right)!}} P_{n|m|}\ , \tag{2.10}$$

in Eq. (2.10) and after further simplifications, the proposition follows.

Proposition 2.1 implies that we do not have to compute the derivative of the ALFs. Equation (2.9b) includes the second-order derivative of this function and we will present another simple formula for that in Proposition 2.2.

Proposition 2.2:

$$\frac{\partial^2 \bar{P}_{n|m|}}{\partial \theta^2} = b^1_{nm} P_{n,|m|-2} + b^2_{nm} P_{n|m|} + b^3_{nm} P_{n,|m|+2},$$

where

$$b^1_{nm} = \frac{1}{4}\sqrt{n+|m|}\sqrt{n+|m|-1}\sqrt{n-|m|+1}\sqrt{n-|m|+2}\sqrt{\left(2-\delta_{|m|,0}\right)\Big/\left(2-\delta_{|m|-2,0}\right)}\ ,$$

$$b^2_{nm} = -\frac{1}{4}\Big[\left(n+|m|\right)\left(n-|m|+1\right)+\left(n-|m|\right)\left(n+|m+1|\right)\Big],$$

$$b^3_{nm} = \frac{1}{4}\sqrt{n+|m|+2}\sqrt{n+|m|+1}\sqrt{n-|m|}\sqrt{n-|m|-1}\sqrt{\left(2-\delta_{|m|0}\right)\Big/\left(2-\delta_{|m|+2,0}\right)}.$$

Proof. Using Lemma 2.1 twice for the non-normalized ALFs we obtain

$$\frac{\partial^2 P_{n|m|}}{\partial \theta^2} = \frac{\partial}{\partial \theta}\left(\frac{\partial P_{n|m|}}{\partial \theta}\right) = \left\{\frac{1}{2}\left[\left(n+|m|\right)\left(n-|m|+1\right)\frac{\partial P_{n,|m|-1}}{\partial \theta} - \frac{\partial P_{n,|m|+1}}{\partial \theta}\right]\right\}. \tag{2.11}$$

Again, from Lemma 2.1 we obtain also

$$\frac{\partial P_{n,|m|-1}}{\partial\theta}=\frac{1}{2}\Big[\big(n+|m|-1\big)\big(n-|m|+2\big)P_{n,|m|-2}-P_{n|m|}\Big] \tag{2.12}$$

$$\frac{\partial P_{n,|m|+1}}{\partial\theta}=\frac{1}{2}\Big[\big(n+|m|+1\big)\big(n-|m|\big)P_{n|m|}-P_{n,|m|+2}\Big]\ . \tag{2.13}$$

Substituting Eqs. (2.12) and (2.13) into (2.11) and after simplification we obtain

$$\frac{\partial^2 P_{n|m|}}{\partial\theta^2}=\frac{1}{4}\big(n+|m|\big)\big(n-|m|+1\big)\big(n+|m|-1\big)\big(n-|m|+2\big)P_{n,|m|-2}-$$
$$-\frac{1}{4}\Big[\big(n+|m|\big)\big(n-|m|+1\big)+\big(n-|m|\big)\big(n+|m|+1\big)\Big]P_{n|m|}+\frac{1}{4}P_{n,|m|+2}\,. \tag{2.14}$$

After normalization based on Eq. (2.10) and further simplifications the proposition is proved.

Removal of singular factor $1/\sin^2\theta$ in Eq. (2.9c) is dealt with in Propositions 2.3 and 2.4.

Lemma 2.2 (Ilk 1983, Eq. Z.1.42):

$$\frac{P_{n|m|}}{\sin\theta}=\frac{1}{2|m|}\Big[\big(n+|m|\big)\big(n+|m|-1\big)P_{n-1,|m|-1}+P_{n-1,|m|+1}\Big]\ , \qquad |m|\neq 0\,.$$

Lemma 2.3 (Ilk 1983, Eq. Z.1.41):

$$\frac{P_{n,|m|}}{\sin\theta}=\frac{1}{2|m|}\Big[\big(n-|m|+1\big)\big(n-|m|+2\big)P_{n+1,|m|-1}+P_{n+1,|m|+1}\Big], \quad |m|\neq 0\,.$$

Lemmas 2.2 and 2.3 present the $P_{n|m|}/\sin\theta$ term in two forward and backward modes with respect to degree n. It means that in the former the degree is n-1 (backward) and in the latter it is n+1(forward). In the following proposition we simplify $mP_{n|m|}/\sin\theta$ in backward mode.

Proposition 2.3:

$$m\,\frac{\bar{P}_{n,|m|}}{\sin\theta}=c^1_{nm}\bar{P}_{n-1,|m|-1}+c^2_{nm}\bar{P}_{n-1,|m|+1}\,, \qquad |m|\neq 0$$

where

$$c^1_{nm}=\frac{m}{2|m|}\sqrt{n+|m|}\sqrt{n+|m|-1}\sqrt{\big(2-\delta_{|m|0}\big)(2n+1)\Big/\big(2-\delta_{|m|-1,0}\big)\Big/(2n-1)}\,,$$

$$c^2_{nm}=\frac{m}{2|m|}\sqrt{n-|m|}\sqrt{n-|m|-1}\sqrt{\big(2-\delta_{|m|0}\big)(2n+1)\Big/\big(2-\delta_{|m|+1,0}\big)\Big/(2n-1)}\,.$$

Proof. The proposition is proved by normalizing the equation of Lemma 2.2.

The $mP_{n|m|}\big/\sin\theta$ term can be simplified in forward mode with respect to n in the following proposition.

Proposition 2.4:

$$m\,\frac{\bar{P}_{n|m|}}{\sin\theta}=c'^{1}_{nm}\bar{P}_{n+1,|m|-1}+c'^{2}_{nm}\bar{P}_{n+1,|m|+1},\qquad |m|\neq 0$$

where

$$c'^{1}_{nm}=\frac{m}{2|m|}\sqrt{n-|m|+1}\sqrt{n-|m|+2}\sqrt{\left(2-\delta_{|m|0}\right)(2n+1)\Big/\left(2-\delta_{|m|-1,0}\right)\Big/(2n+3)}$$

$$c'^{2}_{nm}=\frac{m}{2|m|}\sqrt{n+|m|+1}\sqrt{n+|m|+2}\sqrt{\left(2-\delta_{|m|0}\right)(2n+1)\Big/\left(2-\delta_{|m|+1,0}\right)\Big/(2n+3)}$$

Proof. The proposition is proved by normalizing the equation in Lemma 2.3.

Proposition 2.5:

$$m^{2}\,\frac{\bar{P}_{n,|m|}}{\sin^{2}\theta}=d^{1}_{nm}\bar{P}_{n,|m|-2}+d^{2}_{nm}\bar{P}_{n|m|}+d^{3}_{nm}\bar{P}_{n,|m|+2},\quad |m|\neq 0,1\quad,$$

where

$$d^{1}_{nm}=\frac{m^{2}}{4|m|\left(|m|-1\right)}\sqrt{\frac{2-\delta_{|m|0}}{2-\delta_{|m|-2,0}}}\sqrt{n+|m|}\sqrt{n-|m|+1}\sqrt{n-|m|+2}\sqrt{n+|m|-1}\ ,$$

$$d^{2}_{nm}=\frac{m^{2}}{4|m|}\left[\frac{\left(n+|m|\right)\left(n+|m|-1\right)}{|m|-1}+\frac{\left(n-|m|\right)\left(n-|m|-1\right)}{|m|+1}\right],$$

$$d^{3}_{nm}=\frac{m^{2}}{4|m|\left(|m|+1\right)}\sqrt{\frac{2-\delta_{|m|0}}{2-\delta_{|m|+2,0}}}\sqrt{n-|m|}\sqrt{n-|m|-1}\sqrt{n+|m|+2}\sqrt{n+|m|+1}\,.$$

Proof. Using Lemma 2.2 twice for non-normalized ALFs we have

$$\frac{P_{n|m|}}{\sin^{2}\theta}=\frac{1}{\sin\theta}\frac{P_{n|m|}}{\sin\theta}=\frac{1}{2|m|\sin\theta}\left[\left(n+|m|\right)\left(n+|m|-1\right)\frac{P_{n-1,|m|-1}}{\sin\theta}+\frac{P_{n-1,|m|+1}}{\sin\theta}\right],\quad(2.15)$$

and according to Lemma 2.2 and Eq. (2.15) we can write

$$\frac{P_{n-1,|m|-1}}{\sin\theta}=\frac{1}{2\left(|m|-1\right)}\left[\left(n-|m|+1\right)\left(n-|m|+2\right)P_{n,|m|-2}+P_{n|m|}\right]\qquad(2.16)$$

and

$$\frac{P_{n-1,|m|+1}}{\sin\theta}=\frac{1}{2\left(|m|+1\right)}\left[\left(n-|m|-1\right)\left(n-|m|\right)P_{n|m|}+P_{n,|m|+2}\right]. \tag{2.17}$$

Substituting Eqs. (2.16) and (2.17) into (2.15) we obtain

$$\frac{P_{n,|m|}}{\sin^2\theta}=\frac{1}{4|m|}\left\{\frac{\left(n+|m|\right)\left(n+|m|-1\right)\left(n-|m|+1\right)\left(n-|m|+2\right)}{|m|-1}P_{n,|m|-2}+\right.$$
$$\left.+\left[\frac{\left(n+|m|\right)\left(n+|m|-1\right)}{|m|-1}+\frac{\left(n-|m|\right)\left(n-|m|-1\right)}{|m|+1}\right]P_{n,|m|}+\frac{1}{|m|+1}P_{n,|m|+2}\right\}. \tag{2.18}$$

After normalization and further algebraic simplifications the proposition is proved.

Equation (2.9f) includes the problem of the factor $\sin^{-1}\theta$ and the derivative with respect to θ, which will be eliminated by Propositions 2.6 and 2.7 with Lemmas 2.1 and 2.3. It can also be simplified in backward and forward modes. Proposition 2.6 simplifies the formula in backward mode.

Proposition 2.6:

$$\frac{m}{\sin\theta}\frac{\partial\overline{P}_{n|m|}}{\partial\theta}=e^1_{nm}\overline{P}_{n-1,|m|-2}+e^2_{nm}\overline{P}_{n-1,|m|}+e^3_{nm}\overline{P}_{n-1,|m|+2}.\ |m|\neq 1,$$

where

$$e^1_{nm}=\frac{m}{4\left(|m|-1\right)}\sqrt{\frac{\left(2-\delta_{|m|0}\right)\left(2n+1\right)}{\left(2-\delta_{|m|-2,0}\right)\left(2n-1\right)}}\sqrt{n+|m|}\sqrt{n-|m|+1}\sqrt{n+|m|-1}\sqrt{n+|m|-2},$$

$$e^2_{nm}=\frac{m}{4}\left[\frac{\sqrt{\left(n+|m|\right)}\left(n-|m|+1\right)}{|m|-1}-\frac{\left(n+|m|+1\right)\sqrt{\left(n+|m|\right)}}{|m|+1}\right]\sqrt{\frac{\left(2n+1\right)\left(n-|m|\right)}{\left(2n-1\right)}},$$

$$e^3_{nm}=-\frac{m}{4\left(|m|+1\right)}\sqrt{\frac{\left(2-\delta_{|m|0}\right)\left(2n+1\right)}{\left(2-\delta_{|m|+2,0}\right)\left(2n-1\right)}}\sqrt{n-|m|}\sqrt{n+|m|+1}\sqrt{n-|m|-1}\sqrt{n-|m|-2}.$$

Proof. According to Lemma 2.1 we have

$$\frac{1}{\sin\theta}\frac{\partial P_{n,|m|}}{\partial\theta}=\frac{1}{2}\left[\left(n+|m|\right)\left(n-|m|+1\right)\frac{P_{n,|m|-1}}{\sin\theta}-\frac{P_{n,|m|+1}}{\sin\theta}\right], \tag{2.19}$$

and by considering Lemma 2.2, $P_{n,|m|-1}/\sin\theta$ and $P_{n,|m|+1}/\sin\theta$ can be rewritten as

$$\frac{P_{n,|m|-1}}{\sin\theta}=\frac{1}{2\left(|m|-1\right)}\left[\left(n+|m|-1\right)\left(n+|m|-2\right)P_{n-1,|m|-2}+P_{n-1,|m|}\right] \tag{2.20}$$

$$\frac{P_{n,|m|+1}}{\sin\theta}=\frac{1}{2\left(|m|+1\right)}\left[\left(n+|m|+1\right)\left(n+|m|\right)P_{n-1,|m|}+P_{n-1,|m|+2}\right]. \tag{2.21}$$

Finally, substituting Eqs. (2.20) and (2.21) into (2.19) and further simplifications lead to

$$\frac{1}{\sin\theta}\frac{\partial P_{n|m|}}{\partial\theta}=\frac{1}{4}\left\{\frac{\left(n+|m|\right)\left(n-|m|+1\right)\left(n+|m|-1\right)\left(n+|m|-2\right)}{|m|-1}P_{n-1,|m|-2}+\right.$$
$$\left.+\left[\frac{\left(n+|m|\right)\left(n-|m|+1\right)}{|m|-1}-\frac{\left(n+|m|+1\right)\left(n+|m|\right)}{|m|+1}\right]P_{n-1,|m|}-\frac{1}{|m|+1}P_{n-1,|m|+2}\right\}. \tag{2.22}$$

Further, after normalization based on Eq. (2.10) and simplifications, the proposition is derived.

Proposition 2.7 is the forward mode of the formula.

Proposition 2.7:

$$\frac{m}{\sin\theta}\frac{\partial\bar{P}_{n|m|}}{\partial\theta}=e'^{1}_{nm}\bar{P}_{n+1,|m|-2}+e'^{2}_{nm}\bar{P}_{n+1,|m|}+e'^{3}_{nm}\bar{P}_{n+1,|m|+2},\ |m|\neq 1,$$

where

$$e'^{1}_{nm}=\frac{m}{4\left(|m|-1\right)}\sqrt{\frac{\left(2-\delta_{|m|0}\right)\left(2n+1\right)}{\left(2-\delta_{|m|-2,0}\right)\left(2n+3\right)}}\sqrt{n+|m|}\sqrt{n-|m|+1}\sqrt{n-|m|+2}\sqrt{n-|m|+3}$$

$$e'^{2}_{nm}=\frac{m}{4}\left[\frac{n-|m|}{|m|+1}-\frac{n+|m|}{|m|-1}\right]\sqrt{\frac{2n+1}{2n+3}}\sqrt{n-|m|+1}\sqrt{n+|m|+1}$$

$$e'^{3}_{nm}=-\frac{m}{4\left(|m|+1\right)}\sqrt{\frac{\left(2-\delta_{|m|0}\right)\left(2n+1\right)}{\left(2-\delta_{|m|+2,0}\right)\left(2n+3\right)}}\sqrt{n-|m|}\sqrt{n+|m|+1}\sqrt{n+|m|+2}\sqrt{n+|m|+3}.$$

Proof. By considering Eq. (2.19) and Lemma 2.3, we can write

$$\frac{P_{n,|m|-1}}{\sin\theta}=\frac{1}{2\left(|m|-1\right)}\left[\left(n-|m|+2\right)\left(n-|m|+3\right)P_{n+1,|m|-2}+P_{n+1,|m|}\right], \tag{2.23}$$

$$\frac{P_{n,|m|+1}}{\sin\theta}=\frac{1}{2\left(|m|+1\right)}\left[\left(n-|m|\right)\left(n-|m|+1\right)P_{n+1,|m|}+P_{n+1,|m|+2}\right]. \tag{2.24}$$

Finally, substitution of Eqs. (2.23) and (2.24) into (2.19) and further simplifications lead to

$$\frac{1}{\sin\theta}\frac{\partial P_{n,|m|}}{\partial\theta}=\frac{1}{4}\left\{\frac{\left(n+|m|\right)\left(n-|m|+1\right)\left(n-|m|+2\right)\left(n+|m|+3\right)}{|m|-1}P_{n+1,|m|-2}+\right.$$
$$\left.+\left(\frac{n-|m|}{|m|+1}-\frac{n+|m|}{|m|-1}\right)\left(n-|m|+1\right)P_{n+1,|m|}-\frac{1}{|m|+1}P_{n+1,|m|+2}\right\}, \qquad (2.25)$$

further after normalization and simplifications Proposition 2.7 is derived.

2.3.2 New expressions for gravitational vector and tensor in a geocentric frame

In the previous section we simplified some relations by considering the presented propositions and Eqs. (2.7a)-(2.7c) we have (Eshagh 2008):

$$T_r\left(P\right)=-\frac{GM}{R^2}\sum_{n=2}^{N_{\max}}\sum_{m=-n}^{n}\left(n+1\right)\left(\frac{R}{r}\right)^{n+2}t_{nm}Q_m\left(\lambda\right)\overline{P}_{n|m|}, \qquad (2.26a)$$

$$T_\theta\left(P\right)=\frac{GM}{R^2}\sum_{n=2}^{N_{\max}}\sum_{m=-n}^{n}\left(\frac{R}{r}\right)^{n+2}t_{nm}Q_m\left(\lambda\right)\left\{a_{nm}^1\overline{P}_{n,|m|-1}+a_{nm}^2\overline{P}_{n,|m|+1}\right\}, \qquad (2.26b)$$

$$T_\lambda\left(P\right)=\frac{GM}{R^2}\sum_{n=2}^{N_{\max}}\sum_{m=-n}^{n}\left(\frac{R}{r}\right)^{n+2}t_{nm}Q_{-m}\left(\lambda\right)\left\{c_{nm}^1\overline{P}_{n-1,|m|-1}+c_{nm}^2\overline{P}_{n-1,|m|+1}\right\}, \qquad (2.26c)$$

and

$$T_\lambda\left(P\right)=\frac{GM}{R^2}\sum_{n=2}^{N_{\max}}\sum_{m=-n}^{n}\left(\frac{R}{r}\right)^{n+2}t_{nm}Q_{-m}\left(\lambda\right)\left\{c_{nm}'^1\overline{P}_{n+1,|m|-1}+c_{nm}'^2\overline{P}_{n+1,|m|+1}\right\}. \qquad (2.26d)$$

According to Propositions 2.4-2.7 and Eqs.(2.9a)-(2.9f) we can present new relations for the gravitational tensor as follows (Eshagh 2008):

$$T_{rr}\left(P\right)=\frac{GM}{R^3}\sum_{n=2}^{N_{\max}}\sum_{m=-n}^{n}\left(n+1\right)\left(n+2\right)\left(\frac{R}{r}\right)^{n+3}t_{nm}Q_m\left(\lambda\right)\overline{P}_{n|m|}, \qquad (2.27a)$$

$$T_{\theta\theta}\left(P\right)=\frac{GM}{R^3}\sum_{n=2}^{N_{\max}}\sum_{m=-n}^{n}\left(\frac{R}{r}\right)^{n+3}t_{nm}Q_m\left(\lambda\right)\left\{b_{nm}^1\overline{P}_{n,|m|-2}+b_{nm}^2\overline{P}_{n|m|}+b_{nm}^3\overline{P}_{n,|m|+2}\right\}, \qquad (2.27b)$$

$$T_{\lambda\lambda}\left(P\right)=\frac{GM}{R^3}\sum_{n=2}^{N_{\max}}\sum_{\substack{m=-n\\|m|\neq1}}^{n}\left(\frac{R}{r}\right)^{n+3}t_{nm}Q_m\left(\lambda\right)\left\{d_{nm}^1\overline{P}_{n,|m|-2}+d_{nm}^2\overline{P}_{n|m|}+d_{nm}^3\overline{P}_{n,|m|+2}\right\}, \qquad (2.27c)$$

$$T_{r\theta}\left(P\right)=-\frac{GM}{R^3}\sum_{n=2}^{N_{\max}}\sum_{m=-n}^{n}\left(n+1\right)\left(\frac{R}{r}\right)^{n+3}t_{nm}Q_m\left(\lambda\right)\left\{a_{nm}^1\overline{P}_{n,|m|-1}+a_{nm}^2\overline{P}_{n,|m|+1}\right\}, \qquad (2.27d)$$

$$T_{r\lambda}(P)=-\frac{GM}{R^3}\sum_{n=2}^{N_{\max}}\sum_{m=-n}^{n}(n+1)\left(\frac{R}{r}\right)^{n+3}t_{nm}Q_{-m}(\lambda)\left\{c_{nm}^{1}\bar{P}_{n-1,|m|-1}+c_{nm}^{2}\bar{P}_{n-1,|m|+1}\right\}, \quad (2.27e)$$

$$T_{r\lambda}(P)=-\frac{GM}{R^3}\sum_{n=2}^{N_{\max}}\sum_{m=-n}^{n}(n+1)\left(\frac{R}{r}\right)^{n+3}t_{nm}Q_{-m}(\lambda)\left\{c_{nm}'^{1}\bar{P}_{n+1,|m|-1}+c_{nm}'^{2}\bar{P}_{n+1,|m|+1}\right\}, \quad (2.27f)$$

$$T_{\theta\lambda}(P)=\frac{GM}{R^3}\sum_{n=2}^{N_{\max}}\sum_{\substack{m=-n\\|m|\neq 1}}^{n}\left(\frac{R}{r}\right)^{n+3}t_{nm}Q_{-m}(\lambda)\left\{e_{nm}^{1}\bar{P}_{n-1,|m|-2}+e_{nm}^{2}\bar{P}_{n-1,|m|}+e_{nm}^{3}\bar{P}_{n-1,|m|+2}\right\}, \quad (2.27g)$$

$$T_{\theta\lambda}(P)=\frac{GM}{R^3}\sum_{n=2}^{N_{\max}}\sum_{\substack{m=-n\\|m|\neq 1}}^{n}\left(\frac{R}{r}\right)^{n+3}t_{nm}Q_{-m}(\lambda)\left\{e_{nm}'^{1}\bar{P}_{n+1,|m|-2}+e_{nm}'^{2}\bar{P}_{n+1,|m|}+e_{nm}'^{3}\bar{P}_{n+1,|m|+2}\right\}. \quad (2.27h)$$

These expressions do not contain the singular terms at the poles, and all relations are summed up in terms of the adjacent ALFs. All the constant coefficients of the ALFs in the relations can be computed once for all computations. Another advantage of the above relations is that we just have to compute the ALFs and not its derivatives, but it should be computed to two additional degrees and orders.

The expressions of $T_{\lambda\lambda}(P)$ and $T_{\theta\lambda}(P)$ do not include the order 1 because the coefficients of the ALFs in these expressions are singular if $|m|=1$. One may interpret this matter as transferring the singularity from the space domain to the spectral domain at the poles. For solving this problem, it is recommended to use the traditional expression for $|m|=1$. In this case, we can easily show that $1/\sin^2\theta$ and $1/\sin\theta$ do not make singularity at the poles as

$$\lim_{\theta\to 0^\circ,180^\circ}\frac{P_{n1}(\cos\theta)}{\sin^2\theta}=0\ , \quad (2.28)$$

and

$$\lim_{\theta\to 0^\circ,180^\circ}\frac{\partial P_{n1}(\cos\theta)/\partial\theta}{\sin\theta}=0\ , \quad (2.29)$$

yielding no contribution from terms with $|m|=1$. Figure 2.1 shows the gravitational gradients, which were generated at 250 km level in the geocentric frame. The EGM96 geopotential model (Lemoine et al. 1998) was used to generate the gradients to degree and order 360 with $0.5^\circ\times 0.5^\circ$ resolution and using the fully-vectorized method; see Eshagh (2009a). Figure 2.1 illustrates that T_{rr} is the largest gradient compared with the others, and $T_{\theta\lambda}$ is the smallest. Their statistics are presented in Table 2.1.

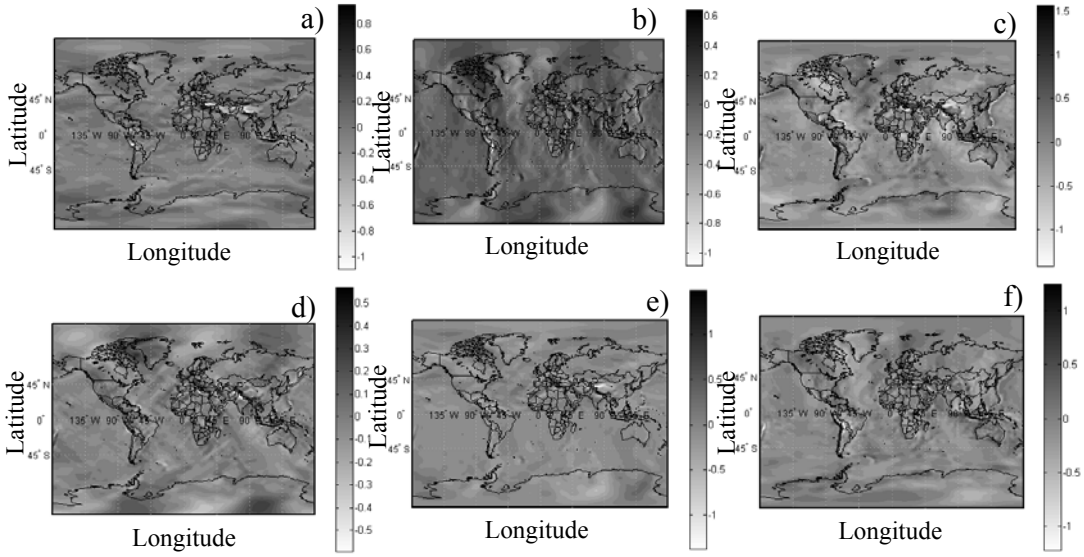

Figure 2.1. Gravitational gradients in geocentric frame. (a) $T_{\theta\theta}$, (b) $T_{\lambda\lambda}$, (c) T_{rr}, (d) $T_{\theta\lambda}$, (e) $T_{r\theta}$ and (f) $T_{r\lambda}$. Unit: 1 E

2.4 Gravitational gradients in LNOF

The LNOF is defined as the frame whose *z*-axis is pointing upwards in the geocentric radial direction, the *x*-axis towards the north (see Figure 2.2) and the *y*-axis is directed to the west to complete a right handed frame.

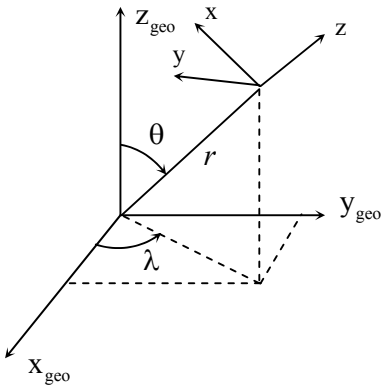

Figure 2.2. Geocentric frame (x_{geo}, y_{geo}, z_{geo}) and LNOF (*x*, *y*, *z*)

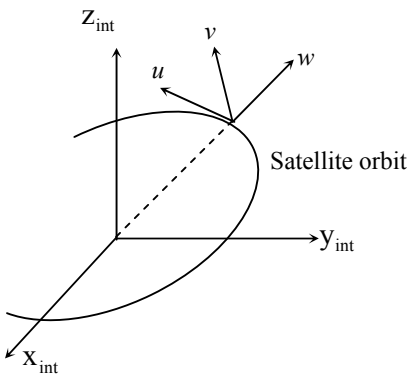

Figure 2.3. ORF (*u*, *v*, *w*) and inertial frame (x_{int}, y_{int}, z_{int})

The traditional expressions for the gravitational gradients in the LNOF are obtained by using the tensor product of the gradient operator as presented by Reed (1973):

$$T_{zz}(P) = \frac{\partial^2 T(P)}{\partial r^2}, \tag{2.30a}$$

$$T_{xx}\left(P\right)=\frac{\partial T\left(P\right)}{r\partial r}+\frac{\partial^2 T\left(P\right)}{r^2\partial\theta^2}, \tag{2.30b}$$

$$T_{yy}\left(P\right)=\frac{\partial T\left(P\right)}{r\partial r}+\cot\theta\frac{\partial T\left(P\right)}{r^2\partial\theta}+\frac{\partial^2 T\left(P\right)}{r^2\sin^2\theta\partial\lambda^2}, \tag{2.30c}$$

$$T_{xy}\left(P\right)=\frac{\partial^2 T\left(P\right)}{r^2\sin\theta\partial\theta\partial\lambda}-\cot\theta\frac{\partial T\left(P\right)}{r^2\sin\theta\partial\lambda}, \tag{2.30d}$$

$$T_{xz}\left(P\right)=\frac{\partial T\left(P\right)}{r^2\partial\theta}-\frac{\partial^2 T\left(P\right)}{r\partial r\partial\theta}, \tag{2.30e}$$

and

$$T_{yz}\left(P\right)=\frac{\partial T\left(P\right)}{r^2\sin\theta\partial\lambda}-\frac{\partial^2 T\left(P\right)}{r\sin\theta\partial r\partial\lambda}. \tag{2.30f}$$

Based on these formulas Petrovskaya and Vershkov (2006, Eqs. 4-9) presented the following relations after some simplifications:

$$T_{zz}(P)=\frac{GM}{R^3}\sum_{n=2}^{N_{\max}}\left(n+1\right)\left(n+2\right)\left(\frac{R}{r}\right)^{n+3}\sum_{m=-n}^{n}t_{nm}Q_m\left(\lambda\right)\overline{P}_{n|m|}, \tag{2.31a}$$

$$T_{xx}(P)=\frac{GM}{R^3}\sum_{n=2}^{N_{\max}}\left(\frac{R}{r}\right)^{n+3}\sum_{m=-n}^{n}t_{nm}Q_m\left(\lambda\right)\left[-\left(n+1\right)\overline{P}_{n|m|}+\frac{\partial^2\overline{P}_{n|m|}}{\partial\theta^2}\right], \tag{2.31b}$$

$$T_{yy}(P)=\frac{GM}{R^3}\sum_{n=2}^{N_{\max}}\left(\frac{R}{r}\right)^{n+3}\sum_{m=-n}^{n}t_{nm}Q_m\left(\lambda\right)\left[-\left(n+1\right)\overline{P}_{n|m|}+\cot\theta\frac{\partial\overline{P}_{n|m|}}{\partial\theta}+\frac{m^2}{\sin^2\theta}\overline{P}_{n|m|}\right], \tag{2.31c}$$

$$T_{xy}(P)=\frac{GM}{R^3}\sum_{n=2}^{N_{\max}}\left(\frac{R}{r}\right)^{n+3}\sum_{m=-n}^{n}mt_{nm}Q_{-m}\left(\lambda\right)\left[\frac{1}{\sin\theta}\frac{\partial\overline{P}_{n|m|}}{\partial\theta}-\frac{\cos\theta}{\sin^2\theta}\overline{P}_{n|m|}\right], \tag{2.31d}$$

$$T_{xz}(P)=\frac{GM}{R^3}\sum_{n=2}^{N_{\max}}\left(n+2\right)\left(\frac{R}{r}\right)^{n+3}\sum_{m=-n}^{n}t_{nm}Q_m\left(\lambda\right)\frac{\partial\overline{P}_{n|m|}}{\partial\theta}, \tag{2.31e}$$

and

$$T_{yz}(P)=\frac{GM}{R^3}\sum_{n=2}^{N_{\max}}\left(n+2\right)\left(\frac{R}{r}\right)^{n+3}\sum_{m=-n}^{n}mt_{nm}Q_{-m}\left(\lambda\right)\frac{\overline{P}_{n|m|}}{\sin\theta}. \tag{2.31f}$$

These expressions include also the terms $1/\sin\theta$ and $1/\sin^2\theta$ which are singular at the poles. They include combinations of ALFs and/or their first- and second-order derivatives. In the following section we further simplify these formulas. It should be mentioned that our derivations differ in simplifications and normalization with those presented by Petrovskaya and Vershkov (2006).

2.4.1 Alternative expressions for gravitational gradients in the LNOF

Equation (2.31a), which is the second-order radial derivative of the potential, does not need to be simplified. Therefore we start our mathematical derivations with Eq.

(2.31c), which is related to $T_{yy}\left(P\right)$. Let us first consider the following lemma, which is useful through the derivations.

Lemma 2.4 (Ilk 1983, p. 114):

$$\sin\theta\cos\theta\frac{\partial P_{n|m|}}{\partial\theta}=|m|P_{n|m|}+(n+1)\sin^2\theta P_{n|m|}-\sin\theta P_{n+1,|m|+1}\ .$$

It should be mentioned that the lemma is also valid for the non-normalized ALFs. Now we start simplification of Eq. (2.31c) by the following proposition.

Proposition 2.8:

$$-(n+1)\bar{P}_{n|m|}+\cot\theta\frac{\partial\bar{P}_{n|m|}}{\partial\theta}-\frac{m^2}{\sin^2\theta}\bar{P}_{n|m|}=f_{nm}^{1}\bar{P}_{n,|m|-2}+f_{nm}^{2}\bar{P}_{n|m|}+f_{nm}^{3}\bar{P}_{n,|m|+2},$$

where

$$f_{nm}^{1}=\frac{1}{4}\sqrt{\frac{2-\delta_{|m|0}}{2-\delta_{|m|-2,0}}}\sqrt{n+|m|}\sqrt{n-|m|+1}\sqrt{n-|m|+2}\sqrt{n+|m|-1}\ ,$$

$$f_{nm}^{2}=\frac{1}{4}\left[(n+|m|)(n+|m|-1)+\frac{|m|-1}{|m|+1}(n-|m|)(n-|m|-1)+\frac{2(n+|m|+1)(n+|m|+2)}{|m|+1}\right]$$

$$f_{nm}^{3}=\frac{1}{4}\sqrt{\frac{2-\delta_{|m|0}}{2-\delta_{|m|+2,0}}}\sqrt{n-|m|}\sqrt{n-|m|-1}\sqrt{n+|m|+2}\sqrt{n+|m|+1}\ .$$

Proof. According to Petrovskaya and Vershkov (2006, Eq. 21, p. 120) and Lemma 2.4 the left hand side of the proposition can be written

$$-(n+1)P_{n|m|}+\cot\theta\frac{\partial P_{n|m|}}{\partial\theta}-\frac{m^2}{\sin^2\theta}P_{n|m|}=\left[|m|(|m|-1)\frac{P_{n|m|}}{\sin^2\theta}+\frac{P_{n+1,|m|+1}}{\sin\theta}\right]\ . \quad (2.32)$$

According to Lemma 2.2 we obtain

$$\frac{P_{n+1,|m|+1}}{\sin\theta}=\frac{1}{2(|m|+1)}\left[(n+|m|+2)(n+|m|+1)P_{n|m|}+P_{n,|m|+2}\right]\ . \quad (2.33)$$

Substituting Eqs. (2.33) and Proposition 2.4 divided by m^2 into the right hand-side of Eq. (2.32), and after a long simplification and normalization of the results (based Eq. 2.10), the proposition is proved.

Equation (2.31d) can also be simplified in two different ways. We can derive a linear combination of the adjacent ALFs and the backward and forward mode with respect to degree *n*. Proposition 2.9 simplifies the complicated part of Eq. (2.31d) in backward mode in degree.

Proposition 2.9:

$$m\left[\frac{1}{\sin\theta}\frac{\partial \bar{P}_{n|m|}}{\partial\theta}-\frac{\cos\theta}{\sin^2\theta}\bar{P}_{n|m|}\right]=g^1_{nm}\bar{P}_{n-1,|m|-2}+g^2_{nm}\bar{P}_{n-1,|m|}+g^3_{nm}\bar{P}_{n-1,|m|+2},\ |m|\neq 0,$$

where

$$g^1_{nm}=\frac{m}{4|m|}\sqrt{\frac{\left(2-\delta_{|m|0}\right)(2n+1)}{\left(2-\delta_{|m|-2,0}\right)(2n-1)}}\sqrt{n+|m|}\sqrt{n+|m|-1}\sqrt{n+|m|-2}\sqrt{n-|m|+1},$$

$$g^2_{nm}=\frac{m}{2}\sqrt{n+|m|}\sqrt{n-|m|}\sqrt{\frac{2n+1}{2n-1}},$$

$$g^3_{nm}=\frac{m}{4|m|}\sqrt{\frac{\left(2-\delta_{|m|0}\right)(2n+1)}{\left(2-\delta_{|m|+2,0}\right)(2n-1)}}\sqrt{n-|m|}\sqrt{n-|m|-1}\sqrt{n-|m|-2}\sqrt{n+|m|+1}.$$

Proof. According to Petrovskaya and Vershkov (2006, Eq. 31, p. 121) we can write

$$\frac{1}{\sin\theta}\frac{\partial P_{n|m|}}{\partial\theta}-\frac{\cos\theta}{\sin^2\theta}P_{n|m|}=\frac{1}{2|m|}\left[\left(|m|-1\right)\left(n+|m|\right)\left(n-|m|+1\right)\frac{P_{n,|m|-1}}{\sin\theta}-\left(|m|+1\right)\frac{P_{n,|m|+1}}{\sin\theta}\right] \tag{2.34}$$

and using Lemma 2.2 we obtain

$$\frac{P_{n,|m|-1}}{\sin\theta}=\frac{1}{2\left(|m|-1\right)}\left[\left(n+|m|-1\right)\left(n+|m|-2\right)P_{n-1,|m|-2}+P_{n-1,|m|}\right], \tag{2.35}$$

$$\frac{P_{n,|m|+1}}{\sin\theta}=\frac{1}{2\left(|m|+1\right)}\left[\left(n+|m|+1\right)\left(n+|m|\right)P_{n-1,|m|}+P_{n-1,|m|+2}\right]. \tag{2.36}$$

Substituting Eqs. (2.35) and (2.36) into the right hand side of Eq. (2.34) and after simplification we derive

$$m\left[\frac{1}{\sin\theta}\frac{\partial P_{n|m|}}{\partial\theta}-\frac{\cos\theta}{\sin^2\theta}P_{n|m|}\right]=\frac{m}{4|m|}\left[\left(n+|m|\right)\left(n-|m|+1\right)\left(n+|m|-1\right)\left(n+|m|-2\right)\right.$$
$$\left.P_{n-1,|m|-2}-2|m|\left(n+|m|\right)P_{n-1,|m|}-P_{n-1,|m|+2}\right]. \tag{2.37}$$

After normalizing Eq. (2.37) (using Eq. 2.10) the proposition is proved.

Now the complicated part of Eq. (2.31d) is simplified forward in Proposition 2.10 we mean that the degree of the adjacent ALFs in right hand side is n+1.

Proposition 2.10:

$$m\left[\frac{1}{\sin\theta}\frac{\partial \bar{P}_{n|m|}}{\partial\theta}-\frac{\cos\theta}{\sin^2\theta}\bar{P}_{n|m|}\right]=g'^{1}_{nm}\bar{P}_{n+1,|m|-2}+g'^{2}_{nm}\bar{P}_{n+1,|m|}+g'^{3}_{nm}\bar{P}_{n+1,|m|+2},\ |m|\neq 0$$

where

$$g'^{1}_{nm}=\frac{m}{4|m|}\sqrt{\frac{\left(2-\delta_{|m|0}\right)(2n+1)}{\left(2-\delta_{|m|-2,0}\right)(2n-1)}}\sqrt{n+|m|}\sqrt{n+|m|-1}\sqrt{n+|m|-2}\sqrt{n-|m|+1},$$

$$g'^{2}_{nm}=\frac{m}{4|m|}\left[\left(n+|m|\right)\left(n-|m|+1\right)-\left(n-|m|\right)\left(n-|m|+1\right)\right]\sqrt{\frac{(2n+1)\left(n+|m|+1\right)}{(2n+3)\left(n-|m|+1\right)}},$$

$$g'^{3}_{nm}=-\frac{m}{4|m|}\sqrt{\frac{\left(2-\delta_{|m|0}\right)(2n+1)}{\left(2-\delta_{|m|+2,0}\right)(2n+3)}}\sqrt{n-|m|}\sqrt{n+|m|+1}\sqrt{n+|m|+2}\sqrt{n+|m|+3}.$$

Proof. Using Lemma 2.3 we obtain

$$m\left[\frac{1}{\sin\theta}\frac{\partial P_{n|m|}}{\partial\theta}-\frac{\cos\theta}{\sin^2\theta}P_{n|m|}\right]=\frac{m}{4|m|}\left[\left(n+|m|\right)\left(n-|m|+1\right)\left(n-|m|-2\right)\left(n-|m|+3\right)\right.$$
$$\left.P_{n+1,|m|-2}+\left[\left(n+|m|\right)\left(n-|m|+1\right)-\left(n-|m|\right)\left(n-|m|+1\right)\right]P_{n+1,|m|}-P_{n+1,|m|+2}\right].(2.38)$$

After normalizing Eq. (2.38) using Eq.(2.10) the proposition is proven.

Our mathematical derivations summarized in Propositions 2.8, 2.9 and 2.10. Next we start to present our alternative expressions using the propositions. First, let us start with Eq. (2.31b). This equation is involved with the second-order derivative of the fully-normalized ALFs were already simplified in Proposition 2.2. Using this proposition and Eq. (2.31b), which is the traditional expression for $T_{xx}\left(P\right)$, we can write

$$T_{xx}(P)=\frac{GM}{R^3}\sum_{n=2}^{N_{\max}}\left(\frac{R}{r}\right)^{n+3}\sum_{m=-n}^{n}t_{nm}Q_m\left(\lambda\right)\left\{b^{1}_{nm}\bar{P}_{n,|m|-2}+\left[b^{2}_{nm}-\left(n+1\right)\right]\bar{P}_{n|m|}+b^{3}_{nm}\bar{P}_{n,|m|+2}\right\} \tag{2.39a}$$

Also $T_{yy}\left(P\right)$, which was presented in Eq. (2.31c), can be simplified according to Proposition 2.6 as:

$$T_{yy}(P)=\frac{GM}{R^3}\sum_{n=2}^{N_{\max}}\left(\frac{R}{r}\right)^{n+3}\sum_{m=-n}^{n}t_{nm}Q_m\left(\lambda\right)\left\{f^{1}_{nm}\bar{P}_{n,|m|-2}+f^{2}_{nm}\bar{P}_{n|m|}+f^{3}_{nm}\bar{P}_{n,|m|+2}\right\} \tag{2.39b}$$

where f^{1}_{nm}, f^{2}_{nm} and f^{3}_{nm} were presented in the proposition. Alternatively, based on $T_{xx}\left(P\right)+T_{yy}\left(P\right)+T_{zz}\left(P\right)=0$ (Laplacian equation), we can also develop our expressions for $T_{xx}\left(P\right)$ and $T_{yy}\left(P\right)$:

$$T_{xx}(P)=-\frac{GM}{R^3}\sum_{n=2}^{N_{\max}}\left(\frac{R}{r}\right)^{n+3}\sum_{m=-n}^{n}t_{nm}Q_m(\lambda)\Big\{b_{nm}^1\bar{P}_{n,|m|-2}+ \\ +\Big[b_{nm}^2+(n+1)(n+2)\Big]\bar{P}_{n|m|}+b_{nm}^3\bar{P}_{n,|m|+2}\Big\}, \tag{2.39c}$$

and

$$T_{yy}(P)=-\frac{GM}{R^3}\sum_{n=2}^{N_{\max}}\left(\frac{R}{r}\right)^{n+3}\sum_{m=-n}^{n}t_{nm}Q_m(\lambda)\Big\{a_{nm}^1\bar{P}_{n,|m|-2}+ \\ +\Big[a_{nm}^2+(n+1)(n+2)\Big]\bar{P}_{n|m|}+a_{nm}^3\bar{P}_{n,|m|+2}\Big\}. \tag{2.39d}$$

The coefficients of the ALFs in Eqs. (2.39c) and (2.39d) are the same as those presented in Propositions 2.2 and 2.4. Two alternative similar expressions can also be presented for $T_{xy}(P)$:

$$T_{xy}(P)=\frac{GM}{R^3}\sum_{n=2}^{N_{\max}}\left(\frac{R}{r}\right)^{n+3}\sum_{m=-n}^{n}\bar{t}_{nm}Q_{-m}(\lambda)\Big\{g_{nm}^1\bar{P}_{n-1,|m|-2}+g_{nm}^2\bar{P}_{n-1,|m|}+g_{nm}^3\bar{P}_{n-1,|m|+2}\Big\} \tag{2.39e}$$

and

$$T_{xy}(P)=\frac{GM}{R^3}\sum_{n=2}^{N_{\max}}\left(\frac{R}{r}\right)^{n+3}\sum_{m=-n}^{n}t_{nm}Q_{-m}(\lambda)\Big\{g_{nm}'^1\bar{P}_{n+1,|m|-2}+g_{nm}'^2\bar{P}_{n+1,|m|}+g_{nm}'^3\bar{P}_{n+1,|m|+2}\Big\}, \tag{2.39f}$$

where g_{nm}^1, g_{nm}^2, g_{nm}^3, $g_{nm}'^1$, $g_{nm}'^2$ and $g_{nm}'^3$ have been presented in Propositions 2.9 and 2.10. Until now some alternative expressions were formulated which are the HH components of the gravitational tensor. Formulation of the VH components $T_{xz}(P)$ and $T_{yz}(P)$ is rather simple than those mentioned above. Let us start with $T_{xz}(P)$ in the following. Equation (2.59) which is related to $T_{xz}(P)$ is involved with the derivatives of the fully-normalized ALFs, which were simplified in Proposition 2.1. Considering this proposition and substituting it in Eq. (2.59) we have

$$T_{xz}(P)=\frac{GM}{R^3}\sum_{n=2}^{N_{\max}}\left(\frac{R}{r}\right)^{n+3}\sum_{m=-n}^{n}t_{nm}Q_m(\lambda)\Big[h_{nm}^1\bar{P}_{n,|m|-1}+h_{nm}^2\bar{P}_{n,|m|+1}\Big], \tag{2.39g}$$

where $h_{nm}^1=(n+2)a_{nm}^1/2$ and $h_{nm}^2=-(n+2)a_{nm}^2/2$. Two alternative expressions can be formulated for $T_{yz}(P)$:

$$T_{yz}(P)=\frac{GM}{R^3}\sum_{n=2}^{N_{\max}}\left(\frac{R}{r}\right)^{n+3}\sum_{m=-n}^{n}t_{nm}Q_{-m}(\lambda)\Big[k_{nm}^1\bar{P}_{n-1,|m|-1}+k_{nm}^2\bar{P}_{n-1,|m|+1}\Big], \tag{2.39h}$$

where $k_{nm}^1=(n+2)c_{nm}^1/2$, $k_{nm}^2=(n+2)c_{nm}^2/2$ and

$$T_{yz}(P)=\frac{GM}{R^3}\sum_{n=2}^{N_{\max}}\left(\frac{R}{r}\right)^{n+3}\sum_{m=-n}^{n}t_{nm}Q_{-m}(\lambda)\Big[k_{nm}'^1\bar{P}_{n+1,|m|-1}+k_{nm}'^2\bar{P}_{n+1,|m|+1}\Big] \tag{2.39i}$$

where $k'^{1}_{nm} = (n+2)c'^{1}_{nm}/2$ and $k'^{2}_{nm} = (n+2)c'^{2}_{nm}/2$. The coefficients c^{1}_{nm}, c^{2}_{nm}, c'^{1}_{nm} and c'^{2}_{nm} are derived in Propositions 2.3 and 2.4.

Petrovskaya and Vershkov (2006) also presented similar expressions for the gradients in LNOF. They considered the zero- and first-order of the expansions separately. However, in our derivation we did not use their method and we found a more general form for the coefficients of the adjacent ALFs. According to our comparisons, the derived coefficients will lead to the same values of the coefficients and one can compute the zero- and first-orders coefficients without any separation. This is due to our different way of simplification and normalization. Two expressions for $T_{xx}(P)$, $T_{yy}(P)$, $T_{xy}(P)$ and $T_{yz}(P)$ were presented here, and they are capable of synthesizing the gravitational gradients without neither computing the first- or second-order derivatives of the ALFs nor singularity at poles. The formulas may be used for filling-in the gaps of the Polar Regions due to inclined GOCE orbit, so that the quadrature formulas and TSHs, which are globally orthogonal, can be employed to generate the geopotential coefficients. Figure 1 shows globally synthesized gravitational gradients in the LNOF based on our alternative formulas. Again, EGM96 is used to degree and order 360 to generate the gradients with $0.5^{\circ} \times 0.5^{\circ}$ resolution at 250 km. A semi-vectorization algorithm was used to speed up the computations; see Eshagh and Abdollahzadeh (2009a).

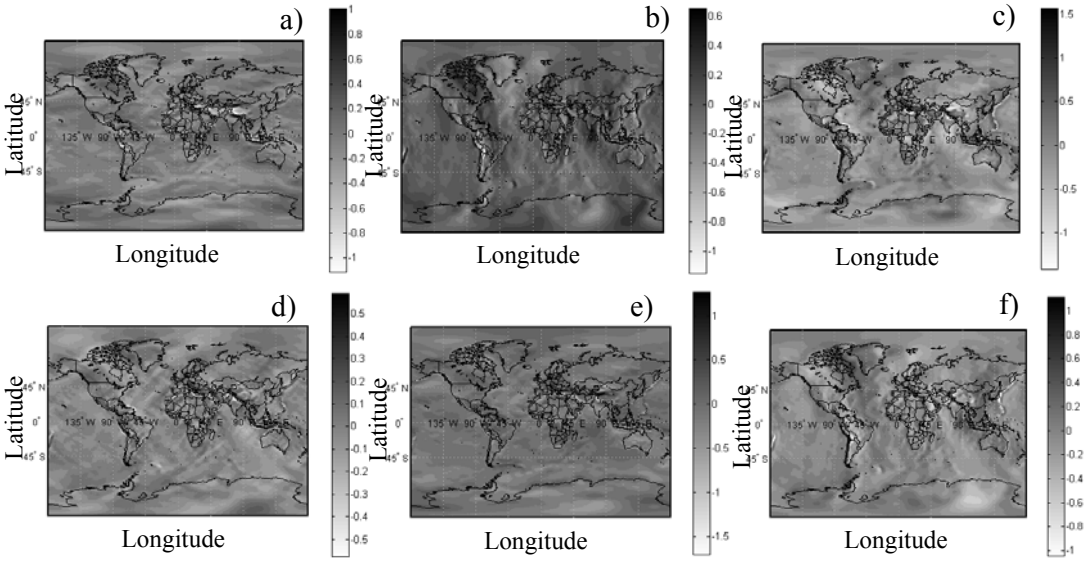

Figure 2.4. Gravitational gradients in LNOF. (a) T_{xx}, (b) T_{yy}, (c) T_{zz}, (d) T_{xy}, (e) T_{xz} and (f) T_{yz}. Unit: 1 E

As expected, T_{rr} is the same as T_{zz} as the *r*- and *z*-axis are common axis of the geocentric and LNOF. This gradient is also the largest gradient, and T_{xy} is the smallest. The statistics of the gradients of disturbing potential in the geocentric frame and the LNOF are presented in Tables 2.1 and 2.2.

Table 2.1. Statistics of second-order gradients of disturbing potential in geocentric frame. Unit: 1 E

	min	mean	max	std
$T_{\theta\theta}$	-1.12	0.00	1.10	± 0.12
$T_{\lambda\lambda}$	-0.11	0.00	0.74	± 0.13
T_{rr}	-1.44	0.00	1.76	± 0.24
$T_{\theta\lambda}$	-0.61	0.00	-0.65	± 0.09
$T_{r\theta}$	-1.42	0.00	1.70	± 0.13
$T_{r\lambda}$	-1.26	0.00	1.39	± 0.16

Table 2.2. Statistics of second-order gradients of disturbing potential in LNOF. Unit: 1 E

	min	mean	max	std
T_{xx}	-1.12	0.00	1.15	± 0.14
T_{yy}	-1.16	0.00	0.76	± 0.14
T_{zz}	-1.44	0.00	1.76	± 0.24
T_{xy}	-0.59	0.00	0.66	± 0.07
T_{xz}	-1.76	-0.01	1.45	± 0.16
T_{yz}	-1.07	0.00	1.25	± 0.16

As a comparison we can say that the gradients are more or less at the same level. Both tables show larger standard deviations for the gradients in the LNOF (except for the second order-radial derivatives, which are exactly the same). The differences are in the 1 cE level, but they are significant.

2.5 Gravitational gradients in ORF

The ORF is a special local frame which is not north-oriented. We consider the frame $\{u, v, w\}$, where the w-axis coincides with z-axis of the LNOF, v-axis points towards the instantaneous angular momentum vector and u-axis complements the right-hand triad as shown in Figure 2.3. The subscripts of int for x-, y- and z-axes stand for inertial frame. The ORF differs from LNOF by a simple rotation around their common axis. The transformation between the LNOF and ORF is (Petrovskaya and Vershkov 2006):

$$\begin{bmatrix} u \\ v \\ w \end{bmatrix} = \begin{bmatrix} \cos\alpha & \sin\alpha & 0 \\ -\sin\alpha & \cos\alpha & 0 \\ 0 & 0 & 1 \end{bmatrix} \begin{bmatrix} x \\ y \\ z \end{bmatrix} = \mathbf{R}_3(\alpha) \begin{bmatrix} x \\ y \\ z \end{bmatrix} \tag{2.40}$$

where α is the satellite track azimuth (i.e. the angle between the local meridian and direction of u-axis at the observation point). Based on the above transformation, it is easy to transform the gravitational tensor from the LNOF $\mathbf{T}_{xyz}(P)$ to the ORF $\mathbf{T}_{uvw}(P)$ using the following transformation:

$$\mathbf{T}_{uvw}(P,\alpha) = \mathbf{R}_3(\alpha)\mathbf{T}_{xyz}(P)\mathbf{R}_3^T(\alpha), \tag{2.41}$$

and therefore the entries of the gravitational tensor in the ORF will be:

$$T_{uu}(P,\alpha) = -\left(\cos^2\alpha - \sin^2\alpha\right)T_{yy}(P) - \cos^2\alpha T_{zz}(P) + 2\cos\alpha\sin\alpha T_{xy}(P), \tag{2.42a}$$

$$T_{vv}(P,\alpha) = \left(\cos^2\alpha - \sin^2\alpha\right)T_{yy}(P) - \sin^2\alpha T_{zz}(P) - 2\cos\alpha\sin\alpha T_{xy}(P), \tag{2.42b}$$

$$T_{uv}(P,\alpha) = 2\cos\alpha\sin\alpha T_{yy}(P) + \cos\alpha\sin\alpha T_{zz}(P) + \left(\cos^2\alpha - \sin^2\alpha\right)T_{xy}(P), \tag{2.42c}$$

$$T_{uw}\left(P,\alpha\right)=\cos\alpha T_{xz}\left(P\right)+\sin\alpha T_{yz}\left(P\right), \tag{2.42d}$$

$$T_{vw}\left(P,\alpha\right)=-\sin\alpha T_{xz}\left(P\right)+\cos\alpha T_{yz}\left(P\right), \tag{2.42e}$$

and

$$T_{ww}\left(P\right)=T_{zz}\left(P\right). \tag{2.42f}$$

In a similar way one can also obtain the reverse transformation by:

$$\mathbf{T}_{xyz}\left(P,\alpha\right)=\mathbf{R}_3^T\left(\alpha\right)\mathbf{T}_{uvw}\left(P\right)\mathbf{R}_3\left(\alpha\right). \tag{2.43}$$

The relation between the gradients in the LNOF and ORF can also be written according to Eq. (2.43):

$$T_{xx}\left(P,\alpha\right)=\cos^2\alpha T_{uu}\left(P\right)+\sin^2\alpha T_{vv}\left(P\right)-2\cos\alpha\sin\alpha T_{uv}\left(P\right), \tag{2.44a}$$

$$T_{yy}\left(P,\alpha\right)=\sin^2\alpha T_{uu}\left(P\right)+\cos^2\alpha T_{vv}\left(P\right)+2\cos\alpha\sin\alpha T_{uv}\left(P\right), \tag{2.44b}$$

$$T_{xy}\left(P,\alpha\right)=\cos\alpha\sin\alpha\left[T_{uu}\left(P\right)-T_{vv}\left(P\right)\right]+\left(\cos^2\alpha-\sin^2\alpha\right)T_{uv}\left(P\right), \tag{2.44c}$$

$$T_{xz}\left(P,\alpha\right)=\cos\alpha T_{uw}\left(P\right)-\sin\alpha T_{vw}\left(P\right), \tag{2.44d}$$

$$T_{yz}\left(P,\alpha\right)=\sin\alpha T_{uw}\left(P\right)+\cos\alpha T_{vw}\left(P\right), \tag{2.44e}$$

and

$$T_{ww}\left(P\right)=T_{zz}\left(P\right). \tag{2.44f}$$

We have already presented the traditional and alternative expressions for the gravitational gradients in the LNOF as well as the relation between the LNOF and the ORF. Consequently, if we put the traditional expressions of the gradients in the NLOF into Eqs. (2.44a)-(2.44f) we will obtain the expression of the gradients in ORF; and if we put the our expression into these equations we will obtain the corresponding alternative one. In the following we present our alternative expressions for the gradients in the ORF (Petrovskaya and Vershkov 2006):

$$T_{uu}\left(P,\alpha\right)=\frac{GM}{R^3}\sum_{n=2}^{N_{\max}}\sum_{m=-n}^{n}\left(\frac{R}{r}\right)^{n+3}t_{nm}\left\{Q_m\left(\lambda\right)\left[\cos 2\alpha f_{nm1}-\cos^2\alpha\left(n+1\right)\left(n+2\right)\bar{P}_{n|m|}\right]+\right.$$
$$\left.+Q_{-m}\left(\lambda\right)\sin 2\alpha f_{nm2}\right\}, \tag{2.45a}$$

$$T_{vv}\left(P,\alpha\right)=-\frac{GM}{R^3}\sum_{n=2}^{N_{\max}}\sum_{m=-n}^{n}\left(\frac{R}{r}\right)^{n+3}t_{nm}\left\{Q_m\left(\lambda\right)\left[\cos 2\alpha f_{nm1}+\sin^2\alpha\left(n+1\right)\left(n+2\right)\bar{P}_{n|m|}\right]+\right.$$
$$\left.+Q_{-m}\left(\lambda\right)\sin 2\alpha f_{nm2}\right\}, \tag{2.45b}$$

$$T_{uv}\left(P,\alpha\right)=-\frac{GM}{R^3}\sum_{n=2}^{N_{\max}}\sum_{m=-n}^{n}\left(\frac{R}{r}\right)^{n+3}t_{nm}\left\{Q_m\left(\lambda\right)\left[\sin 2\alpha f_{nm1}-\cos\alpha\sin\alpha\right.\right.$$
$$\left.\left.\left(n+1\right)\left(n+2\right)\bar{P}_{n|m|}-Q_{-m}\left(\lambda\right)\cos 2\alpha f_{nm2}\right\}, \tag{2.45c}$$

$$T_{uw}\left(P,\alpha\right)=\frac{GM}{R^3}\sum_{n=2}^{N_{\max}}\sum_{m=-n}^{n}\left(\frac{R}{r}\right)^{n+3}t_{nm}\left[Q_m\left(\lambda\right)\cos\alpha f_{nm3}+Q_{-m}\left(\lambda\right)\sin\alpha f_{nm4}\right], \quad (2.45d)$$

$$T_{vw}\left(P,\alpha\right)=-\frac{GM}{R^3}\sum_{n=2}^{N_{\max}}\sum_{m=-n}^{n}\left(\frac{R}{r}\right)^{n+3}t_{nm}\left[Q_m\left(\lambda\right)\sin\alpha f_{nm3}-Q_{-m}\left(\lambda\right)\cos\alpha f_{nm4}\right], \quad (2.45e)$$

and

$$T_{ww}\left(P,\alpha\right)=\frac{GM}{R^3}\sum_{n=2}^{N_{\max}}\sum_{m=-n}^{n}\left(n+1\right)\left(n+2\right)\left(\frac{R}{r}\right)^{n+3}t_{nm}Q_m\left(\lambda\right)\bar{P}_{n|m|}, \quad (2.45f)$$

where

$$f_{nm1}\left(\theta\right)=b^1_{nm}\bar{P}_{n,|m|-2}+b^2_{nm}\bar{P}_{n|m|}+b^3_{nm}\bar{P}_{n,|m|+2}, \quad (2.46a)$$

$$f_{nm2}\left(\theta\right)=g^1_{nm}\bar{P}_{n-1,|m|-2}+g^2_{nm}\bar{P}_{n-1,|m|}+g^3_{nm}\bar{P}_{n-1,|m|+2}, \quad (2.46b)$$

$$f_{nm3}\left(\theta\right)=h^1_{nm}\bar{P}_{n,|m|-1}+h^2_{nm}\bar{P}_{n,|m|+1}, \quad (2.46c)$$

and

$$f_{nm4}\left(\theta\right)=k^1_{nm}\bar{P}_{n-1,|m|-1}+k^2_{nm}\bar{P}_{n-1,|m|+1}. \quad (2.46d)$$

The above formulas are valid when the satellite track azimuth is given. The azimuth, in the simplest case, is a function of inclination of orbit and the co-latitude of the observation point. Vermeer (1990) presented the following formula for the azimuth:

$$\sin\alpha=\cos I/\sin\theta, \quad (2.47)$$

where I stands for the orbit inclination and θ is the co-latitude of the observation point at satellite level. However, we know that co-latitude and satellite inclination are not constant during satellite revolutions because of existence of perturbing forces. The geopotential force is the largest gravitational perturbing force. In the following we express the differential equation of a satellite in the presence of the Earth gravitational force which can numerically be integrated to estimate the satellite position.

2.5.1 Equations of motion of a satellite

As we mentioned in the beginning of this chapter, a truncated spherical harmonic series is used to approximate the Earth gravitational field. We presented this series in Eq. (2.1) for the disturbing potential. The same relation can be used for the geopotential by replacing the disturbing potential (T) with the geopotential (W) and also the SHCs of the disturbing potential t_{nm} to the geopotential w_{nm}. The second-order derivative of the geopotential with respect to time is the satellite acceleration vector in a geocentric inertial frame:

$$\ddot{x}\left(P\right)=W_x\left(P\right)=W_r\left(P\right)r_x+W_\theta\left(P\right)\theta_x+W_\lambda\left(P\right)\lambda_x, \quad (2.48a)$$

$$\ddot{y}\left(P\right)=W_y\left(P\right)=W_r\left(P\right)r_y+W_\theta\left(P\right)\theta_y+W_\lambda\left(P\right)\lambda_y, \quad (2.48b)$$

$$\ddot{z}\left(P\right)=W_z\left(P\right)=W_r\left(P\right)r_z+W_\theta\left(P\right)\theta_z+W_\lambda\left(P\right)\lambda_z, \quad (2.48c)$$

where $\ddot{x}$, $\ddot{y}$ and $\ddot{z}$ are the satellite accelerations in x-, y- and z-direction of an inertial frame, respectively. $W_r(P)$, $W_\lambda(P)$ and $W_\theta(P)$ are the partial derivatives of the spherical harmonic expansion of gravitational field with respect to the geocentric distance, longitude and co-latitude. r_i, θ_i, λ_i, $i = x, y$ and z are the partial derivatives of the spherical coordinates with respect to Cartesian ones. The relations among these triple parameters r, λ, θ and the Cartesian inertial coordinates of x, y, and z are:

$$r = \sqrt{x^2 + y^2 + z^2}\,, \tag{2.49a}$$

$$\theta = \pi/2 - arc\sin(z/r)\,, \tag{2.49b}$$

$$\lambda = arc\tan(y/x) - \Theta\,. \tag{2.49c}$$

where Θ is the Greenwich apparent sidereal time. The partial derivatives of the curvilinear and Cartesian coordinates are (Hwang and Lin 1998):

$$\begin{bmatrix} \ddot{x}(P) \\ \ddot{y}(P) \\ \ddot{z}(P) \end{bmatrix} = \begin{bmatrix} x/r & xz\Big/\left(r\sqrt{x^2+y^2}\right) & -y\Big/\sqrt{x^2+y^2} \\ y/r & yz\Big/\left(r\sqrt{x^2+y^2}\right) & x\Big/\sqrt{x^2+y^2} \\ z/r & -\sqrt{x^2+y^2}\Big/r & 0 \end{bmatrix} \begin{bmatrix} W_r(P) \\ W_\theta(P) \\ W_\lambda(P) \end{bmatrix}. \tag{2.50}$$

Equation (2.50) is the differential equations of satellite motion in the presence of the geopotential field. It is a second-order vector differential equation, and it can be solved using numerical integrator, like Runge-Kutta, Adams-Bashforth, Adams-Moulton. Some investigations about orbit integration was done by Eshagh (2003a) and (2003b), Eshagh and Najafi-Alamdari (2005a) and (2005b), Also Eshagh (2005a) and (2009b) has presented two approaches for variable step orbit integration and orbit integration in non-inertial frames. Eshagh et al. (2009) simplified the geopotential perturbing force. This alternative formulation is nothing else than simplification of Eq. (2.50) and this expression is shortly presented in the next subsection.

2.5.2 Simplification of the geopotential perturbing force acting on a satellite

As was shown in the previous section, to carry out the integration steps of satellite orbit in the inertial frame (while the geopotential model (e.g., EGM96) as the source of geopotential is given in an Earth fixed (non-inertial) curvilinear coordinates system) one has to transfer the satellite position from the inertial frame to the Earth fixed frame, for the acceleration computation out of the EGM. This requires the Cartesian and curvilinear coordinates of the satellite to be computed in both the inertial and the earth fixed frames. Let us start with Eq. (2.50) and present it in terms of curvilinear coordinates:

$$\begin{bmatrix} \ddot{x}(P) \\ \ddot{y}(P) \\ \ddot{z}(P) \end{bmatrix} = \begin{bmatrix} \sin\theta\cos\lambda^* & \cos\lambda^*\cos\theta & -\sin\lambda^* \\ \sin\theta\sin\lambda^* & \sin\lambda^*\cos\theta & \cos\lambda^* \\ \cos\theta & -\sin\theta & 0 \end{bmatrix} \begin{bmatrix} W_r(P) \\ W_\theta(P) \\ W_\lambda(P) \end{bmatrix}, \tag{2.51}$$

where $\lambda^* = \lambda + \Theta$ as defined previously. By inserting the components of the gravitational vector (Eqs. 2.7a-2.7c) into Eq. (2.51) and after simplifications, we obtain :

$$\ddot{x}(P) = \frac{GM}{R^2} \sum_{n=0}^{N_{\max}} \sum_{m=-n}^{n} \left(\frac{R}{r}\right)^{n+2} w_{nm} \left[\cos\lambda^* Q_{-m}(\lambda) K_{nm}(\theta) - \sin\lambda^* Q_m(\lambda) L_{nm}(\theta)\right], \tag{2.52a}$$

$$\ddot{y}(P) = \frac{GM}{R^2} \sum_{n=0}^{N_{\max}} \sum_{m=-n}^{n} \left(\frac{R}{r}\right)^{n+2} w_{nm} \left[\sin\lambda^* Q_m(\lambda) K_{nm}(\theta) - \cos\lambda^* Q_{-m}(\lambda) L_{nm}(\theta)\right], \tag{2.52b}$$

$$\ddot{z}(P) = -\frac{GM}{R^2} \sum_{n=0}^{N_{\max}} \sum_{m=-n}^{n} \left(\frac{R}{r}\right)^{n+2} w_{nm} Q_m(\lambda) \left[(n+1)\cos\theta \bar{P}_{n|m|} + \sin\theta \frac{\partial \bar{P}_{n|m|}}{\partial\theta}\right], \tag{2.52c}$$

where

$$K_{nm}(\theta) = -(n+1)\sin\theta \bar{P}_{n|m|} + \cos\theta \frac{\partial \bar{P}_{n|m|}}{\partial\theta}, \tag{2.53a}$$

$$L_{nm}(\theta) = m \frac{\bar{P}_{n,|m|}}{\sin\theta} = c_{nm}^1 \bar{P}_{n-1,|m|-1} + c_{nm}^2 \bar{P}_{n-1,|m|+1}. \tag{2.53b}$$

The terms in the bracket of Eq. (2.52c) can be simplified further. To do that we start the mathematical derivations by introducing the following lemmas.

Lemma 2.5 (Ilk 1983, Z. 1.43):

$$\sin\theta \frac{\partial P_{n|m|}}{\partial\theta} = -\frac{(n+1)(n+|m|)}{(2n+1)} P_{n-1,|m|} + \frac{n(n-|m|+1)}{(2n+1)} P_{n+1,|m|}.$$

Lemma 2.6 (Ilk 1983, Z.1.37):

$$\cos\theta P_{n|m|} = \frac{n+|m|}{2n+1} P_{n-1,|m|} + \frac{n-|m|+1}{2n+1} P_{n+1,|m|}.$$

Note: these relations only hold for non-normalized ALFs.

Proposition 2.11:

$$(n+1)\cos\theta \bar{P}_{n|m|} + \sin\theta \frac{\partial \bar{P}_{n|m|}}{\partial\theta} = \sqrt{n-|m|+1}\sqrt{n+|m|+1}\sqrt{\frac{2n+1}{2n+3}} \bar{P}_{n+1,|m|}.$$

Proof. By multiplying the equation of Lemma 2.6 by (n+1) and adding to that of Lemma 2.5 we obtain:

$$(n+1)\cos\theta P_{n|m|} + \sin\theta \frac{\partial P_{n|m|}}{\partial \theta} = (n - |m| + 1) P_{n+1,|m|}. \tag{2.54}$$

By considering normalization factors of Eq. (2.10) inserting them into Eq. (2.54) and after further simplifications, Proposition 2.11 is proved.

The function $K_{nm}(\theta)$ presented in Eq. (2.53a) can also be simplified. Let us first introduce the following lemma.

Lemma 2.7 (Ilk 1983, Z.1.40):

$$\sin\theta P_{n|m|} = -\frac{1}{2n+1} P_{n-1,|m|+1} + \frac{1}{2n+1} P_{n+1,|m|+1}\ .$$

Here the function $K_{nm}(\theta)$ is simplified by Proposition 2.12.

Proposition 2.12:

$$K_{nm}(\theta) = l^1_{nm} \bar{P}_{n-1,|m|-1} + l^2_{nm} \bar{P}_{n-1,|m|+1} + l^3_{nm} \bar{P}_{n-1,|m|+1} + l^4_{nm} \bar{P}_{n+1,|m|+1}$$

where

$$l^1_{nm} = \frac{n-|m|}{2} \sqrt{\left(2-\delta_{|m|0}\right)(n+|m|)(n+|m|-1) \Big/ \left(2-\delta_{|m|-1,0}\right) \Big/ (2n+1)/(2n-1)}\ ,$$

$$l^2_{nm} = \frac{n-|m|}{2} \sqrt{\left(2-\delta_{|m|0}\right)(n-|m|)(n-|m|-1) \Big/ \left(2-\delta_{|m|+1,0}\right) \Big/ (2n+1)/(2n-1)}\ ,$$

$$l^3_{nm} = \frac{n+|m|+1}{2} \sqrt{\left(2-\delta_{|m|0}\right)(n-|m|+1)(n-|m|+2) \Big/ \left(2-\delta_{|m|-1,0}\right) \Big/ (2n+1)/(2n+3)}\ ,$$

$$l^4_{nm} = -\frac{3n-|m|+1}{2} \sqrt{\left(2-\delta_{|m|0}\right)(n+|m|+1)(n+|m|+2) \Big/ \left(2-\delta_{|m|-1,0}\right) \Big/ (2n+1)/(2n+3)}$$

Proof. We have to derive a relation for $\cos\theta \frac{\partial P_{n|m|}}{\partial \theta}$. In this case let us differentiate the equation of Lemma 2.6 with respect to θ (co-latitude)

$$-\sin\theta P_{n|m|} + \cos\theta \frac{\partial P_{n|m|}}{\partial \theta} = \frac{n+|m|}{2n+1} \frac{\partial P_{n-1,|m|}}{\partial \theta} + \frac{n-|m|+1}{2n+1} \frac{\partial P_{n+1,|m|}}{\partial \theta}. \tag{2.55}$$

Considering Lemma 2.1 for the derivatives of the non-normalized ALFs and inserting them in Eq. (2.55) we finally obtain

$$-\sin\theta P_{n|m|} + \cos\theta \frac{\partial P_{n|m|}}{\partial \theta} = \frac{n+|m|}{2(2n+1)} \left[(n+|m|-1)(n-|m|) P_{n-1,|m|-1} - P_{n-1,|m|+1} \right] +$$
$$+ \frac{n-|m|+1}{2(2n+1)} \left[(n+|m|+1)(n-|m|+2) P_{n+1,|m|-1} - P_{n+1,|m|+1} \right]. \tag{2.56}$$

By taking the most left part of Eq. (2.56) ($-\sin\theta P_{n|m|}$) into the right hand side of the equation and considering Lemma 2.7 we obtain

$$\cos\theta\frac{\partial P_{n|m|}}{\partial\theta}=\frac{\left(n+|m|\right)\left(n+|m|-1\right)\left(n-|m|\right)}{2\left(2n+1\right)}P_{n-1,|m|-1}-\frac{n+|m|+2}{2\left(2n+1\right)}P_{n-1,|m|+1}+$$
$$+\frac{\left(n-|m|+1\right)\left(n+|m|+1\right)\left(n-|m|+2\right)}{2\left(2n+1\right)}P_{n+1,|m|-1}-\frac{n-|m|-1}{2\left(2n+1\right)}P_{n+1,|m|+1}. \quad (2.57)$$

Multiplying Eq. (2.56) by –(n+1) and adding to Eq. (2.57) we have

$$\cos\theta\frac{\partial P_{n|m|}}{\partial\theta}-\left(n+1\right)\sin\theta P_{n|m|}=\frac{\left(n+|m|\right)\left(n+|m|-1\right)\left(n-|m|\right)}{2\left(2n+1\right)}P_{n-1,|m|-1}+\frac{n-|m|}{2\left(2n+1\right)}P_{n-1,|m|+1}+$$
$$+\frac{\left(n-|m|+1\right)\left(n+|m|+1\right)\left(n-|m|+2\right)}{2\left(2n+1\right)}P_{n+1,|m|-1}-\frac{3n-|m|+1}{2\left(2n+1\right)}P_{n+1,|m|+1}. \quad (2.58)$$

The proposition is proved by normalizing Eq. (2.58) and considering Eq. (2.10) as the normalizing factor.

According to Propositions 2.11 and 2.12 one can also write Eqs. (2.52a)-(2.52c) in the following forms:

$$\ddot{x}\left(P\right)=\frac{GM}{R^2}\sum_{n=0}^{N_{\max}}\left(\frac{R}{r}\right)^{n+2}\sum_{m=-n}^{n}w_{nm}\left[\cos\lambda^{*}Q_m\left(\lambda\right)F'_{nm}\left(\theta\right)-\sin\lambda^{*}Q_{-m}\left(\lambda\right)G'_{nm}\left(\theta\right)\right], \quad (2.59a)$$

$$\ddot{y}\left(P\right)=\frac{GM}{R^2}\sum_{n=0}^{N_{\max}}\left(\frac{R}{r}\right)^{n+2}\sum_{m=-n}^{n}w_{nm}\left[\sin\lambda^{*}Q_m\left(\lambda\right)F'_{nm}\left(\theta\right)-\cos\lambda^{*}Q_{-m}\left(\lambda\right)G'_{nm}\left(\theta\right)\right], \quad (2.59b)$$

and

$$\ddot{z}\left(P\right)=-\frac{GM}{R^2}\sum_{n=0}^{N_{\max}}\left(\frac{R}{r}\right)^{n+2}\sum_{m=-n}^{n}w_{nm}Q_m\left(\lambda\right)\sqrt{n-|m|+1}\sqrt{n+|m|+1}\sqrt{\frac{2n+1}{2n+3}}\bar{P}_{n+1,|m|}, \quad (2.59c)$$

where

$$G'_{nm}\left(\theta\right)=c^1_{nm}\bar{P}_{n-1,|m|-1}+c^2_{nm}\bar{P}_{n-1,|m|+1}, \quad (2.59d)$$

and

$$F'_{nm}\left(\theta\right)=l^1_{nm}\bar{P}_{n-1,|m|-1}+l^2_{nm}\bar{P}_{n-1,|m|+1}+l^3_{nm}\bar{P}_{n+1,|m|-1}+l^4_{nm}\bar{P}_{n+1,|m|+1}. \quad (2.59e)$$

Note: $G'_{n0}\left(\theta\right)=0$.

Equations (2.45a)-(2.45f) are the gravitational gradient expressions in the ORF, and they are functions of the satellite position in its orbit as well as satellite track azimuth.

The SGG data are also affected by the orbital perturbations. Although in the time-wise approach and the least-squares solution of space-wise approach these

perturbations are not important, but if one wants to use the spectral solution of the GBVPs, the SGG data should be interpolated (Sjöberg 1982 and Keller 1997), or continued upward/downward to the mean orbital sphere (Toth et al. 2004). Such an orbit would be close to the Keplerian orbit. The Keplerian orbit is an ellipse and the SGG data should be corrected further to transfer on the mean orbital sphere. However if the orbit is circular, one might neglect this transfer. In such a case, consideration of the effect of satellite perturbations is important to give some idea about magnitude of the changes on SGG data during this upward and downward continuation process.

In Figure 2.5 we present the orbital perturbation of a satellite during one-day revolution. The EGM96 was employed to generate the orbit and the SGG data at 250 km level. The maximum degree of the EGM to generate the orbit is 261 (Eshagh et al. 2009) based on the average power of the acceleration vector; see Hwang and Lin (1998). The presented expression for the geopotential acceleration of the satellite (Eqs. 259a-259c) was used to integrate the orbit, and after that the Keplerian orbit (the orbit without any perturbation) was subtracted from the generated orbit to compute the perturbations. (The integration step size was 5 second and the integrated orbit was compared with the simulated orbit of Bonn University to test the correctness of the simulation; and the differences are below millimeter level after one day). The perturbations are transformed into the orbital elements using the well-known formulas in celestial mechanics; see e.g. Seeber (2003, Ch. 3, p. 70).

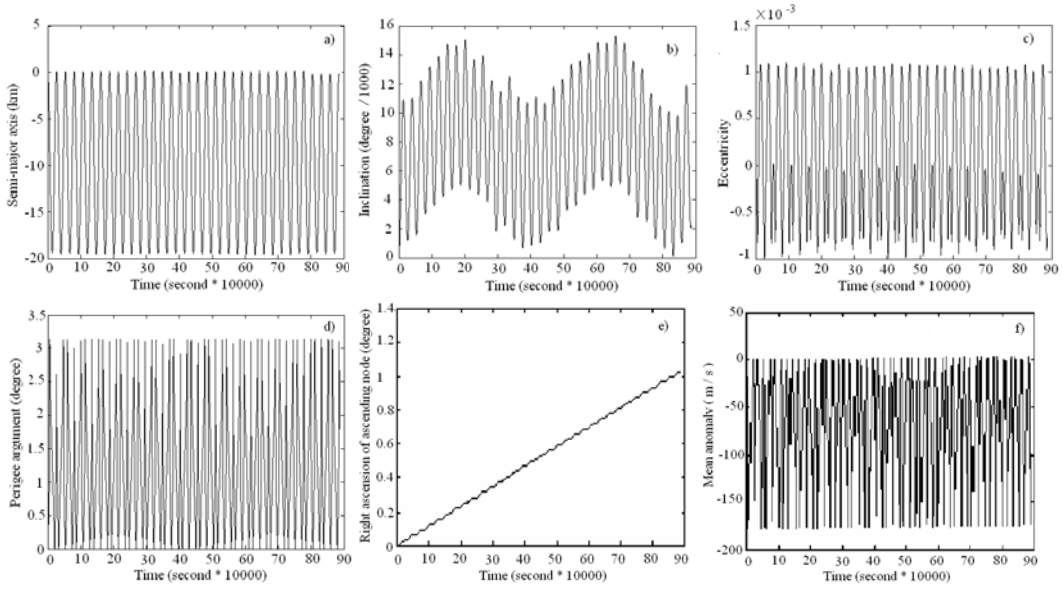

Figure 2.5. Orbital perturbations of GOCE in one day revolution. (a) semi-major axis of orbital ellipse, (b)) inclination, (c) eccentricity, (d) perigee argument, (e) , right ascension of ascending node and (f) mean motion.

As Figure 2.5 shows the semi-major axis of the orbital ellipse will change during one day revolution about 20 km and inclination of the orbital frame varies about 0.016°. Eccentricity and perigee argument change about 0.001 and 3.5°, respectively. The right ascension of ascending node has secular behaviour and it changes to 1.03° in one day revolution. The mean motion varies between -180 and 0 m/s during these revolutions.

In order to study the orbital perturbation effects, the gravitational gradients were generated in the LNOF on the Keplerian and generated orbits and the SGG data generated on the Keplerian orbit was subtracted from those generated on the integrated one. Figure 2.6 shows these differences.

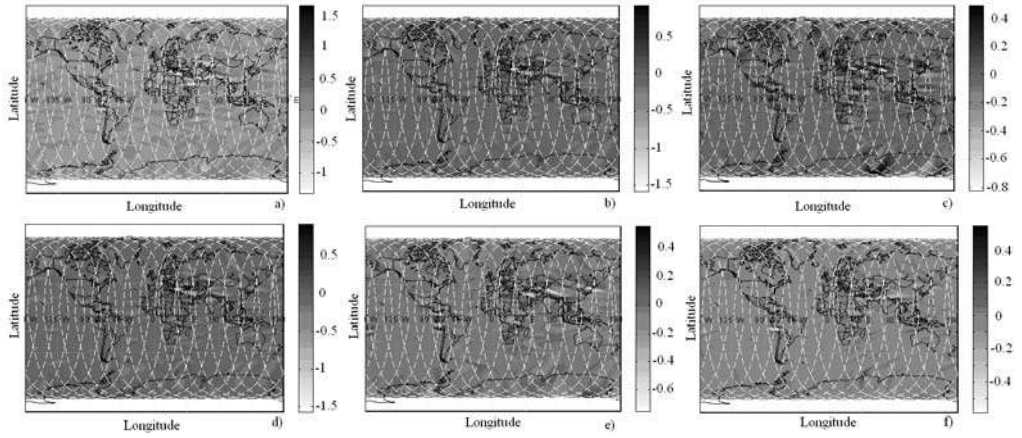

Figure 2.6 Effect of orbital perturbations on (a) T_{xx} , (b) T_{yy} , (c) T_{zz} , (d) T_{xy} , (e) T_{xz} and (f) T_{yz} . Unit : 1 E

The largest effects are seen when the satellite is approaching the topographically rough parts of the globe, which are the Hymalyan and Zagros mountains. Obviously, the satellite orbit is much more affected when it passes over these rough regions than the other parts. We illustrate the details in Table 2.3. It shows that the maximum orbital perturbation effect is related to δT_{xx} and the minimum effect is related to δT_{yz} . However, as the table illustrates, δT_{xx} , δT_{yy} and δT_{xy} are more affected by the orbital perturbation than the VV components as their standard deviations are larger than the others. This investigation is restricted to one-day revolution of the satellite and the Earth gravitational perturbations.

Table 2.3. Statistics of effect of orbital perturbations on SGG data. Unit: 1 E

	min	mean	Max	std
δT_{xx}	-1.36	-5.39×10^{-4}	1.89	$\pm$ 0.18
δT_{yy}	-0.68	10×10^{-4}	0.99	$\pm$ 0.13
δT_{zz}	-0.85	22×10^{-4}	0.57	$\pm$ 0.10
δT_{xy}	-1.63	7.80×10^{-4}	1.10	$\pm$ 0.13
δT_{xz}	-0.78	-2.41×10^{-4}	0.67	$\pm$ 0.09
δT_{yz}	-0.62	1.88×10^{-5}	0.62	$\pm$ 0.06

In the above numerical study, we considered the gravitational gradients in the LNOF because the expressions are functions of the satellite track azimuth in the ORF, which is perturbed as well. In the following, we will demonstrate the effect of perturbations of the satellite track azimuth on the SGG data. In order to show this, the gravitational gradients were generated on the Keplerian orbit and the satellite track azimuth was computed based on the Keplerian elements (the elements without perturbations). After that we will consider the Keplerian orbit to generate the gravitational gradients. In this case we consider the perturbed inclination and co-latitude for computing the gradients in the ORF according to Eq. (2.47).

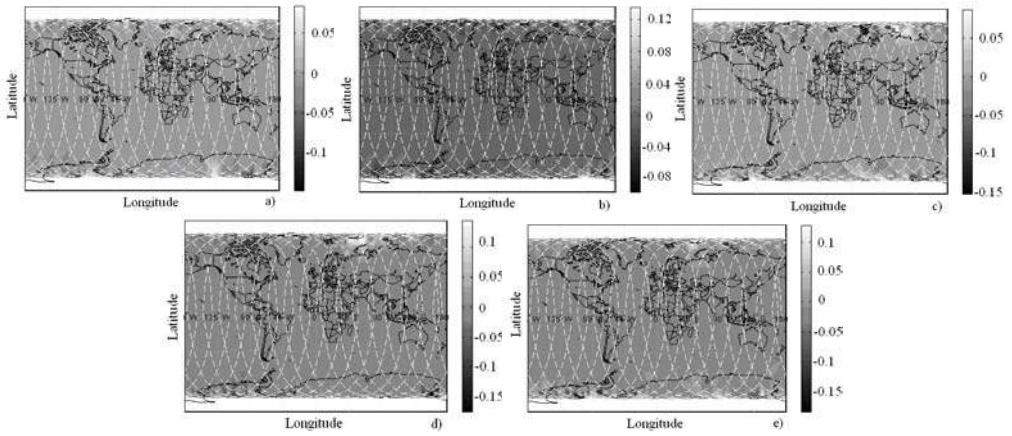

Figure 2.7. Effect of satellite track azimuth perturbations in ORF on (a) T_{uu} , (b) T_{vv} , (c) T_{uv} , (d) T_{uw} and (e) T_{vw} . Unit: 1 E

Figure 2.7 shows that the gravitational gradients are influenced when the satellite is approaching the poles. This could be expected according to Eq. (2.4) the satellite track azimuth has more deviation from the non-perturbed case. The statistics of these computations are presented in Table 2.4.

Table 2.4. Statistics of effect of perturbed satellite track azimuth on SGG data in ORF. Unit: 1 E

	min	mean	max	std
δT_{uu}	-0.16	-1.74×10^{-4}	0.10	± 0.01
δT_{vv}	-0.10	1.74×10^{-4}	0.16	± 0.01
δT_{uv}	-0.15	-3.28×10^{-4}	0.11	± 0.01
δT_{uw}	-0.18	2.14×10^{-4}	0.16	± 0.01
δT_{vw}	-0.19	2.07×10^{-4}	0.15	± 0.01

The statistics shows that the magnitude of the satellite track azimuth perturbation is within 0.2 E. Eshagh and Abdolahzadeh (2009b) showed that the perturbation of the co-latitude is larger than the satellite inclination.

2.6 The GBVPs

This section describes how the gravitational gradients can be used to compute an EGM, and how the gradients and the TSHs are related. The new expressions for the gradients and the TSHs are employed to compute the geopotential coefficients. A numerical test is made to show the correctness of the derived formulas, and the ability of the spectral solution of the GBVPs to continue the SGG data downward to the sea level from a satellite at 250 km altitude using spherical harmonics. We will briefly summarize the theory of the solution of the GBVPs. The interested reader is referred, for example, to Martinec (2003, Eq. 6, p. 42) to see how such GBVPs are solved. Let the gravitational tensor be expressed by:

$$\mathbf{T}_{xyz}(P)=T_{zz}(P)e_{zz}+2T_{xz}(P)\mathbf{e}_{r\theta}+2T_{xz}(P)\mathbf{e}_{r\lambda}+\frac{1}{2}\left[T_{xx}(P)-T_{yy}(P)\right]\left(\mathbf{e}_{\theta\theta}-\mathbf{e}_{\lambda\lambda}\right)+$$
$$+2T_{xy}(P)\mathbf{e}_{\theta\lambda}+\frac{1}{2}\left[T_{xx}(P)+T_{yy}(P)\right]\left(\mathbf{e}_{\theta\theta}+\mathbf{e}_{\lambda\lambda}\right). \qquad (2.60)$$

Five independent components of the gravitational tensor can be grouped into three second-order gradiometric tensors $\mathbf{T}^{(1)}(P)$, $\mathbf{T}^{(2)}(P)$, and $\mathbf{T}^{(3)}(P)$ as follows (Rummel and Gelderen 1992):

$$\mathbf{T}^{(1)}(P)=T_{zz}(P)\mathbf{e}_{zz}, \qquad (2.61a)$$
$$\mathbf{T}^{(2)}(P)=2T_{xz}(P)\mathbf{e}_{r\theta}+2T_{yz}(P)\mathbf{e}_{r\lambda}, \qquad (2.61b)$$

and

$$\mathbf{T}^{(3)}(P)=\frac{1}{2}\left[T_{xx}(P)-T_{yy}(P)\right]\left(\mathbf{e}_{\theta\theta}-\mathbf{e}_{\lambda\lambda}\right)+2T_{xy}(P)\mathbf{e}_{\theta\lambda}. \qquad (2.61c)$$

where $\mathbf{e}_{ij}=\left(\mathbf{e}_i\otimes\mathbf{e}_j\right)$ is the symmetric spherical dyadics, $i,j=(r,\theta,\lambda)$ spherical coordinate components and $\otimes$ is the tensor product. These combinations are made so that the orthogonality of the TSHs holds. In other words, the combinations are in accordance with these harmonic expressions, so that the orthogonality of them can be used to derive integral formulas for computing the geopotential coefficients. Equations (2.61a)-(2.61c) are the boundary values of the Laplace partial differential equation, $\Delta T=0$. The boundary values for this equation are $\mathbf{T}^{(1)}$, $\mathbf{T}^{(2)}$, and $\mathbf{T}^{(3)}$, which are called the VV, VH and HH boundary values, respectively (Martinec 2003). If we use a double gradient of the disturbing potential and substitute the result into the conditions of Eqs. (2.61a)-(2.61c) we obtain (Martinec 2003, Eq. 12):

$$\mathbf{T}^{(1)}(P)=\frac{GM}{R^3}\sum_{n=2}^{N_{\max}}(n+1)(n+2)\sum_{m=-n}^{n}t_{nm}\mathbf{Z}_{nm}^{(1)}(P), \qquad (2.62a)$$
$$\mathbf{T}^{(2)}(P)=-\frac{2GM}{R^3}\sum_{n=2}^{N_{\max}}(n+2)\sum_{m=-n}^{n}t_{nm}\mathbf{Z}_{nm}^{(2)}(P), \qquad (2.62b)$$

and

$$\mathbf{T}^{(3)}(P)=\frac{GM}{2R^3}\sum_{n=2}^{N_{\max}}\sum_{m=-n}^{n}t_{nm}\mathbf{Z}_{nm}^{(3)}(P). \qquad (2.62c)$$

In these equations $\mathbf{Z}_{nm}^{(1)}(P)$, $\mathbf{Z}_{nm}^{(2)}(P)$ and $\mathbf{Z}_{nm}^{(3)}(P)$ are TSHs corresponding to the gradiometric boundary values and t_{nm} are the SHCs of the disturbing potential.

Here, it is worth reviewing the definition of these harmonics to clarify their benefits in solving the GBVPs. Any second-order symmetric tensor $\mathbf{T}_{xyz}(P)$, whose components are square-integrable functions, like the gradiometric tensor, can be expanded in a series of TSHs of $\mathbf{Z}_{nm}^{(k)}(P)$ as (Martinec 2003, Eq. A9):

$$\mathbf{T}_{xyz}\left(P\right)=\sum_{n=2}^{N_{\max}}\sum_{m=-n}^{n}\sum_{i=1}^{6}t_{nm}^{(k)}\mathbf{Z}_{nm}^{(k)}\left(P\right), \tag{2.63}$$

where $t_{nm}^{(k)}$ are the expansion coefficients, which are obtained by taking advantage of the orthogonality properties:

$$\iint_{\sigma}\mathbf{Z}_{nm}^{(k)}\left(Q\right):\left[\mathbf{Z}_{n'm'}^{(k')}\left(Q\right)\right]d\sigma=4\pi\left[N_{n}^{(k)}\right]^{2}\delta_{nn'}\delta_{mm'}\delta_{kk'}, \tag{2.64}$$

where the colon denotes the double-dot product of the tensors and $\left[N_{n}^{(k)}\right]^{2}$ is the square norm of the base functions $\mathbf{Z}_{nm}^{(k)}\left(P\right)$(Martinec 2003, A8) :

$$\left[N_{n}^{(k)}\right]^{2}=\begin{cases}1 & k=1\\ n(n+1)/2 & k=2\\ 2(n-1)n(n+1)(n+2) & k=3\\ 2n^{2}(n+1)^{2} & k=4\\ n(n+1)/2 & k=5\\ (n-1)n(n+1)(n+2)/2 & k=6\end{cases}. \tag{2.65}$$

According to Zerilli (1970) the TSHs have the following form

$$\mathbf{Z}_{nm}^{(1)}\left(Q\right)=\tilde{Y}_{nm}\left(Q\right)\mathbf{e}_{rr}, \tag{2.66a}$$
$$\mathbf{Z}_{nm}^{(2)}\left(Q\right)=\tilde{E}_{nm}\left(Q\right)\mathbf{e}_{r\theta}+\tilde{F}_{nm}\left(Q\right)\mathbf{e}_{r\lambda}, \tag{2.66b}$$
$$\mathbf{Z}_{nm}^{(3)}\left(Q\right)=\tilde{G}_{nm}\left(Q\right)\left(\mathbf{e}_{\theta\theta}-\mathbf{e}_{\lambda\lambda}\right)+2\tilde{H}_{nm}\left(Q\right)\mathbf{e}_{\theta\lambda}, \tag{2.66c}$$
$$\mathbf{Z}_{nm}^{(4)}\left(Q\right)=-n(n+1)\tilde{Y}_{nm}\left(Q\right)\left(\mathbf{e}_{\theta\theta}+\mathbf{e}_{\lambda\lambda}\right), \tag{2.66d}$$
$$\mathbf{Z}_{nm}^{(5)}\left(Q\right)=-\tilde{F}_{nm}\left(Q\right)\mathbf{e}_{r\theta}+\tilde{E}_{nm}\left(Q\right)\mathbf{e}_{r\lambda}, \tag{2.66e}$$

and

$$\mathbf{Z}_{nm}^{(6)}\left(Q\right)=\tilde{G}_{nm}\left(Q\right)\mathbf{e}_{\theta\lambda}-\tilde{H}_{nm}\left(Q\right)\left(\mathbf{e}_{\theta\theta}-\mathbf{e}_{\lambda\lambda}\right), \tag{2.66f}$$

where

$$\tilde{Y}_{nm}\left(Q\right)=\left(\frac{R}{r}\right)^{n+1}Y_{nm}\left(Q\right), \tag{2.66g}$$

$$\begin{pmatrix}\tilde{E}_{nm}\left(Q\right)\\ \tilde{F}_{nm}\left(Q\right)\end{pmatrix}=-\frac{n+1}{R}\left(\frac{R}{r}\right)^{n+1}\begin{pmatrix}E_{nm}\left(Q\right)\\ F_{nm}\left(Q\right)\end{pmatrix}, \tag{2.66h}$$

and

$$\begin{pmatrix}\tilde{G}_{nm}\left(Q\right)\\ \tilde{H}_{nm}\left(Q\right)\end{pmatrix}=\left(\frac{R}{r}\right)^{n+1}\begin{pmatrix}G_{nm}\left(Q\right)\\ H_{nm}\left(Q\right)\end{pmatrix}, \tag{2.66i}$$

and $E_{nm}\left(Q\right)$, $F_{nm}\left(Q\right)$, $G_{nm}\left(Q\right)$ and $H_{nm}\left(Q\right)$ will be described in the next section.

According to the orthogonality property of $\mathbf{Z}_{nm}^{(k)}(P)$ we can write

$$t_{nm}^{(k')}=\frac{1}{4\pi\left[N_n^{(k')}\right]^2}\iint_{\sigma}\mathbf{T}^{(k')}(Q):\mathbf{Z}_{nm}^{(k')}(Q)d\sigma \quad \text{and} \quad k'=1,\,2 \text{ and } 3. \tag{2.67}$$

Since we have considered three independent combinations of the gradiometric boundary values we will have three different sets of solutions for the geopotential coefficients (Martinec 2003):

$$t_{nm}^{(1)}=\frac{R^3/(4\pi GM)}{(n+1)(n+2)}\left(\frac{r}{R}\right)^{n+3}\iint_{\sigma}T_{zz}(Q)Y_{nm}(Q)d\sigma, \tag{2.67a}$$

$$t_{nm}^{(2)}=-\frac{R^3/(4\pi GM)}{n(n+1)(n+2)}\left(\frac{r}{R}\right)^{n+3}\iint_{\sigma}\left[T_{xz}(Q)E_{nm}(Q)+T_{yz}(Q)F_{nm}(Q)\right]d\sigma, \tag{2.67b}$$

and

$$t_{nm}^{(3)}=\frac{R^3/(4\pi GM)}{(n-1)n(n+1)(n+2)}\left(\frac{r}{R}\right)^{n+3}\iint_{\sigma}\left\{\left[T_{xx}(Q)-T_{yy}(Q)\right]G_{nm}(Q)+2T_{xy}(Q)H_{nm}(Q)\right\}d\sigma \tag{2.67c}$$

Equations (2.67)-(2.67c) yield three different sets of solutions for the geopotential coefficients.

2.6.1 Traditional expressions for the TSHs

In this subsection, we will present the traditional expressions of the TSHs and after that we continue our mathematical derivations by simplifying and deriving alternative expressions for them. We can write $Y_{nm}(Q)$, $E_{nm}(Q)$, $F_{nm}(Q)$, $G_{nm}(Q)$ and $H_{nm}(Q)$ in the following form:

$$Y_{nm}(Q)=Q_m(\lambda)\bar{P}_{n|m|}, \tag{2.68a}$$

$$E_{nm}(Q)=\frac{\partial Y_{nm}(Q)}{\partial\theta}=Q_m(\lambda)\frac{\partial\bar{P}_{n|m|}}{\partial\theta}, \tag{2.68b}$$

$$F_{nm}(Q)=\frac{1}{\sin\theta}\frac{\partial Y_{nm}(Q)}{\partial\lambda}=mQ_{-m}(\lambda)\frac{\bar{P}_{n|m|}}{\sin\theta}, \tag{2.68c}$$

$$\begin{aligned}G_{nm}(Q)&=\left(\frac{\partial^2}{\partial\theta^2}-\cot\theta\frac{\partial}{\partial\theta}-\frac{1}{\sin^2\theta}\frac{\partial^2}{\partial\lambda^2}\right)Y_{nm}(Q)\\&=Q_m(\lambda)\left(\frac{\partial^2\bar{P}_{n|m|}}{\partial\theta^2}-\cot\theta\frac{\partial\bar{P}_{n|m|}}{\partial\theta}+m^2\frac{\bar{P}_{n|m|}}{\sin^2\theta}\right),\end{aligned} \tag{2.68d}$$

and

$$H_{nm}(Q) = 2\frac{\partial}{\partial\theta}\left(\frac{1}{\sin\theta}\frac{\partial Y_{nm}(Q)}{\partial\lambda}\right) = 2mQ_{-m}(\lambda)\frac{\partial}{\partial\theta}\left(\frac{\bar{P}_{n|m|}}{\sin\theta}\right). \quad (2.68e)$$

Clearly, the functions $E_{nm}(Q)$, $F_{nm}(Q)$, $G_{nm}(Q)$ and $H_{nm}(Q)$ have complicated forms depending on the first- and second-order derivatives of the ALFs as well as singular terms at the poles. $E_{nm}(Q)$ is related to the first-order derivative of the ALFs and in $F_{nm}(Q)$ there is the term $1/\sin\theta$. $G_{nm}(Q)$ is the most complicated function involving first- and second-order derivatives of the ALFs as well as the terms $1/\sin\theta$ and $1/\sin^2\theta$ and $H_{nm}(Q)$ is related to $\bar{P}_{nm}(\cos\theta)/\sin\theta$ and its first-order derivative with respect to co-latitude. In the next section we will present simpler expressions for these functions.

2.6.2 Alternative expressions for the TSHs

Let us introduce the following lemma, which will be useful in our derivations.

Lemma 2.5 (Zielinski and Petrovskaya 2003, Eq. 7):

$$\frac{\partial P_{n|m|}}{\partial\theta} = |m|\cot\theta P_{n|m|} - P_{n,|m|+1}.$$

The first term of $G_{nm}(Q)$ is related to the second-order derivative of the ALFs and the second term is related to the first-order derivative of the ALFs as well as the term $1/\sin\theta$ and the third term contains the term $1/\sin^2\theta$. In this section we will construct a very simple form for $G_{nm}(Q)$ in terms of three adjacent ALFs. Let us first start our derivations by Proposition 2.13.

Proposition 2.13:

$$\frac{\partial^2\bar{P}_{n|m|}}{\partial\theta^2} - \cot\theta\frac{\partial\bar{P}_{n|m|}}{\partial\theta} - m^2\frac{\bar{P}_{n|m|}}{\sin^2\theta} = p^1_{nm}\bar{P}_{n,|m|-2} + p^2_{nm}\bar{P}_{n|m|} + p^3_{nm}\bar{P}_{n,|m|+2},$$

where

$$p^1_{nm} = \frac{1}{2}\sqrt{\frac{2-\delta_{|m|0}}{2-\delta_{|m|-2,0}}}\sqrt{n+|m|}\sqrt{n+|m|-1}\sqrt{n-|m|+1}\sqrt{n-|m|+2},$$

$$p^2_{nm} = m^2,$$

$$p^3_{nm} = \frac{1}{2}\sqrt{\frac{2-\delta_{|m|0}}{2-\delta_{|m|+2,0}}}\sqrt{n-|m|}\sqrt{n-|m|-1}\sqrt{n+|m|+1}\sqrt{n+|m|+2}.$$

Proof. The second term of $G_{nm}(Q)$ is nothing else than multiplication of the first-order derivative of the ALFs with $\cot\theta$. Premultiplying the equation of Lemma 2.5 with $\cot\theta$ we obtain

$$\cot\theta\frac{\partial P_{n|m|}}{\partial\theta}=|m|\cot^2\theta P_{n|m|}-\cot\theta P_{n,|m|+1}, \tag{2.69}$$

and again by using Lemma 2.5, we can write

$$\cot\theta P_{n|m|}=\frac{1}{|m|}\frac{\partial P_{n|m|}}{\partial\theta}+\frac{1}{|m|}P_{n,|m|+1}. \tag{2.70}$$

From Lemma 2.1 and after simplification we have

$$\cot\theta P_{n|m|}=\frac{1}{2|m|}\left\{(n+|m|)(n-|m|+1)P_{n,|m|-1}+P_{n,|m|+1}\right\}. \tag{2.71}$$

After multiplication by another $\cot\theta$, we obtain

$$\cot^2\theta P_{n|m|}=\frac{1}{2|m|}\left\{(n+|m|)(n-|m|+1)\cot\theta P_{n,|m|-1}+\cot\theta P_{n,|m|+1}\right\}. \tag{2.72}$$

By using Eq. (2.71) we derive the following formulas

$$\cot\theta P_{n,|m|-1}=\frac{1}{2(|m|-1)}\left\{(n+|m|-1)(n-|m|+2)P_{n,|m|-2}+P_{n|m|}\right\}, \tag{2.73}$$

$$\cot\theta P_{n,|m|+1}=\frac{1}{2(|m|+1)}\left\{(n+|m|+1)(n-|m|)P_{n|m|}+P_{n,|m|+2}\right\}, \tag{2.74}$$

and by inserting these equations into Eq. (2.72) we obtain

$$\begin{aligned}\cot^2\theta P_{n|m|}=\frac{1}{2|m|}\Bigg\{&\frac{(n+|m|)(n-|m|+1)}{2(|m|-1)}\left[(n+|m|-1)(n-|m|+2)P_{n,|m|-2}+P_{n|m|}\right]+\\&+\frac{(n-|m|)(n+|m|+1)}{2(|m|+1)}P_{n|m|}+\frac{1}{2(|m|+1)}P_{n,|m|+2}\Bigg\}\end{aligned}. \tag{2.75}$$

Finally, by inserting Eq. (2.75) and Eq. (2.74) into Eq. (2.69) we obtain

$$\begin{aligned}\cot\theta\frac{\partial P_{n|m|}}{\partial\theta}=\Bigg\{&\frac{(n+|m|)(n-|m|+1)(n+|m|-1)(n-|m|+2)}{4(|m|-1)}P_{n,|m|-2}+\\&+\left[\frac{(n+|m|)(n-|m|+1)}{4(|m|-1)}-\frac{(n+|m|+1)(n-|m|)}{4(|m|+1)}\right]P_{n|m|}-\frac{P_{n,|m|+2}}{2(|m|+1)}\Bigg\}.\end{aligned} \tag{2.76}$$

By normalizing Eq. (2.76) using Eq. (2.10) we obtain

$$\cot\theta\frac{\partial\bar{P}_{n|m|}}{\partial\theta}=p'^{1}_{nm}\bar{P}_{n,|m|-2}+p'^{2}_{nm}\bar{P}_{n|m|}+p'^{3}_{nm}\bar{P}_{n,|m|+2},\quad |m|\neq 1 \tag{2.77}$$

where

$$p'^{1}_{nm}=\frac{1}{4(|m|-1)}\sqrt{\frac{2-\delta_{|m|0}}{2-\delta_{|m|-2,0}}}\sqrt{n+|m|}\sqrt{n-|m|+1}\sqrt{n-|m|+2}\sqrt{n+|m|-1},$$

$$p'^{2}_{nm}=\left[\frac{(n+|m|)(n-|m|+1)}{4(|m|-1)}-\frac{(n+|m|+1)(n-|m|)}{4(|m|+1)}\right],$$

$$p'^{3}_{nm}=\frac{-1}{4(|m|+1)}\sqrt{\frac{2-\delta_{|m|0}}{2-\delta_{|m|+2,0}}}\sqrt{n-|m|}\sqrt{n-|m|-1}\sqrt{n+|m|+2}\sqrt{n+|m|+1}.$$

Substituting Propositions 2.2, 2.4 and Eq. (2.77) into left hand side of the equation of Proposition 2.13, and after a relatively long simplifications the proposition is proven.

Equation (2.67c), involves $G_{nm}(Q)$ and $H_{nm}(Q)$ and $G_{nm}(Q)$ was simplified in Proposition 2.13. $H_{nm}(Q)$ can also be simplified in two ways: forwarded or backwarded with respect to degree *n*. Let us start the derivations by the forward mode in which the degree of the adjacent ALFs in right hand side of the equations becomes *n*+1. The formulation is presented in Proposition 2.14.

Proposition 2.14:

$$2m\frac{\partial}{\partial\theta}\left(\frac{\bar{P}_{n,|m|}}{\sin\theta}\right)=q^{1}_{nm}\bar{P}_{n+1,|m|-2}+q^{2}_{nm}\bar{P}_{n+1,|m|}+q^{3}_{nm}\bar{P}_{n+1,|m|+2},\qquad |\mathrm{m}|\neq 0$$

where

$$q^{1}_{nm}=\frac{m}{2|m|}\sqrt{\frac{(2-\delta_{|m|0})(2n+1)}{(2-\delta_{|m|-2,0})(2n+3)}}\sqrt{n+|m|}\sqrt{n-|m|+3}\sqrt{n-|m|+2}\sqrt{n-|m|+1}$$

$$q^{2}_{nm}=\frac{m}{2|m|}\sqrt{\frac{(2n+1)(n+|m|+1)}{(2n+3)(n-|m|+1)}}\left[(n+|m|+2)(n-|m|+1)-(n-|m|+2)(n-|m|+1)\right]$$

$$q^{3}_{nm}=-\frac{m}{2|m|}\sqrt{\frac{(2-\delta_{|m|0})(2n+1)}{(2-\delta_{|m|+2,0})(2n+3)}}\sqrt{n-|m|}\sqrt{n+|m|+3}\sqrt{n+|m|+2}\sqrt{n+|m|+1}.$$

Proof. Let us consider the last term, i.e. $H_{nm}(Q)$. It is better to simplify the term in the parenthesis according to Lemma 2.3, before differentiation with respect to co-latitude:

$$2m\frac{\partial}{\partial\theta}\left(\frac{P_{n|m|}}{\sin\theta}\right)=\frac{\partial}{\partial\theta}\left\{\frac{m}{|m|}\left[\left(n-|m|+1\right)\left(n-|m|+2\right)P_{n+1,|m|-1}+P_{n+1,|m|+1}\right]\right\}$$
$$=\frac{m}{|m|}\left[\left(n-|m|+1\right)\left(n-|m|+2\right)\frac{\partial P_{n+1,|m|-1}}{\partial\theta}+\frac{\partial P_{n+1,|m|+1}}{\partial\theta}\right] \quad (2.78)$$

According to Lemma 2.1 we can write

$$\frac{\partial P_{n+1,|m|-1}}{\partial\theta}=\frac{1}{2}\left[\left(n+|m|\right)\left(n-|m|+3\right)P_{n+1,|m|-2}-P_{n+1,|m|}\right] \quad (2.79)$$

$$\frac{\partial P_{n+1,|m|+1}}{\partial\theta}=\frac{1}{2}\left[\left(n+|m|+2\right)\left(n-|m|+1\right)P_{n+1,|m|}-P_{n+1,|m|+2}\right]. \quad (2.80a)$$

Substituting Eqs.(2.79) and (2.80a) into Eq. (2.78) yields

$$2m\frac{\partial}{\partial\theta}\left(\frac{P_{n|m|}}{\sin\theta}\right)=\frac{m}{2|m|}\left\{\left(n-|m|+1\right)\left(n-|m|+2\right)\left[\left(n+|m|\right)\left(n-|m|+3\right)P_{n+1,|m|-2}-\right.$$
$$\left.-P_{n+1,|m|}\right]+\left(n-|m|+1\right)\left(n-|m|+2\right)P_{n+1,|m|}-P_{n+1,|m|+2}\Big\}. \quad (2.80b)$$

The proposition is proven by normalization and simplification.

Now, $H_{nm}(Q)$ is formulated in backwarded mode in which n changes to n-1 for the ALFs in the right-hand side of the equation.

Proposition 2.15:

$$2m\frac{\partial}{\partial\theta}\left(\frac{\bar{P}_{n|m|}}{\sin\theta}\right)=q'^{1}_{nm}\bar{P}_{n-1,|m|-2}+q'^{2}_{nm}\bar{P}_{n-1,|m|}+q'^{3}_{nm}\bar{P}_{n-1,|m|+2},$$

where

$$q'^{1}_{nm}=\frac{m}{2|m|}\sqrt{\frac{\left(2-\delta_{|m|0}\right)\left(2n+1\right)}{\left(2-\delta_{|m|-2,0}\right)\left(2n-1\right)}}\sqrt{n+|m|}\sqrt{n+|m|-3}\sqrt{n+|m|-2}\sqrt{n-|m|+1},$$

$$q'^{2}_{nm}=-m\sqrt{\frac{\left(2n+1\right)}{\left(2n-1\right)}}\sqrt{n-|m|}\sqrt{n+|m|},$$

$$q'^{3}_{nm}=-\frac{m}{2|m|}\sqrt{\frac{\left(2-\delta_{|m|0}\right)\left(2n+1\right)}{\left(2-\delta_{|m|+2,0}\right)\left(2n-1\right)}}\sqrt{n-|m|}\sqrt{n-|m|-1}\sqrt{n-|m|-2}\sqrt{n+|m|+1}.$$

Proof. By using Lemma 2.2 for $P_{n|m|}/\sin\theta$ we write

$$2m\frac{\partial}{\partial\theta}\left(\frac{P_{n|m|}}{\sin\theta}\right)=\frac{\partial}{\partial\theta}\left\{\frac{m}{|m|}\left[\left(n+|m|\right)\left(n+|m|-1\right)P_{n-1,|m|-1}+P_{n-1,|m|+1}\right]\right\}$$
$$=\frac{m}{|m|}\left[\left(n+|m|\right)\left(n+|m|-1\right)\frac{\partial P_{n-1,|m|-1}}{\partial\theta}+\frac{\partial P_{n-1,|m|+1}}{\partial\theta}\right] \quad , \quad (2.81)$$

and according to Lemma 2.1 we deliver

$$\frac{\partial P_{n-1,|m|-1}}{\partial\theta}=\frac{1}{2}\left[\left(n+|m|-2\right)\left(n-|m|+1\right)P_{n-1,|m|-2}-P_{n-1,|m|}\right], \quad (2.82)$$

$$\frac{\partial P_{n-1,|m|+1}}{\partial\theta}=\frac{1}{2}\left[\left(n+|m|\right)\left(n-|m|-1\right)P_{n-1,|m|}-P_{n-1,|m|+2}\right]. \quad (2.83)$$

Substituting Eqs.(2.82) and (2.83) into Eq. (2.81) yields

$$2m\frac{\partial}{\partial\theta}\left(\frac{P_{n|m|}}{\sin\theta}\right)=\frac{m}{2|m|}\left\{\left(n+|m|\right)\left(n+|m|-1\right)\left(n+|m|-2\right)\left(n-|m|+1\right)P_{n-1,|m|-2}+\right.$$
$$\left.\left(n+|m|\right)\left(-2|m|\right)P_{n-1,|m|}-P_{n-1,|m|+2}\right\} \quad (2.84)$$

The proposition is proven by normalizing Eq. (2.84) using Eq. (2.10).

The most difficult part of the derivations was related to those parts of the TSHs involving the $G_{nm}(Q)$ and $H_{nm}(Q)$. However these terms were simplified in Propositions 2.13, 2.14 and 2.15. Consequently we are at the step to present the simplified forms of these harmonics.

According to Eq. (2.68a) and normalized form of the equation of Lemma 2.1, the function $E_{nm}(Q)$ is:

$$E_{nm}(Q)=Q_m(\lambda)\frac{\partial\bar{P}_{n|m|}}{\partial\theta}=Q_m(\lambda)\left\{a^1_{nm}\bar{P}_{n,|m|-1}+a^2_{nm}\bar{P}_{n,|m|+1}\right\}, \quad (2.85a)$$

Normalizing the equations of Lemmas 2.2 and 2.3 and considering Eq. (2.10) we obtain (Eshagh 2009c):

$$F_{nm}(Q)=Q_m(\lambda)\frac{\bar{P}_{n|m|}}{\sin\theta}=Q_m(\lambda)\left\{c^1_{nm}\bar{P}_{n-1,|m|-1}+c^2_{nm}\bar{P}_{n-1,|m|+1}\right\}, \quad (2.85b)$$

$$F_{nm}(Q)=Q_m(\lambda)\frac{\bar{P}_{n|m|}}{\sin\theta}=Q_m(\lambda)\left\{c'^1_{nm}\bar{P}_{n+1,|m|-1}+c'^2_{nm}\bar{P}_{n+1,|m|+1}\right\}. \quad (2.85c)$$

$G_{nm}(Q)$ and $H_{nm}(Q)$ follow from Propositions 2.13 and 2.14 as:

$$G_{nm}(Q)=Q_m(\lambda)\left\{\frac{\partial^2\bar{P}_{n|m|}}{\partial\theta^2}-\cot\theta\frac{\partial\bar{P}_{n|m|}}{\partial\theta}+m^2\frac{\bar{P}_{n|m|}}{\sin^2\theta}\right\}$$
$$=Q_m(\lambda)\left\{p^1_{nm}\bar{P}_{n,|m|-2}+p^2_{nm}\bar{P}_{n|m|}+p^3_{nm}\bar{P}_{n,|m|+2}\right\},\qquad(2.85d)$$

and

$$H_{nm}(Q)=2Q_m(\lambda)\frac{\partial}{\partial\theta}\left\{\frac{\bar{P}_{n|m|}}{\sin\theta}\right\}=Q_m(\lambda)\left\{q^1_{nm}\bar{P}_{n+1,|m|-2}+q^2_{nm}\bar{P}_{n+1,|m|}+q^3_{nm}\bar{P}_{n+1,|m|+2}\right\},$$

or (2.85e)

$$H_{nm}(Q)=2Q_m(\lambda)\frac{\partial}{\partial\theta}\left\{\frac{\bar{P}_{n|m|}}{\sin\theta}\right\}=Q_m(\lambda)\left\{q'^1_{nm}\bar{P}_{n-1,|m|-2}+q'^2_{nm}\bar{P}_{n-1,|m|}+q'^3_{nm}\bar{P}_{n-1,|m|+2}\right\}.$$

(2.85f)

2.7 Numerical studies

In order to verify the new formulas, they are used to synthesize the gravitational gradients on the mean Earth sphere using the EGM96 (Lemoine et al. 1998) with 0.5° by 0.5° resolution. After that we compute the geopotential coefficients by Eqs. (2.67a)-(2.67c) and using the new expressions for the TSHs. In this step, the spherical harmonics and the combinations of the gradients are used to compute geopotential coefficients. Theoretically Eqs. (2.67a)-(2.67c) yield the same results; but practically, they do not because of the dicretization error of the integrals and noise of the gradients. Let the gradients be free of noise then the discretization error will be the main source of the differences. Figure 2.8 shows the relative error degree variances between the true (the geopotential coefficients of EGM96) and computed values of the geopotential coefficients in the presence of discretization error.

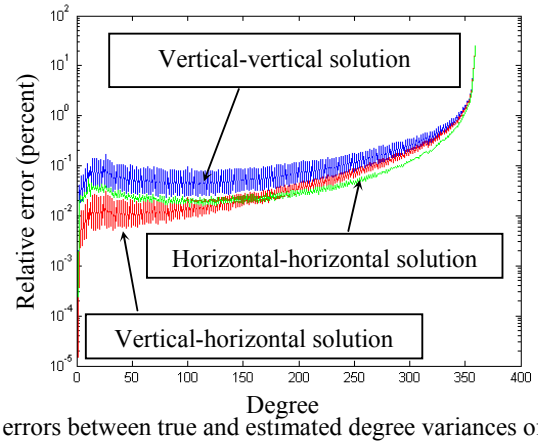

Figure 2.8. Relative errors between true and estimated degree variances of the geopotential field in percent.

According to Figure 2.8 it can be concluded that the VH and HH solutions of the GBVP are less affected by discretization error than the VV solution. It is interesting to see that the discretization error due the HH solution is smaller than the other solutions after about degree 180. The discretization errors of the solutions are small and in acceptable level. In order to make sure that these errors are really due to discretization of the integrals, we consider a higher resolution ($15'\times15'$) in the synthesis and

analysis. The results of these computations are presented in Figures 2.9(a)-(c) which confirms that the numerical integration error is reduced by increasing the resolution.

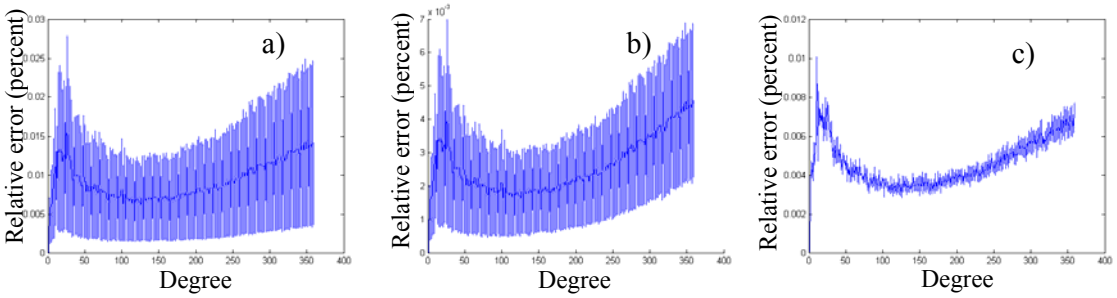

Figure 2.9. (a), (b) and (c) are the percentage relative error degree variances of true and computed EGM with $15' \times 15'$ resolution

Next we will test the capability of downward continuation of the SGG data from 250 km altitude to sea level using spherical harmonic expansion. In this case, the SGG data were globally synthesized at satellite level in the LNOF, and Eqs. (2.67a)-(2.67c) are used to compute the geopotential coefficients from the SGG data. Different resolutions of the data ($30' \times 30'$, $15' \times 15'$, $10' \times 10'$ and $5' \times 5'$ grids) are tested to see the resolution of the maximum useful degree of geopotential coefficients. Figure 2.10 shows the results of these computations.

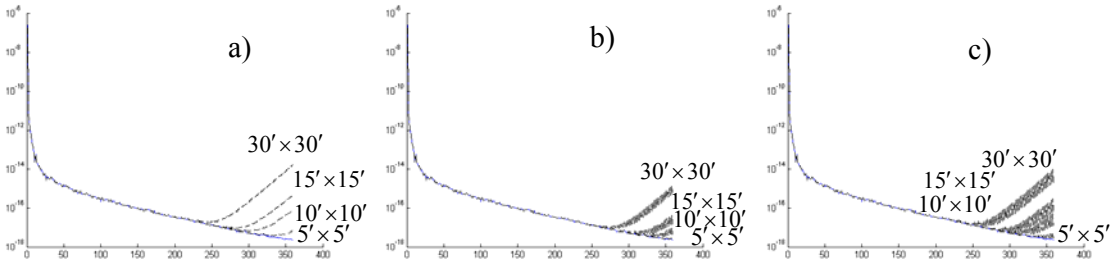

Figure 2.10. Degree variances of geopotential model determined from SGG data at 250 km level with different resolutions. (a), (b) and (c) are the solutions of the first, second and third integrals in Eqs. (2.67a)-(2.67c), respectively.

Figures 2.10 (a), (b) and (c) show the degree variances of the recovered geopotential models by the integral formulas of Eqs. (2.67a)-(2.67c), respectively. Since the recovered signal is very close to the true one, only one curve is visible in the figures as they are coinciding before a certain degree. Clearly, all three integral formulas have not the same ability to continue the SGG data down to sea level by spherical harmonics. At first view one can see that by increasing the resolution of the SGG data, higher degree geopotential coefficients can be recovered. The spectral solution of the VH GBVP, Eqs. (2.67b), computes to higher degrees than the other solutions. Also we can see more or less the same ability for the first and third integral to recover geopotential coefficients. Graphical interpretation is not precise enough to judge about the capability of downward continuation of the geopotential field, the figures show that the numerical discretization error of the integral formulas increase considerably after a certain degree. The question is, what this specific degree is. It is not easy to answer this question unless we have a criterion. For that reason, we will only accept those degrees with relative errors less than 1% and 0.1%. The result of

this investigation is summarized in Table 2.5, which shows the relative errors of the degree variances. According to the table the solution of the GBVPs of VV and HH (Eqs. 2.67a and 2.67c) show more or less the same capability to downward continue the gradient using spherical harmonics.

Table 2.5. Maximum degree of the geopotential coefficients determined from SGG data at 250 km level within 1% (0.1%) relative error of degree variances

	$30' \times 30'$	$15' \times 15'$	$10' \times 10'$	$5' \times 5'$
VV $T_{zz}(P)$	198(1%) 134(0.1%)	238(1%), 185(0.1%)	257(1%) 202(0.1%)	288(1%) 238(0.1%)
VH $T_{xz}(P)$ and $T_{yz}(P)$	233(1%) 161(0.1%)	269(1%) 203(0.1%)	289(1%) 244(0.1%)	313(1%) 269(0.1%)
HH $T_{xx}(P)-T_{yy}(P)$ and $2T_{xy}(P)$	199(1%) 150(0.1%)	249(1%) 195(0.1%)	259(1%) 207(0.1%)	295(1%) 251(0.1%)

A simple comparison of the maximum degrees presented in Table 2.5 shows that the VH GBVP solution is one step further than the others. More coefficients can be determined using VH solution with lower resolution than the other solutions.

2.8 Error propagation

Until now we have considered just the discretization error for the geopotential modelling. However, we already know that the random error of the geopotential coefficients can be estimated using the error propagation law. The three integrals of Eqs. (2.67a)-(2.67c) can be written in the following vectorized froms:

$$t_{nm}^{(1)} = \mathbf{b}_{zz}^{nm}\ \mathbf{t}_{zz}\ , \tag{2.97a}$$

$$t_{nm}^{(2)} = \mathbf{b}_{xz}^{nm}\mathbf{t}_{xz} + \mathbf{b}_{yz}^{nm}\ \mathbf{t}_{yz}\ , \tag{2.97b}$$

$$t_{nm}^{(3)} = \mathbf{b}_{xx}^{nm}\ \mathbf{t}_{xx} + \mathbf{b}_{yy}^{nm}\ \mathbf{t}_{yy} + \mathbf{b}_{xy}^{nm}\ \mathbf{t}_{xy}\ , \tag{2.97c}$$

where $\mathbf{b}_{zz}^{nm}$, $\mathbf{b}_{xx}^{nm}$, $\mathbf{b}_{yy}^{nm}$, $\mathbf{b}_{xy}^{nm}$, $\mathbf{b}_{xz}^{nm}$ and $\mathbf{b}_{yz}^{nm}$ are row vectors obtained by discretizing Eqs. (2.97a)-(2.97c) and $\mathbf{t}_{zz}$, $\mathbf{t}_{xx}$, $\mathbf{t}_{yy}$, $\mathbf{t}_{xy}$, $\mathbf{t}_{xz}$ and $\mathbf{t}_{yz}$ are the column vectors of $T_{zz}(Q)$, $T_{xx}(Q)$, $T_{yy}(Q)$, $T_{xy}(Q)$, $T_{xz}(Q)$ and $T_{yz}(Q)$ observations, respectively. By using such a vectorized model it is easy to use the error propagation law to estimate the error of each geopotential coefficient at degree *n* and order *m*. For example, if we assume to have uncorrelated observations we obtain:

$$\sigma_{t_{nm}^{(1)}} = \pm\sqrt{\mathbf{b}_{zz}^{nm}\left(\mathbf{b}_{zz}^{nm}\right)^{T}}\,\sigma_{\mathbf{t}_{zz}}\ , \tag{2.98a}$$

$$\sigma_{t_{nm}^{(2)}} = \pm\sqrt{\mathbf{b}_{xz}^{nm}\left(\mathbf{b}_{xz}^{nm}\right)^{T}\sigma_{\mathbf{t}_{xz}}^{2} + \mathbf{b}_{yz}^{nm}\left(\mathbf{b}_{yz}^{nm}\right)^{T}\sigma_{\mathbf{t}_{yz}}^{2}}\ , \tag{2.98b}$$

$$\sigma_{t_{nm}^{(3)}} = \pm\sqrt{\mathbf{b}_{xx}^{nm}\left(\mathbf{b}_{xx}^{nm}\right)^{T}\sigma_{\mathbf{t}_{xx}}^{2} + \mathbf{b}_{yy}^{nm}\left(\mathbf{b}_{yy}^{nm}\right)^{T}\sigma_{\mathbf{t}_{yy}}^{2} + \mathbf{b}_{xy}^{nm}\left(\mathbf{b}_{xy}^{nm}\right)^{T}\sigma_{\mathbf{t}_{xy}}^{2}}\ , \tag{2.98c}$$

where $\sigma_{\mathbf{t}_{zz}}$, $\sigma_{\mathbf{t}_{xz}}$, $\sigma_{\mathbf{t}_{yz}}$, $\sigma_{\mathbf{t}_{xx}}$, $\sigma_{\mathbf{t}_{yy}}$ and $\sigma_{\mathbf{t}_{xy}}$ are the standard errors of the data, which is equal with 0.01 E for each set of gradient.

The errors are propagated according to Eqs. (2.97a)-(2.97c) which are discretized integral solutions. The higher resolution, the lower discretization error and the higher degree of resolution. Actually the degree of resolution shows the maximum acceptable truncation for the spherical harmonic analysis, and it is not meaningful to estimate higher degrees of geopotential coefficients than this degree. This could therefore be one criterion for the maximum degree of the geopotential model. Theoretically, the integral formulas are perfect and able to continue the SGG data down to sea level using spherical harmonics for all frequencies. However, in practice this is not true as the integrals should be discretized and solved. Discretization of these integrals is in accordance with the resolution of the available SGG data, and we have not continues coverage for the SGG data and we are restricted to a certain resolution. In Table 2.6 we present the minimum degree at which the relative error degree variances are larger than 0.1% as well as the degree of resolution obtained based on the error propagation of the random noise.

Table 2.6. Maximum degree of the geopotential coefficients determined from SGG data at 250 km level until 1% relative errors degree variances between true and estimated coefficients as well as degree of resolution.

	$30' \times 30'$	$15' \times 15'$	$10' \times 10'$	$5' \times 5'$
VV $T_{zz}(P)$	148-175	186-190	206-202	240-218
VH $T_{xz}(P)$ and $T_{yz}(P)$	179-175	215-190	235-202	267-218
HH $T_{xx}(P)-T_{yy}(P)$ and $2T_{xy}(P)$	155-164	191-181	211-189	245-202

For each solution of the gradiometric analysis and resolution we have given two numbers. The first number is the signal degree at which the relative error degree variance exceeds 1% and the second number is the degree of resolution discussed above. The table shows slow changes in the degree of resolution by increasing the resolution of numerical integration. The degree of resolution is the same for the first and second integrals.

2.9 Average power of gravitational gradients

Another way to estimate the cut-off degree of the spherical harmonic expansion is to use the average power of the gravitational gradients. In this section we consider the three solutions of the GBVPs to estimate this cut-off degree. In other words, we are going to find a way to see how much the attenuation factor reduce the gravitational signal. We start to formulate the average acceleration power in the following.

The average power of the VV solution of the GBVPs is derived by squaring Eq. (2.62a) and taking the global average:

$$\frac{1}{4\pi}\iint_{\sigma}\left[\mathbf{T}^{(1)}\right]^2 d\sigma=\left(\frac{GM}{R^3}\right)^2\sum_{n=2}^{\infty}\sum_{n'=2}^{\infty}(n+1)(n+2)(n'+1)(n'+2)\sum_{m=-n}^{n}\sum_{m'=-n'}^{n'} t_{nm}t_{n'm'}\frac{1}{4\pi}\iint_{\sigma}\mathbf{Z}_{nm}^{(1)}(Q)\mathbf{Z}_{n'm'}^{(1)}(Q)d\sigma\,. \tag{2.99}$$

Considering the orthogonality property of the TSHs (see Eq. 2.66) we can write:

$$\frac{1}{4\pi}\iint_{\sigma}\left[\mathbf{T}^{(1)}\right]^2 d\sigma = \left(\frac{GM}{R^3}\right)^2 \sum_{n=2}^{\infty}(n+1)^2(n+2)^2\left(\frac{R}{r}\right)^{2n+6} t_n \,, \qquad (2.100)$$

where $t_n = \sum_{m=-n}^{n} t_{nm}^2$ is the degree variance of the disturbing potential.

In a very similar way, the average power acceleration of the VH solution of the GBVP is derived by squaring and global averaging of Eq. (2.62b):

$$\frac{1}{4\pi}\iint_{\sigma}\left[\mathbf{T}^{(2)}\right]^2 d\sigma = 4\left(\frac{GM}{R^3}\right)^2 \sum_{n=2}^{\infty}\sum_{n'=2}^{\infty}(n+2)(n'+2)\sum_{m=-n}^{n}\sum_{m'=-n'}^{n'} t_{nm}t_{n'm'}\frac{1}{4\pi}\iint_{\sigma}\mathbf{Z}_{nm}^{(2)}(Q)\mathbf{Z}_{n'm'}^{(2)}(Q)d\sigma \,, \qquad (2.101a)$$

Correspondingly we have:

$$\frac{1}{4\pi}\iint_{\sigma}\left[\mathbf{T}^{(2)}\right]^2 d\sigma = 2\left(\frac{GM}{R^3}\right)^2 \sum_{n=2}^{\infty}(n+2)^2 n(n+1)\left(\frac{R}{r}\right)^{2n+6} t_n \,. \qquad (2.101b)$$

and the average power of the HH solution of the GBVP is obtained by squaring and global averaging Eq. (2.63):

$$\frac{1}{4\pi}\iint_{\sigma}\left[\mathbf{T}^{(3)}\right]^2 d\sigma = 4\left(\frac{GM}{R^3}\right)^2 \sum_{n=2}^{\infty}\sum_{n'=2}^{\infty}\sum_{m=-n}^{n}\sum_{m'=-n'}^{n'} t_{nm}t_{n'm'}\frac{1}{4\pi}\iint_{\sigma}\mathbf{Z}_{nm}^{(3)}(Q)\mathbf{Z}_{n'm'}^{(3)}(Q)d\sigma \,, \qquad (2.102a)$$

and finally

$$\frac{1}{4\pi}\iint_{\sigma}\left[\mathbf{T}^{(3)}\right]^2 d\sigma = \frac{1}{2}\left(\frac{GM}{R^3}\right)^2 \sum_{n=2}^{\infty}(n-1)n(n+1)(n+2)\left(\frac{R}{r}\right)^{2n+6} t_n \,. \qquad (2.102b)$$

Actually these average powers of the gravitational gradients were presented by Rummel (1997). In Eqs. (2.100), (2.101b) and (2.102b) the upper bound of the summation goes to infinity, which is not meaningful in practice. Here we will limit this upper bound to a certain value using the method presented by Hwang and Lin (1998) to estimate the cut-off degree of this average power. Let $p_k^{(i)}$, *i=1*,2 and 3, be the average power of the gradients at degree *k*:

$$p_k^{(1)} = \left(\frac{GM}{R^3}\right)^2 \sum_{n=2}^{k}(n+1)^2(n+2)^2\left(\frac{R}{r}\right)^{2n+6} t_n \,, \qquad (2.103a)$$

$$p_k^{(2)} = 2\left(\frac{GM}{R^3}\right)^2 \sum_{n=2}^{k}(n+2)^2 n(n+1)\left(\frac{R}{r}\right)^{2n+6} t_n \,, \qquad (2.103b)$$

$$p_k^{(3)} = \frac{1}{2}\left(\frac{GM}{R^3}\right)^2 \sum_{n=2}^{k}(n-1)n(n+1)(n+2)\left(\frac{R}{r}\right)^{2n+6} t_n \,. \qquad (2.103c)$$

By assuming that a satellite at 250 km level cannot sense higher frequencies than $N_{\max} = 360$, we can compute the full average power of the gradients. After that we compute these average powers at different degrees up to $N_{\max}$ to present the average power in larger relative errors. The following parameter is introduced as a criterion for this truncation degree:

$$\left(1 - \frac{p_k^{(i)}}{p_{N_{\max}}^{(i)}}\right) \le c \,, \qquad (2.104)$$

We should investigate at which cut-off degree *k*, the ratio $p_k^{(i)} \big/ p_{N_{\max}}^{(i)}$ is equal to 1. However, we know that this ratio will not be equal to 1 and we have to select a value for *c* which shows how this ratio is close to 1. Table 2.7 shows the cut-off degree based on different values of *c*.

Table 2.7. Cut-off degrees of the gradients based on different criteria

c	10^{-10}	10^{-11}	10^{-12}	10^{-13}	10^{-14}
$\mathbf{T}^{(1)}$	249	278	307	334	353
$\mathbf{T}^{(2)}$	254	283	312	338	355
$\mathbf{T}^{(3)}$	271	300	328	350	358
average	254	282	311	338	355

Hwang and Lin (1998) considered $c = 10^{-14}$ according to Institute of Electrical and Electronics Engineers (IEEE) double-precision environment. It means that the beyond degrees, these presented cut-off degrees are in the noise level according to the IEEE convention. The cut-off degree for $\mathbf{T}^{(3)}$ is larger than for the others, which is not in agreement with those cut-off degrees obtained based on degree of resolution and discretization. However, it can be mentioned, that in the best possible case, the gravitational gradients do not sense higher frequencies than 360, or in other words, there is no information beyond cut-off degree in gravitational gradients. It should also be mentioned that these results are based on $c = 10^{-14}$, but one can change this number to change the cut-off degree. If we assume that $c = 10^{-14}$ the cut-off degree is about 360 for a satellite at 250 km level. If we decrease the satellite altitude higher cut-off degree is delivered.

Chapter 3

Topographic and atmospheric effects

3. 1 Introduction

The satellite gravity gradiometry (SGG) data are affected by the masses of topography and the atmosphere. The topographic effect (TE) has been considered by several geodesists (e.g. Martinec et al. 1993, Martinec and Vaníček 1994, Sjöberg 1998a, Sjöberg and Nahavandchi 1999, Tsoulis 2001, Heck 2003, Seitz and Heck 2003, Sjöberg 2000 and 2007). The main goal of these efforts was to compute the TE on geoid and terrestrial gravimetric data and also considering terrain correction. Wild and Heck (2004a) and (2004b) have considered this effect on SGG data. Makhloof and Ilk (2005) and (2006) worked on the topographic-isostatic effects on airborne gravimetry, satellite gravimetry and gradiometry. More details about their work can be found in Makhloof (2007). Novák and Grafarend (2006) presented a method for computing the TE and atmospheric effect (AE) in SGG. Considering a constant density (2.67 g/cm^3) for the topographic masses introduces errors in harmonitisation of the space before downward continuation. Most of the efforts in this subject were done for geoid determination aspects, see e.g., Martinec (1993), Martinec et al. (1995), Kuhtreiber (1998), Pagiatakis and Armenkis (1999), Tziavos and Featherstone (2000) and Huang et al. (2001). Sjöberg (2004) showed that the total effect on the geoid due to the lateral density variation (LDV) of topographic masses at deepest and highest parts of the Earth is about 1.5 cm and 1.78 m, respectively. Kiamehr (2006a) and (2006b) showed that the lateral density variation effect (LDVE) of topographic masses can reach to 30 cm in Iran. Eshagh (2009d) estimated the LDVE of the crustal density on the SGG data. Since at satellite altitude the geopotential can be regarded as harmonic, the external type of spherical harmonic expansions of the global topography and atmosphere is considered, and converted them into harmonic series of the potentials. Knowing the gravitational potentials generated by topography and atmosphere would allow for removing these effects from the geopotential. The result is the no-topography and no-atmosphere geopotentials, which is thus harmonic all the way down to sea level and the SGG data can be directly continued downward to the sea level for the local gravity field

determination. Therefore it is necessary to consider the gravitational effects of the topography and static atmosphere to smooth the gravity field and simplify the downward continuation process. Some primary assumptions are needed for considering the AEs. The atmosphere is usually assumed to be layered spherically above a sphere approximating the Earth surface. Also Moritz (1980), Sjöberg (1993), (1998b), (1999), and (2001), Sjöberg and Nahavandchi (2000) and Nahavandchi (2004) used spherical approximation of sea level and considered the topographic heights with respect to this sphere in geoid determination purpose.

Ecker and Mittermayer (1969) used an ellipsoidal approach to study the atmospheric gravitational potential and acceleration; they proposed a mathematical model for the direct AE, which is well-known as the International Association of Geodesy (IAG) approach. Anderson et al. (1975) considered the effect of the atmospheric masses in physical geodesy problems and computed the global values of the AE on gravity and the geoid. Sjöberg (1993) investigated the effect of terrain in the atmospheric gravity and geoid corrections, Sjöberg (1998b) presented the atmospheric correction on the gravity anomaly, geoid and on the satellite derived geopotential coefficients. Sjöberg (1999) found some shortcomings in the IAG approach in atmospheric geoid correction and proposed a new strategy to solve the shortcomings. Sjöberg and Nahavandchi (2000) investigated the direct and indirect effects of the atmosphere in the modified Stokes formula and they showed that the AE on the geoid can reach 40 cm. Novák (2000) presented a density model for the atmosphere based on a simple polynomial fitting and used that model to compute the AE on the geoid. The polynomial function was used only for atmospheric mass density modeling within the topography, i.e., below the elevation of highest spot on the Earth (approximately 10 km above the mean sea level). The atmospheric masses above 10-km elevation can be considered by using United States Standard Atmospheric model (USSA76) (United State atmosphere 1976). For more details about his method see e.g. Novák (2000). Sjöberg (2001) investigated the atmospheric correction and found that the atmosphere contributes with the zero-degree harmonic of magnitude of 1 cm on the geoid. Nahavandchi (2004) presented another strategy for the direct atmospheric gravity effect in geoid determination. He numerically compared his new strategy with old formulas in Iran and found 17 cm difference on the geoid between both formulas in that region, but as Sjöberg (1998b) argued the direct effect is considerably reduced after restoring the AE. Sjöberg (2006) showed that the AE in geoid determination needs a correction for the geometry when applying the spherical approximation of Stokes' formula. According to his conclusions the correction needed to the AE in spherical Stokes formula varies between 0.3 and 4.0 cm on the geoid at the equator and pole, respectively. Tenzer et al. (2006) considered the effect of atmospheric masses with concentration on the direct and secondary indirect AEs for Stokes problem. They found the complete effect of the atmosphere on the ground gravity anomaly varies between 1.75 and 1.81 mGal in Canada, and the effects are mainly dependent on the accuracy of the atmospheric density model (ADM). Novák and Grafarend (2006) proposed a method to compute the effect of topographic and atmospheric masses on space-borne data based on a spherical harmonic expansion with a numerical study in North America.

In this chapter the topographic and atmospheric potentials are formulated in spherical harmonics. The LDV of the topographic masses is considered and numerically tested. The SHCs are formulated based on different analytical ADMs for the atmospheric densities and a new model is proposed. By substituting the formulated and derived SHCs into the spherical harmonic expressions of the gravitational gradients, the corresponding effects can be computed. The topographic and atmospheric biases are also formulated in spherical harmonics at the end of the chapter.

3. 2 Topographic and atmospheric potentials in spherical harmonics

In order to explain how the SHCs of the topographic and atmospheric potential are derived, we start our mathematical explanation with the well-known Newtonian volume integral

$$V^{\,\mathrm{t,a}}(P) = G \iint_{\sigma} \int_{a}^{b} \frac{\rho(r') r'^2 dr'}{l} d\sigma, \tag{3.1}$$

for the topographic and atmospheric potential at point P, where G is the Newtonian gravitational constant, l is the distance between any points P and Q, a and b are the integral limits depending on what potential is being considered, either topographic or atmospheric potential. For the former $a=R$ and $b=R+H$ and for the latter $a = R + H$ is the geocentric radius of the Earth surfaces (H is orthometric height), $b = R + Z$ is the radius of the upper bound of the atmosphere. $\rho(r')$ is either the topographic or atmospheric density at geocentric radius of point Q, σ is the unit sphere of integration and $d\sigma$ is the integration element. The inverse distance l can be expanded in an external or internal series of the Legendre polynomial as:

$$\frac{1}{l} = \frac{1}{r} \sum_{n=0}^{\infty} \left(\frac{r'}{r} \right)^n P_n(\cos\psi), \text{ if } r > r' \tag{3.2a}$$

$$\frac{1}{l} = \frac{1}{r'} \sum_{n=0}^{\infty} \left(\frac{r}{r'} \right)^n P_n(\cos\psi), \text{ if } r' > r. \tag{3.2b}$$

Equations (3.2a) and (3.2b) are the external and internal types of the Legendre expansion of $1/l$. $P_n(\cos\psi)$ is the Legendre polynomial of degree n and ψ stands for the geocentric angle between points P and Q. Equations (3.3a) and (3.3b) are used in generating the external and internal type of atmospheric potentials, respectively. Another useful formula is the addition theorem of the fully-normalized spherical harmonics (Heiskanen and Moritz 1967, p.33, Eq. 1-82'):

$$P_n(\cos\psi) = \frac{1}{(2n+1)} \sum_{m=-n}^{n} Y_{nm}(Q) Y_{nm}(P). \tag{3.3}$$

The gravitational potential $V(P)$ is harmonic out side the Earth's surface and can be expanded into an external harmonic series. Based on it, the computation point is outside or inside the topographic and atmospheric masses, we can consider the external and internal type of spherical harmonic expressions for their corresponding potentials as follow:

$$V_{\text{ext}}(P)=\frac{GM}{R}\sum_{n=0}^{\infty}\left(\frac{R}{r}\right)^{n+1}\sum_{m=-n}^{n}\left(v_{\text{ext}}\right)_{nm}Y_{nm}(P)\quad\text{where}\quad r\geq R \tag{3.4a}$$

and

$$V_{\text{int}}(P)=\frac{GM}{R}\sum_{n=0}^{\infty}\left(\frac{r}{R}\right)^{n}\sum_{m=-n}^{n}\left(v_{\text{int}}\right)_{nm}Y_{nm}(P)\quad\text{where}\quad r<R\,, \tag{3.4b}$$

respectively, where GM is the geocentric gravitational constant, R stands for the mean radius of the Earth, r is the geocentric radius of any point P with angular spherical coordinates (spherical co-latitude and longitude), $\left(v_{\text{ext}}\right)_{nm}$ and $\left(v_{\text{int}}\right)_{nm}$ are the SHCs of the external and internal types of the atmospheric potential, respectively, and δ is Kronecker's delta. We assume that the point P is at satellite level, which means that the topographic and atmospheric masses are below P and Eq. (3.4a) hold for the external potential of the atmosphere and topography.

3.3 External and internal topographic potentials in spherical harmonics

The external type of the topographic potential is the case where the point P is outside of topographic features, in other words, it is above the topography. However, when this point is inside the topography, say at the geoid the potential of the topography is of internal type. The problem in this section is to derive the mathematical models of the SHCs of topography both in external and internal types. In the following we present the mathematical formulas of the external topographic potential.

Proposition 3.1 *The external type of SHCs of the topographic potential are*:

$$\left(V_{\text{ext}}^{\text{t}}\right)_{nm}\approx\frac{3}{\rho^{\text{e}}(2n+1)}\left[\frac{\left(\rho^{\text{t}}H\right)_{nm}}{R}+(n+2)\frac{\left(\rho^{\text{t}}H\right)^{2}_{nm}}{2R^{2}}+(n+2)(n+1)\frac{\left(\rho^{\text{t}}H\right)^{3}_{nm}}{6R^{3}}\right].$$

where $\left(\rho^{\text{t}}H\right)_{nm}$, $\left(\rho^{\text{t}}H^{2}\right)_{nm}$ *and* $\left(\rho^{\text{t}}H^{3}\right)_{nm}$ *are the SHCs of* $\rho^{\text{t}}H$, $\rho^{\text{t}}H^{2}$ *and* $\rho^{\text{t}}H^{3}$, *respectively.* ρ^{t} *is the topographic density with a global coverage, H,* H^{2} *and* H^{3} *are the powers of the topographic height all over the globe and* $\rho^{e}\approx 5500\ kg/m^{3}$ *is the mean density of the Earth's mass,*

Proof. Considering the external type of Legendre's series of $1/l$, i.e. Eq. (3.2a) into Newton's integral Eq. (3.1) and assuming the topographic density to change laterally we can write:

$$V^{\mathrm{t}}(P)=G\sum_{n=0}^{\infty}r^{-(n+1)}\iint_{\sigma}\frac{\rho^{t}R^{n+3}}{n+3}\left[\left(1+\frac{H}{R}\right)^{n+3}-1\right]P_{n}(\cos\psi)d\sigma\,. \tag{3.5}$$

Considering binomial expansion up to third-order for the first term in the square bracket and using addition theorem of the spherical harmonics, Eq. (3.3), we can further simplify Eq. (3.5)

$$V^{t}(P)\approx GR^{2}\sum_{n=0}^{\infty}\left(\frac{R}{r}\right)^{(n+1)}\frac{1}{2n+1}\sum_{m=-n}^{n}\iint_{\sigma}\left[\frac{\rho^{t}H}{R}+(n+2)\frac{\left(\rho^{t}H\right)^{2}}{2R^{2}}+(n+1)(n+2)\right.$$
$$\left.\frac{\left(\rho^{t}H\right)^{3}}{6R^{3}}\right]Y_{nm}(Q)d\sigma Y_{nm}(P)\,. \tag{3.6}$$

By solving the integral which is spherical harmonic analysis of the terms inside the square bracket and considering

$$GM=4\pi R^{3}\rho_{e}G/3\,, \tag{3.7}$$

the proposition is proven.

Proposition 5.1 is not a new formulas for the SHCs of topographic potential, but we have re-derived it as it is fitted to the spherical harmonic expansions that we have mentioned in the beginning of this chapter.

Corollary 3.1 *If* $\rho^{t}\approx 26667\ kg/\mathrm{m}^{3}$ *is the mean density of the topography the SHCs has the following form*:

$$\left(V^{\mathrm{t}}_{\mathrm{ext}}\right)_{nm}=\frac{3\rho^{\mathrm{t}}}{\rho^{\mathrm{e}}(2n+1)}\left[\frac{H_{nm}}{R}+(n+2)\frac{H^{2}{}_{nm}}{2R^{2}}+(n+2)(n+1)\frac{H^{3}{}_{nm}}{6R^{3}}\right],$$

where H_{nm}, H^{2}_{nm} *and* H^{3}_{nm} *are the SHCs of H,* H^{2} *and* H^{3}, *respectively. These coefficients can be obtained by a general spherical harmonic analysis of a global digital elevation model (DEM) such as GTOPO or SRTM (Wieczorek 2007).*

Proposition 3.2 *The internal type of SHCs of topographic potential is (Eshagh and Sjöberg 2008a)*:

$$\left(V^{\mathrm{t}}_{\mathrm{int}}\right)_{nm}=\frac{3}{\rho^{\mathrm{e}}(2n+1)}\left[\frac{\left(\rho^{\mathrm{t}}H\right)_{nm}}{R}-(n-1)\frac{\left(\rho^{\mathrm{t}}H\right)^{2}{}_{nm}}{2R^{2}}+n(n-1)\frac{\left(\rho^{\mathrm{t}}H\right)^{2}{}_{nm}}{6R^{3}}\right].$$

Proof. The proof is very similar to that of Proposition 3.1.

3.3.1 TE on the SGG data in LNOF

In order to compute the TE on the SGG data in LNOF, the generated SHCs of the TE are inserted to the harmonic expression of the gravitational gradients. In Chapter 2 we have considered the disturbing potential instead of true potential of the Earth's gravitational field, those expressions and the software developed based on them can be modified by adding the portion of the zero- and first-degree harmonics. The effect of these SHCs can be presented as (Eshagh and Sjöberg 2009a):

$$V_{zz}^{0,1}(P)=\frac{2GMR}{r^4}\left\{\frac{r}{R}C_{00}+3\sqrt{3}\left[C_{10}\cos\theta+\left(C_{11}\cos\lambda+S_{11}\sin\lambda\right)\sin\theta\right]\right\}, \quad (3.8a)$$

$$V_{xx}^{0,1}(P)=-\frac{GMR}{r^4}\left\{\frac{r}{R}C_{00}+3\sqrt{3}\left[C_{10}\cos\theta+\left(C_{11}\cos\lambda+S_{11}\sin\lambda\right)\sin\theta\right]\right\}, \quad (3.8b)$$

$$V_{yy}^{0,1}(P)=-\frac{GMR}{r^4}\left\{\frac{r}{R}C_{00}+3\sqrt{3}\left[C_{10}\cos\theta+\left(C_{11}\cos\lambda+S_{11}\sin\lambda\right)\sin\theta\right]\right\}, \quad (3.8c)$$

$$V_{xy}^{0,1}(P)=0, \quad (3.8d)$$

$$V_{xz}^{0,1}(P)=3\sqrt{3}\frac{GMR}{r^4}\left\{-C_{10}\sin\theta+\left(C_{11}\cos\lambda+S_{11}\sin\lambda\right)\cos\theta\right\}, \quad (3.8e)$$

and

$$V_{yz}^{0,1}(P)=3\sqrt{3}\frac{GMR}{r^4}\left(-C_{11}\sin\lambda+S_{11}\cos\lambda\right), \quad (3.8f)$$

where the superscripts 0 and 1 stand for the effects of the zero- and first-degree harmonics and C and S are the cosine and sine fully-normalized SHCs of the topographic potential. It is interesting to notice that the effect of these coefficients on $V_{xy}(P)$ is theoretically zero, and the zero-degree SHCs vanish also in $V_{xz}(P)$ and $V_{yz}(P)$. As can be seen, Eqs.(3.8a)-(3.8c) include both zero- and first-degree SHCs, therefore they could be large in magnitude. Eqs. (3.8e) and (3.8f) include just the first-degree harmonic, and since these harmonics are usually smaller than the zero-degree coefficients, the corresponding gravitational gradients can be expected to be smaller than the terms with zero-degree coefficients but larger than the higher degree effects. Equation (3.8d) shows that $V_{xy}(P)$ does not include these harmonics, and, consequently, it should have the smallest magnitude relative to the other gradients.

3.3.2 Numerical studies on TE on the SGG data over Fennoscandia and Iran

Numerical studies are performed for the regions limited by latitudes 55° and 70° and longitudes between 5° and 30° (Fennoscandia) and by the latitudes 25° and 40° and longitudes 44° and 64° (Iran); see Figure 3.1. The SHCs of the global topography

JGP95e (H. Fan private communication) was employed in the harmonic expansion to degree and order 360 for our computations. Novák and Grafarend (2006) suggested to select 180 as the maximum degree and order for the current orbital elevations of CHAMP and GRACE satellite missions (approximately 400 km), but we have considered GOCE satellite orbiting at approximate altitude of 250 km, which calls for a higher order set of potential coefficients.

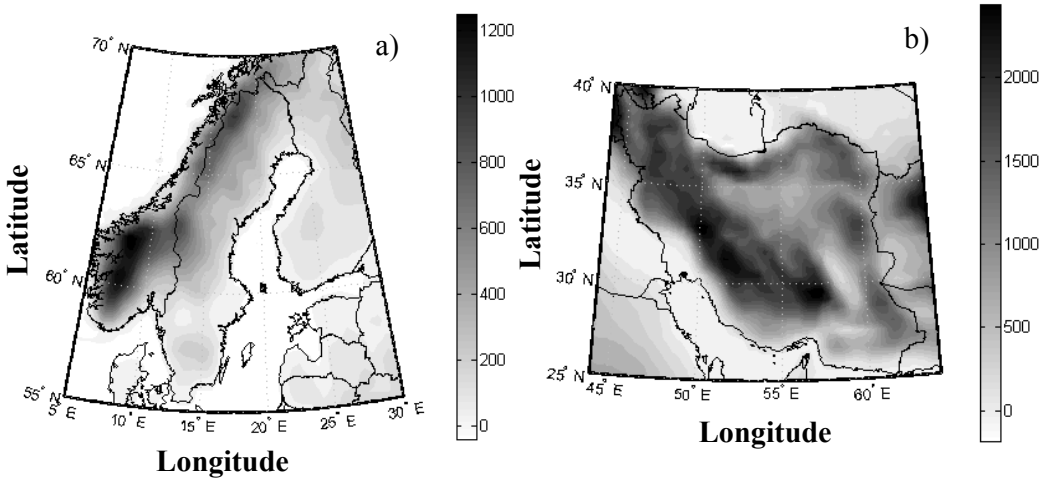

Figure 3.1. Long-wavelength topographic height of Fennoscandia and Iran obtained by SHCs of JGP95e global model to degree and order 360. Unit: 1 m

According to Figure 3.1 one can see that the topography of Iran is extended from south to north-west part, and the topography of Fennoscandia is extended from southern part of Norway to the north of Sweden. Figure 3.1 shows that the large volume of the topography is placed in the middle and south parts of Iran and it is placed in Norwegian mountains in the west of Fennoscandia.

A MATLAB program code was written, and it computes the SHCs of topographic and atmospheric potentials. These potential models are used to compute the SGG data in the LNOF according to the formulas presented in previous chapter and Eqs. (3.8a)-(3.8f). The program was used to compute maps of the TE at altitude of 250 km over the two study areas as well as their statistics. Figures 3.2 and 3.3 (a), (b), (c), (d), (e) and (f) present the TE on the SGG data $V_{xx}^{\mathrm{t}}(P)$, $V_{yy}^{\mathrm{t}}(P)$, $V_{zz}^{\mathrm{t}}(P)$, $V_{xy}^{\mathrm{t}}(P)$, $V_{xz}^{\mathrm{t}}(P)$ and $V_{yz}^{\mathrm{t}}(P)$, respectively in Fennoscandia and Iran. As can be seen, they are all in the order of a few Eötvös or less. According to Table 3.1 the maximum mean effect 0.10 E of the TE in Fennoscandia is related to $V_{zz}^{\mathrm{t}}(P)$, and the minimum mean effect is about 0.01 E and related to $V_{xy}^{\mathrm{t}}(P)$. The corresponding values are 0.64 E and -0.65 E in Iran, respectively. The effect is larger in magnitude in Iran, which topography is rougher and more massive than that in Fennoscandia.

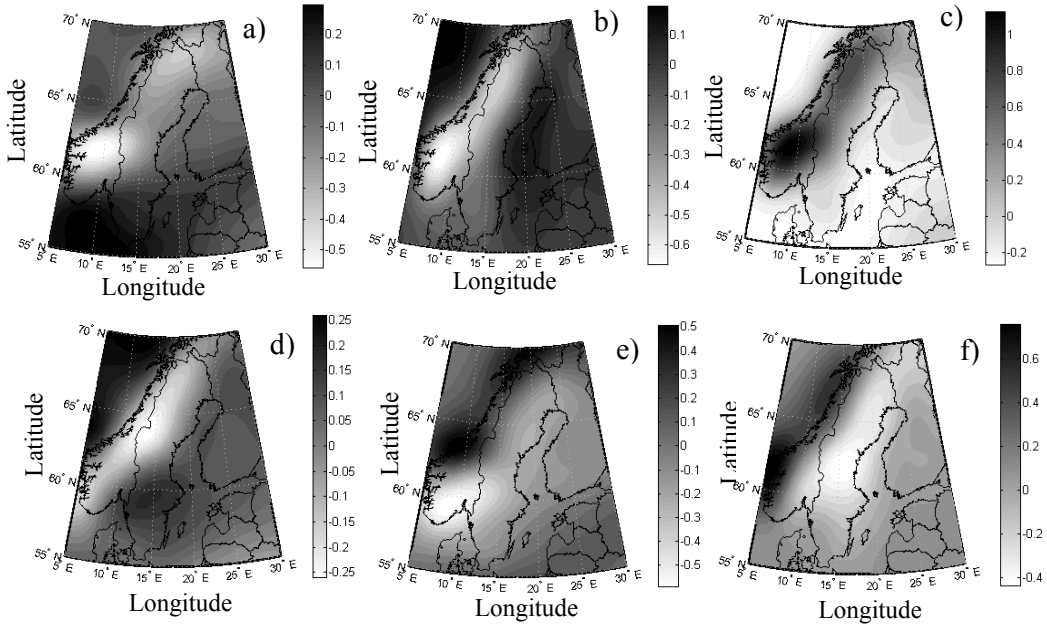

Figure 3.2. TE on SGG data in Fennoscandia in LNOF. Unit: 1 E.

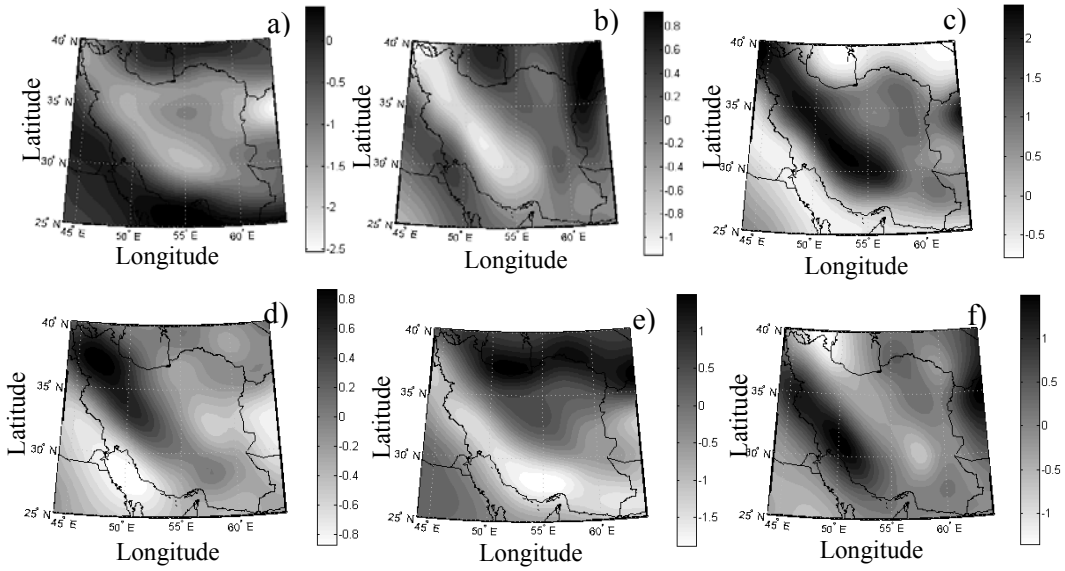

Figure 3.3. TE on SGG data in Iran in LNOF. Unit: 1 E.

Some geophysical interpretations can be made for the correlations of TE. For more details about geophysical interpretations of gravity gradients in exploration see Pawlowski and Prieto (1997), Pawlowski (1998), Mickus and Hinojosa (2001) and Li (2001a), (2001b) and (2001c). We consider such interpretations just for TE. (AE can be interpreted in a similar way). $V_{zz}^{\mathrm{t}}(P)$ is better related to topographic features compared to other gravitational gradients. $V_{xx}^{\mathrm{t}}(P)$ and $V_{yy}^{\mathrm{t}}(P)$ are related with the lateral extension of topographic features. If topography were aligned along meridians

the northern and southern sides of feature are related with $V_{xx}^{t}(P)$. The corresponding relation is true for $V_{yy}^{t}(P)$, when topography is extended along parallels. This matter can easily be seen in Figures 3.2(a) and 3.2(b) and Figures 3.3(a) and 3.3(b). $V_{xy}^{t}(P)$ is related to the corners of topographic features. By comparing Figures 3.2(d) and 3.3(d) with their corresponding topographic heights one can see this matter. Whenever topographic masses exist we can see very large negative values for this gravitational gradient in south-west and north-east sides of topography in both regions and large positive values can be seen in north-west and south-east parts of topography. $V_{yz}^{t}(P)$ and $V_{xz}^{t}(P)$ are related with the lateral dimension of topography with similar interpretation as $V_{xx}^{t}(P)$ and $V_{yy}^{t}(P)$. $V_{xx}^{t}(P)$ and $V_{yy}^{t}(P)$ are related to the extension with large positive *or* negative values, but $V_{yz}^{t}(P)$ and $V_{xz}^{t}(P)$ are related to the topographic features with positive *and* negative values, i.e. in one dimension we see positive values and in the other dimension we see the negative.

Table 3.1. Statistics of TE on SGG data in Fennoscandia and Iran in LNOF. Unit: 1 E.

	Fennoscandia				Iran			
	max	mean	min	std	max	mean	min	std
$V_{xx}^{t}(P)$	0.34	-0.02	-0.57	$\pm$ 0.19	0.59	-0.65	-2.57	$\pm$ 0.68
$V_{yy}^{t}(P)$	0.25	-0.07	-0.67	$\pm$ 0.20	1.05	0.01	-1.17	$\pm$ 0.48
$V_{zz}^{t}(P)$	1.23	0.10	-0.27	$\pm$ 0.34	2.63	0.64	-0.81	$\pm$ 0.94
$V_{xy}^{t}(P)$	0.29	0.06	-0.27	$\pm$ 0.11	0.98	-0.14	-0.89	$\pm$ 0.41
$V_{xz}^{t}(P)$	0.58	0.01	-0.60	$\pm$ 0.22	1.71	-0.10	-1.92	$\pm$ 0.92
$V_{yz}^{t}(P)$	0.84	0.08	-0.45	$\pm$ 0.24	1.66	0.20	-1.38	$\pm$ 0.57

3.3.1 LDVE of topography on the SGG data

In the above formulation the main assumption was a constant topographic density in radial direction. However, the LDV can also be considered. To this end, the LDV of topography using spherical harmonics we need a global model of the topographic density. Until know only CRUST2 model is available for the crustal density, which is the updated version of CRUST5.1 (Mooney et al. 1998). In this model the crust is divided into three layers, upper crust, middle crust and lower crust (Bassin et al. 2000). The crustal density and topography of the boundaries between each layer have been measured by seismic data with $2^{\circ} \times 2^{\circ}$ resolution corresponding degree and order of 90 in spherical harmonic expansion. Figure 3.4 shows the general structure of the crust in CRUST2 model. The topographic data of the crustal boundaries (boundaries between the crustal layers) are given with respect to sea level as Figure 3.4 shows. Figure 3.5 shows the LDV of the topographic features with respect to mean value of the upper crust in both regions of Fennoscandia and Iran.

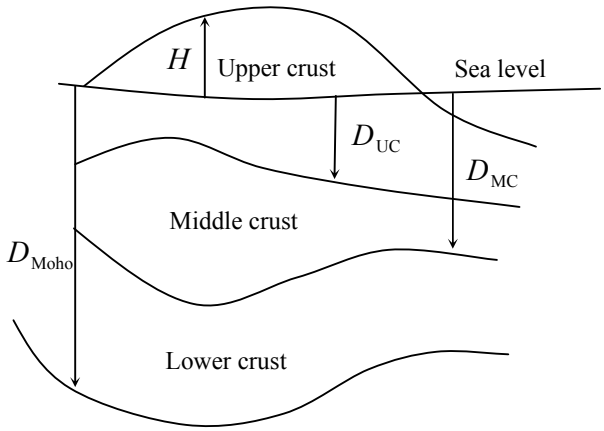

Figure 3.4 General schematic structure of crust in CRUST2

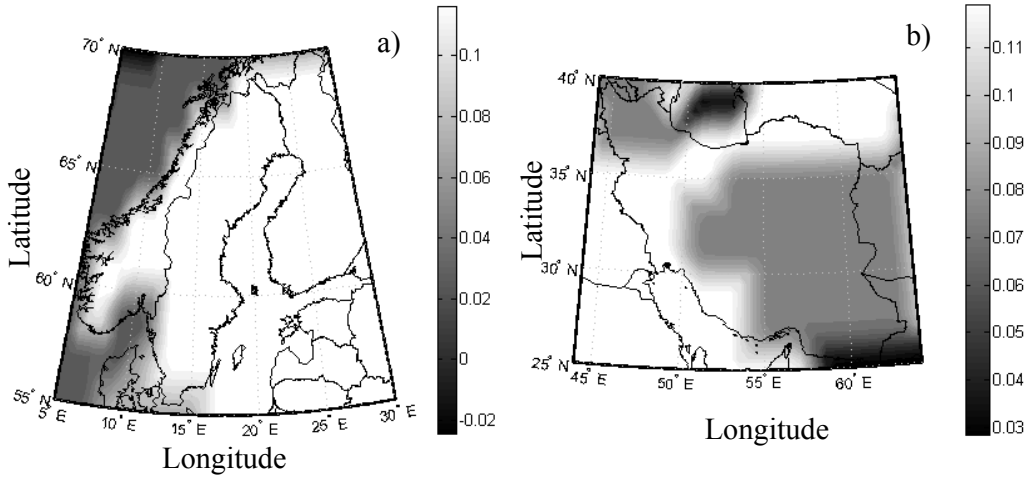

Figure 3.5. Long-wavelength LDV of upper crust in (a) Fennoscandia and (b) Iran. Unit: 1 g/cm^3

The topographic potential can be formulated in two different ways in spherical harmonics: one can use either the SHCs of the LDV or by the formulas presented for the topographic potential (Proposition 3.1). In the former method we will be involved with products of the SHCs of the height and LDV models and Clebsh-Gordan series, which will be slightly complicated; for formulation of this matter the reader is referred to Novák and Grafrarend (2006, pages 555-556). However, the method presented here is easier to use. As we know, topographic feature is a part of the upper crust. Therefore the LDV of the topography can also be considered by Proposition 3.1, but in this case we should replace ρ^t by $\Delta\rho^t$ as the LDV of the topography. In a similar way as topographic potential we can consider the LDV effect (LDVE) of the topography on the SGG data.

For numerical investigation we consider JGP95e global topographic model as we did for the previous numerical example for the TE. CRUST2 was generated with $2^\circ \times 2^\circ$ resolution corresponding degree and order 90 in spherical harmonic expansion. A grid of $0.5^\circ \times 0.5^\circ$ global density model was created based on a simple

interpolation, and the SHCs of $\left(\Delta\rho^{t}H\right)_{nm}$, $\left(\Delta\rho^{t}H^{2}\right)_{nm}$ and $\left(\Delta\rho^{t}H^{3}\right)_{nm}$ were generated based on a global spherical harmonic analysis up to degree and order 360, and the SHCs of the topographic potential was produced using Proposition 3.1. The formulas presented in the previous chapter for the gravitational gradients in the LNOF were used for generating the TE on the SGG data.

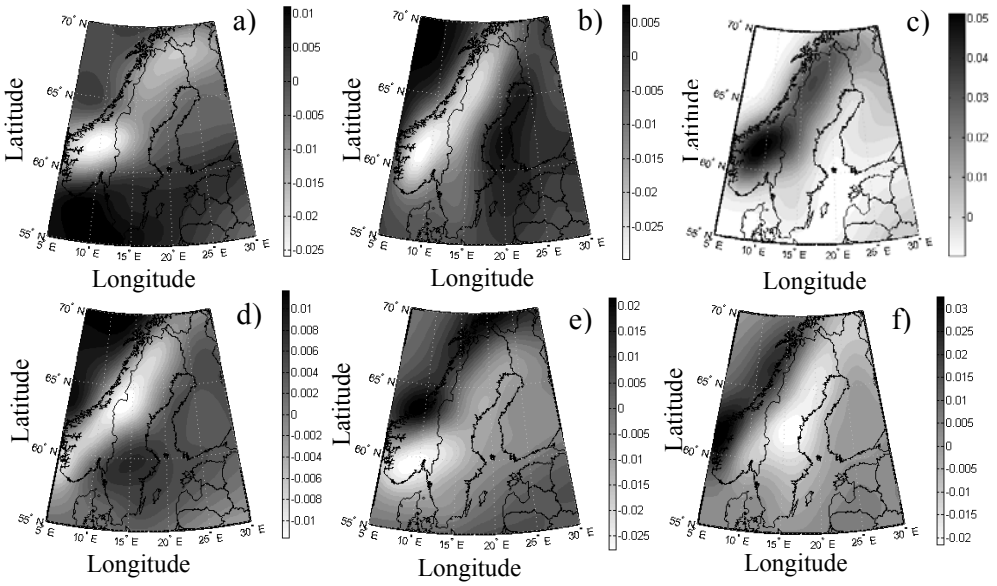

Figure 3.6. LDVE of topography in Fennoscandia in LNOF on (a) $V_{xx}(P)$, (b) $V_{yy}(P)$, (c) $V_{zz}(P)$, (d) $V_{xy}(P)$, (e) $V_{xz}(P)$ and (f) $V_{yz}(P)$, respectively. Unit: 1 E.

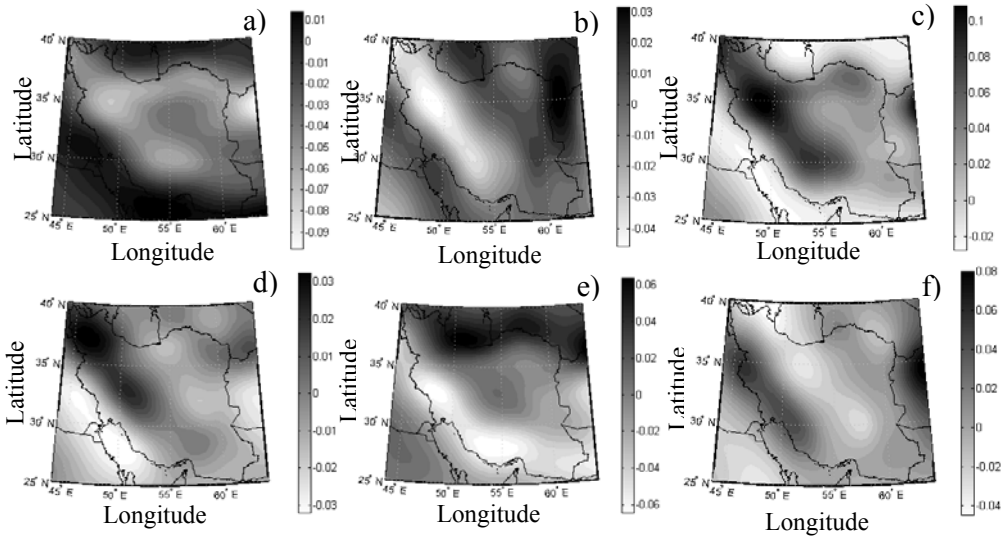

Figure 3.7. LDVE of topography in Iran in LNOF on (a) $V_{xx}(P)$, (b) $V_{yy}(P)$, (c) $V_{zz}(P)$, (d) $V_{xy}(P)$, (e) $V_{xz}(P)$ and (f) $V_{yz}(P)$, respectively. Unit: 1 E.

Figures 3.6 and 3.7 (a), (b), (c), (d), (e) and (f) present the LDVE of topography on the SGG data $V_{xx}(P)$, $V_{yy}(P)$, $V_{zz}(P)$, $V_{xy}(P)$, $V_{xz}(P)$ and $V_{yz}(P)$,

respectively, in Fennoscandia and Iran. Since Iran is topographically rougher than Fennoscandia we can see larger LDVE of topography in Iran than Fennoscandia. More details of the statistics of these computations are tabulated in Table 3.2.

Table 3.2. Statistics of LDVE of topography in Fennoscandia and Iran in LNOF. Unit: 1 mE.

	Fennoscandia				Iran			
	max	mean	min	std	max	mean	min	std
$V_{xx}(P)$	13.37	-1.88	-26.53	± 85.56	21.12	-23.04	-99.98	± 25.14
$V_{yy}(P)$	9.66	-4.25	-30.34	± 8.76	36.30	-1.38	-46.45	± 17.84
$V_{zz}(P)$	55.73	6.12	-10.22	± 15.32	116.72	24.41	-28.54	± 34.44
$V_{xy}(P)$	13.14	2.78	-12.05	± 5.36	36.28	-4.96	-32.61	± 14.71
$V_{xz}(P)$	24.98	0.44	-28.31	± 10.42	71.73	-3.39	-65.90	± 34.24
$V_{yz}(P)$	36.16	2.40	-22.04	± 11.06	88.14	4.60	-45.56	± 23.73

The maximum value of the LDVE of the topography is 116.72 mE in Iran and 55.73 mE in Fennoscandia and both are related to $V_{zz}(P)$. The minimum value is -99.98 mE in Iran related to $V_{xx}(P)$ but in Fennoscandia it is -30.34 mE on $V_{yy}(P)$. Maximum and minimum mean values of the LDVE of topography are 24.41 mE and -23.04 mE in Iran; and 6.12 mE and -4.25 mE in Fennoscandia.

3.4 External and internal atmospheric potentials in spherical harmonics

Unlike formulation of the SHCs of topographic potential, which was presented in previous section, we cannot assume that the atmospheric density changes laterally. The atmospheric density is very much related to the altitude, and this is reasonable to use some analytical models to formulate the atmospheric density. In this part of the study we assume that the LDV of the atmosphere is very small and negligible and the atmospheric density is modeled by some simple analytical formulas varying by elevation. We will present some analytical ADMs and express how to develop the atmospheric potential in spherical harmonics.

3.4.1 The ADMs

There are different models for the density of the atmosphere. One of the most well-known models was issued by NOAA (National Oceanic and Atmospheric Administration), NASA (National Aeronautics and Space Administration) and USAF(United State Air Force) as United States Standard Atmospheric model in 1976 (USSA76) (United State Standard Atmosphere 1976). This model is a complicated model depending on atmospheric pressure and molecular-scale temperature. For considering these parameters, the atmospheric masses (up to the height of 86 km), are divided into seven layers, and in each layer a molecular-scale temperature, and

pressure is defined according to some other mathematical model. In the following we review some ADMs and present a new ADM.

3.4.1.1 The Standard ADM (USSA76)

Among different ADMs, the one which is frequently used is the standard atmospheric density model (United State Standard Atmosphere 1976):

$$\rho^a(H) = \frac{\mu P(H)}{\kappa T(H)} \tag{3.9}$$

where κ = 8314.32 (N m km^{-1}K^{-1}) is the universal gas constant, μ = 28.9644 (kgkmol^{-1}) is mean molecular weight of the atmospheric masses, P = 101325 (Nm^{-2}) is the atmospheric pressure, and T = 288.12 K is the molecular-scale temperature of the atmosphere in K at sea level.

In this model the atmosphere between topography and height at 86 km is divided into 7 layers, in which the molecular-scale temperature and atmospheric pressure are modeled as:

$$\forall i = 1,2,...,7: \quad T(H) = T_i + \tau_i (H - H_i), \tag{3.10a}$$

$$\forall i \in \{1,3,4,6,7\}: P(H) = P_i \left[\frac{T_i}{T(H)}\right]^{\frac{g\mu}{\kappa\tau_i}}, \tag{3.10b}$$

$$\forall i \in \{2,5\}: P(H) = P_i \exp\left[\frac{-g\mu(H - H_i)}{\kappa\tau_i}\right], \tag{3.10c}$$

where H is the height within and H_i is the reference height of each layer, T_i is the reference value of the molecular-scale temperature for the i-th layer, τ_i is the molecular-scale temperature gradient; cf. Table 3.3, P_i stands for the reference pressure, g = 9.80665 ms^{-2} is the gravity value at sea level. The molecular temperature gradient of each layer is presented in Table 3.3.

Table 3.3. Molecular temperature gradients. Novák (2000)

Layer	Height (km)	τ_i (K km^{-1})
1	0-11	-6.5
2	11-20	+0.0
3	20-32	+1.0
4	32-48	+2.8
5	48-51	+0.0
6	51-71	-2.8
7	71-86	-2.0

This model is an updated version of standard ADM published in 1961. Table 3.4 shows the ascosporic density of these two standard ADMs and their differences.

Table 3.4. Values of the atmospheric mass density based on the USSA61 and USSA76. Unit: 1 kg/ m^3

Elevation (km)	USSA61	USSA76	difference
0	1.22	1.22	0.02×10^{-2}
2	1.01	1.00	-0.20×10^{-2}
4	8.24×10^{-1}	8.18×10^{-1}	-0.06×10^{-3}
6	6.65×10^{-1}	6.59×10^{-1}	-0.06×10^{-3}
8	5.27×10^{-1}	5.25×10^{-1}	-0.02×10^{-3}
10	4.09×10^{-1}	4.13×10^{-1}	0.03×10^{-3}
12	3.11×10^{-1}	3.11×10^{-1}	0.04×10^{-4}
14	2.32×10^{-1}	2.27×10^{-1}	-0.05×10^{-3}
16	1.70×10^{-1}	1.66×10^{-1}	-0.04×10^{-3}
18	1.23×10^{-1}	1.21×10^{-1}	-0.01×10^{-3}
20	8.80×10^{-2}	8.87×10^{-2}	0.07×10^{-4}
30	1.84×10^{-2}	1.84×10^{-2}	-0.35×10^{-4}
40	4.00×10^{-3}	3.99×10^{-3}	-0.79×10^{-5}
50	1.03×10^{-3}	1.02×10^{-3}	-0.21×10^{-5}

Later we will assume that the USSA76 model is a true ADM.

3.4.1.2 Exponential ADM

An exponential function for the atmospheric density can be considered as (Lambeck 1988):

$$\rho^{a}(r) = \rho_0 e^{-\alpha''(r-R)} = \rho_0 e^{\alpha'' R} e^{-\alpha'' r}, \tag{3.11}$$

where ρ_0 = 1.2227 kg/ m^3 the atmospheric density at sea level, R is the mean radius of the Earth, r is the radial distance of any point inside the atmosphere and α'' is a constant, which we will estimate later.

3.4.1.3 Sjöberg's ADM (KTHA)

The Sjöberg model is:

$$\rho^{a}(r) = \rho_0 \left(\frac{R}{r}\right)^{\nu}, \text{ where } \quad R \le r, \tag{3.12}$$

where, $\rho^{a}(r)$ is the atmospheric density, R (set to 6378137 m) is the Earth's mean radius, $R \le r \le R+Z$ is the geocentric radius of any point inside the atmosphere, ρ_0 =1.2227 kg/ m^3 is the atmospheric density at the sea level. We name this model

KTHA. The constant ν was derived by a simple fitting to the logarithmic scale of the atmospheric density too. The Sjöberg (1993) fitting was based on the USSA1961 (Reference Atmosphere Committee 1961) and this model was updated based on the USSA76 by Eshagh and Sjöberg (2009b). In the former case the exponent ν = 850 was derived, but in the latter (updated) model ν = 930 was achieved.

3.4.1.4 Novák's ADM (NADM)

The maximum value of the atmospheric density is at sea level and decreases fast with increasing elevation. Novák (2000) proposed the following model to approximate the vertical behaviour of the atmospheric density (NADM):

$$\rho^a(r) = \rho_0\left[1+\alpha H+\beta H^2\right], \tag{3.13}$$

where, α = -7.6495×10^{-5} m^{-1}, β = 2.2781×10^{-9} m^{-2} and $H = r\text{-}R$ with $0 \le H <$10 km. The other parameters of this model are the same as defined in the previous section. As Novák (2000) mentioned, his model fits the USSA76 with the accuracy of about 10^{-3} to up to 10 km above sea level. For higher elevations the USSA76 should be used.

3.4.1.5 New KTH ADM (NKTHA)

We now propose the following model (NKTHA) for the atmospheric density, which in fact is a direct combination of the NADM and KTHA. This model was proposed by Eshagh and Sjöberg (2009b):

$$\rho^a(r) = \begin{cases} \rho_0\left[1+\alpha H+\beta H^2\right], & 0 \le H \le H_0 \\ \rho^a(H_0)\left(\dfrac{R+H_0}{r}\right)^{\nu''}, & H_0 \le H \le Z \end{cases}, \tag{3.14}$$

where H_0=10 km and $\rho^a(H_0)$=0.4127 kg/m^3 is based on the NADM. By using this ADM we approximate the atmospheric density at higher levels by a simple model and it can be considered up to satellite level. The parameter ν''=890 was derived based on a simple least-squares fit to the USSA76 elevations of above 10 km.

3.4.2 External and internal atmospheric potential based on NADM and USSA76

Generally, a spherical approximation of sea level of the Earth and no atmosphere outside a sphere extending 86 km above sea level (maximum height considered in the standard atmospheric model) is assumed. As Ecker and Mittemayer (1969) presented, more than 99% of the atmospheric masses are included up to the elevation of 50 km. This is why some users select this level as the upper bound of the atmospheric masses

(see e.g., Novák and Grafarend 2006). However, Wallace and Hobbs (1977) believes that this value is at 30 km and also Lambeck (1988) mentioned that 80% of the atmospheric masses are below 12 km; therefore Novák's (2000) proposition to consider a simple polynomial to formulate the atmospheric density below 10 km height is not so far from reality.

Based on Eq. (3.11) the external atmospheric potential can easily be formulated using the Newtonian integral and spherical harmonics. In this case we can write the SHCs of the atmospheric potential in the following.

Proposition 3.3 *(Novák and Grafarend 2006):*

$$\left(V_{\text{ext}}^{\text{a}}\right)_{nm} \approx \frac{3\rho^{a}}{\rho^{e}\left(2n+1\right)}\left\{\frac{Z\,\delta_{n0}-H_{nm}}{R}+\left(n+2-\alpha' R\right)\frac{Z^{2}\delta_{n0}-H_{nm}^{2}}{2R^{2}}+\left[\left(n+2\right)\right.\right.$$
$$\left.\left.\left(n+1-2\alpha' R\right)+2\beta' R^{2}\right]\frac{Z^{3}\delta_{n0}-H_{nm}^{3}}{6R^{3}}\right\}\ .$$

Since the constant Z is the upper bound of the atmospheric masses and only contributes to the zero-degree harmonic. H_{nm}, H_{nm}^{2} and H_{nm}^{3} are the SHCs of H, H^{2} and H^{3}, respectively. The internal potential of the atmosphere in spherical harmonics will have the form.

Proposition 3.4 *The internal type of SHCs of the atmospheric potential based on NADM is (Eshagh and Sjöberg 2008a)*:

$$\left(V_{\text{int}}^{a}\right)_{nm} \approx \frac{3\rho^{a}}{\rho^{e}\left(2n+1\right)}\left\{\frac{Z\,\delta_{n0}-H_{nm}}{R}-\left(n-1-\alpha' R\right)\frac{Z^{2}\delta_{n0}-H_{nm}^{2}}{2R^{2}}+\left[\left(1-n\right)\left(n+2\alpha' R\right)-\right.\right.$$
$$\left.\left.-2\beta' R^{2}\right]\frac{Z^{3}\delta_{n0}-H_{nm}^{3}}{6R^{3}}\right\}.$$

Proof. In order to obtain the direct AE, $1/l$ is expanded using Eq. (3.2a) which is the external expansion of $1/l$. Inserting Eqs.(3.11) and (3.3b) into Eq. (3.1) and considering $b \approx R+Z$ and $a \approx R+H$ in Eq.(3.2) the external atmospheric potential is (subscript ext stands for external type of potential):

$$V_{\text{ext}}^{\text{a}}\left(P\right)=G\rho_{0}\sum_{n=0}^{\infty}r^{n}\iint_{\sigma}\int_{R+H}^{R+Z}\left[1+\alpha'\left(r'-R\right)+\beta'\left(r'-R\right)^{2}\right]r'^{\left(-n+1\right)}dr'P_{n}\left(\cos\psi\right)d\sigma\,. \tag{3.15}$$

The radial integral can be separately written as:

$$\int_{R+H}^{R+Z}\left[1+\alpha'\left(r'-R\right)+\beta'\left(r'-R\right)^2\right]r'^{-n+1}dr' = \left(1-\alpha R+\beta R^2\right)\int_{R+H}^{R+Z} r'^{-n+1}dr' + \left(\alpha-2R\beta\right)$$
$$\int_{R+H}^{R+Z} r'^{-n+2}dr' + \beta\int_{R+H}^{R+Z} r'^{-n+3}dr' = I_n \ , \tag{3.16}$$

and the solution of this integral is

$$I_n = \frac{\left(1-\alpha' R+\beta' R^2\right)R^{-n+2}}{-n+2}\left[\left(1+\frac{Z}{R}\right)^{-n+2}-\left(1+\frac{H}{R}\right)^{-n+2}\right]+\frac{\left(\alpha'-2\beta' R\right)R^{-n+3}}{-n+3}$$
$$\left[\left(1+\frac{Z}{R}\right)^{-n+3}-\left(1+\frac{H}{R}\right)^{-n+3}\right]+\frac{\beta' R^{-n+4}}{-n+4}\left[\left(1+\frac{Z}{R}\right)^{-n+4}-\left(1+\frac{H}{R}\right)^{-n+4}\right]. \tag{3.17}$$

Using the binomial expansion for the above terms in the brackets up to third-order the singularities in Eq. (3.17) are cancelled out. After relatively long derivations we obtain

$$F_{\text{int}}^{\text{a}}\left(Q\right) = R^{-n+2}\left\{\frac{Z-H}{R}-\left(n-1-\alpha' R\right)\frac{Z^2-H^2}{2R^2}-\left[\left(1-n\right)\left(n+2\alpha' R\right)-2\beta' R^2\right]\right.$$
$$\left.\frac{Z^3-H^3}{6R^3}\right\}. \tag{3.18}$$

Considering Eqs. (3.18) and (3.15) we obtain

$$V_{\text{int}}^{\text{a}}\left(P\right) = GR^2\rho_0\sum_{n=0}^{\infty}\left(\frac{r}{R}\right)^n\iint_{\sigma}F_{\text{int}}^{\text{a}}\left(Q\right)P_n\left(\cos\psi\right)d\sigma \tag{3.19}$$

According to the addition theorem of the fully-normalized spherical harmonics the proposition is proven.

The atmospheric model presented by Novák (2000) is valid just to 10 km elevation. His main goal for providing such a model was just to formulate the atmospheric roughness. For the atmospheric densities above 10 km, we use the standard atmospheric model (United State Atmosphere, 1976). We can consider atmospheric shells from 10 km to 86 km (which is the upper bound of the atmosphere in USSA76) with a thickness of 100 m (710 atmospheric shells) to generate the corresponding potentials. The effect of these shells, which contributes to the zero-degree harmonic of the atmospheric potential, are formulated in the following.

Proposition 3.5 *The external type of atmospheric potential due to the atmospheric shells above 10 km based on USSA76 is (Eshagh and Sjöberg 2008a)*:

$$\left(\delta V^{\mathrm{a}}_{\mathrm{ext}}\right)_0 = \frac{3}{\rho^{\mathrm{e}}}\left\{\left(1+\frac{Z_{j+1}}{R}\right)^3 \rho^{\mathrm{a}}_j - \left(1+\frac{Z_i}{R}\right)^3 \rho^{\mathrm{a}}_i + \sum_{k=i+1}^{j}\left(1+\frac{Z_k}{R}\right)^3\left(\rho^{\mathrm{a}}_{k-1}-\rho^{\mathrm{a}}_k\right)\right\},$$

where, ρ^{a}_i is the atmospheric density of each shell, Z_{j+1} and Z_i are the highest and lowest bounds of the atmospheric masses. Z_k is the upper bound of the atmospheric shell which is inside the atmospheric masses. i, j and k are the atmospheric shell numbers.

Proof. The integral formulas of the external type of potential of a spherical shell with the density ρ^{a}_i is (see also Sjöberg 2007, Eq. 16):

$$V^{\mathrm{a}}_{\mathrm{ext}}(P) = \frac{4\pi G\rho^{\mathrm{a}}_i}{r_P}\int_{R+Z_i}^{R+Z_{i+1}} r'^2 dr' = \frac{4\pi G\rho^{\mathrm{a}}_i}{3r_P}\left[\left(R+Z_{i+1}\right)^3 - \left(R+Z_i\right)^3\right], \quad (3.20)$$

The solution of this integral will be

$$V^{\mathrm{a}}_{\mathrm{ext}}\left(P\right) = \frac{GM}{R}\frac{R}{r_P}\frac{3\rho^{\mathrm{a}}_i}{\rho^{\mathrm{e}}}\left[\left(R+Z_{i+1}\right)^3 - \left(R+Z_i\right)^3\right], \quad (3.21)$$

yielding

$$\left(\delta V^{\mathrm{a}}_{\mathrm{ext}}\right)_0 = \frac{\rho^{\mathrm{a}}_i}{\rho^{\mathrm{e}}}\left[\left(1+\frac{Z_{i+1}}{R}\right)^3 - \left(1+\frac{Z_i}{R}\right)^3\right]. \quad (3.22)$$

This potential contributes only to the zero-degree harmonic is related to one atmospheric shell confined between Z_{i+1} and Z_i elevations. The subscript 0 means the potential which is added just to the zero-degree harmonic. The total potential of all shells is a summation of potential of each atmospheric shell as in Eq.(3.22).

Proposition 3.6 *The internal type of atmospheric potential of the atmospheric shells, contributing with the zero-degree harmonic can be written (Eshagh and Sjöberg 2008a)*:

$$\left(\delta V^{\mathrm{a}}_{\mathrm{int}}\right)_0 = \frac{3}{2\rho^{\mathrm{e}}}\left\{\left(1+\frac{Z_{j+1}}{R}\right)^2 \rho^{\mathrm{a}}_j - \left(1+\frac{Z_i}{R}\right)^2 \rho^{\mathrm{a}}_i + \sum_{k=i+1}^{j}\left(1+\frac{Z_k}{R}\right)^2\left(\rho^{\mathrm{a}}_{k-1}-\rho^{\mathrm{a}}_k\right)\right\},$$

where. i, j and k are the same as those introduced in Proposition 3.5.

Proof. In a similar manner, the integral formula of internal type of the potential of a spherical shell with the density ρ^{a}_i is (Sjöberg 2007):

$$\left(\delta V^{\,\mathrm{a}}_{\mathrm{int}}\right)_0 = 4\pi G\,\rho_i^{\mathrm{a}} \int_{R+Z_i}^{R+Z_{i+1}} r'dr' = 2\pi G\,\rho_i^{\mathrm{a}}\left[\left(R+Z_{i+1}\right)^2 - \left(R+Z_i\right)^2\right], \qquad (3.23a)$$

also

$$\left(\delta V^{\,\mathrm{a}}_{\mathrm{int}}\right)_0 = \frac{GM}{R}\frac{3\rho_i^{\mathrm{a}}}{2\rho^{\mathrm{e}}}\left[\left(1+\frac{Z_{i+1}}{R}\right)^2 - \left(1+\frac{Z_i}{R}\right)^2\right], \qquad (3.23b)$$

and the summation of all the atmospheric shells can be written in the form of the equation presented in this proposition.

3.4.2.1 Numerical studies on AE on the SGG data over Iran and Fennoscandia

Again, we consider Iran and Fennoscandia in the numerical investigations. The same data is used in this study as in the previous case study on TE. However, in this study we use NADM and USSA76 in order to generate the SHCs of the atmospheric potential. The AEs on the SGG data at satellite altitude 250 km are presented in Figures 3.8 and 3.9.

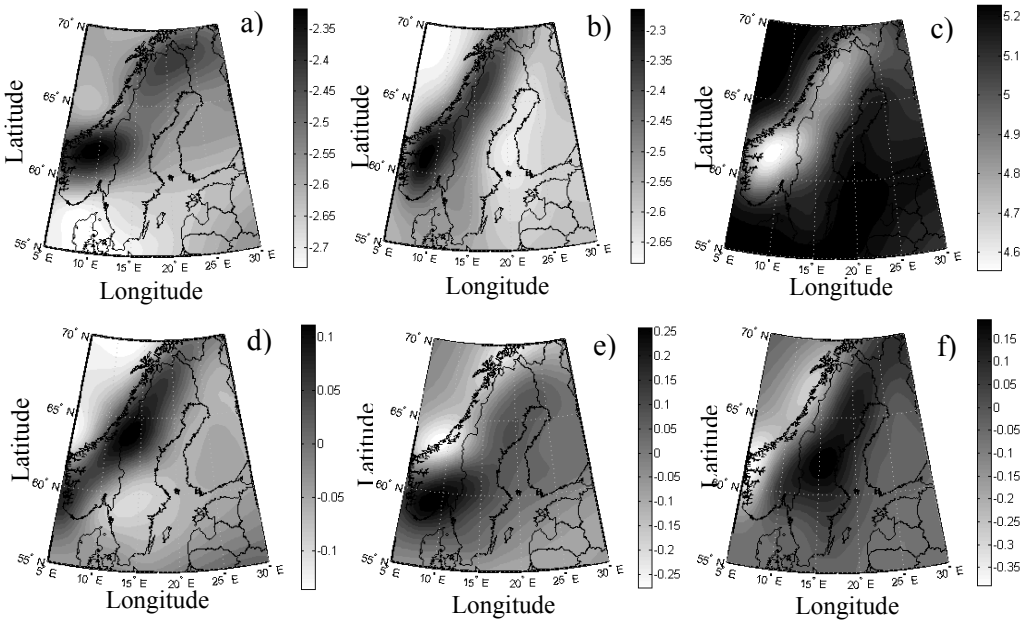

Figure 3.8. AE on SGG data in Fennoscandia in LNOF. Unit: 1 mE.

The statistics of the AE are presented in Table 3.5 as well. The maximum mean value of the effects in both areas are about 5 mE, and their minima are about -2 mE related to $V^{\,\mathrm{a}}_{zz}\left(P\right)$ and $V^{\,\mathrm{a}}_{xx}\left(P\right)$, respectively.

As can be seen from Table 3.6, strong, positive correlations exist between topographic heights and the TE on $V_{zz}^{t}(P)$ component. Strong negative correlations can be seen in the TE on $V_{xx}^{t}(P)$ and $V_{yy}^{t}(P)$ (see also Figures 3.1a and 3.1b). The correlations of the AE and topographic height is similar to correlation of topographic height and the TE but with opposite sign. Weaker correlations can be seen for topographic height and AE on $V_{xy}^{t}(P)$ but with opposite signs. Very weak correlations exist between $V_{xz}^{t}(P)$ and $V_{yz}^{t}(P)$ and topography. The correlations for $V_{zz}^{t}(P)$ and topographic heights are approximately the same in both regions. The correlations for $V_{xy}^{t}(P)$ and $V_{yy}^{t}(P)$ with the heights are smaller in Iran and the correlation between $V_{xx}^{i}(P)$ and the heights is slightly increased vs. Fennoscandia. The diagonal elements of the gradiometric tensor, $V_{xx}^{t}(P)$, $V_{yy}^{t}(P)$ and $V_{zz}^{t}(P)$, are very similar in correlation with topography. However, the off-diagonal elements, such as $V_{yz}^{t}(P)$, $V_{xz}^{t}(P)$ and $V_{xy}^{t}(P)$, have different signs in different regions. Also, notice the larger correlation in $V_{xy}^{t}(P)$ vs. topography in both regions, but with different signs. We expect that this difference in sign be due to the dominant topographic orientation. It is oriented from south-west to north-east in Fennoscandia, while in Iran it is oriented from north-west to south-east.

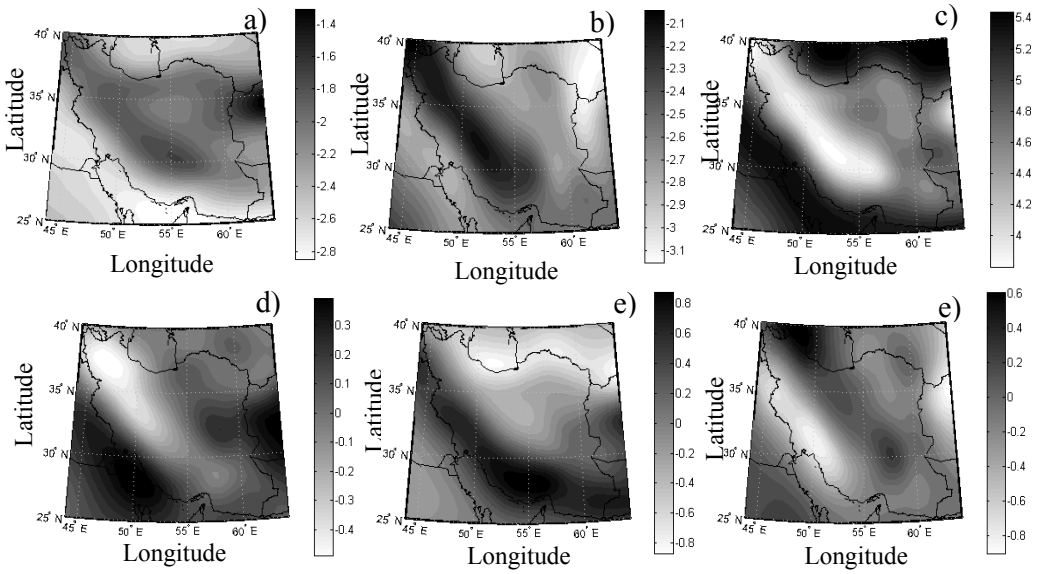

Figure 3.9. AE on SGG data in Iran in LNOF. Unit: 1 mE.

Table 3.5. Statistics of AE on SGG data in Fennoscandia and Iran in LNOF. Unit: 1 mE.

	Fennoscandia				Iran			
	max	mean	min	std	max	Mean	min	std
$V_{xx}^{a}(P)$	-2. 29	-2.56	-2.74	± 0.09	-1.20	-2.23	-2.86	± 0.35
$V_{yy}^{a}(P)$	-2.24	-2.54	-2.69	± 0.09	-1.97	-2.59	-3.16	± 0.25
$V_{zz}^{a}(P)$	5.27	5.10	4.53	± 0.16	5.53	4.82	3.78	± 0.48
$V_{xy}^{a}(P)$	0.13	-0.03	-0.14	± 0.05	0.45	0.07	-0.50	± 0.21
$V_{xz}^{a}(P)$	0.29	-0.01	-0.28	± 0.11	0.99	0.06	-0.89	± 0.47
$V_{yz}^{a}(P)$	0.23	-0.02	-0.40	± 0.12	-1.20	-2.23	-2.86	± 0.35

Table 3.6. Correlation coefficients between topographic height, and TE and AE in Fennoscandia and Iran

	Fennoscandia		Iran	
	TE	AE	TE	AE
$V_{xx}^{i}(P)$	-0.75	0.76	-0.81	0.81
$V_{yy}^{i}(P)$	-0.83	0.81	-0.63	0.62
$V_{zz}^{i}(P)$	0.90	-0.90	0.91	-0.91
$V_{xy}^{i}(P)$	-0.68	0.68	0.52	-0.53
$V_{xz}^{i}(P)$	-0.04	0.04	-0.10	0.10
$V_{yz}^{i}(P)$	-0.04	0.05	0.08	-0.09

3.4.3 Atmospheric potential based on KTHA

In this section, we derive the SHCs of the atmospheric potentials considering Sjöberg's ADM denoted KTHA. The external type of the SHCs of the atmospheric potential can be expressed as:

Proposition 3.7 *The SHCs of the external type of the atmospheric potential based on KTHA is (Eshagh and Sjöberg 2009b)*:

$$\left(v_{\text{ext}}^{a}\right)_{nm} \approx \frac{3\rho_0}{(2n+1)\rho^{e}}\left\{\frac{Z\,\delta_{n0}-H_{nm}}{R}+(n+2-\nu)\frac{Z^{2}\delta_{n0}-H^{2}{}_{nm}}{2R^{2}}+(n+2-\nu)\right.$$
$$\left.(n+1-\nu)\frac{Z^{3}\delta_{n0}-H^{3}{}_{nm}}{6R^{3}}\right\}.$$

Proof. By substituting Eq. (3.12) into Eq. (3.3) and considering Eq. (3.2a) as the ADM we have:

$$V_{\text{ext}}^{\text{a}}(P) = G\sum_{n=0}^{\infty}\rho_0\frac{R^{\nu}}{r^{n+1}}\iint_{\sigma}\int_{r_S}^{r_Z} r'^{n+2-\nu}dr'P_n(\cos\psi)d\sigma\,, \tag{3.24}$$

and after performing the radial integral and regarding $r_S = R + H$ and $r_Z = R + Z$ (where H is a function of position whereas Z is the upper bound of the atmospheric masses and constant) we obtain:

$$V_{\text{ext}}^{\text{a}}(P) = G\rho_0\sum_{n=0}^{\infty}\frac{R^{n+3}}{r^{n+1}(n+3-\nu)}\iint_{\sigma}\left[\left(1+\frac{Z}{R}\right)^{n+3-\nu} - \left(1+\frac{H}{R}\right)^{n+3-\nu}\right]P_n(\cos\psi)d\sigma\,. \tag{3.25}$$

The two terms in square bracket can be expanded into a binomial series and eventually truncated. |Since the series is converging fast. We consider the expansion to third-order (cf. Sun and Sjöberg (2001) for an investigation about the convergence of this binomial series). Further simplifications yield:

$$V_{\text{ext}}^{\text{a}}(P) = G\rho_0\sum_{n=0}^{\infty}\frac{R^{n+3}}{r^{n+1}}\iint_{\sigma}F_{\text{ext}}^{\text{a}}(Q)P_n(\cos\psi)d\sigma\,, \tag{3.26a}$$

where

$$F_{\text{ext}}^{\text{a}}(Q) = \frac{Z-H}{R} + (n+2-\nu)\frac{Z^2-H^2}{2R^2} + (n+2-\nu)(n+1-\nu)\frac{Z^3-H^3}{6R^3}\,. \tag{3.26b}$$

Considering addition theorem of spherical harmonics (Eq. 3.4) and after simplification we obtain:

$$V_{\text{ext}}^{\text{a}}(P) = 4\pi G\rho_0 R^2\sum_{n=0}^{\infty}\left(\frac{R}{r}\right)^{n+1}\frac{1}{2n+1}\sum_{m=-n}^{n}\left(F_{\text{ext}}^{\text{a}}\right)_{nm}Y_{nm}(P)\,, \tag{3.27}$$

$\left(F_{\text{ext}}^{\text{a}}\right)_{nm}$ is derived based on a simple spherical harmonic analysis of Eq. (3.26b) and the proposition is proven.

It is now worth comparing Proposition 3.7 with Proposition 3.3. By comparing the second-order terms in those equations, we observe that there is a constant $\alpha R = -596.55$ in the Novák and Grafarend model, while we have $\nu = 850$ in KTHA. Also, the coefficient of the third term in the equation of Proposition 3.7 after a simple manipulation is $\left[(n+2)(n+1-\nu)-(n+1)\nu+\nu^2\right]$, and as one can see an extra term appears vs. Novák and Grafarend's model. The constant terms of both formulas are not comparable as they are $2\beta R^2 = 226623.09$ and $\nu^2 = 722500$. However, when the terms are divided by $6R^3$ the effect of the third term is considerably reduced. In comparison with Sjöberg's (1998) solution, we can say that, since Sjöberg's emphasis was on the AE of the gravity anomaly and geoid, the upper limit of the radial integral

in Eq. (3.24) was set to infinity, and the internal type of Legendre's expansion was used instead of Eq. (3.2b), but in our case that we want to obtain the AE on the SGG data we can limit this upper bound to the specific value r_z=R+Z=6628137 m. It means that we assume the massive part of the atmosphere is below r_z level from the seal level, or in other words, we assume the computation point is out side of the atmospheric masses.

Now, consider the computation point to be below the atmospheric masses (on the geoid), in such a case the internal atmospheric potential should be formulated because the removed atmospheric effect should be restored after downward continuation. Similar to the external atmospheric potential formulation in spherical harmonics, we start with the Newtonian volume integral, Eq. (3.1) and consider Eq. (3.12) as the ADM (KTHA). If we expand $1/l$ into Legendre's series of internal type by Eq. (3.2b), the following proposition is obtained:

Proposition 3.8 *The SHCs of the external type of the atmospheric potential based on KTHA is (Eshagh and Sjöberg 2009b)*:

$$\left(v^{\mathrm{a}}_{\mathrm{int}}\right)_{nm} \approx \frac{3\rho_0}{(2n+1)\rho^{\mathrm{e}}}\left\{\frac{Z\,\delta_{n0}-H_{nm}}{R}-\frac{(n+\nu-1)}{2R^2}\left(Z^2\delta_{n0}-H^2{}_{nm}\right)+\frac{(n+\nu-1)(n+\nu)}{6R^3}\right.$$
$$\left.\left(Z^3\delta_{n0}-H^3{}_{nm}\right)\right\}.$$

Proof. Inserting Eq. (3.2b) into Eq. (3.1) and after some further simplifications we have

$$V^{\mathrm{a}}_{\mathrm{int}}(P)=G\sum_{n=0}^{\infty}\rho_0 R^{\nu}r^n\iint_{\sigma}\int_{r_S}^{r_Z} r'^{1-n-\nu}dr'P_n(\cos\psi)d\sigma. \tag{3.28}$$

In a similar way as for the external atmospheric potential we obtain

$$V^{\mathrm{a}}_{\mathrm{int}}(P)=G\rho_0\sum_{n=0}^{\infty}\frac{-R^{-n+2}r^n}{(n+\nu-2)}\iint_{\sigma}\left[\left(1+\frac{Z}{R}\right)^{-(n+\nu-2)}-\left(1+\frac{H}{R}\right)^{-(n+\nu-2)}\right]P_n(\cos\psi)d\sigma. \tag{3.29}$$

If the two terms in the square bracket are expanded into a binomial series up to third-order, and after some simplifications we obtain:

$$V^{\mathrm{a}}_{\mathrm{int}}(P)=G\rho_0\sum_{n=0}^{\infty}\frac{R^{-n+2}r^n}{2n+1}\sum_{m=-n}^{n}\iint_{\sigma}F^{\mathrm{a}}_{\mathrm{int}}(Q)Y_{nm}(Q)d\sigma Y_{nm}(P), \tag{3.30a}$$

where

$$F_{\text{int}}^{a}(Q)=\frac{Z-H}{R}-(n+\nu-1)\frac{\left(Z^{2}-H^{2}\right)}{2R^{2}}+(n+\nu-1)(n+\nu)\frac{\left(Z^{3}-H^{3}\right)}{6R^{3}}. \tag{3.30b}$$

Again, spherical harmonic expansion of H and Z yields

$$V_{\text{int}}^{a}(P)=4\pi G\rho_{0}R^{2}\sum_{n=0}^{\infty}\frac{1}{2n+1}\left(\frac{r}{R}\right)^{n}\sum_{m=-n}^{n}\left(F_{\text{int}}^{a}\right)_{nm}Y_{nm}(P). \tag{3.31}$$

The SHCs of the internal type of the atmospheric potential are derived by inserting Eq. (3.30b) into Eq. (3.30a) and further simplifications.

In formulation of the SHCs of the atmospheric potential based on KTHA, there is no restriction in elevation, and it can theoretically be considered up to infinity. However, the approximations used in generating the atmospheric potential may not be accurate enough for higher elevations based on this model. It is obvious that when increasing the elevation of the upper boundary of the atmosphere, the magnitude of this harmonic can increase unboundedly. We propose to use the following relation for the zero-degree harmonic coefficient of the atmospheric potential (which follows from Eq. 3.25 for n=0):

$$\left(v_{\text{ext}}^{\text{a}}\right)_{0}=\frac{3\rho_{0}}{\rho^{\text{e}}(3-\nu)}\left\{\left(1+\frac{Z}{R}\right)^{3-\nu}-\bar{H}\right\}, \tag{3.32a}$$

where

$$\bar{H}=\frac{1}{4\pi}\iint_{\sigma}\left(1+\frac{H}{R}\right)^{3-\nu}d\sigma. \tag{3.32b}$$

The integral of Eq.(3.32b) can be solved numerically.

In the following figure, the USSA76, NADM and KTHA are visualized with respect to the elevation

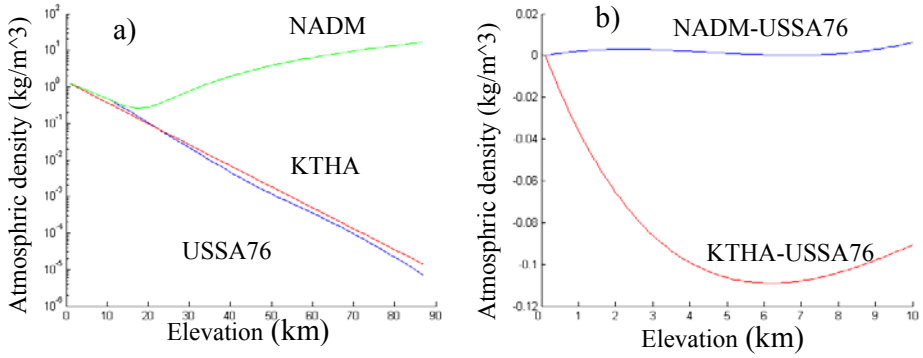

Figure 3.10. (a) NADM in green, KTHA in red and USSA76 in blue versus elevation (vertical axis is in logarithmic scale), (b) deference between NADM and USSA76 in blue, KTHA and USSA76 in red, respectively to 10 km elevation

Figure 3.10 shows that the NADM is valid up to 10 km elevation above sea level; see Novák (2000). The KTHA agrees with the USSA76 more or less, but underestimates the atmospheric density below 20 km and overestimates it in higher altitudes. It should be mentioned that the main aim of Novák (2000) was to formulate the atmospheric topography. This is why he considered a simple polynomial to model the atmospheric density up to 10 km. Since 80% of atmospheric masses are below 12 km (Lambeck 1988), it is reasonable to use a simple polynomial to express the effect of atmospheric topography although Wallace and Hobbs (1977) believes that 99% of the masses lie within the lowest 30 km above sea level.

3.4.3.1 AE on the SGG data in ORF

For computing the AE on the SGG data based on NADM and KTHA, they are generated from the atmospheric masses below 10 km. The ORF is used to generate the AE at 250 km level with 2-months revolution of an imaginary satellite at 250 km level over Fennoscandia. The mathematical models of the gravitational gradients in the ORF were presented in Chapter 2. Since these equations were developed to consider disturbing potential instead of true potential we can easily modify the developed software by adding the zero- and first-degree harmonics with the solution.

The contribution of the zero- and the first-degree harmonics of the AE can be derived based on the original formulas of the gravitational gradients in the ORF as (Eshagh and Sjöberg 2009b):

$$V_{uu}^{0,1}(P) = -\frac{GMR}{r^4}\left\{\frac{r}{R}C_{00} + 3\sqrt{3}\left[C_{10}\cos\theta + \left(C_{11}\cos\lambda + S_{11}\sin\lambda\right)\sin\theta\right]\right\}, \quad (3.33a)$$

$$V_{vv}^{0,1}(P) = -\frac{GMR}{r^4}\left\{\frac{r}{R}C_{00} + 3\sqrt{3}\left[C_{10}\cos\theta + \left(C_{11}\cos\lambda + S_{11}\sin\lambda\right)\sin\theta\right]\right\}, \quad (3.33b)$$

$$V_{ww}^{0,1}(P) = \frac{2GMR}{r^4}\left\{\frac{r}{R}C_{00} + 3\sqrt{3}\left[C_{10}\cos\theta + \left(C_{11}\cos\lambda + S_{11}\sin\lambda\right)\sin\theta\right]\right\}, \quad (3.33c)$$

$$V_{uv}^{0,1}(P) = 0, \quad (3.33d)$$

$$V_{uw}^{0,1}(P) = \frac{3\sqrt{3}GMR}{r^4}\left\{\cos\alpha\left[C_{10}\sin\theta + \left(C_{11}\cos\lambda + S_{11}\sin\lambda\right)\cos\theta\right] + \right.$$
$$\left. + \sin\alpha\left(-C_{11}\sin\lambda + S_{11}\cos\lambda\right)\right., \quad (3.33e)$$

$$V_{vw}^{0,1}(P) = \frac{3\sqrt{3}GMR}{r^4}\left\{-\sin\alpha\left[-C_{10}\sin\theta + \left(C_{11}\cos\lambda + S_{11}\sin\lambda\right)\cos\theta\right] + \right.$$
$$\left. + \cos\alpha\left(-C_{11}\sin\lambda + S_{11}\cos\lambda\right)\right., \quad (3.33f)$$

where superscripts of 0 and 1 stand for the zero- and the first-degree harmonics, respectively. C_{00}, C_{10},C_{11},S_{10} and S_{11} are the fully-normalized zero- and the first-degree harmonics of the atmospheric potential.

The position of the satellite can be generated using a numerical integration technique and an existing geopotential model. For more details the reader is referred to, e.g., Hwang and Lin (1998), Eshagh (2003a) and (2003b), Eshagh (2005a) and Eshagh and Najafi-Alamdari (2006) and (2007).

The statistics of the numerical comparison of the AE based on NADM and KTHA generated from the atmospheric masses below 10 km are summarized in Table 3.7. The KTHA shows small effects since it underestimates the massive part of the atmosphere in the lower altitudes. This underestimation of the atmospheric density directly affects the zero-degree harmonic coefficient of the atmospheric potential. Since $V_{uu}(P)$, $V_{vv}(P)$ and $V_{ww}(P)$ include this harmonic in their formulation, we can expect to see larger AE based on the NADM than the KTHA. $V_{uv}(P)$, $V_{uw}(P)$ and $V_{vw}(P)$ are more or less in the same order in both approaches because of their independency from the zero-degree harmonic. However, it should be noted that $V_{uw}(P)$ and $V_{vw}(P)$ include also the first-degree harmonics.

Table 3.7. AE on the SGG data at 250 km level based on NADM and KTHA up to 10 km in ORF. Unit: 1 mE

	NADM				KTHA			
	max	mean	min	std	max	mean	min	std
$V_{uu}(P)$	-2.01	-2.21	-2.39	± 0.08	-0.69	-0.88	-1.04	± 0.07
$V_{vv}(P)$	-1.92	-2.22	-2.41	± 0.11	-0.61	-0.88	-1.05	± 0.10
$V_{ww}(P)$	4.62	4.44	3.94	± 0.15	1.93	1.77	1.32	± 0.14
$V_{uv}(P)$	0.07	-0.03	-0.11	± 0.04	0.07	-0.02	-0.10	± 0.04
$V_{uw}(P)$	0.30	0.01	-0.30	± 0.11	0.26	0.01	-0.27	± 0.10
$V_{vw}(P)$	0.35	0.01	-0.20	± 0.09	0.32	0.01	-0.18	± 0.09

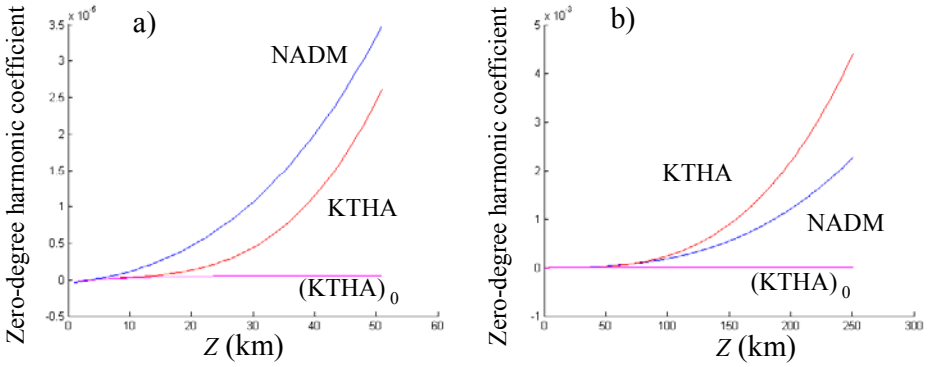

Figure 3.11. Behaviour of unitless zero-degree harmonic of the atmospheric potential versus various *Z*. (a) *Z*=0 to 50 km and (b) *Z*=0 to 250 km

Figure 3.11 illustrates values of the zero-degree harmonic based on the NADM and KTHA. As we know, the NADM is valid just up to 10 km height, and it is not surprising to see larger values when applying it for the external potential to higher elevations. The horizontal line presented in the figure is the true value of the zero-degree harmonic computed by Eq. (3.32b). As could be expected, this harmonic should be treated as a bounded function when increasing the elevation. However, Figure 3.11a shows that the approximations of the true mathematical expressions with binomial expansion, which was used in Eq. (3.32b), is good just for elevations lower than 20 km. The zero-degree harmonic has smaller value up to 50 km when KTHA is used vs. the NADM, while it is larger at 250 km. It means that the approximation used Eq. (3.32b) is not good enough for higher elevations and can destroy the solution even worse than the NADM see Figure 3.11a. The simplest way to get a non-diverging value for the zero-degree harmonic is to avoid approximations in this harmonic in the KTHA using Eq. (3.32b). As we previously mentioned we can consider the atmospheric shells above 10 km and compute the atmospheric potential corresponding to each shell and add it in this harmonic; see Novák (2000).

3.4.4 Reformulation of the SHCs of atmospheric potentials based on KTHA

In the previous section we presented that the zero-degree harmonic varies unboundedly because of the approximation used in formulation of the SHCs. In this section we propose another expression in order to solve this problem. In other words, we reformulate the SHCs of the atmospheric potentials so that there is no need to consider the zero-degree harmonic separately.

Proposition 3.9 *The SHCs of the external atmospheric potential based on KTHA are (Eshagh 2009e)*:

$$\left(V^{\,\mathrm{a}}_{\mathrm{ext}}\right)_{nm} \approx \frac{3\rho_0}{(2n+1)\rho^e}\left\{\left[\left(1+\frac{Z}{R}\right)^{3-\nu}-1\right]\frac{\delta_{n0}}{3-\nu}-\frac{H_{nm}}{R}-\frac{n+2-\nu}{2R^2}H^2{}_{nm}-\right.$$
$$\left.-\frac{(n+2-\nu)(n+1-\nu)}{6R^3}H^3{}_{nm}\right\}.$$

Proof. Considering Eqs. (3.2) and (3.3a) we can write the external potential as

$$V^{\,\mathrm{a}}_{\mathrm{ext}}(P)=G\rho_0\iint_{\sigma}\frac{R^{\nu}}{r^{n+1}}\int_{r_S}^{r_Z} r'^{n+2-\nu}dr'P_n(\cos\psi)d\sigma\,. \tag{3.34}$$

The radial integral can be separated into two parts

$$\int_{r_S}^{r_Z} r'^{n+2-\nu}dr'=\int_{R}^{R+Z} r'^{n+2-\nu}dr'-\int_{R}^{R+H} r'^{n+2-\nu}dr'\,. \tag{3.35}$$

The solution of the above integral is

$$\int_{R}^{R+Z} r'^{n+2-\nu} dr' = \frac{R^{n+3-\nu}}{n+3-\nu}\left[\left(1+\frac{Z}{R}\right)^{n+3-\nu}-1\right] - R^{n+3-\nu}\left[\frac{H}{R}+\frac{n+2-\nu}{2R^2}H^2+ \right.$$
$$\left. +\frac{(n-\nu+2)(n-\nu+1)}{6R^3}H^3\right] \qquad (3.36)$$

Eq. (3.36) is substituted into Eq. (3.34), and we have

$$V_{\text{ext}}^{a}(P) = G\rho_0 R^2 \sum_{n=0}^{\infty}\left(\frac{R}{r}\right)^{n+1} \iint_{\sigma}\left\{\left[\left(1+\frac{Z}{R}\right)^{n+3-\nu}-1\right]\frac{\delta_{n0}}{n+3-\nu} - \left[\frac{H}{R}+\frac{n+2-\nu}{2R^2}H^2+ \right.\right.$$
$$\left.\left. +\frac{(n-\nu+2)(n-\nu+1)}{6R^3}H^3\right]\right\} P_n(\cos\psi)\, d\sigma\,. \qquad (3.37)$$

By using Eq. (3.3) and further simplifications the proposition is proven.

Proposition 3.10 *The SHCs of the internal atmospheric potential based on KTHA are (Eshagh 2009e)*:

$$\left(V_{\text{int}}^{\text{a}}\right)_{nm} \approx \frac{3\rho_0}{(2n+1)\rho^{\text{e}}}\left\{\left[1-\left(1+\frac{Z}{R}\right)^{2-\nu}\right]\frac{\delta_{n0}}{\nu-2} - \frac{H_{nm}}{R}+\frac{n+\nu-1}{2R^2}H^2{}_{nm} - \right.$$
$$\left. -\frac{(n+\nu-1)(n+\nu)}{6R^3}H^3{}_{nm}\right\}.$$

Proof. According to Eqs. (3.2) and (3.3b) and also Eq. (3.12) we can write the internal type of the atmospheric potential

$$V_{\text{int}}^{a}(P) = G\rho_0 \sum_{n=0}^{\infty} R^{\nu} r^{n} \iint_{\sigma}\int_{R+H}^{R+Z} r'^{1-\nu-n} dr' P_n(\cos\psi)\, d\sigma\,. \qquad (3.38)$$

Similar to Eq. (3.35) we can divide the radial integral into two parts. Solution of the radial integral is:

$$\int_{R+H}^{R+Z} r'^{1-\nu-n} dr' = \frac{R^{2-\nu-n}}{2-\nu-n}\left[\left(1+\frac{Z}{R}\right)^{2-\nu-n}-1\right] - R^{2-\nu-n}\left[\frac{H}{R}+\frac{1-\nu-n}{2R^2}H^2+ \right.$$
$$\left. +\frac{(1-\nu-n)(-\nu-n)}{6R^3}H^3\right]. \qquad (3.39)$$

Inserting Eqs. (3.39) into Eq. (3.38) we derive

$$V^{\,a}_{\text{int}}(P)=G\rho_0R^2\sum_{n=0}^{\infty}\left(\frac{r}{R}\right)^n\iint_{\sigma}\left\{\left[\left(1+\frac{Z}{R}\right)^{2-\nu-n}-1\right]\frac{\delta_{n0}}{2-\nu-n}-\frac{H}{R}-\frac{1-\nu-n}{2R^2}H^2+\right.$$
$$\left.+\frac{(1-\nu-n)(-\nu-n)}{6R^3}H^3\right\}P_n(\cos\psi)d\sigma\,. \qquad (3.40)$$

and by considering Eq. (3.3) and simplification the proposition is proved.

3.4.5 External and internal atmospheric potentials based on exponential ADM

Ecker and Mittermayer (1969) have used an exponential model for approximating the atmospheric density. Because of the complicated formulation process (based on exponential model) most people prefer not to use this model and this is why it has not been further developed and applied. In this section we formulate and develop the atmospheric potential based on this model. Simple formulas for the harmonic coefficients of the spherical harmonic expansion of atmospheric potentials are presented. The SHCs of the atmospheric potentials based on exponential ADM is considered in this section.

Proposition 3.11 *The SHCs of external atmospheric potential based on the exponential ADM are (Eshagh 2009e)*:

$$\left(v^{\,a}_{ext}\right)_{nm}\approx\frac{3\rho_0}{(2n+1)\rho_e}\left\{\left\{\left[1-\left(1+\frac{Z}{R}\right)e^{-\alpha''Z}\right]\left(\frac{2+\alpha''(R+Z)}{\alpha''^2R^2}\right)+\frac{2\left(1-e^{-\alpha''Z}\right)}{\alpha''^3R^3}-\frac{Z}{R^2\alpha''}\right\}\delta_{n0}-\right.$$
$$\left.-\left[\frac{H_{nm}}{R}+\frac{n+2-\alpha''R}{2R^2}H^2{}_{nm}+\frac{(n+2)(n+1-2\alpha''R)+\alpha''^2R^2}{6R^3}H^3{}_{nm}\right]\right\}. \qquad (3.41)$$

Proof. Equation (3.41) is obtained from Eq. (3.1) by substituting from Eqs. (3.3a) and (3.13):

$$V^{\,a}_{\text{ext}}(P)=G\rho_0e^{\alpha''R}\sum_{n=0}^{\infty}\frac{1}{r^{n+1}}\iint_{\sigma}\int_{r_S}^{r_Z}e^{-\alpha''r'}r'^{n+2}dr'P_n(\cos\psi)d\sigma\,. \qquad (3.41)$$

The radial integral can be separated into

$$\int_{r_S}^{r_Z}e^{-\alpha r'}r'^{n+2}dr'=\int_{R}^{R+Z}e^{-\alpha''r'}r'^{n+2}dr'-\int_{R}^{R+H}e^{-\alpha''r'}r'^{n+2}dr'=I_n-\int_{R}^{R+H}e^{-\alpha''r'}r'^{n+2}dr'\,. \qquad (3.42)$$

Let the solution of the second integral from left be I_n and we will see that we just need I_0 in our derivations, and there is no need to perform partial integration to solve the integral. The exponential function in the third integral from left of Eq. (3.42) is expanded by Taylor series and the integration performs:

$$\int_R^{R+H} e^{-\alpha'' r'} r'^{n+2} dr' = \sum_{k=0}^{\infty} \frac{\left(-\alpha''\right)^k}{k!} \int_R^{R+H} r'^{n+k+2} dr' = \sum_{k=0}^{\infty} \frac{\left(-\alpha''\right)^k}{k!\left(n+k+3\right)} r'^{n+k+3} \Bigg|_R^{R+H} =$$

$$= \sum_{k=0}^{\infty} \frac{\left(-\alpha''\right)^k R^{n+k+3}}{k!\left(n+k+3\right)} \left[\left(1+\frac{H}{R}\right)^{n+k+3} - 1 \right]. \tag{3.43}$$

If we use binomial expansion up to third-order for the first term in the squared bracket in Eq. (3.43) we obtain

$$\sum_{k=0}^{\infty} \frac{\left(-\alpha''\right)^k}{k!} \int_R^{R+H} r'^{n+k+2} dr' \approx \sum_{k=0}^{\infty} \frac{\left(-\alpha''\right)^k R^{n+k+3}}{k!} \left[\frac{H}{R} + \frac{n+k+2}{2} \left(\frac{H}{R}\right)^2 + \right.$$

$$\left. + \frac{\left(n+k+2\right)\left(n+k+1\right)}{6} \left(\frac{H}{R}\right)^3 \right]. \tag{3.44}$$

Inserting Eq. (3.44) into Eq. (3.42) substituting the result into Eq. (3.41) we obtain

$$V_{\text{ext}}^{\text{a}}\left(P\right) = G\rho_0 e^{\alpha R} \sum_{n=0}^{\infty} \frac{1}{r^{n+1}} \iint_{\sigma} \left\{ I_n - \sum_{k=0}^{\infty} \frac{\left(-\alpha''\right)^k R^{n+k+3}}{k!} \left[\frac{H}{R} + \frac{n+k+2}{2R^2} H^2 + \right. \right.$$

$$\left. \left. + \frac{\left(n+k+2\right)\left(n+k+1\right)}{6R^3} H^3 \right] \right\} P_n\left(\cos\psi\right) d\sigma. \tag{3.45}$$

Using Eq. (3.3) which is the addition theorem of the fully-normalized spherical harmonics, Eq. (3.45) can further be simplified

$$V_{\text{ext}}^{a}\left(P\right) = 4\pi G\rho_0 e^{\alpha'' R} R^2 \sum_{n=0}^{\infty} \left(\frac{R}{r}\right)^{n+1} \frac{1}{\left(2n+1\right)} \sum_{m=-n}^{n} \left\{ \frac{I_n \delta_{n0}}{R^{n+3}} - \sum_{k=0}^{\infty} \frac{\left(-\alpha''\right)^k R^k}{k!} \left[\frac{H_{nm}}{R} + \right. \right.$$

$$\left. \left. + \frac{n+k+2}{2R^2} H^2{}_{nm} + \frac{\left(n+k+2\right)\left(n+k+1\right)}{6R^3} H^3{}_{nm} \right] \right\} Y_{nm}\left(P\right). \tag{3.46}$$

Considering Eq. (3.7) and after further simplifications we obtain

$$\left(v_{\text{ext}}^{\,a}\right)_{nm} = \frac{3\rho_0}{(2n+1)\rho_e}\left\{\frac{I_n e^{\alpha'' R}}{R^{n+3}}\delta_{n0} - e^{\alpha'' R}\sum_{k=0}^{\infty}\frac{(-\alpha'')^k R^k}{k!}\left[\frac{H_{nm}}{R} + \frac{n+k+2}{2R^2}H^2{}_{nm} + \right.\right.$$
$$\left.\left. + \frac{(n+k+2)(n+k+1)}{6R^3}H^3{}_{nm}\right]\right\} = \frac{3\rho_0}{(2n+1)\rho_e}\left\{A\,\delta_{n0} - B\right\}. \qquad (3.47)$$

The first term in the squared bracket consists of the solution of the first integral of Eq. (3.42) and we have:

$$A = \frac{I_0 e^{\alpha'' R}}{R^3} = \left\{\left[1 - \left(1 + \frac{Z}{R}\right)e^{-\alpha'' Z}\right]\left[\frac{2 + \alpha''(R+Z)}{\alpha''^2 R^2}\right] + \frac{2\left(1 - e^{-\alpha'' Z}\right)}{\alpha''^3 R^3} - \frac{Z}{R^2\alpha''}\right\}. \qquad (3.48)$$

The second term of the squared bracket of Eq. (3.47) needs more consideration and simplification. Let us start with Taylor expansion of $e^{-\alpha'' R}$

$$e^{-\alpha'' R} = \sum_{k=0}^{\infty}\frac{(-\alpha'')^k R^k}{k!}. \qquad (3.49)$$

Then we can write

$$B = e^{\alpha'' R}\frac{H_{nm}}{R}\sum_{k=0}^{\infty}\frac{(-\alpha'')^k R^k}{k!} + e^{\alpha'' R}\left\{\frac{H^2{}_{nm}}{2R^2}\left[(n+2)\sum_{k=0}^{\infty}\frac{(-\alpha'')^k R^k}{k!} + \right.\right.$$
$$\left. + (-\alpha'' R)\sum_{k=1}^{\infty}\frac{(-\alpha'')^{k-1} R^{k-1}}{(k-1)!}\right] + \frac{H^3{}_{nm}}{6R^3}\left[\sum_{k=0}^{\infty}\frac{(-\alpha'')^k R^k}{k!}k^2 + (2n+3)\sum_{k=0}^{\infty}\frac{(-\alpha'')^k R^k}{k!}k + \right.$$
$$\left.\left. + (n+2)(n+1)\sum_{k=0}^{\infty}\frac{(-\alpha'')^k R^k}{k!}\right]\right\}. \qquad (3.50)$$

The first term of the second square bracket can be simplified more as:

$$\sum_{k=0}^{\infty}\frac{(-\alpha'')^k R^k}{k!}k^2 = -\alpha'' R + \sum_{k=2}^{\infty}\frac{(-\alpha'')^k R^k}{(k-1)!}(k-1+1) = -\alpha'' R + \sum_{k=2}^{\infty}\frac{(-\alpha'')^k R^k}{(k-1)!}(k-1) +$$
$$+\sum_{k=2}^{\infty}\frac{(-\alpha'')^k R^k}{(k-1)!} = (-\alpha'')^2 R^2\sum_{k=2}^{\infty}\frac{(-\alpha'')^{k-2} R^{k-2}}{(k-2)!} - \alpha'' R\sum_{k=1}^{\infty}\frac{(-\alpha'')^{k-1} R^{k-1}}{(k-1)!} =$$
$$= \alpha'' R\,(\alpha'' R - 1)e^{-\alpha'' R}. \qquad (3.51)$$

Considering Eq. (3.49) we have

$$B = e^{\alpha'' R}\frac{H_{nm}}{R}e^{-\alpha'' R} + e^{\alpha'' R}\left\{\frac{H^2{}_{nm}}{2R^2}\left[(n+2)e^{-\alpha'' R} + (-\alpha R)e^{-\alpha'' R}\right] + \right.$$

$$+\frac{H^{3}{}_{nm}}{6R^{3}}\left[\left(-\alpha''R+\alpha''^{2}R^{2}\right)e^{-\alpha''R}+\left(2n+3\right)\left(-\alpha''R\right)e^{-\alpha''R}+\left(n+2\right)\left(n+1\right)e^{-\alpha''R}\right]\Bigg\}. \tag{3.52}$$

After further simplification we derive Eq. (3.53).

$$B=\left\{\frac{H_{nm}}{R}+\frac{n+2-\alpha''R}{2R^{2}}H^{2}{}_{nm}+\frac{\left(n+2\right)\left(n+1-2\alpha''R\right)+\alpha''^{2}R^{2}}{6R^{3}}H^{3}{}_{nm}\right\}. \tag{3.53}$$

Inserting Eqs. (3.53) and (3.48) into Eq. (3.47) the proposition is proved.

Proposition 3.12 *The SHCs of internal atmospheric potential based on the exponential ADM are (Eshagh 2009e)*:

$$\left(v^{\,\mathrm{a}}_{\,\mathrm{int}}\right)_{nm}\approx\frac{3\rho_{0}}{\left(2n+1\right)\rho^{\mathrm{e}}}\left\{\left\{\frac{1}{\alpha''R}\left[1-\left(1+\frac{Z}{R}\right)e^{-\alpha''Z}\right]+\frac{\left(1-e^{-\alpha''Z}\right)}{\alpha''^{2}R^{2}}\right\}\delta_{n0}-\left[\frac{H_{nm}}{R}+\right.\right.$$
$$\left.\left.+\frac{-n+1-\alpha''R}{2R^{2}}H^{2}{}_{nm}+\frac{\left(n-1\right)\left(n+2\alpha''R\right)+\alpha''^{2}R^{2}}{6R^{3}}H^{3}{}_{nm}\right]\right\}.$$

Proof. Considering Eqs. (3.2) and (3.3b) as the internal type of the Legendre expansion for $1/l$ we can write

$$V^{\,\mathrm{a}}_{\,\mathrm{int}}\left(P\right)=G\rho_{0}e^{\alpha''R}\iint_{\sigma}\sum_{n=0}^{\infty}\frac{1}{r^{n}}\int_{r_{S}}^{r_{Z}}e^{-\alpha''r'}r'^{-n+1}dr'P_{n}\left(\cos\psi\right)d\sigma\,. \tag{3.54}$$

Similar to Proposition 3.11 we can divide the radial integral into two parts; see Eq. (3.42). Let the solution of the radial integral of Eq. (3.54) be J_{n}, the exponential function in the second radial integral is expanded into the binomial series and integration performs as:

$$\sum_{k=0}^{\infty}\frac{\left(-\alpha''\right)^{k}}{k\,!}\int_{R}^{R+H}r'^{k-n+1}dr'=\sum_{k=0}^{\infty}\frac{\left(-\alpha''\right)^{k}}{k\,!\left(k-n+2\right)}r'^{k-n+2}\Bigg|_{R}^{R+H}=$$
$$=\sum_{k=0}^{\infty}\frac{\left(-\alpha''\right)^{k}R^{\,k-n+2}}{k\,!\left(k-n+2\right)}\left[\left(1+\frac{H}{R}\right)^{n+k+3}-1\right]. \tag{3.55}$$

After expanding the first term in the square bracket up to third-order we derive

$$\sum_{k=0}^{\infty}\frac{\left(-\alpha''\right)^k}{k!}\int_R^{R+H} r'^{k-n+1}dr' \approx \sum_{k=0}^{\infty}\frac{\left(-\alpha''\right)^k R^{k-n+2}}{k!}\left[\frac{H}{R}+\frac{k-n+1}{2}\left(\frac{H}{R}\right)^2+\right.$$
$$\left.+\frac{\left(k-n+1\right)\left(k-n\right)}{6}\left(\frac{H}{R}\right)^3\right]. \qquad (3.56)$$

Inserting Eq. (3.56) into Eq. (3.54) and using Eq. (3.3) the internal potential is

$$V_{\text{int}}^{\,a}\left(P\right)=4\pi G\rho_0 e^{\alpha''R}\sum_{n=0}^{\infty}\left(\frac{r}{R}\right)^n\frac{1}{\left(2n+1\right)}\sum_{m=-n}^{n}\left\{\frac{J_n\delta_{n0}}{R^{-n+2}}-\sum_{k=0}^{\infty}\frac{\left(-\alpha''\right)^k R^k}{k!}\right.$$
$$\left.\left[\frac{H_{nm}}{R}+\frac{k-n+1}{2R^2}H^2{}_{nm}+\frac{\left(k-n+1\right)\left(k-n\right)}{6R^3}H^3{}_{nm}\right]\right\}Y_{nm}\left(P\right), \qquad (3.57)$$

considering Eq. (3.7) and further simplifications we obtain:

$$\left(v_{\text{int}}^{\,a}\right)_{nm}=\frac{3\rho_0}{\left(2n+1\right)\rho_e}\left\{\frac{J_n e^{\alpha''R}}{R^{n+2}}\delta_{n0}-e^{\alpha''R}\sum_{k=0}^{\infty}\frac{\left(-\alpha''\right)^k R^k}{k!}\left[\frac{H_{nm}}{R}+\frac{-n+1-\alpha''R}{2R^2}H^2{}_{nm}+\right.\right.$$
$$\left.\left.+\frac{\left(k-n+1\right)\left(k-n\right)}{6R^3}H^3{}_{nm}\right]\right\}=\frac{3\rho_0}{\left(2n+1\right)\rho_e}\left\{C\,\delta_{n0}-D\right\}\ . \qquad (3.58)$$

The first term in the bracket is

$$C=\frac{J_0 e^{\alpha''R}}{R^2}=\frac{1}{\alpha''R}\left[1-\left(1+\frac{Z}{R}\right)e^{-\alpha''Z}\right]+\frac{\left(1-e^{-\alpha''Z}\right)}{\alpha''^2R^2}, \qquad (3.59)$$

and similar to the proof of Proposition 3.11 the second term is simplified as:

$$D=\left\{\frac{H_{nm}}{R}+\frac{-n+1-\alpha''R}{2R^2}H^2{}_{nm}+\frac{\left(n-1\right)\left(n+2\alpha''R\right)+\alpha''^2R^2}{2R^2}H^3{}_{nm}\right\}. \qquad (3.60)$$

Substituting Eq. (3.60) and Eq. (3.59) into Eq. (3.58) and after further simplifications the proposition is proved.

Comparing Propositions 3.8 and 3.10, we can say that the main difference between these harmonic coefficients is related to the first terms in the brackets. These terms are the potential of the atmospheric shell from sea surface to any point *P* inside the atmosphere. The values of these terms are about 1.132×10^{-3} and 1.127×10^{-3} derived according to the exponential ADM and KTHA, respectively. The second terms in Propositions 3.8 and 3.11 are related to the atmospheric roughness. In fact we have assumed that there are atmospheric masses between sea surfaces and the surface of

the Earth instead of topographic masses, which are subtracted from the atmospheric shell potential. This way of formulation is beneficial otherwise the derived zero-degree harmonic coefficient cannot yield the real value because of the approximations used in the binomial expansion. In fact, we avoid using this expansion for expressing the shell between the sea levels and upper bound of the atmosphere.

For further interpretation, let us compare the formulas numerically. First we have to determine the value α'' in Eq. (3.11). In this case we considered USSA76. The atmospheric density was generated based on this model up to 86 km (maximum elevation for the atmospheric density in this model) and by fitting a line into the logarithm of the atmospheric density versus elevation $\alpha''=1.3886\times10^{-4}$ was estimated. Also by similar fitting we can obtain value $\nu=890$ for the Eq. (3.12). The exponential ADM and KTHA are equations of two coinciding lines in logarithmic scale of the atmospheric density; see Figure 3.14d. The atmospheric density which is estimated by standard model is not linear versus elevation, and the KTHA and exponential ADM both underestimate the most massive part of the atmospheric density below 10 km height. This matter does not affect the formulation, as we can fit both functions to get better match to this first 10 km level. Now let us return to our comparison of the topographic terms of Propositions 3.8 and 3.11. The first terms are exactly the same, but the second topographic terms are very similar. It is interesting to see that value $\alpha''R$ =885.6680=886 (R=6378137 m) and very close the $\nu=890$ thus the second terms of the topography are also the same. The coefficients of the third roughness term is $\alpha''^2R^2+(n+2)(n+1-2\alpha''R)$ in Proposition 3.11 corresponding to

$$\nu^2+(n+2)\left[n+1-\nu\left(\frac{n+1}{n+2}+1\right)\right] \tag{3.61}$$

in KTHA in Proposition 3.9 (after little simplification). It is easy to see that if n=0 then $\nu^2+(n+2)(n+1-1.5\nu)$ and when n increases the term $(n+1)/(n+2)+1$ goes to 2. Therefore in high degrees the SHCs of external potential of the atmosphere are more or less the same as $\alpha''R\approx\nu$. Similar comparison can be done for the harmonics of the internal type as above.

For a numerical study a satellite orbit at 250 km altitude was generated by 4-th order Runge-Kutta algorithm for two-month revolutions at sampling rate of 30 seconds. The SHCs of the height function H and its powers H_{nm}, $H^2{}_{nm}$ and $H^3{}_{nm}$ have to be generated through the global spherical harmonic synthesis and analysis. The SRTM global topographic height model (Wieczorek 2007) with resolution $0.5^\circ\times0.5^\circ$ corresponding to degree of 360 was considered in this process. Figure 3.12 shows the maps of the AE based on the exponential ADM on SGG data over Fennoscandia.

In Figure 3.12, $V_{uu}^{a}(P)$, $V_{vv}^{a}(P)$, $V_{ww}^{a}(P)$, $V_{uv}^{a}(P)$, $V_{uw}^{a}(P)$ and $V_{vw}^{a}(P)$ are the AEs on the gravitational gradients in ORF. $V_{ww}^{a}(P)$ is the largest because of including the zero-degree harmonic while $V_{uv}^{a}(P)$ is the smallest as it excludes zero- and first-degree harmonics. The statistics of the AEs on the SGG data over Fennoscandia are presented in Table 3.8, which shows that the AE on the SGG data based on both models are more or less the same in practice and the differences are very small.

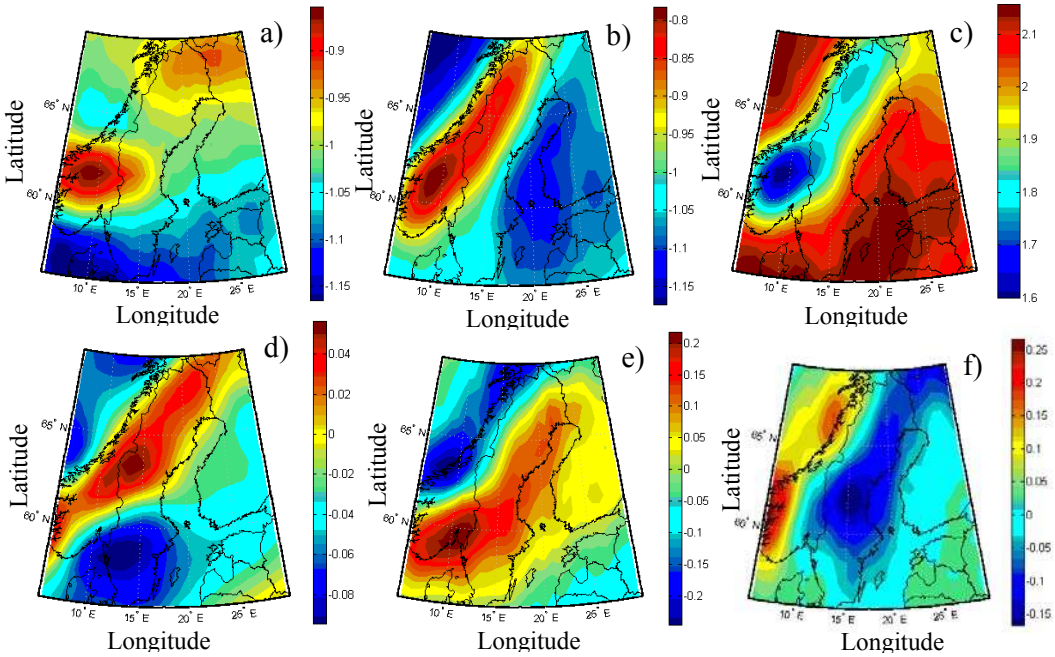

Figure 3.12. AE on SGG data at 250 km elevation, based on the exponential ADM in Fennoscandia in ORF, (a) V_{uu}^{a}, (b) V_{vv}^{a}, (c) V_{ww}^{a}, (d) V_{uv}^{a}, (e) V_{uw}^{a} and (f) V_{vw}^{a}. Unit: 1 mE

Table 3.8. Statistics of AE on SGG data at 250 km level over Fennoscandia based on exponential ADM and KTHA in ORF. Unit: 1 mE

	Exponential ADM				KTHA			
	max	mean	min	std	max	mean	min	std
$V_{uu}^{a}(P)$	-0.83	-1.01	-1.17	±0.07	-0.82	-1.01	-1.17	±0.07
$V_{vv}^{a}(P)$	-0.75	-1.01	-1.18	±0.10	-0.74	-1.01	-1.17	±0.10
$V_{ww}^{a}(P)$	2.20	2.03	1.58	±0.14	2.19	2.02	1.57	±0.14
$V_{uv}^{a}(P)$	0.07	-0.02	-0.10	±0.04	0.07	-0.02	-0.10	±0.04
$V_{uw}^{a}(P)$	0.26	0.01	-0.27	±0.10	0.26	0.01	-0.27	±0.10
$V_{vw}^{a}(P)$	0.32	0.01	-0.18	±0.08	0.32	0.01	-0.18	±0.08

The gravity anomaly and disturbing potential can be derived from the SGG data in local gravity field determination using inversion of the second-order derivatives of the extended Stokes and Abel-Poisson integrals, see Chapter 5. In this case the removed AEs should be restored on these quantities as the indirect AE. Since these indirect effects are also dependent on the type of the ADM, we just present the map of the difference between indirect effects in Figures 3.13a and 3.13b in Fennoscandia.

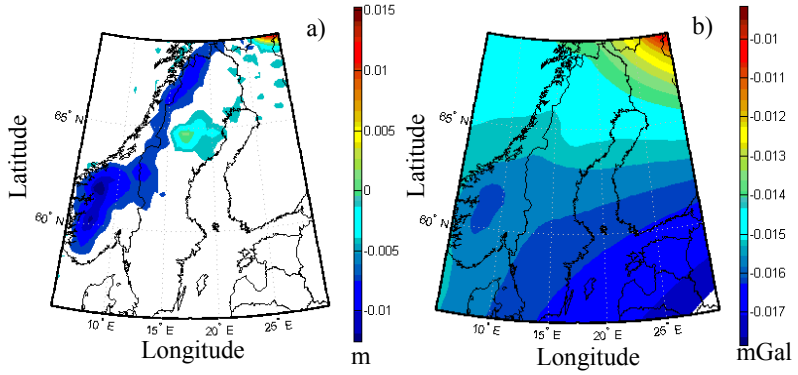

Figure 3.13. (a) and (b) difference between the indirect AEs due to the exponential ADM and KTHA, on the gravity anomaly and geoid, respectively.

The value of this effect is about -4.6 m and 1.4 mGal on the geoid and gravity anomaly, respectively (using both exponential ADM and KTHA). The maximum difference between the indirect effects is less than 2 cm on the geoid and 0.02 mGal on gravity anomaly (in mountainous regions) and may be negligible in ordinary practical works.

The SHCs of the external and internal atmospheric potentials derived based on the exponential function do not include any exponential function in the atmospheric roughness terms. The first term, contributing the zero-degree harmonic, includes the exponential function $e^{-\alpha Z}$, which is very close to zero when Z is large, for example at satellite level. No partial integration is needed for generating the potential of the atmosphere based on this model. The constant ν in the KTHA is equivalent to $\alpha'' R$ in exponential ADM. This implies that the attenuation factor (R/r) in this model corresponds to $\exp(1-r/R)$ in exponential ADM. The first and second terms of the atmospheric topography are more or less the same and the difference is related to the third term. The difference in the third terms is related to the coefficient 2 of $\alpha'' R$ and $\left[(n+1)/(n+2)+1\right]$ of ν. When n=0 this coefficients is 1.5 and it goes to 2 by increasing the degrees. However, this difference is negligible when it is divided by $6R^3$. The main difference is related to the zero-degree harmonic including the potential of the atmospheric shell from sea level up to the elevation $R+Z$. They are completely different in formulation but the same in value. Numerical studies on the AEs on the SGG data over Fennoscandia shows insignificant difference for the direct AEs due to these ADMs (less than 0.01 mE). This difference is mainly related to the largest SHCs and its different formulations based on both exponential ADM and

KTHA. However, the maximum AE is about 2 mE when the satellite passes over this region based on both models. The indirect AE on the geoid and gravity anomaly is dependent on the type of ADM. In this study we found the maximum difference 2 cm and 0.02 mGal on the geoid and gravity anomaly in roughest part of Fennoscandia.

3.4.6 Atmospheric potential based on the NKTHA

Now we consider the NKTHA that we proposed in Subsection 3.4. This model is a combination of the NADM and the KTHA. In the following we express how to use this NKTHA for formulating the external and internal atmospheric potentials in spherical harmonics.

Proposition 3.13 *The SHCs of the external type of the atmospheric potential based on NKTHA are (Eshagh and Sjöberg 2009b)*:

$$\left(V^{\,\mathrm{a}}_{\mathrm{ext}}\right)_{nm} \approx \frac{3}{(2n+1)\rho^{\mathrm{e}}}\left\{\rho_0\left[\frac{H_0\delta_{n0}-H_{nm}}{R}+(n+2-\alpha' R)\frac{H_0^2\delta_{n0}-H^{\,2}{}_{nm}}{2R^2}+\left[(n+2)(n+1-2\alpha' R)+\right.\right.\right.$$
$$\left.\left.\left.+2\beta' R^2\right]\frac{H_0^3\delta_{n0}-H^{\,3}{}_{nm}}{6R^3}+\frac{\rho(H_0)}{n+3-\nu}\left[\left(1+\frac{H_0}{R}\right)^{\nu}\left(1+\frac{Z}{R}\right)^{n+3-\nu}-\left(1+\frac{H_0}{R}\right)^{n+3}\right]\delta_{n0}\right\}.$$

Proof. Inserting the NKTHA into Eq. (3.1) and considering Eq. (3.2a) and the external type of expansion of $1/l$ we obtain

$$V^{\,\mathrm{a}}_{\mathrm{ext}}(P)=G\sum_{n=0}^{\infty}\frac{1}{r^{n+1}}\iint_{\sigma}\left[\int_{r_S}^{H_0}\rho^{\mathrm{a}}(r')r'^{n+2}dr'+\int_{H_0}^{r_Z}\rho^{\mathrm{a}}(r')r'^{n+2}dr'\right]P_n(\cos\psi)d\sigma\,. \quad (3.62)$$

The ADM in the first integral in the square bracket is related the upper function of Eq.(3.3a) and the second integral relates to the lower function. Therefore the solution of the first term is the same as in Proposition 3.3. Considering the second part of Eq. (3.62) as the ADM above H_0, the solution of the second integral becomes

$$\rho(H_0)(R+H_0)^{\nu}\int_{R+H_0}^{R+Z}r'^{n+2-\nu}dr'=\frac{\rho(H_0)R^{n+3}}{n+3-\nu}\left[\left(1+\frac{H_0}{R}\right)^{\nu}\left(1+\frac{Z}{R}\right)^{n+3-\nu}-\left(1+\frac{H_0}{R}\right)^{n+3}\right] \quad (3.63)$$

Since this term is a constant with respect to integration point Q in Eq. (3.63), it associates just with the zero-degree harmonic. The unitless SHCs of the external atmospheric potential can thus be written in the following form

$$\left(v^{\,a}_{ext}\right)_{nm}=\frac{3}{(2n+1)\rho_e}\left(\rho_0\left(F^{a}_{ext}\right)_{nm}+\rho(H_0)G_n\right), \quad (3.64)$$

where $\left(\mathrm{F}_{\mathrm{ext}}^{\mathrm{a}}\right)_{\mathrm{nm}}$ was defined in Proposition 3.3, and

$$G_n = \frac{1}{n+3-\nu}\left[\left(1+\frac{H_0}{R}\right)^{\nu}\left(1+\frac{Z}{R}\right)^{n+3-\nu} - \left(1+\frac{H_0}{R}\right)^{n+3}\right]\delta_{n0}. \qquad (3.65)$$

Inserting Eqs. (3.65) and Proposition 3.3 into Eq. (3.64) and setting $Z\delta_{n0} = H_0\delta_{n0}$ the proposition is proved.

We can also consider our new atmospheric model NKTHA to generate the internal type of the atmospheric potential. By considering Proposition 3.4 and Eq. (3.14) (the NKTHA) and reinserting into Eq. (3.1) we obtain

Proposition 3.14 *The SHCs of the internal type of the atmospheric potential based on NKTHA are (Eshagh and Sjöberg 2009b)*:

$$\left(V_{\mathrm{int}}^{a}\right)_{nm} \approx \frac{3}{(2n+1)\rho_e}\left\{\rho_0\left[\frac{H_0\delta_{n0}-H_{nm}}{R} - (n-1-\alpha R)\frac{H^2{}_0\delta_{n0}-H^2{}_{nm}}{2R^2} - \left[(1-n)(n+2\alpha R)-2\beta R^2\right]\times\right.\right.$$
$$\left.\left.\times\frac{H^3{}_0\delta_{n0}-H^3{}_{nm}}{6R^3}\right] + \frac{\rho(H_0)}{-n-\nu+2}\left[\left(1+\frac{H_0}{R}\right)^{\nu}\left(1+\frac{Z}{R}\right)^{-n-\nu+2} - \left(1+\frac{H_0}{R}\right)^{-n+2}\right]\delta_{n0}\right\}.$$

Proof. Inserting Eq. (3.14) into (3.2) considering (3.3b) we obtain:

$$V_{\mathrm{int}}^{a}(P) = G\sum_{n=0}^{\infty} r^n\left[\int_{r_S}^{H_0}\rho^a(r')r'^{-n+1}dr' + \int_{H_0}^{r_Z}\rho^a(r')r'^{-n+1}dr'\right]P_n(\cos\psi)d\sigma. \quad (3.66)$$

The first integral in the square bracket is the same as in the internal type of the NADM and is also the same as Proposition 3.3. The second part can be written

$$\rho(H_0)(R+H_0)^{\nu}\int_{R+H_0}^{R+Z} r'^{-n+1-\nu}dr' = \frac{\rho(H_0)R^{-n+2}}{-n-\nu+2}\left[\left(1+\frac{H_0}{R}\right)^{\nu}\left(1+\frac{Z}{R}\right)^{-n-\nu+2} - \right.$$
$$\left. - \left(1+\frac{H_0}{R}\right)^{-n+2}\right], \qquad (3.67)$$

and the SHCs of the internal atmospheric potential can thus be written

$$\left(v_{\mathrm{int}}^{a}\right)_{nm} = \frac{3}{(2n+1)\rho_e}\left(\rho_0\left(F_{\mathrm{int}}^{a}\right)_{nm} + \rho(H_0)K_n\right), \qquad (3.68)$$

where $\left(F_{\mathrm{int}}^{\mathrm{a}}\right)_{nm}$ is the same as in Eq. (3.19) and

$$K_n = \frac{1}{-n-\nu+2}\left[\left(1+\frac{H_0}{R}\right)^{\nu}\left(1+\frac{Z}{R}\right)^{-n-\nu+2} - \left(1+\frac{H_0}{R}\right)^{-n+2}\right]\delta_{n0}. \qquad (3.69)$$

It should be noted that these SHCs should be inserted into Eq. (3.69) for generating the internal atmospheric potential.

In the following figure we present the atmospheric densities generated by each ADM versus the height up to 90 km.

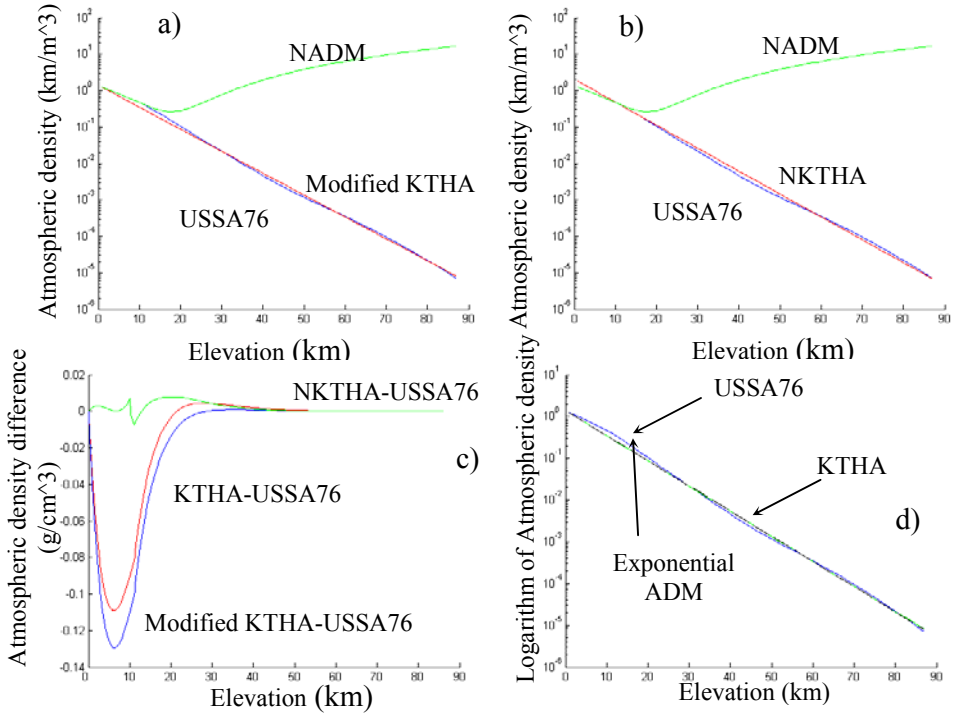

Figure 3.14. (a) Modified KTHA in red (vertical axis is in logarithmic scale), (b) NKTHA based on the USSA76 in red (vertical axis is in logarithmic scale), (c) differences between approximating models of KTHA, modified KTHA New KTHA and USSA76. (d) fitting of the exponential ADM and KTHA to the atmospheric density of the standard model

By fitting the KTHA to the USSA76 we obtain the value $\nu \doteq 930$. This modified KTHA is visualized in Figure 3.14a, which figure shows that, although the modified KTHA has very good fit to the USSA76 in higher elevations, it underestimates the density of the most massive part of the atmosphere in low levels. Therefore it is expected to see small AE on the SGG data. In Table 3.9 the statistics of these AEs based on the KTHA and the modified KTHA over Fennoscandia are presented. The differences are again mainly related to the diagonal elements V_{uu}, V_{vv} and V_{ww} of the gradiometric tensor as they, unlike the other elements, include the zero-degree harmonic. The difference between the AEs generated based on the original and modified KTHA is related to the underestimation of the atmospheric density in the

modified KTHA and also to significant overestimation of KTHA in higher elevation. However, since the most massive part of the atmosphere lies below 10 km level we can expect that the underestimation of the atmospheric density in the modified KTHA is the main reason for these differences. The only advantage of the modified KTHA relative to the original KTHA is thus to have a better fit in the higher elevations. Consequently, the modified KTHA is inferior to the original KTHA in context of the gravimetric data processing.

Table 3.9. Statistics of AE on SGG data at 250 km level based on KTHA and modified KTHA in ORF. Unit: 1 mE

	KTHA				Modified KTHA			
	max	mean	min	std	max	mean	min	std
V_{uu}	-0.87	-1.06	-1.22	$\pm$ 0.07	-0.78	-0.97	-1.12	$\pm$ 0.07
V_{vv}	-0.79	-1.06	-1.22	$\pm$ 0.10	-0.70	-0.96	-1.13	$\pm$ 0.10
V_{ww}	2.29	2.12	1.67	$\pm$ 0.14	2.10	1.93	1.48	$\pm$ 0.14
V_{uv}	0.07	-0.03	-0.10	$\pm$ 0.04	0.07	-0.02	-0.10	$\pm$ 0.04
V_{uw}	0.26	0.01	-0.27	$\pm$ 0.10	0.26	0.01	-0.27	$\pm$ 0.10
V_{vw}	0.32	0.01	-0.18	$\pm$ 0.08	0.32	0.01	-0.18	$\pm$ 0.08

We also consider another approach in which the NADM is used for the heights below 10 km and another modified KTHA for considering higher levels. In this case the atmospheric density generated by the NADM at 10 km is considered as a reference value and the KTHA model is modified to get best fit to the densities of the USSA76 after 10 km. Figure 3.14b shows the result of this fitting. The figure shows that the atmospheric densities are overestimated by the NKTHA with respect to the USSA76 between 20 and 60 km levels. However since the atmospheric density decreases fast by increasing the elevation we can expect that such misfitness is insignificant in higher levels. In this case we estimate $\nu = 890.1727 \doteq 890$, see Eq. (3.12). The RMSEs of the model fittings are 0.038, 0.032 and 0.0027 kg/m^3 for KTHA, modified KTHA and new KTHA, respectively. In Table 3.10 the statistics of the AE on the SGG data over Fennoscandia are presented based on the NKTHA.

Table 3.10. Statistics of AE on SGG data at 250 level based on NKTHA in ORF. Unit: 1 mE

	NKTHA			
	max	mean	min	std
V_{uu}	-2.36	-2.56	-2.74	$\pm$ 0.08
V_{vv}	-2.27	-2.57	-2.76	$\pm$ 0.11
V_{ww}	5.32	5.14	4.63	$\pm$ 0.15
V_{uv}	0.07	-0.03	-0.11	$\pm$ 0.04
V_{uw}	0.30	0.01	-0.30	$\pm$ 0.11
V_{vw}	0.35	0.01	-0.20	$\pm$ 0.09

Since in the NKTHA we use the NADM for the elevations below 10 km, we expect to see a good fit to the effects for these ADMs, which are confirmed by the statistics presented in the tables.

In the following we present the maps of the AE on the SGG data over Fennoscandia. Again two-month revolution of the satellite with 30 second integration step size was considered in our investigation over Fennoscandia. The lower boundary of the atmosphere was considered the Earth surface and the upper bound at satellite level. The JGP95e global topographic model was also used to generate the topographic harmonics to degree and order 360.

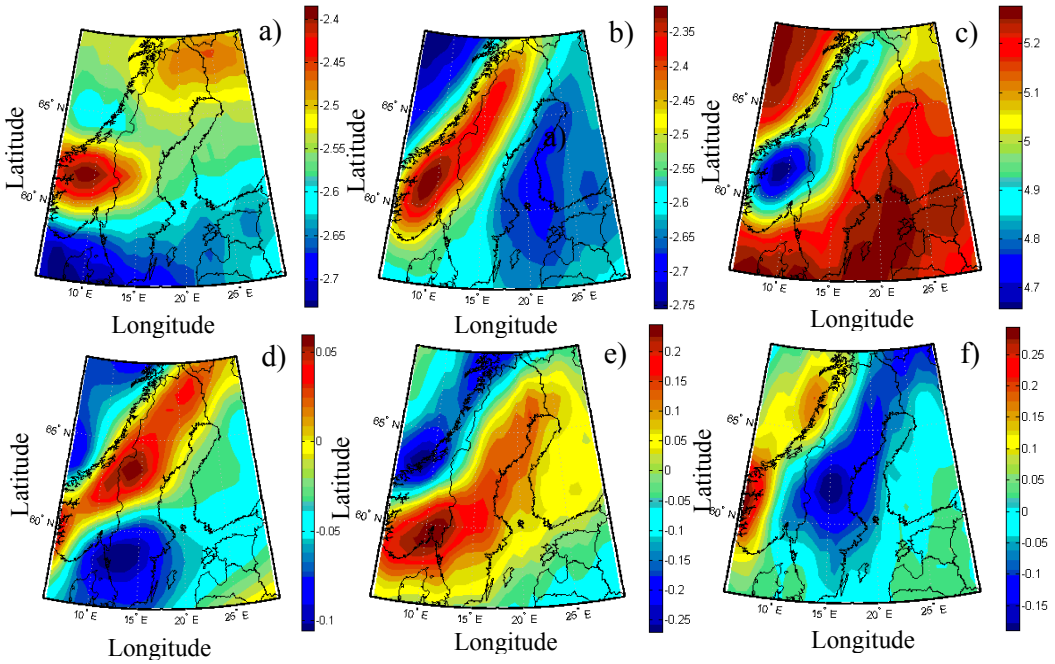

Figure 3.15. AE on the SGG at 250 km based on the NKTHA, (a) V_{uu}, (b) V_{vv}, (c) V_{ww}, (d) V_{uv}, (e) V_{uw} and (f) V_{vw}. Unit: 1 mE

Figure 3.15 illustrates the AE on the SGG data at 250 km based on the NKTHA. (a), (b), (c), (d), (e) and (f) are V_{uu}, V_{vv}, V_{ww}, V_{uv}, V_{uw} and V_{vw}, respectively. The largest AE is about 5.1381 mE and related to V_{ww} as would we expect, and the smallest effect (about -0.0276 mE) is related to V_{uv}.

3.4.7 Summary of AEs

The KTHA was modified so that it yields better fit to the USSA76 than the original one (which was derived based on USSA61), and the constant ν=930 was obtained for the modified model. Numerical studies show that this model underestimates the most massive part of the atmosphere which is below 10 km more than the original one, but it has better fit for higher elevations, and this effect on the SGG is less than 1

mE. A combination of both ADMs presented by Novák (2000) and Sjöberg (1998) with a simple modification was proposed as the NKTHA. This model has good fit with the USSA76 for low and high levels. The SHCs of the atmospheric potential generated based on this new model were used to compute the AEs on the SGG data in the ORF. Numerical results show that the maximum effect is related to V_{ww} and about 5.13 mE. In comparison with Novák (2000) model, which generate the corresponding value 4.44 mE, one can state that the effect of the atmospheric masses above 10 km is less than 1 mE but significant for validation or downward continuation of the SGG. We recommend the use of NKTHA in considering AEs in the SGG data processing and any other gravimetric applications.

3.5 Remove-Compute-Restore scheme

In the remove-compute-restore approach, the external topographic and atmospheric potentials are removed and the result will be a space with no-topography and no-atmosphere. The effect of the topographic and atmospheric masses must be restored after computations (this is why the method is called remove-compute-restore). The gravity field can also be determined locally from SGG data using inversion of the second-order derivatives of extended Stokes or Abel-Poisson integrals. The downward continued gravity anomaly or disturbing potential at sea level is the results of this inversion process. One can also downward continue the SGG data directly to geoid height or gravity anomaly at sea level. In any case, the effect of the removed atmospheric potential should be restored on these quantities. In the following we present these indirect AEs on the gravity anomaly and geoid height.

The direct and indirect effects are used in remove-compute-restore technique. However, when analytical continuation is considered one can perform downward continuation disregarding these effects and add the total effect (combination of direct and indirect effects) on the downward continued quantities. As mentioned in the introduction the downward continued quantities are the gravity anomaly or geoid. Based on the fundamental theorem of physical geodesy (Heiskanen and Moritz 1967) we have:

$$\delta\Delta g\left(P\right) = -\frac{\partial \delta V\left(P\right)}{\partial r} - \frac{2}{r}\delta V\left(P\right), \tag{3.70}$$

where $V\left(P\right)$ is either external or internal topographic potential. Therefore the direct and indirect effect on the gravity anomaly will be

$$\delta\Delta g_{\text{ext}}^{\text{t,a}}\left(P\right) = \frac{GM}{R^2}\sum_{n=0}^{\infty}\left(n-1\right)\left(\frac{R}{r}\right)^{n+1}\sum_{m=-n}^{n}\left(V_{\text{ext}}^{\text{t,a}}\right)_{nm}Y_{nm}\left(P\right), \tag{3.70a}$$

$$\delta\Delta g_{\text{int}}^{\text{t,a}}\left(P\right) = -\frac{GM}{R^2}\sum_{n=0}^{\infty}\left(n+1\right)\left(\frac{r}{R}\right)^{n-1}\sum_{m=-n}^{n}\left(V_{\text{int}}^{\text{t,a}}\right)_{nm}Y_{nm}\left(P\right). \tag{3.70b}$$

Restoring the topographic or atmospheric potential on the continued SGG data to sea level can also be formulated using internal type of the spherical harmonic series. By using the internal type of the topographic and atmospheric potentials, Eq. (3.2b), and using the expression of the gravitational gradients in the LNOF presented by Reed (1973) we obtain:

$$V_{xx}^{\mathrm{t,a}}(P)=\frac{GM}{R^3}\sum_{n=0}^{\infty}\left(\frac{r}{R}\right)^{n-2}\sum_{m=-n}^{n}\left(V_{\mathrm{int}}^{\mathrm{t,a}}\right)_{nm}Q_m(\lambda)\left(n\bar{P}_{n|m|}+\frac{\partial^2\bar{P}_{n|m|}}{\partial\theta^2}\right), \tag{3.71a}$$

$$V_{yy}^{\mathrm{t,a}}(P)=\frac{GM}{R^3}\sum_{n=0}^{\infty}\left(\frac{r}{R}\right)^{n-2}\sum_{m=-n}^{n}\left(V_{\mathrm{int}}^{\mathrm{t,a}}\right)_{nm}Q_m(\lambda)\left(n\bar{P}_{n|m|}+\frac{\cos\theta}{\sin\theta}\frac{\partial\bar{P}_{n|m|}}{\partial\theta}-m^2\frac{\bar{P}_{n|m|}}{\sin^2\theta}\right), \tag{3.71b}$$

$$V_{xy}^{\mathrm{t,a}}(P)=\frac{GM}{R^3}\sum_{n=0}^{\infty}\left(\frac{r}{R}\right)^{n-2}\sum_{m=-n}^{n}m\left(V_{\mathrm{int}}^{\mathrm{t,a}}\right)_{nm}Q_{-m}(\lambda)\left(\frac{1}{\sin\theta}\frac{\partial\bar{P}_{n|m|}}{\partial\theta}-\frac{\cos\theta}{\sin^2\theta}\bar{P}_{n|m|}\right), \tag{3.71c}$$

$$V_{xz}^{\mathrm{t,a}}(P)=\frac{GM}{R^3}\sum_{n=0}^{\infty}\left(\frac{r}{R}\right)^{n-2}\sum_{m=-n}^{n}\left(V_{\mathrm{int}}^{\mathrm{t,a}}\right)_{nm}Q_m(\lambda)(1-n)\frac{\partial\bar{P}_{n|m|}}{\partial\theta}, \tag{3.71d}$$

and

$$V_{xz}^{\mathrm{t,a}}(P)=\frac{GM}{R^3}\sum_{n=0}^{\infty}\left(\frac{r}{R}\right)^{n-2}\sum_{m=-n}^{n}m\left(V_{\mathrm{int}}^{\mathrm{t,a}}\right)_{nm}Q_{-m}(\lambda)(1-n)\frac{\bar{P}_{n|m|}}{\sin\theta}. \tag{3.71e}$$

The topographic bias (or the total effect) on the gravity anomaly will be:

$$\delta\Delta g_{\mathrm{bias}}^{\mathrm{t}}(P)=\left[\delta\Delta g_{\mathrm{ext}}^{\mathrm{t}}(P)\right]^{*}-\delta\Delta g_{\mathrm{int}}^{\mathrm{t}}(P)\Big|_{r=R}. \tag{3.71}$$

Inserting Eq. (3.70a) and Eq. (3.70b) for $r=R$ into Eq. (3.71) yields

$$\delta\Delta g_{\mathrm{bias}}^{\mathrm{t}}(P)\doteq\frac{3GM}{R^2\rho^{\mathrm{e}}}\sum_{n=0}^{\infty}\sum_{m=-n}^{n}\left[\frac{\left(\rho^{\mathrm{t}}H\right)_{nm}}{R}+(n-1)(n+2)\frac{\left(\rho^{\mathrm{t}}H\right)^3_{nm}}{6R^3}\right]Y_{nm}(P). \tag{3.72}$$

In a similar way as in Eq. (3.72) we can write the topographic bias on the disturbing potential as:

$$\delta V_{\mathrm{bias}}^{\mathrm{t}}(P)\doteq\frac{3GM}{R\rho^{\mathrm{e}}}\sum_{n=0}^{\infty}\sum_{m=-n}^{n}\left[\frac{\left(\rho^{\mathrm{t}}H\right)^2_{nm}}{2R^2}+\frac{\left(\rho^{\mathrm{t}}H\right)^3_{nm}}{3R^3}\right]Y_{nm}(P), \tag{3.73}$$

which is the same as the topographic bias in Sjöberg (2007).

Theorem 3.1 *The potential of topographic bias is (Ågren 2004, Sjöberg 2007)*:

$$\delta V^{\,\mathrm{t}}_{\mathrm{bias}}(P) \doteq \frac{3GM\,\rho^{\mathrm{t}}}{R^3\rho^{\mathrm{e}}}\left(\frac{H_P^2}{2}+\frac{H_P^3}{3R}\right).$$

3.6 Topographic and atmospheric biases in spherical harmonics on the SGG data

According to the story we mentioned in the previous section, we can write the topographic and atmospheric biases in spherical harmonics as subtraction of the downward continued direct effect and the indirect effects on the geoid. Here we present general formulas for considering the topographic and atmospheric biases on the gravitational gradients:

$$\mathrm{bias}V^{\,\mathrm{t,a}}_{zz}(P)=\frac{GM}{R^3}\sum_{n=0}^{\infty}\sum_{m=-n}^{n}\left[(n+1)(n+2)\left(V^{\,\mathrm{t,a}}_{\mathrm{ext}}\right)_{nm}-n(n-1)\left(V^{\,\mathrm{t,a}}_{\mathrm{int}}\right)_{nm}\right]Y_{nm}(P), \tag{3.74a}$$

$$\mathrm{bias}V^{\,\mathrm{t,a}}_{xx}(P)=\frac{GM}{R^3}\sum_{n=0}^{\infty}\sum_{m=-n}^{n}\left\{\left[-(n+1)\left(V^{\,\mathrm{t,a}}_{\mathrm{ext}}\right)_{nm}-n\left(V^{\,\mathrm{t,a}}_{\mathrm{int}}\right)_{nm}\right]Y_{nm}(P)+\right.$$
$$\left.+\left[\left(V^{\,\mathrm{t,a}}_{\mathrm{ext}}\right)_{nm}-\left(V^{\,\mathrm{t,a}}_{\mathrm{int}}\right)_{nm}\right]\frac{\partial^2 Y_{nm}(P)}{\partial\theta^2}\right\}, \tag{3.74b}$$

$$\mathrm{bias}V^{\,\mathrm{t,a}}_{yy}(P)=\frac{GM}{R^3}\sum_{n=0}^{\infty}\sum_{m=-n}^{n}\left\{\left[-(n+1)\left(V^{\,\mathrm{t,a}}_{\mathrm{ext}}\right)_{nm}-n\left(V^{\,\mathrm{t,a}}_{\mathrm{int}}\right)_{nm}\right]Y_{nm}(P)+\right.$$
$$\left.+\left[\left(V^{\,\mathrm{t,a}}_{\mathrm{ext}}\right)_{nm}-\left(V^{\,\mathrm{t,a}}_{\mathrm{int}}\right)_{nm}\right]\left(\frac{\cos\theta}{\sin\theta}\frac{\partial Y_{nm}(P)}{\partial\theta}-m^2\frac{Y_{nm}(P)}{\sin^2\theta}\right)\right\}, \tag{3.74c}$$

$$\mathrm{bias}V^{\,\mathrm{t,a}}_{xy}(P)=\frac{GM}{R^3}\sum_{n=0}^{\infty}\sum_{m=-n}^{n}\left[\left(V^{\,\mathrm{t,a}}_{\mathrm{ext}}\right)_{nm}-\left(V^{\,\mathrm{t,a}}_{\mathrm{int}}\right)_{nm}\right]$$
$$\left[\frac{1}{\sin\theta}\frac{\partial Y_{nm}(P)}{\partial\theta}-\frac{\cos\theta}{\sin^2\theta}Y_{nm}(P)\right], \tag{3.74d}$$

$$\mathrm{bias}V^{\,\mathrm{t,a}}_{xz}(P)=\frac{GM}{R^3}\sum_{n=0}^{\infty}\sum_{m=-n}^{n}\left[(n+2)\left(V^{\,\mathrm{t,a}}_{\mathrm{ext}}\right)_{nm}-(1-n)\left(V^{\,\mathrm{t,a}}_{\mathrm{int}}\right)_{nm}\right]\frac{\partial Y_{nm}(P)}{\partial\theta}, \tag{3.74e}$$

and

$$\mathrm{bias}V^{\,\mathrm{t,a}}_{xz}(P)=\frac{GM}{R^3}\sum_{n=0}^{\infty}\sum_{m=-n}^{n}\left[(n+2)\left(V^{\,\mathrm{t,a}}_{\mathrm{ext}}\right)_{nm}-(1-n)\left(V^{\,\mathrm{t,a}}_{\mathrm{int}}\right)_{nm}\right]\frac{\partial^2 Y_{nm}(P)}{\sin\theta\partial\theta\partial\lambda}, \tag{3.74f}$$

These formulas are useful for practical computations, but it should be considered that the downward continuation using spherical harmonics is not true as the convergence of the spherical harmonic expansion does not hold. It can also make the results even

worse. Therefore it is recommended to remove the effects before downward continuation and restore them after computations. However, considering the topographic bias can easily be investigated without problem in convergence if the binomial expansion is used up to third-order. In the following we discuss the topographic bias on the gravitational gradients further.

Proposition 3.15 *The topographic bias on second-radial derivative of gravitational gradients at sea level ($R \approx r$) is*:

$$\mathrm{bias}V_{zz}^{\mathrm{t}}(P) \approx \frac{3GM\rho^{\mathrm{t}}}{R^3\rho^{\mathrm{e}}}\left(1+\frac{2H_P}{R}\right).$$

Proof. Double differentiating the equation in Theorem 3.15 with respect to H_P proves the proposition.

Corollary 3.2 *The topographic bias on T_{xz} , T_{yz} and T_{xy} at geoid is zero*.

Proof. As we know, we can generally write

$$\mathrm{bias}V_{xz}(P) = \frac{1}{r^2}\frac{\partial \mathrm{bias}V(P)}{\partial\theta} - \frac{1}{r}\frac{\partial^2 \mathrm{bias}V(P)}{\partial r\partial\theta}, \tag{3.75a}$$

$$\mathrm{bias}V_{xz}(P) = \frac{1}{r^2}\frac{\partial \mathrm{bias}V(P)}{\sin\theta\partial\lambda} - \frac{1}{r}\frac{\partial^2 \mathrm{bias}V(P)}{\sin\theta\partial r\partial\theta}, \tag{3.75b}$$

and

$$\mathrm{bias}V_{xy}(P) = \frac{\partial \mathrm{bias}V(P)}{r^2\sin\theta\partial\theta\partial\lambda} - \frac{\cos\theta\,\partial \mathrm{bias}V(P)}{r^2\sin^2\theta\partial\lambda}. \tag{3.75c}$$

According to Theorem 3.1 the potential of the topographic bias is only function of radial distance and consequently its derivatives with respect to any another horizontal parameter will be zero.

Proposition 3.16:

$$\mathrm{bias}V_{xx}^{\mathrm{t}}(P) = \mathrm{bias}V_{yy}^{\mathrm{t}}(P) = \mathrm{bias}V_{r}^{\mathrm{t}}(P) = \frac{3GM\rho^{\mathrm{t}}}{R^4\rho^{\mathrm{e}}}\left(H_P + \frac{H_P^2}{R}\right).$$

Proof. We already know

$$\mathrm{bias}V_{xx}^{\mathrm{t}}(P) = \frac{1}{R}\frac{\partial \mathrm{bias}V^{\mathrm{t}}(P)}{\partial r} + \frac{1}{R^2}\frac{\partial^2 \mathrm{bias}V^{\mathrm{t}}(P)}{\partial\theta^2}, \tag{3.76a}$$

$$\mathrm{bias}V_{yy}^{t}(P) = \frac{1}{R}\frac{\partial \mathrm{bias}V^{\mathrm{t}}(P)}{\partial r} + \frac{1}{R^2\tan\theta}\frac{\partial \mathrm{bias}V^{\mathrm{t}}(P)}{\partial\theta} + \frac{1}{R^2\sin^2\theta}\frac{\partial^2 \mathrm{bias}V^{\mathrm{t}}(P)}{\partial\lambda^2}, \tag{3.76b}$$

According to Theorem 3.1 the horizontal derivatives of the topographic bias vanish. Therefore the first terms of Eqs. (3.76a)-(3.76c) are the same and

$$\frac{\partial \text{bias} V^{\text{t}}(P)}{\partial r} = \frac{3GM\rho^{\text{t}}}{R^3 \rho^{\text{e}}} \left(H_P + \frac{H_P^2}{R} \right). \tag{3.77}$$

Therefore the proposition is proved.

According to this discussion, one can say that the gravitational gradients $V_{xz}^{\text{t}}(P)$, $V_{yz}^{\text{t}}(P)$ and $V_{xy}^{\text{t}}(P)$ can be continued downward without considering the TE, as the topographic bias on these gradients are zero. The topographic bias can easily be considered after downward continuation using Propositions 3.15 and 3.16 for diagonal elements of the gravitational tensor as they are extremely simple. These propositions show that the total TE (the topographic bias in opposite sign) is only a function of that part of topography which in below the point *P*.

Chapter 4

Least-squares modification

4.1 Introduction

The SGG data should be validated before using. In order to do that different methods have been proposed. A simple way could be the direct comparing of the real SGG data with the synthesized gravitational gradients using an existing EGM. Another idea is to use regional gravity data to generate the gradients at satellite level. Haagmans et al. (2002) and Kern and Haagmans (2004) used the extended Stokes and extended Hotine formulas to generate the gravitational gradients using terrestrial gravity data. Denker (2002) used the least-squares spectral combination technique to generate and validate the gravitational gradients. Bouman et al. (2003) has set up a calibration model based on instrument (gradiometer) characteristics to validate the measurement. Muller et al. (2004) used the terrestrial gravity anomalies to generate the gravitational gradients, and after that Wolf (2007) investigated the deterministic approaches to modify the integrals and validate the SGG data. In fact, the spectral weighting scheme (Sjöberg 1980 and 1981 and Wenzel 1981) was used by Wolf (2007). Stochastic methods of modifying Stokes' formula can be used for the extended Stokes' formula as well; see Sjöberg (1984a), (1984b), (1991) and (2003). Least-squares collocation can be used for validation purposes. Tscherning et al. (2006) considered this method and concluded that the gradients can be predicted with an error of 2-3 mE in the case of an optimal size of the collection area and optimal resolution of data. Zielinski and Petrovskaya (2003) proposed a balloon-borne gradiometer to fly at 20-40 km altitude simultaneously with satellite mission and proposed downward continuation of satellite data and comparing them with balloon-borne data. Bouman and Koop (2003) presented an along-track interpolation method to detect the outliers. Their idea is to compare the along-tack interpolated gradients with measured gradients. If the interpolation error is small enough the differences should be predicted reasonably by an error model. Pail (2003) proposed a combined adjustment method supporting high quality gravity field information within the well-surveyed test area for continuation of local gravity field upward and validating the SGG data. Bouman et al. (2004) stated

that there are some limitations in generating the gravitational gradients using terrestrial gravimetry data and EGMs. When an EGM model is used, high degrees and orders should be taken into account and the recent EGMs seem to be able to remove the greater part of the systematic errors. In regional approach they concluded that the bias of the gradients can accurately be recovered using least-squares collocation. Also, they concluded that the method of validation using high-low satellite-to-satellite tracking data fails unless a higher resolution EGM is available. Kern et al. (2004) and (2005) presented an algorithm for detecting the outliers in the SGG data in the time domain.

In this chapter our goal is to validate the SGG data in the presence of unknown sources of the systematic errors. Since the gravity anomaly is a simple measurement in physical geodetic applications, a way to relate this observable to the SGG data is sought. The second-order partial derivatives of the well-known extended stokes formula is used to generate the gravitational gradients at satellite level. In the geodetic application involved with gravity anomaly and terrestrial data we are restricted to a specific area. Therefore the integral formulas should be modified according to the cap of the existing data. Different ways of modifying these integral formulas exist, but in this chapter the emphasis is on the LSM to modify the second-order partial derivatives of the extended Stokes formula.

The disturbing potential can be expressed by an integral which is well-known as the extended Stokes formula. This integral formula is (Heiskanen and Moritz 1967):

$$T(P)=\frac{R}{4\pi}\iint_{\sigma} S(r,\psi)\Delta g(Q)d\sigma\,, \tag{4.1}$$

where R is the radius of the reference sphere, r is the geocentric distance at computation point P, ψ is the geocentric angle between the computation point P and the integration point Q with the following expression

$$\cos\psi=\cos\theta\cos\theta'+\sin\theta\sin\theta'\cos(\lambda'-\lambda), \tag{4.2}$$

and θ and λ are the co-latitude and longitude of P and θ' and λ' are of the integration point Q. σ is the unit sphere, $\Delta g(Q)$ is the gravity anomaly at sea level and

$$S(r,\psi)=\sum_{n=2}^{\infty}\frac{2n+1}{2}\Omega_n(r)P_n(\cos\psi), \tag{4.3a}$$

is the spectral form of the extended Stokes function (ESF) with the spectrum

$$\Omega_n(r)=\frac{2}{n-1}\left(\frac{R}{r}\right)^{n+1}. \tag{4.3b}$$

Equation (4.1) shows that the integration should be performed globally, which means that $\Delta g(Q)$ with a global coverage is required. Therefore we should look for an approach to modify the integral in such a way that the contribution of the far zone data is minimized. Different methods for modifying Stokes' formula have been presented, but here the concentration is on stochastic approaches as in Sjöberg (1984a) and (1984b). In fact, the theory behind this part of the study was presented by him, but the main difference is that his emphasis was just on Stokes' integral for geoid determination. However, we are going to test the capability of these stochastic approaches in modifying the extended Stokes formula and generating the SGG data for validation purposes. In the following we investigate the LSM and the Molodensky modification (MM) (Molodensky et al. 1962) of the extended Stokes formula.

4.2 LSM and MM of the extended Stokes formula

A general estimator of the disturbing potential based on the extended Stokes formula is very similar to the general geoid estimator of Sjöberg (2003); and the only difference is related to the kernel function and its spectrum. Let us start the discussion by this general disturbing potential estimator:

$$\tilde{T}(P)=\frac{R}{4\pi}\iint_{\sigma_0} S^{L}(r,\psi)\Delta g^{\mathrm{T}}(Q)\,d\sigma+\frac{R}{2}\sum_{n=2}^{L} b_n(r)\Delta g_n^{\mathrm{EGM}}(P), \qquad (4.4a)$$

where L is the maximum degree of modification, $b_n(r)$ is a parameter, which differs with the type of the disturbing potential estimator, and

$$S^{L}(r,\psi)=S(r,\psi)-\sum_{n=2}^{L}\frac{2n+1}{2}s_n(r)P_n(\cos\psi), \qquad (4.4b)$$

is the modified ESF and $s_n(r)$ are the modification parameters, which are estimated. The closed form of the ESF is (Heiskanen and Moritz 1967, p. 93, Eq. 2-162):

$$S(r,\psi)=\frac{2R}{l}+\frac{R}{r}-3\frac{Rl}{r^2}-\frac{R^2}{r^2}\cos\psi\left(5+3\ln\frac{r-R\cos\psi+l}{2r}\right), \qquad (4.4c)$$

where

$$l=\sqrt{r^2+R^2-2Rr\cos\psi}\,, \qquad (4.4d)$$

is the spatial distance between points P and Q. Also

$$\Delta g_n^{\mathrm{EGM}}(P)=\frac{GM}{R^2}(n-1)\sum_{m=-n}^{n} t_{nm}Y_{nm}(P), \qquad (4.4e)$$

is the Laplace harmonic expansion of $\Delta g(P)$ (Heiskanen and Moritz 1967, p. 97), t_{nm} is the SHCs of the disturbing potential derived from subtraction of the normal gravitational field from an EGM. $Y_{nm}(P)$ is the surface spherical harmonic of degree *n* and order *m*. *GM* is the geocentric gravitational constant. In order to show from which sources the gravity anomaly is derived we separate them into Δg^{T} for the terrestrial and Δg^{EGM} for the EGM based data.

In the MM the idea is to determine the modification parameters $s_n(r)$ in such a way that the upper bound of the truncation error the estimator (Eq. 4.4a) is minimized. These parameters are attained by differentiating the following integral:

$$\iint_{\sigma-\sigma_0} \left[S^L(r,\psi)\right]^2 \sin\psi d\psi \,, \tag{4.4f}$$

with respect to the parameters $s_n(r)$ and equating to zero. The result is the system of equations presented in Proposition 4.1. For more details the interested readers are referred to e.g., Molodensky et al. (1962) and Heiskanen and Moritz (1967, p. 263).

Proposition 4.1 *The MM parameters* $s_r(r)$ *of the disturbing potential are derived based on solving of the following system of equations (see e.g. Molodensky et al. 1962, Sjöberg 2003)*:

$$\sum_{r=2}^{M} a_{kr} s_r(r) = h_k(r), \qquad k=2,3,\ldots,M, \tag{4.5a}$$

where

$$a_{kr} = a_{rk} = E_{rk}(\psi_0)\,.\,k\,,\ r=2,3,\ldots,M \tag{4.5b}$$

$$h_k(r) = Q_k(r,\psi_0)\ \ k=2,3,\ldots,M, \tag{4.5c}$$

$$E^0_{rk}(\psi_0) = \frac{2k+1}{2} e^0_{rk}(\psi_0)\,, \tag{4.5d}$$

$$e^0_{rk}(\psi_0) = \int_{\psi_0}^{\pi} P_r(\cos\psi) P_k(\cos\psi) \sin\psi d\psi\,, \tag{4.5e}$$

$$Q_k(r,\psi_0) = \int_{\psi_0}^{\pi} S(r,\psi) P_k(\cos\psi) \sin\psi d\psi\,, \tag{4.5f}$$

$$Q_k(r,\psi_0) = \sum_{n=2}^{\infty} \frac{2n+1}{2} \Omega_n(r) e^0_{nn'}(\psi_0)\,. \tag{4.5g}$$

According to the author's numerical experiences, the Shepperd (1982) recursive formula of computing the truncation coefficients $Q_k(r,\psi_0)$ is unstable and impractical at high altitudes. He mentioned that his formulas might be used for the altitudes below 20 km. Another way is to evaluate these truncation coefficients numerically, but it was found out that the numerical integration error considerably affects the results. We use the spectral form of the truncation coefficients (Eq. 4.5g), involving zero-order Paul's coefficients $e^0_{nn'}(\psi_0)$ which are not difficult to compute using the recursive formulas presented e.g. by Paul (1978).

The LSM method considers the error of terrestrial and EGM data as well as the truncation error of the integral. Three different versions of the LSM method were presented by Sjöberg (2003) such as BLSM, ULSM and OLSM. The extended Stokes formula can be modified by these methods as well. In the following propositions, the elements of the system of equations, from which the modification parameters are derived, are presented.

Proposition 4.2 *The BLSM parameters for the disturbing potential estimator at satellite level are derived by setting* $b_n(r) = s_n(r)$ *and solving the system of equations Eq. (4.5a) with the following elements (Sjöberg 2003)*:

$$
\begin{aligned}
a_{kr} = a_{rk} &= \left(\sigma_r^2 + dc_r\right)\delta_{kr} - E^0_{kr}(\psi_0)\sigma_r^2 - E^0_{rk}(\psi_0)\sigma_k^2 + \\
&\quad + \sum_{n=2}^{\infty} E^0_{nr}(\psi_0) E^0_{nk}(\psi_0)\left(\sigma_n^2 + c_n\right) \\
h_k(r) &= \left[\Omega_k(r) - Q_k(r,\psi_0)\right]\sigma_k^2 + \\
&\quad + \sum_{n=2}^{\infty}\left[Q_n(r,\psi_0)\left(\sigma_n^2 + c_n\right) - \Omega_k(r)\sigma_n^2\right]E^0_{nk}(\psi_0). \\
&\quad k, r = 2,3,\ldots,M
\end{aligned}
$$

where σ_k^2 *is the error spectrum of the terrestrial gravimetric data and* dc_k *is the error spectrum of the gravity anomaly obtained from an existing EGM.*

For more details about the computation of σ_k^2 the reader is referred e.g. to Sjöberg (1986), Ågren (2004) and Ellmann (2005). The spectrum of the gravity anomaly is evaluated by using the EGM for those degrees below the maximum degree of modification, and analytical models like Kaula (1963), Tscherning and Rapp (1974) are used for the degrees above that maximum degree. According to Ellmann (2004) and (2005) and Ågren (2004) the Tscherning-Rapp model is superior with respect to the others in modification aspect. Relying on their conclusion we use this model in our numerical studies through this thesis.

Proposition 4.3 *The ULSM parameters of the disturbing potential estimator at satellite level are derived, if we select* $b_n(r)=Q_n^L(r,\psi_0)+s_n(r)$ *and solve the system of Eq. (4.5a) with the following elements (Sjöberg 2003)*:

$$a_{kr}=a_{rk}=d_r\delta_{kr}-E_{rk}^0(\psi_0)d_r-E_{kr}^0(\psi_0)d_k+\sum_{n=2}^{\infty}E_{nr}^0(\psi_0)E_{nk}^0(\psi_0)d_n\,,$$

$$h_k(r)=\Omega_k(r)\sigma_k^2-Q_k(r,\psi_0)d_k+\sum_{n=2}^{\infty}\left[Q_n(r,\psi_0)d_n-\Omega_n(r)\sigma_n^2\right]E_{nk}^0(\psi_0),$$

$$k\,,\ r=2,3,\ldots,M$$

where

$$d_n=\sigma_n^2+dc_n\,.$$

Proposition 4.4 *The OLSM parameters of the disturbing potential estimator at satellite level are derived, if we set* $b_n(r)=\left[Q_n^L(r,\psi_0)+s_n(r)\right]c_n/(c_n+dc_n)$ *and solve Eq. (4.5a) with the following elements (Sjöberg 2003)*:

$$a_{kr}=a_{rk}=C_r\delta_{kr}-E_{rk}^0(\psi_0)C_r-E_{kr}^0(\psi_0)C_k+\sum_{n=2}^{\infty}E_{nr}^0(\psi_0)E_{nk}^0(\psi_0)C_n\,,$$

$$k\,,\ r=2,3,\ldots,M$$

$$h_k(r)=\Omega_k(r)\sigma_k^2-Q_k(r,\psi_0)C_k+\sum_{n=2}^{\infty}\left[Q_n(r,\psi_0)C_n-\Omega_n(r)\sigma_n^2\right]E_{nk}^0(\psi_0).$$

where

$$C_k=\sigma_k^2+\begin{cases}c_k dc_k/(c_k+dc_k) & 2\le k\le M\\ c_k & k>M\end{cases}\,. \qquad (4.6)$$

4.2.1 Numerical studies on modification of the extended Stokes formula

In order to test numerical capability of the LSM methods for modifying the extended Stokes formula and generating the disturbing potential at satellite level (250 km), the EGM96 is used to generate the degree variances of the gravity anomaly c_n and its error degree variance dc_n. The error of the terrestrial data is considered to be 5 mGal with a correlation length of 0.1°. The maximum degree of modification is L=M=150. The three LSM methods and the MM are used to modify the formula. Figure 4.1a shows the behaviour of the ESF in different geocentric angles (ψ_0°) within degree 4°. As the figure shows, all three LSM methods can modify the ESF for 3° cap size successfully. The behaviour of the ESF, which is modified using the ULSM and OLSM, is growing up after 3°.

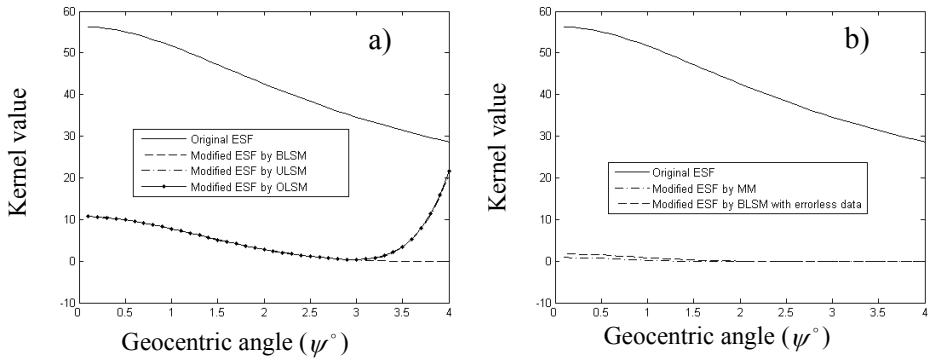

Figure 4.1. (a) Behaviour of ESF before and after different LSM methods. (b) Behaviour of ESF before and after MM and BLSM with errorless data

According to the author's numerical experience it is better to estimate $s_k(r)$, which is a function of geocentric distance instead of s_k (which is the modification parameter of the simple Stokes function). For better comparison we consider the BLSM and MM methods. It should be mentioned that in the MM we do not consider errors in neither for terrestrial nor for satellite data. If we want to compare the LSM with the MM we must put zero for the terrestrial and EGM data errors. Figure 4.1b shows the behaviour of the modified ESF according to the BLSM and the MM. However, it is not clear which one of these modification approaches is better unless we look at the global RMSE of the estimators. Figure 4.2a shows the global RMSE of the estimators modified based on the BLSM, ULSM and OLSM methods.

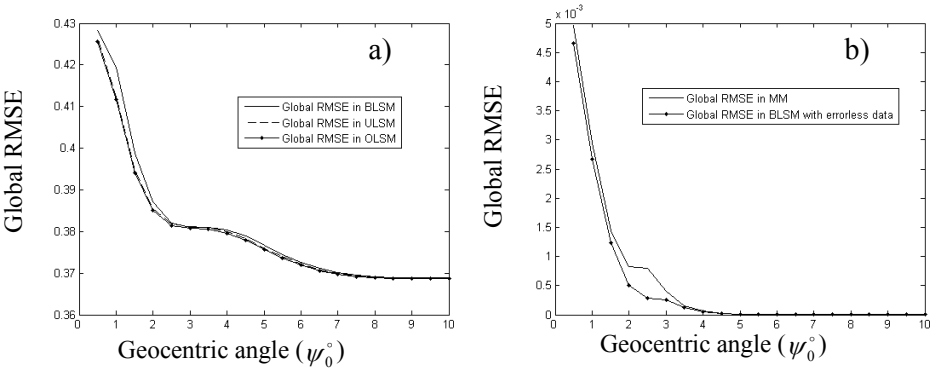

Figure 4.2. (a) Global RMSE of disturbing potential estimators based on different LSM methods. (b) Global RMSE of disturbing potential estimator based on MM and BLSM with errorless data. Unit: 1 m

The figure clearly shows that the ULSM and OLSM yield smaller global RMSE for the estimator than the BLSM. However, this difference is very small and may be negligible in practice. This numerical study shows very similar conclusion with the Ellmann (2005) results about the original Stokes function. Ellmann (2005) concluded that the differences among these types of modifying Stokes' formula are very small and they will have the similar results in geoid determination. Again for comparing the LSM versus the MM, we consider terrestrial and the EGM data free of errors. The

global RMSE of the modified estimator by the BLSM and the MM are presented in Figure 4.2b. As the figure shows the BLSM method is slightly better than the MM for ψ_0° between 2° and 4°.

We select a point above the roughest part of Fennoscandia, which has larger gravity anomalies than other parts of Fennoscandia, to test the capability of the estimators. The latitude and longitude of the computation point are 62° and 10°, respectively. Figure 4.3 shows the test area.

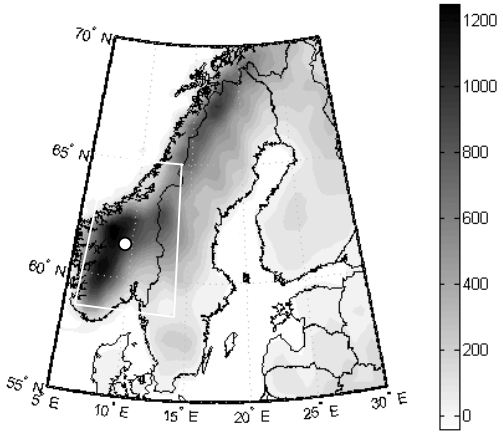

Figure 4.3. Topographic height of Fennoscandia and test area. Unit: 1 m

Table 4.1. Estimated disturbing potential using modified estimators by LSM divided by 9.8 at 250 km level with 1 mGal error for terrestrial data. Unit: 1 m

	BLSM	**ULSM**	**OLSM**
$30' \times 30'$	34.782	34.768	34.766
$15' \times 15'$	34.773	34.761	34.759
$12' \times 12'$	34.772	34.761	34.759
$6' \times 6'$	34.768	34.759	34.757
$3' \times 3'$	34.765	34.757	34.755

Again the EGM96 is used to generate the gravity anomaly in the test region with cap size 3° for integration. Also the value of disturbing potential is estimated by EGM96 at the computation point at 250 km level. For better visualization of the test we divided the values of the disturbing potential roughly by 9.8 $\mathrm{m/s}^2$ to change the units in metre. In this case, the estimated value using the EGM96 at 250 km level is 34.888 m. Table 4.1 shows the estimated disturbing potential using the modified extended Stokes' formula by BSLM, ULSM and OPLSM methods. In these computations we considered 1 mGal error for the terrestrial data. The differences between the BLSM and either the ULSM or OLSM methods in modifying extended Stokes' formula are within 1 cm at 250 km level. Table 4.2 shows the estimated disturbing potential using the modified estimator by LSM at 250 km level when 5 mGal error is selected for the terrestrial data.

Table 4.2. Different estimates of disturbing potential divided by 9.8 $\mathrm{m/s}^2$ at 250 km with 5 mGal error of terrestrial data. Unit: 1 m

	BLSM	**ULSM**	**OLSM**	**MM**	**BLSM0**
$30' \times 30'$	34.857	34.858	34.855	34.888	34.887
$15' \times 15'$	34.854	34.855	34.852	34.888	34.887
$12' \times 12'$	34.853	34.854	34.851	34.888	34.887
$6' \times 6'$	34.852	34.853	34.850	34.888	34.887
$3' \times 3'$	34.851	34.852	34.849	34.888	34.887

Table 4.2 clearly presents that when the accuracy of the terrestrial data decreases the estimated disturbing potential comes closer to 34.888 m (which is considered as the true value). In order to show this matter, we presented the MM and BLSM method with zero error for the terrestrial and the EGM data in Table 4.2.

In the above study we wanted to present the capability of the modification methods to generate the disturbing potential at satellite level. However, in SGG the second-order partial derivatives of the disturbing potential are measured at satellite level. Therefore we should consider how we can use the modification methods to reduce the far zone effects. In the following section we concentrate on the second-order radial derivative (SOD) of the extended Stokes formula because of its simplicity.

4.3 LSM and VV gravitational gradient

The gravitational tensor is a symmetric tensor with 5 independent elements. This tensor is also traceless (trace of this tensor is zero) since the disturbing potential is harmonic outside the Earth's surface. Therefore, if we present a method for validating the simplest components, such as $T_{zz}(P)$, in fact we validate $T_{xx}(P)+T_{yy}(P)$, too, because the disturbing potential is harmonic outside the Earth's surface. If $T_{zz}(P)$ is not equal to $-T_{xx}(P)-T_{yy}(P)$, it means that there is error either in $T_{zz}(P)$ or $-T_{xx}(P)-T_{yy}(P)$. Assuming the former is free of error, we conclude that the latter is erroneous, but we cannot say which one of the components $-T_{xx}(P)$ and $-T_{yy}(P)$ contains the blunder. In this section similar to the previous one we consider the LSM method of modifying the SOD of the extended Stokes formula to generate $T_{zz}(P)$ at point P at satellite level (250 km). The derivation is very similar to the propositions which already presented in Subsection 4.2. We define the following general estimator $\tilde{T}_{zz}(P)$:

$$\tilde{T}_{zz}(P)=\frac{R}{4\pi}\iint_{\sigma_0} S_{zz}^{L}(r,\psi)\Delta g^{\mathrm{T}}(Q)d\sigma+\frac{R}{2}\sum_{n=2}^{L} b_n''(r)\Delta g_n^{\mathrm{EGM}}(P), \qquad (4.7a)$$

where $b_n''(r)$ is a parameter that should be estimated according to the type of estimator, and

$$S_{zz}^{L}(r,\psi)=S_{zz}(r,\psi)-\sum_{n=2}^{L}\frac{2n+1}{2}s_n''(r)P_n(\cos\psi), \qquad (4.7b)$$

where $s_n''(r)$ are the modification parameters to be estimated, and (Reed 1973, Eq. 5.35)

$$S_{zz}^{L}(r,\psi)=\frac{t^3}{R^2}\left\{(1-t\cos\psi)\left[\frac{3(1-t^2)}{D^5}-\frac{4}{D^3}\right]-\frac{1+t^2}{D^3}-\frac{10}{D}-18D+\right.$$

$$+2-3t\cos\psi\left(15+6\ln\frac{1-t\cos\psi+D}{2}\right)\Bigg\}, \tag{4.7c}$$

where $t=R/r$ and $D=\sqrt{1-2t\cos\psi+t^2}$.

The modification parameters are derived in the following subsection.

4.3.1 Modification of the SOD of ESF

The LSM of SOD of the ESF is very similar to that of the ESF itself. If we estimate the modification parameter $s_n''(r)$, the left hand side of the system of equations (Eq. 4.5a) will not change and remain the same with those presented for the LSM of the ESF. The coefficients matrix **A** will have the same properties as that obtained for the ESF. Therefore, in the following we present how the modification parameters $s_n''(r)$ are estimated. At the first step, we start with the following corollary which is related with the MM of the SOD of the ESF.

Corollary 4.1 *The modification parameters $s_n''(r)$ based on the MM method are derived by solving Eq. (4.5a) and considering*

$$h_k(r)=\left[Q_k(r,\psi)\right]_{zz}=\left[Q_{zz}(r,\psi)\right]_k, \tag{4.8a}$$

where

$$\left[Q_k(r,\psi_0)\right]_{zz}=\int_{\psi_0}^{\pi}S_{zz}(r,\psi_{PQ})P_k(\cos\psi)\sin\psi d\psi, \tag{4.8b}$$

or in spectral form

$$\left[Q_k(r,\psi_0)\right]_{zz}=\sum_{n=2}^{\infty}\frac{2n+1}{2}\Omega_n''(r)e_{nk}^0(\psi_0), \tag{4.8c}$$

where

$$\Omega_n''(r)=\frac{(n+1)(n+2)}{r^2}\Omega_n(r), \tag{4.8d}$$

where $\Omega_n(r)$ was introduced in Eq. (4.3b).

Corollary 4.2 *The BLSM parameters are derived by setting $b_n''(r)=s_n''(r)$ and solving the system of equations Eq. (4.5a) with the following right hand side*

$$h_k(r)=\left\{\Omega_k''(r)-\left[Q_k(r,\psi_0)\right]_{zz}\right\}\sigma_k^2+$$
$$+\sum_{n=2}^{\infty}\left[\left[Q_k(r,\psi_0)\right]_{zz}\left(\sigma_n^2+c_n\right)-\Omega_k''(r)\sigma_n^2\right]E_{nk}^0(\psi_0).$$

Proof. The only difference between the biased geoid estimator of Sjöberg (1991) and the biased estimator is related to the truncation coefficients and spectrum of the SOD of ESF. If we consider the errors of terrestrial and satellite data by ε^{T} and $\varepsilon_n^{\mathrm{EGM}}$, respectively. We can write the following form of the error estimator:

$$\delta\tilde{T}_{zz}(P)=\frac{R}{4\pi}\iint_{\sigma_0}S_{zz}^{L}(r,\psi)\varepsilon^{\mathrm{T}}(Q)d\sigma+\frac{R}{2}\sum_{n=2}^{L}s_n''(r)\varepsilon_n^{\mathrm{EGM}}(P). \qquad (4.9)$$

Sjöberg (1991) proved that the integral part of this equation has the following spectral form

$$\frac{R}{4\pi}\iint_{\sigma_0}S_{zz}^{L}(r,\psi)\varepsilon^{T}(Q)d\sigma=\frac{R}{2}\sum_{n=2}^{\infty}\left\{\Omega_n''(r)-s_n''^{*}(r)-\left[Q_n^{L}(r,\psi_0)\right]_{zz}\right\}\varepsilon_n^{\mathrm{T}}, \qquad (4.10)$$

where

$$\left[Q_n^{L}(r,\psi_0)\right]_{zz}=\left[Q_n(r,\psi_0)\right]_{zz}-\sum_{k=2}^{L}s_k''(r)E_{nk}^{0}(\psi_0). \qquad (4.11)$$

Substituting Eq. (4.10) into Eq. (4.9) we obtain

$$\delta\tilde{T}_{zz}(P)=\frac{R}{2}\sum_{n=2}^{\infty}\left\{\Omega_n''(r)-s_n''^{*}(r)-\left[Q_n^{L}(r,\psi_0)\right]_{zz}\right\}\varepsilon_n^{\mathrm{T}}(P)+\frac{R}{2}\sum_{n=2}^{L}s_n''(r)\varepsilon_n^{\mathrm{EGM}}(P). \qquad (4.12)$$

By considering that the errors are random and with zero stochastic expectation,

$$E\left(\varepsilon_n^{\mathrm{T}}\right)=E\left(\varepsilon_n^{\mathrm{EGM}}\right)=0, \qquad (4.13a)$$

we have

$$E\left\{\delta\tilde{T}_{zz}^{2}\right\}=E\left\{\frac{1}{4\pi}\iint_{\sigma}\delta T_{zz}^{2}d\sigma\right\}=$$

$$=\frac{R^2}{4}\sum_{n=2}^{L}\left\{\left\{\Omega_n''(r)-s_n''(r)-\left[Q_n^{L}(r,\psi_0)\right]_{zz}\right\}^2\sigma_n^2+\left[Q_n^{L}(r,\psi_0)\right]_{zz}^2c_n+s_n''^{2}(r)dc_n\right\}+$$

$$+\frac{R^2}{4}\sum_{n=M+1}^{\infty}\left\{\left\{\Omega_n''(r)-\left[Q_n^{L}(r,\psi_0)\right]_{zz}\right\}^2\sigma_n^2+\left[Q_n^{L}(r,\psi_0)\right]_{zz}^2c_n\right\}. \qquad (4.13b)$$

By differentiating Eq. (4.13b) with respect to $s_k''(r)$ and equating the result to zero and rearranging the known and unknown parameters $s_k''(r)$, the proposition is proved.

Corollary 4.3 *The ULSM parameters* $s_n''(r)$ *are derived by considering* $b_n''(r)=\left\{\left[Q_n^L(r,\psi_0)\right]_{zz}+s_n''(r)\right\}$ *and solving the system of equations Eq. (4.5a) by considering*

$$h_k(r)=\Omega_k''(r)\sigma_k^2-\left[Q_k(r,\psi_0)\right]_{zz}d_k+\sum_{n=2}^{\infty}\left\{\left[Q_k(r,\psi_0)\right]_{zz}d_n-\Omega_n''(r)\sigma_n^2\right\}E_{nk}^0(\psi_0)$$

Proof. Similar to the proof presented for Corollary 4.2 we can write the error estimator as:

$$\delta\tilde{T}_{zz}(P)=\frac{R}{4\pi}\iint_{\sigma_0}S_{zz}^L(r,\psi)\varepsilon^{\mathrm{T}}(Q)d\sigma+\frac{R}{2}\sum_{n=2}^{M}\left\{\left[Q_n^L(r,\psi_0)\right]_{zz}+s_n''(r)\right\}\varepsilon_n^{\mathrm{EGM}}(P)-$$
$$-\frac{R}{2}\sum_{n=M+1}^{L}\left\{\left[Q_n^L(r,\psi_0)\right]_{zz}+s_n''(r)\right\}\Delta g_n^T(P)-\frac{R}{2}\sum_{n=L+1}^{\infty}\left[Q_n^L(r,\psi_0)\right]_{zz}\Delta g_n^T(P), \tag{4.14}$$

where $\left[Q_n^L(r,\psi_0)\right]_{zz}$ was already presented in Eq. (4.11). The mathematical expectation of Eq. (4.14) shows that the estimator is unbiased through *M*, which is in fact the maximum degree of the EGM for generating the long wavelength structure of the estimator. By squaring the above equation and considering that the EGM and terrestrial data are not correlated (see Eq. 4.13a) and after taking the statistical expectation and the global average, as we did in Eq. (4.13b) we have the following spectral form for the global MSE:

$$E\left\{\delta\tilde{T}_{zz}^2\right\}=\frac{R^2}{4}\sum_{n=2}^{\infty}\left\{\left\{\Omega_n''(r)-s_n''^*(r)-\left[Q_n^L(r,\psi_0)\right]_{zz}\right\}^2\sigma_n^2+\right.$$
$$\left.+\left\{\left[Q_n^L(r,\psi_0)\right]_{zz}+s_n''^*(r)\right\}^2\right\}dc_n^*, \tag{4.15a}$$

where

$$s_n''^*(r)=\begin{cases}s_n''(r) & 2\le n\le L\\ 0 & n>L\end{cases}\quad\text{and}\quad dc_n^*=\begin{cases}dc_n & 2\le n\le L\\ c_n & n>L\end{cases}. \tag{4.15b}$$

By differentiating Eq. (4.14) with respect to modification parameters $s_k''(r)$ and equating the result to zero and after further simplifications the proposition is proved.

Corollary 4.4 *The OLSM parameters* $s_n''(r)$ *are derived by considering* $b_n''(r)=\left\{\left[Q_n^L(r,\psi_0)\right]_{zz}+s_n''(r)\right\}c_n/(c_n+dc_n)$ *and solving the system of equations Eq. (4.5a) by considering*

$$h_k(r)=\Omega_k''(r)\sigma_k^2-\left[Q_k(r,\psi_0)\right]_{rr}d_k+\sum_{n=2}^{\infty}\left\{\left[Q_k(r,\psi_0)\right]_{rr}d_n-\Omega_n''(r)\sigma_n^2\right\}E_{nk}^0(\psi_0)$$

Proof. If the general error estimator Eq. (4.7a) is written in the following spectral form:

$$\delta\tilde{T}_{zz}(P)=\frac{R}{4\pi}\iint_{\sigma_0}S_{zz}^{L}(r,\psi)\varepsilon^{\mathrm{T}}(Q)d\sigma+\frac{R}{2}\sum_{n=2}^{L}b_n(r)\varepsilon_n^{\mathrm{EGM}}(P),\quad(4.16a)$$

according to Eq. (4.7a) the spectral form of the above error estimator is:

$$\delta\tilde{T}_{zz}(P)=\frac{R}{2}\sum_{n=2}^{\infty}\left\{\Omega_n''(r)-s_n''^{*}(r)-\left[Q_n^{L}(r,\psi_0)\right]_{zz}\right\}\varepsilon_n^{\mathrm{T}}(P)+\frac{R}{2}\sum_{n=2}^{M}b_n(r)\varepsilon_n^{\mathrm{EGM}}(P).\quad(4.16b)$$

The global MSE of the estimator will be:

$$E\left\{\delta\tilde{T}_{zz}\right\}=\frac{R^2}{4}\sum_{n=2}^{\infty}\left\{\left[b_n^{*}(r)-s_n''^{*}(r)-\left[Q_n^{L}(r,\psi_0)\right]_{zz}\right]^2c_n+\right.$$
$$\left.+\left[\Omega_n''(r)-s_n''^{*}(r)-\left[Q_n^{L}(r,\psi_0)\right]_{zz}\right]^2\sigma_n^2\right\}+\frac{R^2}{4}\sum_{n=2}^{M}b_n^2(r)dc_n,\quad(4.16c)$$

Taking the derivative of Eq. (4.16c) with respect to $s_k''(r)$ and after further simplification the proposition is proved.

4.3.2 Numerical studies on modification of the SOD of ESF

Similar to the previous numerical studies on the disturbing potential estimation, we select the EGM96 for generating c_n and dc_n. We consider M=L=150 (we assume the last EGM will have good accuracy up to this degree) and the terrestrial data error 5 mGal. Having assumed the cap size of integration ψ_0=3°, we modify the $\tilde{T}_{zz}(P)$ estimator using different LSM methods as well as the MM approach. The original SOD of ESF and the modified one are visualized in Figures 4.4.

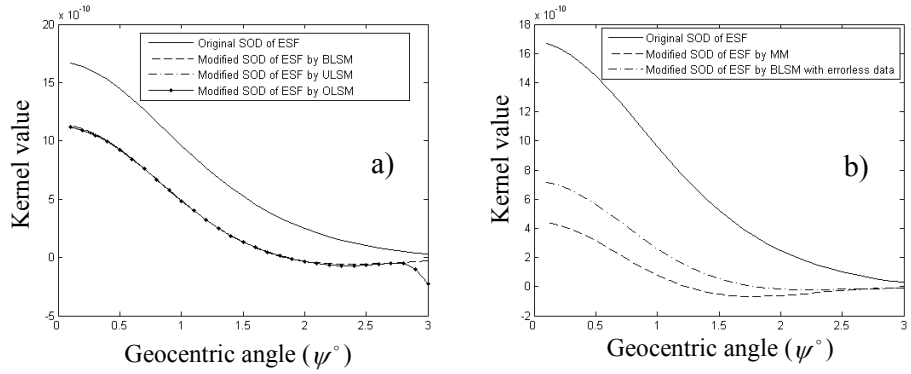

Figure 4.4. (a) Behaviour of original and modified SOD of ESF, (b) behaviour of original and modified SOD of ESF using MM and BLSM with errorless data

Figure 4.4a shows the modified SOD of ESF just up to ψ_0=3. The modified SOD of the ESF by the ULSM and OLSM methods are more or less the same, and both decay before end of the cap size. In order to compare the MM with the LSM method we have to equate the terrestrial and EGM data error to zero until just the truncation error is considered in the estimation. Figure 4.4b shows the modified SOD of ESF by the BLSM and the MM method. As can be seen, the modified SOD of ESF by the BLSM is above the MM. We cannot say which modification method is the better unless we consider the global RMSE of the estimator.

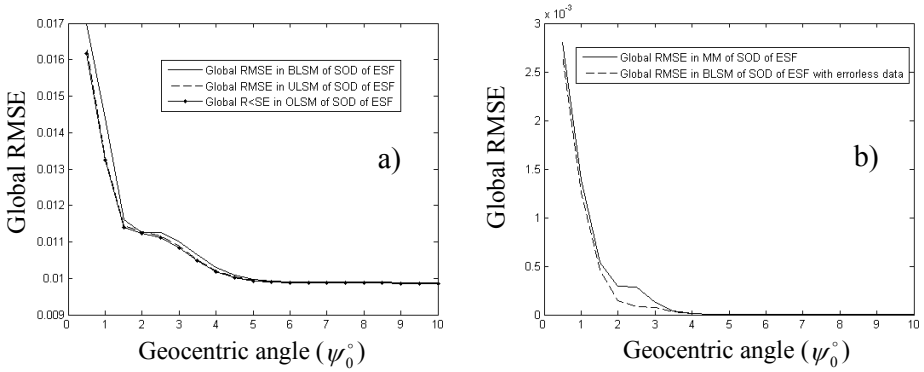

Figure 4.5. (a) Global RMSE of $\tilde{T}_{zz}(P)$ estimators based on different LSM methods. (b) Global RMSE of $\tilde{T}_{zz}(P)$ estimator based on MM and BLSM with errorless data. Unit: 1 E

Figure 4.5a shows very good agreement for the global RMSE of estimators modified by the ULSM and OLSM methods and both are smaller than the BLSM.

We consider the test point considered in Subsection 4.2.2; see Figure 4.3. We estimate $\tilde{T}_{zz}(P)$ = 0.3343 E at 250 km level using the EGM96. We derive the same value using the modified $\tilde{T}_{zz}(P)$ estimators. Since Figure 4.4 illustrates that the original SOD of the ESF decays toward zero, we should investigate if the modification of this integral is meaningful or not. To do this, We estimate $\tilde{T}_{zz}(P)$ using the non-modified formula and compare it with the modified ones in Table 4.3, where BLSM0 means that we have considered errorless data in modifying the estimator. Comparing the non-modified and modified one we can see significant improvements in the estimated $\tilde{T}_{zz}(P)$. It should be emphasized that it is not surprising to get far from the true values when we consider different precision for the data. However, the table shows that all the modified estimators can yield $\tilde{T}_{zz}(P)$ well in 1 mE level of accuracy with different resolutions. In this study we have considered 5 mGal for the terrestrial data error. If the accuracy of the terrestrial data error increases, the solution goes away from the value obtained from the EGM; and it is typical, because contribution of the EGM is reduced. Conversely, if the accuracy of the terrestrial data decreases then contribution of the EGM increases and the obtained value get closer to the estimate value by the EGM.

Table 4.3. Different estimates for $\tilde{T}_{zz}(P)$ at 250 km using modified estimators with capsize of $\psi_0 = 3^\circ$. Unit: 1 cE

	Non-modified	BLSM	ULSM	OLSM	MM	BLSM0
$30' \times 30'$	31.84	33.58	33.79	33.68	33.57	33.17
$15' \times 15'$	31.54	33.51	33.66	33.54	33.61	33.15
$12' \times 12'$	31.48	33.50	33.61	33.50	33.62	33.14
$6' \times 6'$	31.35	33.47	33.53	33.42	33.64	33.13
$3' \times 3'$	31.27	33.45	33.49	33.38	33.65	33.13

4.4 Spectral form of VH gravitational gradients

We name the gradients $T_{xz}(P)$ and $T_{yz}(P)$ VH gradients as they are vertical-horizontal partial derivatives of the disturbing potential. These gradients can be expressed by the second-order VH derivatives of the extended Stokes integral formula:

$$\begin{bmatrix} T_{xz}(P) \\ T_{yz}(P) \end{bmatrix} = \frac{R}{4\pi} \iint_{\sigma} V(r,\psi) \begin{pmatrix} \cos\alpha \\ \sin\alpha \end{pmatrix} \Delta g(Q)\, d\sigma, \tag{4.17a}$$

where

$$V(r,\psi) = \frac{1}{r^2} S_{\psi}(r,\psi) - \frac{1}{r} S_{r\psi}(r,\psi), \tag{4.17b}$$

is the integral kernel. Here we have (Heiskanen and Moritz 1967, Eq. 6-64b, p. 235):

$$\frac{S_{\psi}(r,\psi)}{r^2} = \frac{-t^2 \sin\psi}{r^2} \left(\frac{2}{D^3} + \frac{6}{D} - 8 - 3\frac{1 - t\cos\psi - D}{D\sin^2\psi} - 3\ln\frac{1 - t\cos\psi + D}{2} \right), \tag{4.17c}$$

and (Reed 1973, Eq. 5.36, p. 72):

$$\frac{S_{r\psi}(r,\psi)}{r} = \frac{t^3 \sin\psi}{Rr} \left(\frac{3(1-t^2)}{D^5} + \frac{4}{D^3} + \frac{6}{D} - 13 - 6\ln\frac{1 - t\cos\psi + D}{2} + 3\frac{t\cos\psi(D+1)}{D(1 - t\cos\psi + D)} \right). \tag{4.17d}$$

If we write this kernel function in spectral form, we obtain

$$V(r,\psi) = -\sum_{n=2}^{\infty} \frac{2n+1}{2} \left(\frac{\Omega_n(r)}{r^2} - \frac{\Omega_n'(r)}{r} \right) P_{n1}(\cos\psi), \tag{4.17e}$$

4.4.1 Truncation error for the VH gravitational gradients

The truncation error formulation for VH gradients is done by defining the following kernel for the integral formula:

$$\bar{V}(r,\psi)=\begin{cases}0 & 0\le\psi<\psi_0\\ \dfrac{1}{2}V(r,\psi) & \psi_0\le\psi\le\pi\end{cases}, \tag{4.18a}$$

with the following spectral form for this kernel (see Hagiwara 1972) :

$$\bar{V}(r,\psi)=\sum_{n=2}^{\infty}\frac{2n+1}{2n(n+1)}Q_n^V(r,\psi_0)P_{n1}(\cos\psi), \tag{4.18b}$$

and the truncation error coefficients are derived by:

$$Q_n^V(r,\psi_0)=\frac{1}{2}\int_{\psi_0}^{\pi}V(r,\psi)P_{n1}(\cos\psi)\sin\psi d\psi\,. \tag{4.18c}$$

We can write the truncation error of the VH gravitational gradients by the following integral formula

$$\begin{bmatrix}\delta T_{xz}^1(P)\\ \delta T_{yz}^1(P)\end{bmatrix}=\frac{R}{4\pi}\iint_{\sigma}\bar{V}(r,\psi)\begin{pmatrix}\cos\alpha\\ \sin\alpha\end{pmatrix}\Delta g(Q)\,d\sigma\,. \tag{4.19}$$

A similar spectral form for Eq. (4.19) was presented by Hagiwara (1972), but for Vening-Meinesz's formula. Here, we take advantage of one of his results to find a spectral form for the truncation error of the VH gradients. It is presented in the following theorem.

Theorem 4.1 *(Hagiwara 1972)*:

$$\iint_{\sigma}\Delta g(Q)P_{n1}(\cos\psi)\begin{pmatrix}\cos\alpha\\ \sin\alpha\end{pmatrix}d\sigma=\frac{4\pi}{2n+1}\begin{pmatrix}\dfrac{\partial\Delta g_n(P)}{\partial\theta}\\ \dfrac{\partial\Delta g_n(P)}{\sin\theta\partial\lambda}\end{pmatrix}.$$

Now, by substituting Eq. (4.18b) into Eq. (4.19) we have

$$\begin{bmatrix}\delta T_{xz}^1(P)\\ \delta T_{yz}^1(P)\end{bmatrix}=\frac{R}{4\pi}\sum_{n=2}^{\infty}\frac{2n+1}{2n(n+1)}Q_n^{\mathrm{V}}(r,\psi_0)\iint_{\sigma}\Delta g(Q)P_{n1}(\cos\psi)\begin{pmatrix}\cos\alpha\\ \sin\alpha\end{pmatrix}d\sigma\,. \tag{4.20}$$

According to Theorem 4.1 we can simplify the integral part of Eq. (4.20) to:

$$\begin{bmatrix}\delta T_{xz}^{1}(P)\\ \delta T_{yz}^{1}(P)\end{bmatrix}=\frac{R}{2}\sum_{n=2}^{\infty}Q_{n}^{\mathrm{VH}}(r,\psi_{0})\begin{pmatrix}\dfrac{\partial\Delta g_{n}(P)}{\partial\theta}\\ \dfrac{\partial\Delta g_{n}(P)}{\sin\theta\partial\lambda}\end{pmatrix},\tag{4.21}$$

where

$$Q_{n}^{\mathrm{VH}}(r,\psi_{0})=\frac{Q_{n}^{\mathrm{V}}(r,\psi_{0})}{n(n+1)}.\tag{2.22}$$

Equation (2.21) is the spectral form of the truncation error of the VH derivative of the extended Stokes formula.

4.4.2 Error of terrestrial data in VH derivatives of the extended Stokes formula

The error of the terrestrial data can be expressed by the following integral:

$$\begin{bmatrix}\delta T_{xz}^{0}(P)\\ \delta T_{yz}^{0}(P)\end{bmatrix}=\frac{R}{4\pi}\iint_{\sigma}\left[V(r,\psi)-\bar{V}(r,\psi)\right]\begin{pmatrix}\cos\alpha\\ \sin\alpha\end{pmatrix}\varepsilon^{\mathrm{T}}(Q)\,d\sigma.\tag{4.23}$$

where ε^{T} stands for error of the terrestrial data. Inserting the spectral forms of $V(r,\psi)$ and $\bar{V}(r,\psi)$ into Eq. (4.23) we have

$$\begin{bmatrix}\delta T_{xz}^{0}(P)\\ \delta T_{yz}^{0}(P)\end{bmatrix}=\frac{R}{4\pi}\sum_{n=2}^{\infty}\frac{2n+1}{2}\left[\Omega_{n}^{\mathrm{VH}}(r)-Q_{n}^{\mathrm{VH}}(r,\psi_{0})\right]\iint_{\sigma}\varepsilon^{\mathrm{T}}(Q)P_{n1}(\cos\psi)\begin{pmatrix}\cos\alpha\\ \sin\alpha\end{pmatrix}d\sigma\tag{4.24}$$

According to Theorem 4.1 we can write

$$\begin{bmatrix}\delta T_{xz}(P)\\ \delta T_{yz}(P)\end{bmatrix}=\frac{R}{2}\sum_{n=2}^{\infty}\left[\Omega_{n}^{\mathrm{VH}}(r)-Q_{n}^{\mathrm{VH}}(r,\psi_{0})\right]\begin{pmatrix}\dfrac{\partial\varepsilon_{n}^{T}(P)}{\partial\theta}\\ \dfrac{\partial\varepsilon_{n}^{T}(P)}{\sin\theta\partial\lambda}\end{pmatrix},\tag{4.25}$$

where

$$\Omega_{n}^{\mathrm{VH}}(r)=\frac{\Omega_{n}(r)}{r^{2}}-\frac{\Omega_{n}'(r)}{r}.\tag{4.26}$$

Equation (4.27a) shows that the spectral form of the terrestrial error is derived from the spectrum of the kernel function minus the truncation error coefficients. We will take advantage of this in the LSM of the kernel.

4.4.3 LSM of the VH derivatives of the extended Stokes formula

Let the following general estimator for the VH gravitational gradients:

$$\begin{bmatrix} \tilde{T}_{xz}(P) \\ \tilde{T}_{yz}(P) \end{bmatrix} = \frac{R}{4\pi} \iint_{\sigma_0} V^L(r,\psi) \begin{pmatrix} \cos\alpha \\ \sin\alpha \end{pmatrix} \Delta g^{\mathrm{T}}(Q)\, d\sigma + \frac{R}{2} \sum_{n=2}^{L} b_n(r) \begin{bmatrix} \dfrac{\partial \Delta g_n^{\mathrm{EGM}}(P)}{\partial \theta} \\ \dfrac{\partial \Delta g_n^{\mathrm{EGM}}(P)}{\sin\theta \partial \lambda} \end{bmatrix} \tag{4.27}$$

where

$$V^L(r,\psi) = V(r,\psi) + \sum_{n=1}^{L} \frac{2n+1}{2} v_n(r) P_{n1}(\cos\psi). \tag{4.28}$$

We are going to find the modification parameters $v_n(r)$ in a least-squares sense. As we can see in Eq. (4.17a), the integral kernel is not isotropic as it depends on the azimuth α between the computation point *P* and the integration point *Q*. This problem is very similar with the modification of Vening-Meinesz's integral formula, the truncation error was given by Hagiwara (1972), and the formula was also modified by the least-squares approach for the first time by Sjöberg (1984a), where the modification is performed considering the error of the SHCs and truncation error. Later on Sjöberg (1984b) developed the formulation to consider the error of terrestrial data as well. Neyman et al. (1996) worked further on the modification of this formula, but they used simple MM method in their work. Tziavos and Andritsanos (1998) also used this method and Hwang (1998) presented inverse formulas for Vening-Meinesz's integral to recover gravity anomaly from satellite altimetry data. The LSM of VH derivatives of the extended Stokes formula seems to be new. However, in this section we use the strategy of Sjöberg (1984b) to modify the integral formulas of the VH gravitational gradients.

Proposition 4.5 *The BLSM parameters are derived by setting* $b_n(r) = v_n(r)$ *for the VH components of gravitational tensor and solving Eq. (4.5a) and considering with following elements:*

$$s_n(r) = v_n(r)$$

$$\begin{aligned} a_{rk} = a_{kr} &= k(k+1)\left(\sigma_k^2 + dc_k\right)\delta_{rk} - r(r+1)E_{rk}^1(\psi_0)\sigma_k^2 - \\ &\quad -k(k+1)E_{kr}^1(\psi_0)\sigma_r^2 + \sum_{n=2}^{\infty} E_{nr}^1(\psi_0)E_{nk}^1(\psi_0)n(n+1)\left(\sigma_n^2 + c_n\right), \\ h_k(r) &= k(k+1)\left\{\Omega_k^{\mathrm{VH}}(r) - Q_k^{\mathrm{VH}}(r,\psi_0)\right\}\sigma_k^2 - \sum_{n=2}^{\infty} n(n+1)E_{nk}^1(\psi_0)\times \\ &\quad \times\left\{Q_k^{\mathrm{VH}}(r,\psi_0)\left(\sigma_n^2 + c_n\right) - \Omega_k^{\mathrm{VH}}(r)\sigma_n^2\right\}. \end{aligned}$$

where

$$E_{nk}^1(\psi_0) = \frac{2k+1}{2} e_{nk}^1(\psi_0), \tag{4.29a}$$

$$e_{nk}^1(\psi_0) = -\int_{\psi_0}^{\pi} P_{n1}(\cos\psi) P_{k1}(\cos\psi)\sin\psi d\psi, \tag{4.29b}$$

Proof. We suppose that the global MSE of the estimator contains three terms:

$$\left\|\delta T_{\mathrm{VH}}\right\|^2=\left\|\delta T_{\mathrm{VH}}^0\right\|^2+\left\|\delta T_{\mathrm{VH}}^1\right\|^2+\left\|\delta T_{\mathrm{VH}}^2\right\|^2, \tag{4.30}$$

where $\left\|\delta T_{\mathrm{VH}}^0\right\|^2$ is the term related with terrestrial data error, $\left\|\delta T_{\mathrm{VH}}^1\right\|^2$ is related to the truncation error and $\left\|\delta T_{\mathrm{VH}}^2\right\|^2$ to the error of the geopotential coefficients. Now, we attempt to obtain these terms one by one in the following.

Consider the spectral form of the modified Stokes formulas which is restricted to the cap size that we have data; see Eq. (4.27). Considering the relations between the gravitational gradients in geocentric and local frame and after some manipulation we obtain:

$$\begin{bmatrix}\tilde{T}_{xz}(P)\\ \tilde{T}_{yz}(P)\end{bmatrix}=\frac{R}{2}\sum_{n=2}^{\infty}\left\{\Omega_n^{\mathrm{VH}}(r)+v_n^*(r)-\left[Q_n^{\mathrm{VH}}(r,\psi_0)\right]^L\right\}\begin{bmatrix}\dfrac{\partial\varepsilon_n^{\mathrm{T}}(P)}{\partial\theta}\\ \dfrac{\partial\varepsilon_n^{\mathrm{T}}(P)}{\sin\theta\partial\lambda}\end{bmatrix}. \tag{4.31a}$$

If we square Eq. (4.31a) we obtain

$$\begin{bmatrix}\delta\tilde{T}_{xz}^2(P)\\ \delta\tilde{T}_{yz}^2(P)\end{bmatrix}=\frac{R^2}{4}\sum_{n=2}^{\infty}\sum_{n'=2}^{\infty}\left\{v_{n'}^*(r)-\Omega_{n'}^{\mathrm{VH}}(r)-\left[Q_{n'}^{\mathrm{VH}}(r,\psi_0)\right]^L\right\}$$
$$\left\{v_n^*(r)-\Omega_n^{\mathrm{VH}}(r)-\left[Q_n^{\mathrm{VH}}(r,\psi_0)\right]^L\right\}\begin{bmatrix}\dfrac{\partial\varepsilon_n^{\mathrm{T}}(P)}{\partial\theta}\dfrac{\partial\varepsilon_{n'}^{\mathrm{T}}(P)}{\partial\theta}\\ \dfrac{\partial\varepsilon_n^{\mathrm{T}}(P)}{\sin\theta\partial\lambda}\dfrac{\partial\varepsilon_{n'}^{\mathrm{T}}(P)}{\sin\theta\partial\lambda}\end{bmatrix}, \tag{4.32a}$$

where

$$\left[Q_n^{\mathrm{VH}}(r,\psi_0)\right]^L=Q_n^{\mathrm{VH}}(r,\psi_0)-\sum_{k=2}^{L}v_k(r)E_{nk}^1(\psi_0). \tag{4.32b}$$

According to Heiskanen and Mortiz (1967, Eq. 7-37, p. 262) we can write

$$\left\|\delta T_{\mathrm{VH}}^0\right\|^2=\frac{R^2}{4}\sum_{n=2}^{\infty}\left\{v_n^*(r)-\Omega_n^{\mathrm{VH}}(r)-\left[Q_n^{\mathrm{VH}}(r,\psi_0)\right]^L\right\}^2\left[\left(\frac{\partial\varepsilon_n^{\mathrm{T}}(P)}{\partial\theta}\right)^2+\left(\frac{\partial\varepsilon_n^{\mathrm{T}}(P)}{\sin\theta\partial\lambda}\right)^2\right]$$
$$=\frac{R^2}{4}\sum_{n=2}^{\infty}\left\{v_n^*(r)-\Omega_n^{\mathrm{VH}}(r)-\left[Q_n^{\mathrm{VH}}(r,\psi_0)\right]^L\right\}^2 n(n+1)\sigma_n^2. \tag{4.33a}$$

In a very similar way can obtain:

$$\left\|\delta T_{\mathrm{VH}}^1\right\|^2=\frac{R^2}{4}\sum_{n=2}^{\infty}\left\{\left[Q_n^{\mathrm{VH}}(r,\psi_0)\right]^L\right\}^2 n(n+1)c_n, \tag{4.33b}$$

and

$$\left\|\delta T_{\mathrm{VH}}^2\right\|^2=\frac{R^2}{4}\sum_{n=2}^{L}v_n^2(r)n(n+1)dc_n. \tag{4.33c}$$

Substituting Eqs. (4.33a)-(4.33c) into Eq. (4.30) and considering

$$\frac{\partial \left\| \delta T_{\mathrm{VH}} \right\|^2}{\partial v_k(r)} = 0, \tag{4.34}$$

and after relatively long derivations the proposition is proved.

Proposition 4.6 *The ULSM parameters are derived is we select* $b_n(r) = \left[Q_n^L(r,\psi) \right]^{\mathrm{VH}} + v_n^{\mathrm{VH}}(r)$ *for the VH components of the gravitational tensor and solve Eq. (4.5a) with following elements:*

$$s_n(r) = v_n(r)$$

$$a_{rk} = a_{kr} = k(k+1)\left(\sigma_k^2 + c_k\right)\delta_{rk} - r(r+1)E_{rk}^1(\psi_0)\left(\sigma_k^2 + c_k\right) -$$
$$-k(k+1)E_{kr}^1(\psi_0)\left(\sigma_r^2 + c_r\right) + \sum_{n=2}^{\infty} E_{nr}^1(\psi_0)E_{nk}^1(\psi_0)n(n+1)\left(\sigma_n^2 + c_n\right),$$

$$h_k(r) = k(k+1)\left\{\Omega_k^{\mathrm{VH}}(r)\sigma_k^2 - \left[Q_k(r,\psi_0)\right]^{\mathrm{VH}}\left(\sigma_k^2 + c_k\right)\right\} - \sum_{n=2}^{\infty} n(n+1)E_{nk}^1(\psi_0) \times$$
$$\times\left\{\left[Q_n(r,\psi_0)\right]^{\mathrm{VH}}\left(\sigma_n^2 + c_n\right) - \Omega_k^{\mathrm{VH}}(r)\sigma_n^2\right\}.$$

Proof. Sjöberg (1991) showed that if $b_n(r) = \left[Q_n^{\mathrm{VH}}(r,\psi_0) \right]^L + v_n(r)$, the estimator will be unbiased. In this case, we can consider Eq. (4.30) for the error of the estimator. The first term which is related to the terrestrial data error is the same with the unbiased type; see Eq. (4.33a), but we can merge the truncation and geopotential coefficients errors together. Therefore we can write

$$\left\| \delta T_{\mathrm{VH}}^1 \right\|^2 + \left\| \delta T_{\mathrm{VH}}^2 \right\|^2 = \frac{R^2}{4}\sum_{n=2}^{\infty}\left\{\left[Q_n^{\mathrm{VH}}(r,\psi_0)\right]^L + v_n^*(r)\right\}^2 n(n+1)dc_n, \tag{4.35}$$

After summing up Eq. (4.33a) and the above equation and taking derivative with respect to $v_k^*(r)$ and equating the results to zero and some simplification the proposition is proved. The global MSE of the estimator can be obtained by using Eq. (4.30).

Proposition 4.7 *The OLSM parameters are derived by setting* $b_n(r) = \left\{\left[Q_n^{\mathrm{VH}}(r,\psi_0)\right]^L + v_n(r)\right\} c_n / (c_n + dc_n)$ *for the VH components of gravitational tensor and solving Eq. (4.5a) and with the following elements:*

$$s_n(r) = v_n(r)$$

$$a_{kr} = a_{rk} = k(k+1)C_r\delta_{kr} - r(r+1)E_{rk}^1(\psi_0)C_r - k(k+1)E_{kr}^1(\psi_0)C_k +$$

$$+\sum_{n=2}^{\infty} E_{nr}^{1}(\psi_0) E_{nk}^{1}(\psi_0) n(n+1) C_n, \qquad k, r=2,3,\ldots,M$$

$$h_k(r) = k(k+1)\left\{\Omega_k^{\mathrm{VH}}(r)\sigma_k^2 - \left[Q_k(r,\psi_0)\right]^{\mathrm{VH}} C_k\right\} +$$
$$+\sum_{n=2}^{\infty}\left\{\left[Q_k(r,\psi_0)\right]^{\mathrm{VH}} C_n - \Omega_n^{\mathrm{VH}}(r)\sigma_n^2\right\} n(n+1) E_{nk}^{1}(\psi_0),$$

where C_k has the same definitional as that of Eq. (4.6).

Proof. The global MSE of the estimator is the same with that presented for the SOD of the disturbing potential:

$$\left\|\delta T_{\mathrm{VH}}\right\|^2 = \frac{R^2}{4}\sum_{n=2}^{\infty}\left\{\left[b_n^*(r) - v_n^*(r) - \left[Q_n^{\mathrm{VH}}(r,\psi_0)\right]^L\right]^2 c_n + \right.$$
$$\left. + \left[\Omega_n^{\mathrm{VH}}(r) - v_n^*(r) - \left[Q_n^{\mathrm{VH}}(r,\psi_0)\right]^L\right]^2 \sigma_n^2\right\} + \frac{R^2}{4}\sum_{n=2}^{M} b_n^2(r) dc_n, \qquad (4.36)$$

taking derivative with respect to $v_k(r)$ and equating the results to zero and further simplifications the proposition is proved.

4.5 LSM and HH gravitational gradients

We name the gradients $T_{xx}(P)$, $T_{yy}(P)$ and $T_{xy}(P)$, HH gradients. Similar to the previous subsection, we consider the following integral formula:

$$\begin{bmatrix} T_{xx}(P) - T_{xx}(P) \\ 2T_{xy}(P) \end{bmatrix} = \frac{R}{4\pi}\iint_{\sigma} H(r,\psi)\begin{pmatrix}\cos 2\alpha \\ \sin 2\alpha\end{pmatrix}\Delta g(Q)\, d\sigma, \qquad (4.37a)$$

where (Reed 1973, Eq. 5.37)

$$H(r,\psi) = S_{\psi\psi}(r,\psi) - \cot\psi S_{\psi}(r,\psi), \qquad (4.37b)$$

and

$$S_{\psi\psi}(r,\psi) = -t^2\cos\psi\left(\frac{2}{D^3} + \frac{6}{D} - 8 - 3\frac{1 - t\cos\psi - D}{D\sin^2\psi} - \right.$$
$$\left. -3\ln\frac{1 - t\cos\psi + D}{2}\right) + t^3\sin^2\psi\left[\left(\frac{6}{D^5} + \frac{6}{D^3} + 3\frac{D-1}{D^2\sin^2\psi} + \right.\right.$$
$$\left.\left. +3\frac{D+1}{D(1 - t\cos\psi + D)} - 3\frac{1 - t\cos\psi - D}{D\sin^2\psi}\left(\frac{2\cos\psi}{t\sin^2\psi} + \frac{1}{D^2}\right)\right)\right], \qquad (4.37c)$$

If the spectral form of Eq. (4.37b) is:

$$H\left(r,\psi\right)=\sum_{n=2}^{\infty}\frac{2n+1}{2}\Omega_n\left(r\right)P_{n2}\left(\cos\psi\right), \tag{4.37d}$$

where $\Omega_n\left(r\right)$ is same as that of Eq. (4.3b).

4.5.1 Truncation errors for the HH gravitational gradients

Let the following kernel for the HH gravitational gradients:

$$\bar{H}\left(r,\psi\right)=\begin{cases}0 & 0\le\psi<\psi_0\\ \dfrac{1}{2}H\left(r,\psi\right) & \psi_0\le\psi\le\pi\end{cases}, \tag{4. 38a}$$

with the following spectral form

$$\bar{H}\left(r,\psi\right)=\sum_{n=2}^{\infty}\frac{2n+1}{2\left(n+2\right)\left(n+1\right)n\left(n-1\right)}Q_n^{\mathrm{H}}\left(r,\psi_0\right)P_{n2}\left(\cos\psi\right), \tag{4.38b}$$

and truncation error coefficients

$$Q_n^{\mathrm{H}}\left(r,\psi_0\right)=\frac{1}{2}\int_{\psi_0}^{\pi}H\left(r,\psi\right)P_{n2}\left(\cos\psi\right)\sin\psi d\psi\,. \tag{4.38c}$$

A spectral form for the truncation error of the HH gravitational gradients is sought. Let us first introduce the following lemma before presenting the mathematical derivations. By using the lemma a theorem is presented which is useful for the LSM of the HH derivative of the extended Stokes formula.

Theorem 4.2:

$$\iint_{\sigma}\Delta g\left(Q\right)P_{n2}\left(\cos\psi\right)\begin{pmatrix}\cos2\alpha\\ \sin2\alpha\end{pmatrix}d\sigma=$$

$$=\frac{4\pi}{2n+1}\begin{bmatrix}\dfrac{\partial^2\Delta g_n\left(P\right)}{\partial\theta^2}-\cot\theta\dfrac{\partial\Delta g_n\left(P\right)}{\partial\theta}-\dfrac{1}{\sin^2\theta}\dfrac{\partial^2\Delta g_n\left(P\right)}{\partial\lambda^2}\\ \dfrac{1}{\sin\theta}\dfrac{\partial^2\Delta g_n\left(P\right)}{\partial\lambda\partial\theta}-\cot\theta\dfrac{1}{\sin\theta}\dfrac{\partial\Delta g_n\left(P\right)}{\partial\lambda}\end{bmatrix}.$$

Proof. Let us first consider that part of the theorem containing $\cos2\alpha$, this term can be written as:

$$\iint_{\sigma}\Delta g\left(Q\right)P_{n2}\left(\cos\psi\right)\cos2\alpha d\sigma=$$

$$=\iint_{\sigma}\Delta g\left(Q\right)\left[\frac{\partial^2P_n\left(\cos\psi\right)}{\partial\theta^2}-\cot\theta\frac{\partial P_n\left(\cos\psi\right)}{\partial\theta}-\frac{1}{\sin^2\theta}\frac{\partial^2P_n\left(\cos\psi\right)}{\partial\lambda^2}\right]d\sigma,$$

(4.39)

Equation (4.39) consists of three terms and here we simplified each terms in the following. First, we consider the first term. By using the addition theorem of spherical harmonics, Eq. (3.3) we have

$$\iint_{\sigma} \Delta g(Q) \frac{\partial^2 P_n(\cos\psi)}{\partial\theta^2} d\sigma = \frac{1}{2n+1} \sum_{m=-n}^{n} \frac{\partial^2 Y_{nm}(P)}{\partial\theta^2} \iint_{\sigma} \Delta g(Q) Y_{nm}(Q) d\sigma +$$
$$= \frac{4\pi}{2n+1} \sum_{m=-n}^{n} \Delta g_{nm} \frac{\partial^2 Y_{nm}(P)}{\partial\theta^2} = \frac{4\pi}{2n+1} \frac{\partial^2 \Delta g_n(P)}{\partial\theta^2}, \quad (4.40a)$$

the second term

$$\iint_{\sigma} \Delta g(Q) \cot\theta \frac{\partial P_n(\cos\psi)}{\partial\theta} d\sigma = \frac{\cot\theta}{2n+1} \frac{\partial Y_{nm}(P)}{\partial\theta} \iint_{\sigma} \Delta g(Q) Y_{nm}(Q) d\sigma +$$
$$= \frac{4\pi\cot\theta}{2n+1} \sum_{m=-n}^{n} \Delta g_{nm} \frac{\partial Y_{nm}(P)}{\partial\theta} = \frac{4\pi\cot\theta}{2n+1} \frac{\partial \Delta g_n(P)}{\partial\theta}, \quad (4.40b)$$

and the last term

$$\iint_{\sigma} \Delta g(Q) \frac{1}{\sin^2\theta} \frac{\partial^2 P_n(\cos\psi)}{\partial\lambda^2} d\sigma = \frac{1}{2n+1} \frac{1}{\sin^2\theta} \sum_{m=-n}^{n} \frac{\partial^2 Y_{nm}(P)}{\partial\lambda^2} \iint_{\sigma} \Delta g(Q) Y_{nm}(Q) d\sigma$$
$$= \frac{4\pi}{2n+1} \frac{1}{\sin^2\theta} \sum_{m=-n}^{n} \Delta g_{nm} \frac{\partial^2 Y_{nm}(P)}{\partial\lambda^2} = \frac{4\pi}{2n+1} \frac{1}{\sin^2\theta} \frac{\partial^2 \Delta g_n(P)}{\partial\lambda^2}. \quad (4.40c)$$

Now by substituting Eqs. (4.40a)-(4.40c) into Eq. (4.39) we obtain:

$$\iint_{\sigma} \Delta g(Q) P_{n2}(\cos\psi) \cos 2\alpha d\sigma = \frac{4\pi}{2n+1} \left(\frac{\partial^2 \Delta g_n(P)}{\partial\theta^2} - \right.$$
$$\left. - \cot\theta \frac{\partial \Delta g_n(P)}{\partial\theta} - \frac{1}{\sin^2\theta} \frac{\partial^2 \Delta g_n(P)}{\partial\lambda^2} \right). \quad (4.41a)$$

In a very similar way we can prove that

$$\iint_{\sigma} \Delta g(Q) P_{n2}(\cos\psi) \sin 2\alpha d\sigma = \frac{4\pi}{2n+1} \left(\frac{\partial^2 \Delta g_n(P)}{\sin\theta \partial\lambda \partial\theta} - \cot\theta \frac{\partial \Delta g_n(P)}{\sin\theta \partial\lambda} \right). \quad (4.41b)$$

Therefore the theorem is proved.

By considering Theorem 4.2 it will not be difficult to obtain the spectral form of the truncation error formula. Substituting Eq. (4.38b) into (4.38a) and inserting the result into Eq. (4.37a) we obtain:

$$\begin{bmatrix} \delta T_{xx}^{1}(P)-\delta T_{yy}^{1}(P) \\ 2\delta T_{xy}^{1}(P) \end{bmatrix} = \frac{R}{2}\sum_{n=2}^{\infty}\frac{Q_n^{\mathrm{H}}(r,\psi_0)}{(n+2)(n+1)n(n-1)}\times$$
$$\times\iint_{\sigma}\Delta g^{*}(Q)P_{n2}(\cos\psi)\begin{pmatrix}\cos 2\alpha \\ \sin 2\alpha\end{pmatrix}d\sigma\,, \quad (4.42)$$

According to Theorem 4.2 the integral part of Eq. (4.42) is simplified and finally we can write the spectral form of the truncation error formula as:

$$\begin{bmatrix} \delta T_{xx}^{1}(P)-\delta T_{yy}^{1}(P) \\ 2\delta T_{xy}^{1}(P) \end{bmatrix} = \sum_{n=2}^{\infty}Q_n^{\mathrm{HH}}(r,\psi_0)\times$$
$$\times\begin{bmatrix} \dfrac{\partial^2\Delta g_n(P)}{\partial\theta^2}-\cot\theta\dfrac{\partial\Delta g_n(P)}{\partial\theta}-\dfrac{1}{\sin^2\theta}\dfrac{\partial^2\Delta g_n(P)}{\partial\lambda^2} \\ \dfrac{1}{\sin\theta}\dfrac{\partial^2\Delta g_n(P)}{\partial\lambda\partial\theta}-\cot\theta\dfrac{1}{\sin\theta}\dfrac{\partial\Delta g_n(P)}{\partial\lambda} \end{bmatrix}, \quad (4.43a)$$

where

$$Q_n^{\mathrm{HH}}(r,\psi_0) = \frac{Q_n^{\mathrm{H}}(r,\psi_0)}{(n+2)(n+1)n(n-1)}\,. \quad (4.43b)$$

4.5.2 Error of terrestrial data of HH derivatives of the extended Stokes formula

Let the following integral formula for the error of terrestrial data

$$\begin{bmatrix} \delta T_{xx}^{0}(P)-\delta T_{yy}^{0}(P) \\ 2\delta T_{xy}^{0}(P) \end{bmatrix} = \frac{R}{4\pi}\iint_{\sigma}\left[H(r,\psi)-\bar{H}(r,\psi)\right]\begin{pmatrix}\cos\alpha \\ \sin\alpha\end{pmatrix}\varepsilon^{\mathrm{T}}(Q)\,d\sigma\,. \quad (4.44)$$

Considering the spectral forms of $H(r,\psi)$ and $\bar{H}(r,\psi)$ (see Eqs. 4.37d and 4.38b) and inserting them into Eq. (4.44) we have

$$\begin{bmatrix} \delta T_{xx}^{0}(P)-\delta T_{yy}^{0}(P) \\ 2\delta T_{xy}^{0}(P) \end{bmatrix} = \frac{R}{4\pi}\sum_{n=2}^{\infty}\frac{2n+1}{2}\left[\Omega_n(r)-Q_n^{\mathrm{H}}(r,\psi_0)\right]$$
$$\iint_{\sigma}\varepsilon^{\mathrm{T}}(Q)P_{n2}(\cos\psi)\begin{pmatrix}\cos 2\alpha \\ \sin 2\alpha\end{pmatrix}d\sigma\,. \quad (4.45)$$

According to Theorem 4.2 we obtain

$$\begin{bmatrix} \delta T_{xx}^{0}(P)-\delta T_{yy}^{0}(P) \\ 2\delta T_{xy}^{0}(P) \end{bmatrix} = \frac{R}{2}\sum_{n=2}^{\infty}\left[\Omega_n(r)-Q_n^{\mathrm{H}}(r,\psi_0)\right],$$

$$\times\begin{bmatrix} \dfrac{\partial^2 \varepsilon_n^{\mathrm{T}}(P)}{\partial\theta^2} - \cot\theta \dfrac{\partial \varepsilon_n^{\mathrm{T}}(P)}{\partial\theta} - \dfrac{1}{\sin^2\theta}\dfrac{\partial^2 \varepsilon_n^{\mathrm{T}}(P)}{\partial\lambda^2} \\ \dfrac{1}{\sin\theta}\dfrac{\partial^2 \varepsilon_n^{\mathrm{T}}(P)}{\partial\lambda\partial\theta} - \cot\theta \dfrac{1}{\sin\theta}\dfrac{\partial \varepsilon_n^{\mathrm{T}}(P)}{\partial\lambda} \end{bmatrix}. \qquad (4.46)$$

4.5.3 LSM of the HH derivatives of the extended Stokes formula

Let us consider the following estimator for the HH gravitational gradients:

$$\begin{bmatrix} \tilde{T}_{xx}(P) - \tilde{T}_{yy}(P) \\ 2\tilde{T}_{xy}(P) \end{bmatrix} = \frac{R}{4\pi}\iint_{\sigma_0} H^L(r,\psi)\begin{pmatrix} \cos 2\alpha \\ \sin 2\alpha \end{pmatrix}\Delta g^{\mathrm{T}}(Q)\,d\sigma + \frac{R}{2}\sum_{n=2}^{L} b_n(r)\times$$
$$\times\begin{bmatrix} \dfrac{\partial^2 \Delta g_n^{\mathrm{EGM}}(P)}{\partial\theta^2} - \cot\theta\dfrac{\partial \Delta g_n^{\mathrm{EGM}}(P)}{\partial\theta} - \dfrac{1}{\sin^2\theta}\dfrac{\partial^2 \Delta g_n^{\mathrm{EGM}}(P)}{\partial\lambda^2} \\ \dfrac{1}{\sin\theta}\dfrac{\partial^2 \Delta g_n^{\mathrm{EGM}}(P)}{\partial\theta\partial\lambda} + \dfrac{\cos\theta}{\sin^2\theta}\dfrac{\partial \Delta g_n^{\mathrm{EGM}}(P)}{\partial\lambda} \end{bmatrix}, \qquad (4.47a)$$

where

$$H^L(r,\psi) = H(r,\psi) - \sum_{n=1}^{L}\frac{2n+1}{2}h_n'(r)P_{n2}(\cos\psi). \qquad (4.47b)$$

Similar to the previous derivation the problem is to determine the modification parameters $h_n'(r)$ in such a way that the global MSE of the estimator is minimized in a least-squares scene. In the following, the mathematical derivations are summarized in three propositions as before.

Proposition 4.8 *The BLSM parameters* $h_n'(r)$ *are derived if we set* $b_n(r) = h_n'(r)$ *for the HH components of gravitational tensor and solve Eq. (4.5a) with following elements:*

$$s_n(r) = h_n'(r)$$
$$\begin{aligned} a_{rk} = a_{kr} = {} & (k-1)k(k+1)(k+2)\left(\sigma_k^2 + dc_k\right)\delta_{rk} - \\ & -(r-1)r(r+1)(r+2)E_{rk}^2(\psi_0)\sigma_k^2 - \\ & -(k-1)k(k+1)(k+2)E_{kr}^2(\psi_0)\sigma_r^2 + \\ & +\sum_{n=2}^{\infty}E_{nr}^2(\psi_0)E_{nk}^2(\psi_0)(n-1)n(n+1)(n+2)\left(\sigma_n^2 + c_n\right), \end{aligned}$$
$$\begin{aligned} h_k(r) = {} & (k-1)k(k+1)(k+2)\left\{\Omega_k(r) - Q_k^{\mathrm{HH}}(r,\psi_0)\right\}\sigma_k^2 - \\ & -\sum_{n=2}^{\infty}(n-1)n(n+1)(n+2)E_{nk}^2(\psi_0)\left\{Q_k^{\mathrm{HH}}(r,\psi_0)\left(\sigma_n^2 + c_n\right) - \Omega_k(r)\sigma_n^2\right\}, \end{aligned}$$

where

$$E_{nk}^2(\psi_0) = \frac{2k+1}{2}e_{nk}^2(\psi_0), \qquad (4.48a)$$

$$e_{nk}^2(\psi_0) = \int_{\psi_0}^{\pi} P_{n2}(\cos\psi) P_{k2}(\cos\psi) \sin\psi d\psi \,. \tag{4.48b}$$

Proof. Again the global MSE of the estimator can be written as:

$$\left\|\delta T_{\mathrm{HH}}\right\|^2 = \left\|\delta T_{\mathrm{HH}}^{0}\right\|^2 + \left\|\delta T_{\mathrm{HH}}^{1}\right\|^2 + \left\|\delta T_{\mathrm{HH}}^{2}\right\|^2 . \tag{4.49}$$

The first term is related to the terrestrial data error; the second and the third are related to the truncation and geopotential coefficients errors with following expressions

$$\left\|\delta T_{\mathrm{HH}}^{0}\right\|^2 = \frac{R^2}{4r^2}\sum_{n=2}^{\infty}\left\{h_n^*(r) - \Omega_n(r) - Q_k^{\mathrm{HH}}(r,\psi_0)\right\}^2 (n-1)n(n+1)(n+2)\sigma_n^2 \,, \tag{4.50a}$$

$$\left\|\delta T_{\mathrm{HH}}^{1}\right\|^2 = \frac{R^2}{4r^2}\sum_{n=2}^{\infty}\left[Q_k^{\mathrm{HH}}(r,\psi_0)\right]^2 (n-1)n(n+1)(n+2)c_n \,, \tag{4.50b}$$

$$\left\|\delta T_{\mathrm{HH}}^{2}\right\|^2 = \frac{R^2}{4r^2}\sum_{n=2}^{\infty}\left\{h_n'^*(r)\right\}^2 (n-1)n(n+1)(n+2)dc_n \,, \tag{4.50c}$$

and

$$\left[Q_k^{\mathrm{HH}}(r,\psi_0)\right]^L = Q_k^{\mathrm{HH}}(r,\psi_0) - \sum_{k=2}^{L} h_k'(r) E_{nk}^2(\psi_0) \,. \tag{4.51}$$

According to

$$\frac{\partial\left\|\delta T_{\mathrm{HH}}\right\|^2}{\partial s_k(r)} = 0 \,, \tag{4.52}$$

and simplifying the results the proposition is proved.

Proposition 4.9 *The ULSM parameters* $h_n'(r)$ *of the HH components of gravitational tensor is derived by setting* $b_n(r) = \left[Q_n^{\mathrm{HH}}(r,\psi_0)\right]^L + h_n'(r)$ *and solving Eq. (4.5a) with the following elements*

$$\begin{aligned}
s_n(r) &= h_n'(r) \\
a_{rk} = a_{kr} &= (k-1)k(k+1)(k+2)d_k\delta_{rk} - \\
&\quad -(r-1)r(r+1)(r+2)E_{rk}^2(\psi_0)d_k - \\
&\quad -(k-1)k(k+1)(k+2)E_{kr}^2(\psi_0)d_r + \\
&\quad +\sum_{n=2}^{\infty} E_{nr}^2(\psi_0)E_{nk}^2(\psi_0)(n-1)n(n+1)(n+2)d_n \\
h_k(r) &= (k-1)k(k+1)(k+2)\left\{\Omega_k(r)\sigma_k^2 - Q_k^{\mathrm{HH}}(r,\psi_0)d_k\right\} -
\end{aligned}$$

$$-\sum_{n=2}^{\infty}(n-1)n(n+1)(n+2)E_{nk}^{2}(\psi_0)\left\{Q_k^{\mathrm{HH}}(r,\psi_0)d_n-\Omega_k(r)\sigma_n^2\right\}.$$

Proof. If we consider Eq. (4.31a) for the first term of global MSE of the estimator (Eq. 4.27a) which is related to the terrestrial data error and also

$$\left\|\delta T_{\mathrm{HH}}^{1}\right\|^2+\left\|\delta T_{\mathrm{HH}}^{2}\right\|^2=\frac{R^2}{4r^2}\sum_{n=2}^{\infty}\left\{Q_k^{\mathrm{HH}}(r,\psi_0)+h_n^{\prime *}(r)\right\}^2(n-1)n(n+1)(n+2)dc_n,$$

for truncation and geopotential coefficients error. The proposition is proved in a similar way of Proposition 4.6.

Proposition 4.10 *The OLSM parameters of the HH components of the gravitational tensor are derived by setting* $b_n(r)=\left\{\left[Q_n^{\mathrm{HH}}(r,\psi_0)\right]^L+h_n'(r)\right\}c_n/(c_n+dc_n)$ *solving Eq. (4.5a) with the following elements*

$$\begin{aligned}
s_n(r)&=h_n'(r)\\
a_{rk}&=a_{kr}=(k-1)k(k+1)(k+2)C_k\delta_{rk}-\\
&\quad-(r-1)r(r+1)(r+2)E_{rk}^{2}(\psi_0)C_k-\\
&\quad-(k-1)k(k+1)(k+2)E_{kr}^{2}(\psi_0)C_r+\\
&\quad+\sum_{n=2}^{\infty}E_{nr}^{2}(\psi_0)E_{nk}^{2}(\psi_0)(n-1)n(n+1)(n+2)C_n\\
h_k(r)&=(k-1)k(k+1)(k+2)\left\{\Omega_k(r)\sigma_k^2-Q_k^{\mathrm{HH}}(r,\psi_0)d_k\right\}-\\
&\quad-\sum_{n=2}^{\infty}(n-1)n(n+1)(n+2)E_{nk}^{2}(\psi_0)\left\{Q_k^{\mathrm{HH}}(r,\psi_0)C_n-\Omega_k(r)\sigma_n^2\right\}.
\end{aligned}$$

Proof. The proof is very similar to that of presented for Proposition 4.7.

According to the estimator presented in Eq. (4.7a) and Eq. (4.47a) it is easy to validate the diagonal elements of the gravitational tensor. Since the Laplacian operator shows $T_{zz}(P)=-\left(T_{xx}(P)+T_{yy}(P)\right)$ therefore by estimating the $T_{zz}(P)$ the summation of the $T_{xx}(P)+T_{yy}(P)$ is validated as well as $T_{zz}(P)$. However, Eq. (4.47a) shows that $T_{xx}(P)-T_{yy}(P)$ can also be evaluated, thus each elements of $T_{xx}(P)$ and $T_{yy}(P)$ can easily be estimated by combining these two estimators. No problem is seen for evaluation of the VH gradients according to Eq. (4.28a) as they can be separately estimated. The numerical studies on this matter are left for future work.

4.6. Modification with data in a spherical ring

Modification of Stokes' formula or its second-order derivatives can be done in such a way that the terrestrial data are restricted between two caps or in other words, we have data inside a ring around the computation point. This way of

modification is beneficial for the case where we have no data in the inner zone. This theory was originally presented by Sjöberg and Eshagh (2009) to estimate the geoid with data gaps. Here, we develop the theory to the extended Stokes formula and its second-order partial derivatives. This technique could also be useful to validate the SGG data when the satellite is flying over lakes or deserts with lack of terrestrial data. It can be used to estimate the SGG data to fill-in data in regions lacking the SGG data.

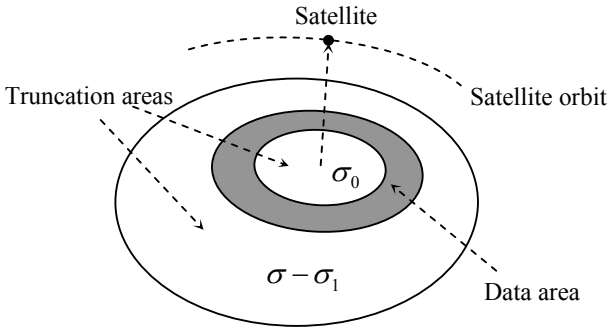

Figure 4.6. Truncation area of restricted data to a ring

Figure 4.6 clearly shows the spherical ring containing the terrestrial gravimetric data. The truncation areas are σ_0 and $\sigma-\sigma_1$. The problem is to modify the extended Stokes formula or its second-order derivatives so that the effect of truncation errors is minimized. First we start with MM, in which the upper bound of the truncation error is minimized. This upper bound can mathematically be expressed by; see also Sjöberg and Eshagh (2009):

$$I=\frac{1}{4\pi}\iint_{\sigma_0}\left[S^L\left(r,\psi\right)\right]^2 d\sigma+\frac{1}{4\pi}\iint_{\sigma-\sigma_1}\left[S^L\left(r,\psi\right)\right]^2 d\sigma\,, \tag{4.53a}$$

or

$$I=\frac{1}{2}\int_{\substack{\psi\le\psi_0\\ \psi\ge\psi_1}}\left[S^L(r,\psi)\right]^2\sin\psi d\psi\,. \tag{4.53b}$$

where $S^L\left(r,\psi\right)$ is the modified extended Stokes formula (Eq. 4.4a). By differentiating Eq. (4.35a) with respect to $s_k\left(r\right)$ and equating the results to zero, a system of equations equivalent to Eq. (4.5a) is obtained, in which the elements of the coefficients matrix is:

$$a_{kr}=\left\{\delta_{kr}+\left[E^0_{kr}\left(\psi_1\right)-E^0_{kr}\left(\psi_0\right)\right]\right\}, \tag{4.54a}$$

and for the right hand side of the system of equations we have:

$$h_k\left(r\right)=\Omega_n\left(r\right)+Q_k\left(r,\psi_1\right)-Q_k\left(r,\psi_0\right). \tag{4.54b}$$

In this case the global mean square truncation error of the disturbing potential estimator becomes:

$$d\bar{T}^2 = \frac{1}{4\pi}\iint_{\sigma} \delta T^2 d\sigma = c^2 \sum_{n=2}^{\infty} \left\{ \Omega_n(r) - s_n^*(r) + Q_n^L(r,\psi_1) - Q_n^L(r,\psi_0) \right\}^2 c_n \,. \tag{4.55}$$

In a very similar way we can obtain the elements of the system of equations (Eq. 4.5a) in such a way that the solution of the system yields the biased type of LSM (BLSM). In this part of the thesis we confine ourselves on the biased type ring modification, which is the simplest type in comparison with the ULSM and OLSM (the discussion about the other types of the LSM is left for future works).

Proposition 4.11 *Solution of system of equations Eq. (4.5a) by the following elements is the BLSM of the disturbing potential estimator at radius r based on a spherical ring between* $\psi_0 < \psi < \psi_1$*:*

$$a_{kr} = (c_r + dc_r)\delta_{kr} - \left\{ \left[E_{rk}^0(\psi_0) - E_{rk}^0(\psi_1) \right] c_k + \left[E_{kr}^0(\psi_0) - E_{kr}^0(\psi_1) \right] c_r \right\} + \\ + \sum_{n=2}^{\infty} \left[E_{nr}^0(\psi_0) - E_{nr}^0(\psi_1) \right] \left[E_{nk}^0(\psi_0) - E_{nk}^0(\psi_1) \right] \left(c_n + \sigma_n^2 \right),$$

and

$$h_k(r) = \left(\Omega_n(r) - Q_n(r,\psi_0) + Q_n(r,\psi_1) \right) c_k + \\ + \sum_{n=2}^{\infty} \left\{ \left[Q_n(r,\psi_0) - Q_n(r,\psi_1) - \Omega_n(r) \right] c_n + \right. \\ \left. + \left[Q_n(r,\psi_0) - Q_n(r,\psi_1) \right] \sigma_n^2 \right\} \left[E_{nk}^0(\psi_0) - E_{nk}^0(\psi_1) \right].$$

Proof. Let the disturbing potential be expressed by the following equation:

$$\tilde{T}(P) = \frac{R}{4\pi} \iint_{\sigma_1 - \sigma_0} S^L(r,\psi) \Delta g^{\mathrm{T}}(Q) d\sigma + \frac{R}{2} \sum_{n=2}^{L} s_n(r) \Delta g_n^{\mathrm{EGM}}(P), \tag{4.56}$$

The spectral form of the above equation is

$$\tilde{T}(P) = \frac{R}{2} \sum_{n=2}^{\infty} \left[Q_n^L(r,\psi_0) - Q_n^L(r,\psi_1) \right] \Delta g_n^{\mathrm{T}}(P) + \frac{R}{2} \sum_{n=2}^{L} s_n(r) \Delta g_n^{\mathrm{EGM}}(P), \tag{4.57}$$

with the error

$$\delta\tilde{T}(P) = \frac{R}{2} \sum_{n=2}^{\infty} \left\{ \left[Q_n^L(r,\psi_0) - Q_n^L(r,\psi_1) \right] \varepsilon_n^{\mathrm{T}}(P) - \right. \\ \left. - \left[\Omega_n(r) - s_n^*(r) + Q_n^L(r,\psi_0) - Q_n^L(r,\psi_1) \right] \Delta g_n(P) \right\} \\ + \frac{R}{2} \sum_{n=2}^{L} s_n^*(r) \varepsilon_n^{\mathrm{EGM}}(P). \tag{4.58}$$

The statistical expectation of the global average of $\delta\tilde{T}(P)$ becomes:

$$E\left\{\delta\overline{T}^{2}\right\}=\frac{R^{2}}{4}\sum_{n=2}^{\infty}\left\{\left[\Omega_{n}(r)-s_{n}^{*}(r)+Q_{n}^{L}(r,\psi_{0})-Q_{n}^{L}(r,\psi_{1})\right]^{2}c_{n}+\right.$$
$$\left.+\left[Q_{n}^{L}(r,\psi_{0})-Q_{n}^{L}(r,\psi_{1})\right]^{2}\sigma_{n}^{2}+\left[s_{n}^{*}(r)\right]^{2}dc_{n}\right\}. \qquad (4.59)$$

Differentiation the above equation with respect to $s_{k}(r)$ and equating the results to zero and after some manipulations the proposition is proved.

Corollary 4.5 *The ring BLSM of the SOD of the extended Stokes function, is derived by selecting the following elements for the right hand side of Eq. (4.5a)*

$$h_{k}(r)=\left(\Omega_{n}''(r)-\left[Q_{n}(r,\psi_{0})\right]_{zz}+\left[Q_{n}(r,\psi_{1})\right]_{zz}\right)c_{k}+$$
$$+\sum_{n=2}^{\infty}\left\{\left(\left[Q_{n}(r,\psi_{0})\right]_{zz}-\left[Q_{n}(r,\psi_{1})\right]_{zz}-\Omega_{n}''(r)\right)c_{n}+\right.$$
$$\left.+\left(\left[Q_{n}(r,\psi_{0})\right]_{zz}-\left[Q_{n}(r,\psi_{1})\right]_{zz}\right)\sigma_{n}^{2}\right\}\left[E_{nk}^{0}(\psi_{0})-E_{nk}^{0}(\psi_{1})\right].$$

Corollary 4.6 *The ring BLSM of the VH derivative of the extended Stokes formula is derived by selecting the following elements for Eq. (4.5a)*

$$a_{kr}=k(k+1)(c_{r}+dc_{r})\delta_{kr}-r(r+1)\left[E_{rk}^{1}(\psi_{0})-E_{rk}^{1}(\psi_{1})\right]c_{k}+$$
$$+k(k+1)\left[E_{kr}^{1}(\psi_{0})-E_{kr}^{1}(\psi_{1})\right]c_{r}+\sum_{n=2}^{\infty}\left[E_{nr}^{1}(\psi_{0})-E_{nr}^{1}(\psi_{1})\right]\times$$
$$\times\left[E_{nk}^{1}(\psi_{0})-E_{nk}^{1}(\psi_{1})\right]n(n+1)\left(c_{n}+\sigma_{n}^{2}\right),$$

and

$$h_{k}(r)=k(k+1)\left\{\Omega_{k}^{\mathrm{VH}}(r)-Q_{k}^{\mathrm{VH}}(r,\psi_{0})+Q_{k}^{\mathrm{VH}}(r,\psi_{1})\right\}c_{k}+$$
$$+\sum_{n=2}^{\infty}\left\{\left[Q_{n}(r,\psi_{0})-Q_{n}(r,\psi_{1})-\Omega_{n}(r)\right]c_{n}+\right.$$
$$\left.+\left[Q_{n}(r,\psi_{0})-Q_{n}(r,\psi_{1})\right]\sigma_{n}^{2}\right\}\left[E_{nk}^{1}(\psi_{0})-E_{nk}^{1}(\psi_{1})\right]n(n+1).$$

Corollary 4.7 *The ring BLSM of the HH derivative of the extended Stokes formula is derived by selecting the following elements for Eq. (4.5a)*

$$a_{kr}=(k-1)k(k+1)(k+2)(c_{r}+dc_{r})\delta_{kr}-$$
$$-(r-1)r(r+1)(r+2)\left[E_{rk}^{2}(\psi_{0})-E_{rk}^{2}(\psi_{1})\right]c_{k}+$$
$$+(k-1)k(k+1)(k+2)\left[E_{kr}^{2}(\psi_{0})-E_{kr}^{2}(\psi_{1})\right]c_{r}+$$
$$+\sum_{n=2}^{\infty}\left[E_{nr}^{2}(\psi_{0})-E_{nr}^{2}(\psi_{1})\right]\left[E_{nk}^{2}(\psi_{0})-E_{nk}^{2}(\psi_{1})\right]\times$$
$$\times(n-1)n(n+1)(n+2)\left(c_{n}+\sigma_{n}^{2}\right),$$

and

$$h_k(r)=(k-1)k(k+1)(k+2)\left\{\Omega_k(r)-Q_k^{\mathrm{HH}}(r,\psi_0)+Q_k^{\mathrm{HH}}(r,\psi_1)\right\}c_k+$$
$$+\sum_{n=2}^{\infty}\left\{\left[Q_n^{\mathrm{HH}}(r,\psi_0)-Q_n^{\mathrm{HH}}(r,\psi_1)-\Omega_n(r)\right]c_n+\right.$$
$$\left.+\left[Q_n^{\mathrm{HH}}(r,\psi_0)-Q_n^{\mathrm{HH}}(r,\psi_1)\right]\sigma_n^2\right\}\left[E_{nk}^2(\psi_0)-E_{nk}^2(\psi_1)\right]\times$$
$$\times(n-1)n(n+1)(n+2).$$

The proofs of Corollary 4.6 and 4.7 are not presented here, as they are very similar to the proof of Proposition 4.10 and we avoid repeating them again.

4.7 Derivations of $e_{nk}^0(\psi_0)$, $e_{nk}^1(\psi_0)$ and $e_{nk}^2(\psi_0)$

The LSM of the gradients are involved with integral product of two ALFs. In the LSM of the VV, VH and HH gradients we are involved with $e_{nk}^0(\psi_0)$, $e_{nk}^1(\psi_0)$ and $e_{nk}^2(\psi_0)$, respectively. We name these coefficients, zero-, first- and second-order Paul's coefficients. Therefore we have to derive some formulas to practically evaluate these coefficients in the LSM respect. The first-order Paul coefficients $e_{nk}^0(\psi_0)$ is the integral of product of two ALFs with order zero. Paul (1973) proposed a recursive formula to generate these coefficients. The first-order Paul coefficients $e_{nk}^1(\psi_0)$ are the integral product of two ALFs with order 1. In general the recursive formulas for the integral product of the two ALFs was obtained by Mainville (1986) and after that Hwang (1995) worked further on this matter and developed a formula to convert this integral product to a simple integral of the ALFs. Since the recursive formula for the integral of the ALFs was derived by Paul (1973), his idea can be used to compute the integral product of two ALFs. However, we already know that higher order terms than 2 is not needed for the LSM goal. Generating the ALFs up to very high degrees and orders may be unstable. Hwang (2008, personal communication) mentioned that he has generated the integral product of the ALFs just to degree and order 50 and generation of higher degrees (in the LSM we need for example 2000) will be unstable. In the LSM nothing has been reported about instability of the recursive algorithm of the associated Legendre polynomial to high degree (at least to 2000). Therefore, it would be preferable to develop some relations between $e_{nk}^1(\psi_0)$ and $e_{nk}^0(\psi_0)$ which is more stable. The computation of $e_{nk}^1(\psi_0)$ which is integral product of two first-order ALFs was also presented by those geodesists working on Vening-Meinesz's formulas and it can easily be shown that $e_{nk}^1(\psi_0)$ is related to $e_{nk}^0(\psi_0)$ by the following relation:

$$e_{nk}^1(\psi_0)=n(n+1)e_{nk}^0(\psi_0)-n\,P_k(\cos\psi_0)\left[P_{n-1}(\cos\psi_0)-\cos\psi_0 P_n(\cos\psi_0)\right]. \tag{4.60}$$

For more details and other forms for this relation the reader is referred e.g. to Chen (1982), Hsu (1984) and Neyman et al. (1996). According to these relations it is not difficult to compute $e_{nk}^1(\psi_0)$. The problem of deriving the second-order

Paul coefficient $e_{nk}^{2}\left(\psi_0\right)$ was not considered until now, because this problem is mostly related to gravity gradiometry, which is a special branch of geodesy. In the following we obtain a relation between this function and the first-order Paul coefficient $e_{nk}^{1}\left(\psi_0\right)$.

Proposition 4.12 *The relation between the second-order* $e_{nk}^{2}\left(\psi_0\right)$ *and the firs-order Paul coefficients* $e_{nk}^{1}\left(\psi_0\right)$ *is:*

$$e_{nk}^{2}\left(\psi_0\right)=-\frac{\cos\psi_0}{2}\left[n\left(n+1\right)+1\right]\left[k\left(k+1\right)+1\right]P_{n1}\left(\cos\psi_0\right)P_{k1}\left(\cos\psi_0\right)+$$
$$+e_{nk}^{1}\left(\psi_0\right)\left[n\left(n+1\right)-2\right]+n\left(n+1\right)k\left[P_{k-1}\left(\cos\psi_0\right)-\cos\psi_0 P_k\left(\cos\psi_0\right)\right].$$

Proof. Let the well-known Legendre equation (Heiskanen and Mortitz 1967, p. 22):

$$\left(1-x^2\right)\frac{d^2P_n\left(x\right)}{dx^2}-2x\,\frac{dP_n\left(x\right)}{dx}=-n\left(n+1\right)P_n\left(x\right), \tag{4.61}$$

we can also write

$$\left(1-x^2\right)^2\frac{d^2P_n\left(x\right)}{dx^2}\frac{d^2P_k\left(x\right)}{dx^2}-2x\left(1-x^2\right)\frac{dP_n\left(x\right)}{dx}\frac{d^2P_k\left(x\right)}{dx^2}=$$
$$=-n\left(n+1\right)\left(1-x^2\right)P_n\left(x\right)\frac{d^2P_k\left(x\right)}{dx^2}, \tag{4.62}$$

After integrating Eq. (4.62), the first term in the left hand side will be nothing else but $e_{nk}^{2}\left(\psi_0\right)$, namely:

$$e_{nk}^{2}\left(x_0\right)=\int_{-1}^{x_0}\left(1-x^2\right)^2\frac{d^2P_n\left(x\right)}{dx^2}\frac{d^2P_k\left(x\right)}{dx^2}dx=\int_{-1}^{x_0}P_{n2}\left(x\right)P_{k2}\left(x\right)dx, \tag{4.63}$$

Therefore Eq. (4.62) can be re-written as:

$$e_{nk}^{2}\left(x_0\right)=2\int_{-1}^{x_0}x\left(1-x^2\right)\frac{dP_n\left(x\right)}{dx}\frac{d^2P_k\left(x\right)}{dx^2}dx-n\left(n+1\right)\int_{-1}^{x_0}\left(1-x^2\right)P_n\left(x\right)\frac{d^2P_k\left(x\right)}{dx^2}dx \tag{4.64}$$

The first and second integrals in the right hand side of Eq. (4.64) can be solved partially

$$e_{nk}^{2}\left(x_0\right)=2x\left(1-x^2\right)\frac{dP_n\left(x\right)}{dx}\frac{d^2P_k\left(x\right)}{dx^2}dx\Bigg|_{-1}^{x_0}-2C-$$
$$-n\left(n+1\right)\left[\left(1-x^2\right)P_n\left(x\right)\frac{d^2P_k\left(x\right)}{dx^2}\Bigg|_{-1}^{x_0}-D\right], \tag{4.65a}$$

where

$$C = \int_{-1}^{x_0} \left(1-x^2\right) \frac{dP_n(x)}{dx} \frac{dP_k(x)}{dx} dx + \int_{-1}^{x_0} x \frac{d}{dx}\left[\left(1-x^2\right)\frac{dP_n(x)}{dx}\right]\frac{dP_k(x)}{dx} dx \ , \quad (4.65b)$$

$$e_{nk}^1(x_0) = \int_{-1}^{x_0} \left(1-x^2\right) \frac{dP_n(x)}{dx} \frac{dP_k(x)}{dx} dx = \int_{-1}^{x_0} P_{n1}(x) P_{n1}(x) dx \ , \quad (4.65c)$$

$$\int_{-1}^{x_0} x \frac{d}{dx}\left[\left(1-x^2\right)\frac{dP_n(x)}{dx}\right]\frac{dP_k(x)}{dx} dx = -n(n+1)\int_{-1}^{x_0} xP_n(x)\frac{dP_k(x)}{dx} dx \ , \quad (4.65d)$$

and after further simplifications

$$C = e_{nk}^1(x_0) + n(n+1)\int_{-1}^{x_0} xP_n(x)\frac{dP_k(x)}{dx} dx \ , \quad (4.65e)$$

$$D = \int_{-1}^{x_0} \frac{d}{dx}\left[\left(1-x^2\right)P_n(x)\right]\frac{dP_k(x)}{dx} dx = \int_{-1}^{x_0}\left[-2xP_n(x) + \left(1-x^2\right)\frac{dP_n(x)}{dx}\right]\frac{dP_k(x)}{dx} dx =$$

$$= -2\int_{-1}^{x_0} xP_n(x)\frac{dP_k(x)}{dx} dx + \int_{-1}^{x_0}\left(1-x^2\right)\frac{dP_n(x)}{dx}\frac{dP_k(x)}{dx} dx$$

$$= -2\int_{-1}^{x_0} xP_n(x)\frac{dP_k(x)}{dx} dx + e_{nk}^1(x_0). \quad (4.65f)$$

Substituting Eqs. (4.65e) and (4.65f) into (4.65) we obtain:

$$e_{nk}^2(x_0) = 2x\left(1-x^2\right)\frac{dP_n(x)}{dx}\frac{dP_k(x)}{dx}\Bigg|_{-1}^{x_0} + \left[n(n+1)-2\right]e_{nk}^1(x_0) -$$

$$-n(n+1)\left(1-x^2\right)P_n(x)\frac{dP_k(x)}{dx}\Bigg|_{-1}^{x_0}, \quad (4.66)$$

and after changing the variable x to $\cos\psi$ we have:

$$e_{nk}^2(\psi_0) = 2\cos\psi\sin^2\psi\frac{dP_n(\cos\psi)}{d\cos\psi}\frac{dP_k(\cos\psi)}{d\cos\psi}\Bigg|_{\psi}^{\pi} + \left[n(n+1)-2\right]e_{nk}^1(\psi_0) -$$

$$-n(n+1)\sin^2\psi P_n(\cos\psi)\frac{dP_k(\cos\psi)}{d\cos\psi}\Bigg|_{\psi_0}^{\pi}. \quad (4.67)$$

Substitution of the limits and further simplifications prove the proposition.

4.8 A simple numerical study on modification with a spherical ring

For a numerical test we consider the extended Stokes function and its SOD. We leave modification of the VH and HH derivatives with spherical ring for future works. At the first step we consider the MM and BLSM. The EGM96 to degree and order 360 is used for generating the spectra of the gravity anomalies and their

corresponding error spectra. Figure 4.7 shows the modified ESF for two rings, a) a ring limited between ψ_0=1° and ψ_1=5° and, b) a ring between ψ_0=5° and ψ_1=20°.

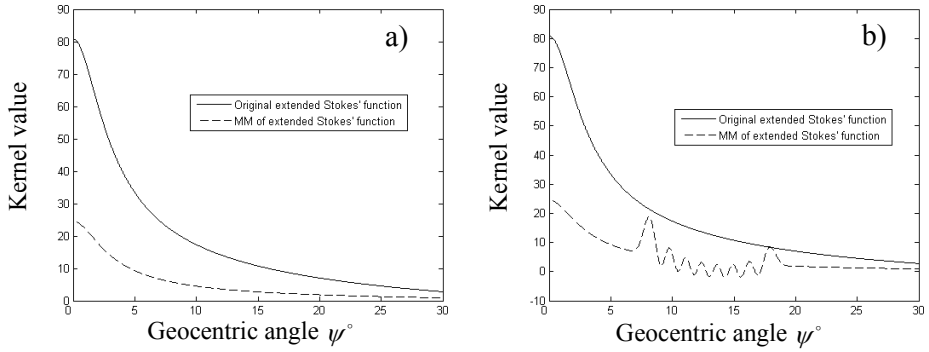

Figure 4.7. (a) MM of ESF for a ring between ψ_0=1° and ψ_1=5° and, (b) ψ_0=5° and ψ_1=20°.

The figure shows that the modified ESF is considerably reduced but as we can see in the figure, minimization of the kernel for the truncation area outside of the ring suppresses the kernel not to change inside the considered ring. In order to show the feasibility of this type of modification, we increase the area of the ring. We select $\psi_0 = 5°$ and $\psi_1 = 20°$ and modify the kernel function using the MM. Figure 4.7b presents the modified kernel versus the original one. As the figure shows the kernel behaviours differ inside the selected ring. Actually, this way of modification amplifies that part of the kernel which is are related with the data inside the ring. Now let us consider the BLSM method with errorless data in order to see its capability to modify the ESF for a spherical ring.

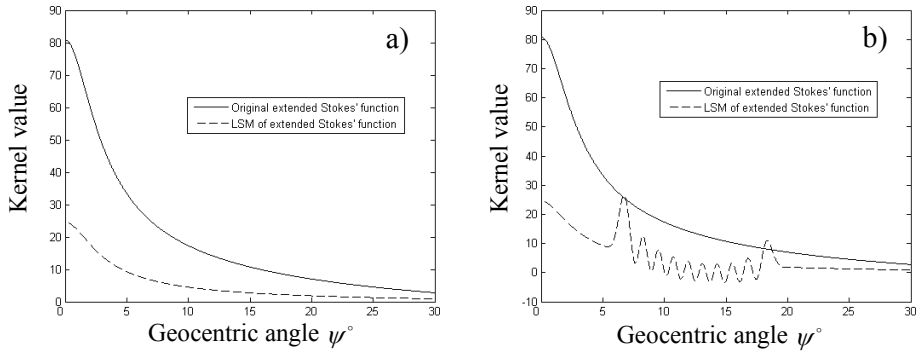

Figure 4.8. (a) BLSM of ESF for a ring between $\psi_0 = 1°$ and $\psi_1 = 5°$ and, (b) $\psi_0 = 5°$ and $\psi_1 = 20°$ with errorless data

Similar to the previous figure, Figure 4.8a shows the modified kernel based on a ring limited to $1° < \psi < 5°$. The same interpretation as that of Figure 4.7a can be made for this figure. Again the area of the ring is increased to $\psi_0 = 5°$ and $\psi_1 = 20°$ caps. In this case, some changes are seen in the modified kernel when the geocentric angle varies from 5° to 20°. The general pattern of Figure 4.8b is very similar with Figure 4.7b, but larger fluctuation is visible in the figure than that of Figure. 4.7b. In order to do better comparison we estimate the global

RMSE of the estimators for both the MM and the BLSM. If we consider the ring between $\psi_0 = 1^\circ$ and $\psi_1 = 5^\circ$ the global RMSE of the estimator will be 2.67 cm for the MM and 9.08×10^{-5} cm for the BLSM, which show better performance of the BLSM in modifying the ESF.

Next, the errors of the terrestrial and EGM data are taken into account. We used the Sjöberg (1984a) model to generate the error spectrum of the terrestrial gravity anomalies. In this case we consider 5 mGal as the standard deviation for the terrestrial data with correlation length of 0.1°. For more details about the numerical computations of the error spectrum of the gravity anomalies the reader is referred to e.g. Ågren (2004) or Ellmann (2005). The following figure shows the results of considering the two aforementioned rings but the kernels are modified by considering the errors of the data as well as the truncation error.

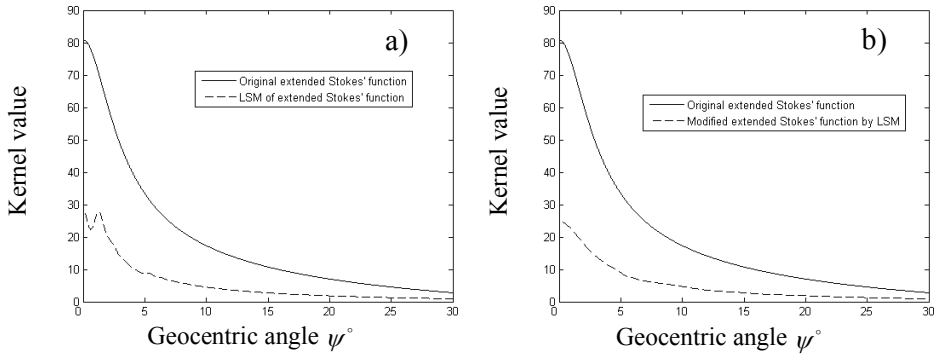

Figure 4.9. (a) BLSM of ESF for ring between $\psi_0 = 1^\circ$ and $\psi_1 = 5^\circ$ and, (b) ψ_0=5° and ψ_1=20° with erroneous data

Figure 4.9a illustrates the modified ESF for a rind restricted between geocentric angles 1° and 5°. As we can see in the figure, a slight change occurs in the modified kernel. If we increase the size of ring and limit it to geocentric angles between 5° and 20° a small changes can be seen in the modified kernel inside the ring. The global RMSE of the estimator is both cases are 4.13 and 4.36 cm when the ring is between $\psi_0 = 1^\circ$ and $\psi_1 = 5^\circ$ and ψ_0=5° and ψ_1=20°, respectively.

The numerical study presented here, discusses the modification of the ESF with a spherical ring. However, in SGG, the emphasis is on the modification of the SOD of the ESF. In the following we numerically investigate the ring modification of the SOD of ESF. Similar to previous study we consider two rings of $2^\circ < \psi < 8^\circ$ and $8^\circ < \psi < 20^\circ$.

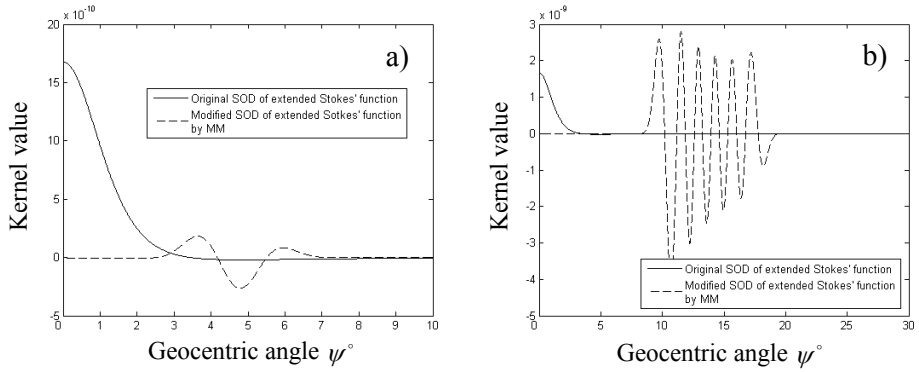

Figure 4.10. (a) MM of SOD of ESF for a ring between ψ_0=2° and ψ_1=8° and, (b) ψ_0=8° and ψ_1=20°

We have selected $2^\circ < \psi < 8^\circ$ in our studies to visualize the variation of the modified kernel better in Figure 4.10a. As the figure shows the SOD of the ESF is better-behave than the ESF. This is why that we present the original and modified kernels to geocentric angle equal to 10°, while it was 30° for the ESF. The SOD of ESF has been modified using MM modification. Figure 4.11 presents the same problem but the modification approach is the BLSM with errorless data.

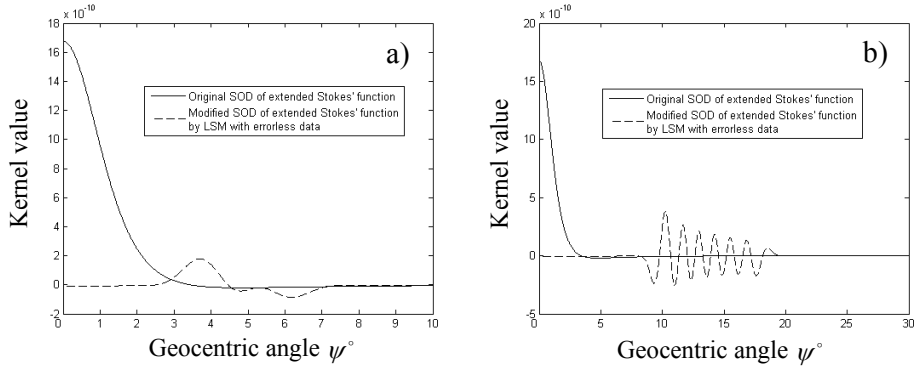

Figure 4.11. (a) BLSM of SOD of ESF for a ring between ψ_0=2° and ψ_1=8° and, (b) ψ_0=8° and ψ_1=20° with errorless data

The figure illustrates different behaviour for the modified kernel by the BLSM. However, the figure demonstrates that the BLSM with errorless data (considering just truncation error) is also capable to modify the SOD of the ESF very well. Figure 4.11b shows smaller variations for the modified kernel by the BLSM than the MM (Figure 4.10b) in the equivalent ring. In order to compare these two modification errors it is enough just to look at the estimated global RMSE of the estimators. The errors are 1.2 mE and 2.46×10^{-5} mE when the MM and the BLSM are used with a spherical ring $2^\circ < \psi < 8^\circ$, respectively. The RMSE of the estimators show that there is no doubt that the BLSM is better than the MM. Let us now take the erroneous data into account in the BLSM process. Figure 4.12 shows that the kernel has been modified very well for both considered rings. The global RMSE of the LSM estimators are 16.86 mE and 17.42 mE for the ring $2^\circ < \psi < 8^\circ$ and $8^\circ < \psi < 20^\circ$, respectively.

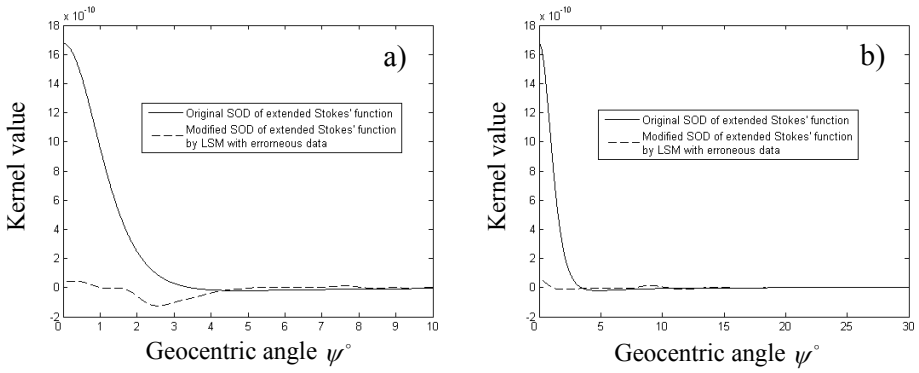

Figure 4.12. (a) BLSM of SOD of ESF for a ring between ψ_0=2° and ψ_1=8° and, (b) ψ_0=8° and ψ_1=20° with errorless data

Chapter 5

Local gravity field determination

5. 1 Introduction

The second-order partial derivatives of the extended Stokes formula can be used to recover the gravity anomaly. In fact, the integral formulas are solved in reverse case by considering them as integral equations, namely the gravitational gradients are observed at satellite level and the unknowns are the gravity anomalies at sea level. In practice, these integral equations have to be descritized prior to computations. The solutions of these integral equations yield the downward continued gravity anomaly. They are classified as the solutions of ill-posed problems, which among other properties are sensitive to the errors of the data. Any small errors in the data can vary the solution considerably. Regularization is one method to stabilize such a system of equations.

Reed (1973) was one of the earliest persons who suggested direct downward continuation of the SGG data in a local gravitational field respect. He derived the corresponding kernels of the second-order partial derivatives of the extended Stokes formula. The performed numerical studies of Reed (1973) were very promising. The ill-posed problems of downward continuation of his simulation were solved by defining some constraints to the system of equations. After that Rummel (1976) theoretically investigated the downward continuation of satellite data in stochastic and deterministic views. Zielinski (1975) considered least-squares collocation for downward continuation and concluded that the additional information is not local but global in statistical characters, and it is impossible to get rigorously exact results. Rummel et al. (1979) compared and presented the relation between regularization and least-squares collocation. Krarup and Tscherning (1984) evaluated the isotropic covariance function of torsion balance observations. Arabelos and Tscherning (1990) used these covariance functions to determine the local gravity field from SGG data. They concluded that the gravity anomaly can be recovered within 8.3 mGal and the geoid within 0.33 m accuracies. Visser (1992) investigated downward continuation of

satellite accelerations. He used the Tikhonov regularization and the least-squares collocation as deterministic and stochastic methods and concluded that collocation is superior to the Tikhonov regularization. Tscherning (1993) derived the covariance of derivatives of the gravity anomalous potential in a rotated frame and later on Arabelos and Tscherning (1995) used the covariance functions to recover the gravity field locally from the observed SGG data in the ORF. Least-squares collocation relies on the a priori information about the unknowns and Xu (1991) investigated the robustness of this method against incorrect prior information of data. Xu (1992) started the discussion of determining the gravity anomaly from the SGG data without a-priori information by using the Tikhonov regularization. He presented a regularization method minimizing the mean square error of the estimated anomalies. Xu and Rummel (1994) investigated the smoothness of the regional gravity field and concluded that the biased estimators improve the least-squares solution, but the improvements are quite different. They proposed an iterative ridge estimator in this respect. The truncated singular value decomposition was used by Xu (1998). Gelderean and Rummel (2001) and (2002) presented the closed form expressions of the Green functions of the GBVPs and removed the zero- and first-degree harmonics from their derivations. Martinec (2003) stated that one can consider these degrees without problem for the VV component and first-degree harmonics for the VH components. Both of the Green functions presented by Gelderen and Rummel (2001) and (2002) and Martinec (2003) can be used to upward or downward continue the gravitational gradient to mean orbital sphere. However, they cannot be used for downward continuation of the gradients to some quantities at sea level. Toth et al. (2004) and (2006) investigated the downward and upward continuation of the gravitational gradient. The difference between their approach and other is to downward/upward continue the gradients to the same type of gradients at mean orbital sphere. They assumed the second-order Taylor expansion for this continuation and derived corresponding kernel formulas in spectral forms. Toth et al. (2007) investigated the practical aspects of this continuation using band limited kernels and concluded that a cap size of 8° is needed, if sufficient suppression of omission errors is required for both upward and downward continuation with band pass filtered kernels. Kotsakis (2007) presented a covariance-adaptive method for regularization and used this method for determining the gravity anomaly at sea level from second-order radial derivative of the gravitational gradients. This method is sensitive to choice of covariance-adaptive matrix which, should a priori be known.

This chapter numerically investigates inversion of all gravitational gradients to recover the gravity anomalies in the presence of Gaussian noise of 1 mE and 1 cE. There are different methods for regularization, but in this chapter, the well-known Tikhonov regularization is used because of its simplicity. The resolution of the SGG data and the required gravity anomalies are tested according to the introduced noise levels. The biases and propagated errors are investigated and discussed as well. At the end, a method to approximate the truncation error of the integrals is proposed.

5.2 Inversion by second-order derivatives of the extended Stokes formula

The second-order partial derivatives of the extended Stokes formulas in the LNOF are:

$$T_{zz}(P)=\frac{R}{4\pi}\iint_{\sigma}S_{rr}(r,\psi)\Delta g^{*}(Q)\,d\sigma, \tag{5.1a}$$

$$T_{xx}(P)=\frac{R}{4\pi}\iint_{\sigma}S_{xx}(r,\psi)\Delta g^{*}(Q)\,d\sigma, \tag{5.1b}$$

$$T_{yy}(P)=\frac{R}{4\pi}\iint_{\sigma}S_{yy}(r,\psi)\Delta g^{*}(Q)\,d\sigma, \tag{5.1c}$$

$$T_{xy}(P)=\frac{R}{4\pi}\iint_{\sigma}S_{xy}(r,\psi)\Delta g^{*}(Q)\,d\sigma, \tag{5.1d}$$

$$T_{xz}(P)=\frac{R}{4\pi}\iint_{\sigma}S_{xz}(r,\psi)\Delta g^{*}(Q)\,d\sigma, \tag{5.1e}$$

and

$$T_{yz}(P)=\frac{R}{4\pi}\iint_{\sigma}S_{yz}(r,\psi)\Delta g^{*}(Q)\,d\sigma, \tag{5.1f}$$

where

$$S_{xx}(r,\psi)=\frac{S_{r}(r,\psi)}{r}+\frac{1}{2r^{2}}\left\{\left[S_{\psi\psi}(r,\psi)+\cot\psi S_{\psi}(r,\psi)\right]+\right.$$
$$\left.+\left[S_{\psi\psi}(r,\psi)-\cot\psi S_{\psi}(r,\psi)\right]\cos 2\alpha\right\},$$
$$S_{yy}(r,\psi)=\frac{S_{r}(r,\psi)}{r}+\frac{1}{2r^{2}}\left\{\left[S_{\psi\psi}(r,\psi)+\cot\psi S_{\psi}(r,\psi)\right]-\right.$$
$$\left.-\left[S_{\psi\psi}(r,\psi)-\cot\psi S_{\psi}(r,\psi)\right]\cos 2\alpha\right\},$$
$$S_{xy}(r,\psi)=\frac{1}{2r^{2}}\left\{\left[S_{\psi\psi}(r,\psi)-\cot\psi S_{\psi}(r,\psi)\right]\sin 2\alpha\right\}$$
$$S_{xz}(r,\psi)=\frac{1}{r}\left[\frac{1}{r}S_{\psi}(r,\psi)-S_{r\psi}(r,\psi)\right]\cos\alpha,$$

and

$$S_{yz}(r,\psi)=\frac{1}{r}\left[\frac{1}{r}S_{\psi}(r,\psi)-S_{r\psi}(r,\psi)\right]\sin\alpha.$$

Here, $T_{ij}(P)$, *i, j = x, y, z* are the gravitational gradients at the computation point *P* (at satellite level), $\Delta g^{*}(Q)$ is the downward continued gravity anomaly at the integration point *Q* (at sea level), *R* is the radius of the sphere approximating sea levels, *r* is the geocentric radius of the computation point *P* and α is the azimuth between *P* and *Q*.

The above integral formulas hold if there is a global coverage of gravity anomalies. However, the problem is not to generate the gravitational gradients, but it is inverse solution of the integral in order to obtain the local gravitational field. Here, the integral formulas must be discretized according to the resolution of the available data (gravitational gradients) and the unknown parameters (gravity anomaly at sea levels). These discretized forms of the above integrals can be written:

$$T_{zz}^{j} = \frac{R}{4\pi}\sum_{i=1}^{n} S_{rr}^{ij}(r,\psi)\Delta g_i^{*}\Delta\sigma_i \text{ , or } \mathbf{T}_{zz} = \mathbf{A}_{zz}\mathbf{\Delta g}, \tag{5.2a}$$

$$T_{xx}^{j} = \frac{R}{4\pi}\sum_{i=1}^{n} S_{xx}^{ij}(r,\psi)\Delta g_i^{*}\Delta\sigma_i \text{ , or } \mathbf{T}_{xx} = \mathbf{A}_{xx}\mathbf{\Delta g}, \tag{5.2b}$$

$$T_{yy}^{j} = \frac{R}{4\pi}\sum_{i=1}^{n} S_{yy}^{ij}(r,\psi)\Delta g_i^{*}\Delta\sigma_i \text{ , or } \mathbf{T}_{yy} = \mathbf{A}_{yy}\mathbf{\Delta g}, \tag{5.2c}$$

$$T_{xy}^{j} = \frac{R}{4\pi}\sum_{i=1}^{n} S_{xy}^{ij}(r,\psi)\Delta g_i^{*}\Delta\sigma_i \text{ , or } \mathbf{T}_{xy} = \mathbf{A}_{xy}\mathbf{\Delta g}, \tag{5.2d}$$

$$T_{xz}^{j} = \frac{R}{4\pi}\sum_{i=1}^{n} S_{xz}^{ij}(r,\psi)\Delta g_i^{*}\Delta\sigma_i \text{ , or } \mathbf{T}_{xz} = \mathbf{A}_{xz}\mathbf{\Delta g}, \tag{5.2e}$$

$$T_{yz}^{j} = \frac{R}{4\pi}\sum_{i=1}^{n} S_{yz}^{ij}(r,\psi)\Delta g_i^{*}\Delta\sigma_i \text{ , or } \mathbf{T}_{yz} = \mathbf{A}_{yz}\mathbf{\Delta g}, \tag{5.2f}$$

where n is the number of cells according to the resolution of the gravity anomaly being determined, i and j are the indices related to P and Q in the integral equations. $\mathbf{A}_{zz}$, $\mathbf{A}_{xx}$, $\mathbf{A}_{yy}$, $\mathbf{A}_{xy}$, $\mathbf{A}_{xz}$, $\mathbf{A}_{yz}$ are the matrix forms of the integrals, $\mathbf{T}_{zz}$, $\mathbf{T}_{xx}$, $\mathbf{T}_{yy}$, $\mathbf{T}_{xy}$, $\mathbf{T}_{xz}$, $\mathbf{T}_{yz}$ are the vectors of the gravitational gradients, $\mathbf{\Delta g}$ is the vector of the unknowns (downward continued gravity anomalies) and $\Delta\sigma_i = \sin\theta_i d\theta_i d\lambda_i$ is the integration element (θ_i and λ_i are the co-latitude and longitude of the point i) .

Equations (5.1a)-(5.1f) are Fredholm integral equations of the first kind, and the inverse solutions of such integrals are ill-posed. The above equations also present the matrix forms of the integral equations, which are suitable for numerical computations. An important matter about these matrix equations is related to the resolution of the data and discretization. In general, we can have different number of unknowns and observables in the solution. Some geoscientists consider equal number of observables and unknowns and some others use more observables than the number of unknowns to have over-determination in their solution. In both cases, we have to solve an ill-posed problem, in which the solution is very sensitive to the existing errors in the observations, which are amplified through the inversion process. In this case, the integral coefficient matrices are ill-conditioned and unstable, and we have to somehow stabilize them by some regulator.

5.3 Singularity investigations on isotropic kernels

In some of the kernels presented in Eqs. (5.1a)-(5.1c) singularity occurs when the integration point Q approaches the computation point P. In this section, we

investigate these numerical singularities theoretically and simplify the kernels in the singular points. It should be mentioned that in our derivation it is assumed that t < 0, as the computation point is at satellite level. No singularity is observed for $S_r(r,\psi)$ and $S_{rr}(r,\psi)$ as they are:

$$S_r(r,0)=-\frac{t^2}{R}\left\{\frac{1+t}{(1-t)^2}+\frac{4}{1-t}-6(1-t)+1-t\left[13+6\ln(1-t)\right]\right\}, \tag{5.3a}$$

$$S_{rr}(r,0)=\frac{t^3}{R^2}\left\{\frac{3(1+t^2)}{(1-t)^4}-\frac{4}{(1-t)^2}-\frac{1+t^2}{(1-t)^3}-\frac{10}{1-t}-18(1-t)+2-3t\left[15+6\ln(1-t)\right]\right\} \tag{5.3b}$$

Therefore we should not worry about singularity of the SOD of the extended Stokes formula and the first terms of the kernels of Eqs. (5.2b) and (5.2c). Consequently, we concentrate on investigating the other kernels. Let us consider the following lemmas, which are useful through the derivations.

Lemma 5.1:

$$\lim_{\psi\to 0}\ \frac{1-t\cos\psi-D}{\sin\psi}=0.$$

Proof. As we presented previously, $D=\left(1-2t\cos\psi+t^2\right)^{\frac{1}{2}}$. Using Hopital's law we obtain

$$\lim_{\psi\to 0}\ \frac{t\sin\psi-t\sin\psi\left(1-2t\cos\psi+t^2\right)^{-\frac{1}{2}}}{\cos\psi}=0. \quad \text{Q.E.D.} \tag{5.4a}$$

Lemma 5.2:

$$\lim_{\psi\to 0}\ \frac{1-t\cos\psi-D}{\sin^2\psi}=-\frac{t^2}{2(1-t)} \quad .$$

Proof. Using Hopital's law we have

$$\lim_{\psi\to 0}\ \frac{t+t\left(1-2t\cos\psi+t^2\right)^{-\frac{1}{2}}}{2\cos\psi}=-\frac{t^2}{2(1-t)}. \quad \text{Q.E.D.} \tag{5.4b}$$

Theorem 5.1:

$$\lim_{\psi\to 0}\left\{\frac{1}{r^2}S_{\psi}(r,\psi)-\frac{1}{r}S_{r\psi}(r,\psi)\right\}=0.$$

Proof. According to Eq. (4.17d) it is easy to show that

$$S_{r\psi}(r,\psi)=0\,, \tag{5.5a}$$

therefore we should show that the first term of the limit is also equal zero. In order to do that we consider Eq. (4.17c) and taking limit of that equation we obtain

$$\lim_{\psi\to 0} S_{\psi}(r,\psi)=\left(\frac{3t^2}{1-t}\right)\lim_{\psi\to 0}\frac{t\sin\psi-t\sin\psi\left(1-t\cos\psi+t^2\right)^{-\frac{1}{2}}}{\cos\psi}=0\,.\ \text{Q.E.D.} \tag{5.5b}$$

Theorem 5.2:

$$\lim_{\psi\to 0}\cot\psi S_{\psi}(r,\psi)=t^2\left[3\ln(1-t)+8-\frac{2}{(1-t)^3}-\frac{6}{1-t}-\frac{3t^2}{2(1-t)^2}\right].$$

Proof. Considering Eq. (4.17c) and after simplifications we have

$$\lim_{\psi\to 0}\cot\psi S_{\psi}(r,\psi)=t^2\left[3\ln(1-t)-\frac{2}{(1-t)^3}-\frac{6}{1-t}+ +8-\left(\frac{3}{1-t}\right)\lim_{\psi\to 0}\left(\frac{1-t\cos\psi-D}{\sin^2\psi}\right)\right]. \tag{5.6}$$

Considering Lemma 5.2 we can further simplify the above relation and prove the theorem.

Theorem 5.3:

$$\lim_{\psi\to 0} S_{\psi\psi}(r,\psi)=t^2\left[3\ln(1-t)+8-\frac{2}{(1-t)^3}-\frac{6}{1-t}-\frac{3t^2}{2(1-t)^2}\right].$$

Proof. Considering Eqs. (4.37c) we obtain in the limit:

$$\lim_{\psi\to 0} S_{\psi\psi}(r,\psi)=-\frac{2t^2}{(1-t)^3}-\frac{6t^2}{1-t}+8t^2+\frac{3t^2}{1-t}\lim_{\psi\to 0}\frac{1-t\cos\psi-D}{\sin^2\psi}+3t^2\ln(1-t) -\frac{3t^4}{(1-t)^2}-\frac{6t^3}{t(1-t)}\lim_{\psi\to 0}\frac{1-t\cos\psi-D}{\sin^2\psi}\,. \tag{5.7}$$

Using Lemma 5.2 the theorem follows.

5.4 Regularization

As was already mentioned, the inverse solution of an integral equation is very sensitive to the errors of the data. A small fluctuation in the data will lead to large changes in the estimated parameters. Therefore, the system of equations is unstable and it should be stabilized. This stabilization problem is called regularization. Let us start our discussion by the following Gauss-Markov model:

$$\mathbf{A}\mathbf{x} = \mathbf{L} - \boldsymbol{\varepsilon}, \tag{5.8}$$

where, $\mathbf{A}$ can be one of the coefficient matrices $\mathbf{A}_{zz}$, $\mathbf{A}_{xx}$, $\mathbf{A}_{yy}$, $\mathbf{A}_{xy}$, $\mathbf{A}_{xz}$, $\mathbf{A}_{yz}$, $\mathbf{L}$ can be one of the vectors $\mathbf{T}_{zz}$, $\mathbf{T}_{xx}$, $\mathbf{T}_{yy}$, $\mathbf{T}_{xy}$, $\mathbf{T}_{xz}$, $\mathbf{T}_{yz}$, $\boldsymbol{\varepsilon}$ is the error of the observations $\mathbf{L}$ and $\mathbf{x}$ is the vector of unknown parameters. Based on this model we consider the well-known Tikhonov regularization method in the following.

5.4.1 Tikhonov regularization

In the Tikhonov regularization the problem is to solve the following optimization problem

$$\left(\left\| \mathbf{A}\mathbf{x} - \mathbf{L} \right\|^2 + \alpha^2 \left\| \mathbf{x} \right\|^2 \right) \rightarrow \min \text{ (with respect to } \mathbf{x}) \tag{5.9a}$$

where $\left\| \mathbf{A}\mathbf{x} - \mathbf{L} \right\|^2$ is the squared norm of the errors, $\left\| \mathbf{x} \right\|^2$ is a norm $\mathbf{x}$. $\alpha^2 > 0$ is the Tikhonov regularization parameter. The regularized solution of Eq. (5.8) based on the Tikhonov regularization is (Tikhonov 1963):

$$\mathbf{x}_{\text{reg}} = \left(\mathbf{A}^T \mathbf{P} \mathbf{A} + \alpha^2 \mathbf{I} \right)^{-1} \mathbf{A}^T \mathbf{P} \mathbf{L} = \mathbf{N}^{-1} \mathbf{A}^T \mathbf{P} \mathbf{L}. \tag{5.9b}$$

The important parameter here is the regularization parameter α^2, which can be estimated in different ways. Here we use the L-curve and the generalized cross-validation (GCV) for estimating this parameter. The interested readers are referred to Hansen (1998) for the details of these methods. If α^2 is large $\mathbf{x}_{\text{reg}}$ contains more bias than the case where α^2 is small. In other words, the former case leads to over-smoothing and the latter to under-smoothing. The over-smoothing means that the solution is smoother than the true one and under-smoothing means that it is rougher; see Hansen (1998) for more details. Here, we take advantage of the regularization toolbox of MATLAB, which was given to the author by a personal communication with Hansen (2008).

5.5 Numerical studies on downward continuation of the SGG data

We start this section with numerical studies on downward continuation of the SGG data to gravity anomalies at sea level. The L-curve and the GCV methods are used to estimate the regularization parameter in the Tikhonov regularization. We need a criterion to select the best method of estimation the regularization parameter; in this case we consider three different simulation studies to see which method yields the closest result to the simulated values.

A regular grid of gravity anomalies are generated using EGM96 to degree and order 360. The integral formulas that we presented for the gravitational gradients at satellite level are employed to generate the SGG data at 250 km level. Two Gaussian noise models of 1 mE and 1 cE are generated and added to the generated SGG data. In fact, considering these Gaussian noise level gives us some ideas about the quality of the inversion, to see which regularization method can provide closer results to the true gravity anomalies.

As before, we select Fennoscandia as our test area, and in order to provide some ideas about the gravity anomalies in this region Figure 5.1 is presented.

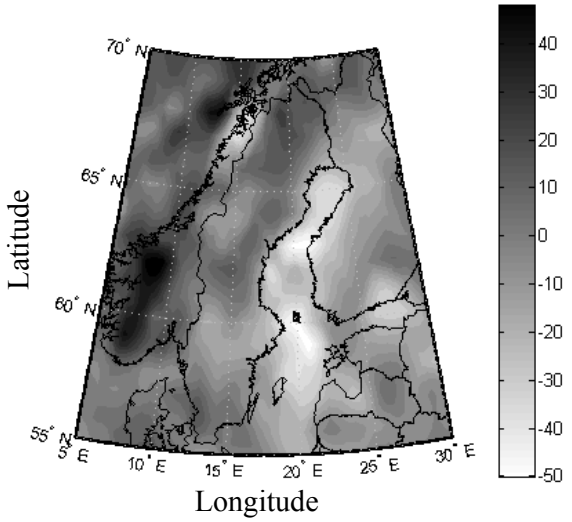

Figure 5.1. Gravity anomalies generated by EGM96 with $1^\circ \times 1^\circ$ resolution in Fennoscandia. Unit: 1 mGal

It shows negative gravity anomalies in the Baltic Sea and positive anomalies over the Norwegian mountains. The maximum, minimum, mean and standard deviation of the gravity anomalies in this area are 57.48, -51.83, 0.09 and 17.84 mGal, respectively.

We consider three simulated examples to test the ability of the regularization methods in recovering the gravity anomalies from gravitational gradients at satellite level. First we test the Tikhonov regularization to recover a grid of $1^\circ \times 1^\circ$ gravity

anomalies from $0.5^\circ \times 0.5^\circ$ grid of the SGG data. In the next subsection, we want to recover a $0.5^\circ \times 0.5^\circ$ grid of gravity anomalies from $0.25^\circ \times 0.25^\circ$ SGG data. In the last part of this numerical simulation studies, we consider the problem of recovering $1^\circ \times 1^\circ$ gravity anomalies from $0.25^\circ \times 0.25^\circ$ SGG data to see how much over-determination can suppress the noise in an ill-posed problem.

5.5.1 Recovery of $1^\circ \times 1^\circ$ gravity anomaly from $0.5^\circ \times 0.5^\circ$ SGG data

We have to consider the condition number of the system of equations related to each gravitational gradient. The condition number is the ratio of the maximum and minimum eigenvalues of the coefficients matrix of the system of equations. A positive-definite matrix has only positive eigenvalues (singular values). A system of equations having a coefficient matrix with a high condition number is more sensitive to data errors than that with a smaller condition number. Here, based on Eqs. (5.2a)-(5.2f) and $1^\circ \times 1^\circ$ synthesized gravity anomalies and $0.5^\circ \times 0.5^\circ$ SGG data by the EGM96, the coefficient matrices are constructed.

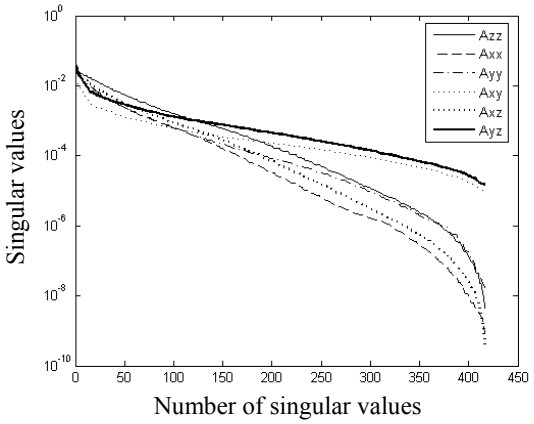

Figure 5.2. Singular values of $\mathbf{A}_{zz}$, $\mathbf{A}_{xx}$, $\mathbf{A}_{yy}$, $\mathbf{A}_{xy}$, $\mathbf{A}_{xz}$ and $\mathbf{A}_{yz}$ matrices, for recovering $1^\circ \times 1^\circ$ gravity anomaly from $0.5^\circ \times 0.5^\circ$ SGG data

Figure 5.2 illustrates the singular values. A very similar pattern can be seen for singular values of $\mathbf{A}_{zz}$, $\mathbf{A}_{xx}$, $\mathbf{A}_{yy}$ and $\mathbf{A}_{xz}$, but this pattern is similar for $\mathbf{A}_{xy}$ and $\mathbf{A}_{yz}$. For the sake of competence, Table 5.1 is given, which presents the maxima and minima singular values of the coefficient matrices of Eqs. (5.2a)-(5.2f) as well as their corresponding condition numbers.

Table 5.1. Maxima and minima of singular values of different system of equations and their corresponding condition numbers κ for recovering $1^\circ \times 1^\circ$ gravity anomaly from $0.5^\circ \times 0.5^\circ$ SGG data

	$\mathbf{A}_{xx}$	$\mathbf{A}_{yy}$	$\mathbf{A}_{zz}$	$\mathbf{A}_{xy}$	$\mathbf{A}_{xz}$	$\mathbf{A}_{yz}$
$\lambda_{\max}$	2.39×10^{-3}	2.44×10^{-3}	2.49×10^{-3}	1.48×10^{-4}	2.54×10^{-3}	3.86×10^{-3}
$\lambda_{\min}$	8.38×10^{-10}	1.67×10^{-8}	4.46×10^{-9}	9.87×10^{-6}	4.35×10^{-10}	1.51×10^{-5}
κ	2.85×10^{7}	1.46×10^{6}	5.57×10^{6}	1.49×10^{3}	5.83×10^{7}	2.56×10^{3}

The smallest condition numbers are related to $\mathbf{A}_{xy}$ and $\mathbf{A}_{yz}$, which means that they are less sensitive to errors in the data compare to other design matrices.

We know that in the real situation the solution are always involved with noise and biases in the data. Here, we consider two Gaussian types of noise levels of 1 mE and 1 cE for the observations. Adding the random noise to the synthesized SGG data at 250 km level may bring the problem closer to reality. Figure 5.3 shows the generated noise for the gravitational gradients.

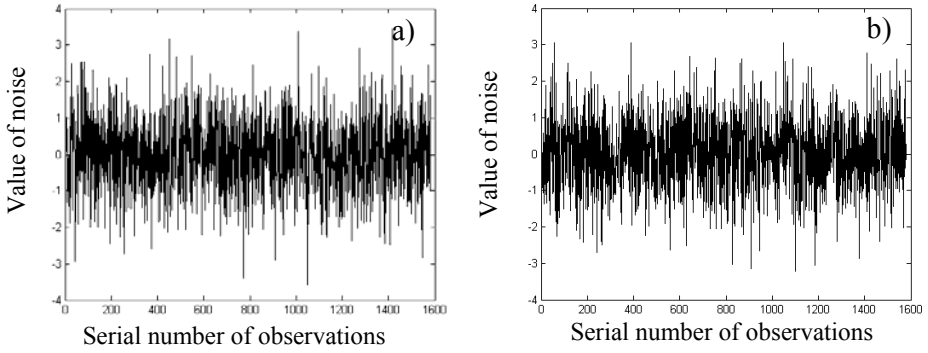

Figure 5.3. Generated Gaussian noise of (a) 1 mE and (b) 1 cE on gravitational gradients

The same noise is considered for all the gradients for easy comparison of results.

The differences between the recovered and the true (simulated) gravity anomalies can be a good criterion to judge about quality of the regularization method. The statistics of these differences are summarized in Table 5.2. The table shows that the GCV method of selecting the regularization parameter yields better results than the L-curve method.

Table 5.2. Statistics of errors of $1^\circ \times 1^\circ$ recovered gravity anomalies from $0.5^\circ \times 0.5^\circ$ SGG data using Tikhonov regularization (based on L-curve and GCV) with Gaussian noise of 1 mE. Unit: 1 mGal

	L-curve				GCV			
	min	mean	max	std	min	mean	max	std
$T_{xx} \rightarrow \Delta g^*$	-18.81	-0.01	17.29	6.02	-19.03	-0.00	16.60	4.97
$T_{yy} \rightarrow \Delta g^*$	-18.33	-0.01	15.30	6.33	-12.44	-0.01	14.75	4.69
$T_{zz} \rightarrow \Delta g^*$	-15.14	0.02	16.92	6.14	-10.10	0.01	9.58	3.32
$T_{xy} \rightarrow \Delta g^*$	-16.85	-0.12	18.90	5.75	-12.96	-0.13	13.78	4.41
$T_{xz} \rightarrow \Delta g^*$	-16.36	0.05	16.98	5.58	-13.42	0.04	12.00	4.11
$T_{yz} \rightarrow \Delta g^*$	-12.92	-0.00	12.82	4.27	-12.28	-0.00	15.02	4.02

Most of the estimated standard deviations of the differences (the difference between the recovered and the true values of the gravity anomalies) by the GCV are smaller than those estimated by the L-curve. Now, let us increase the noise to 1 cE, the statistics of the differences between the recovered and true gravity anomalies are presented below.

Table 5.3. Statistics of errors of $1^\circ \times 1^\circ$ recovered gravity anomalies from $0.5^\circ \times 0.5^\circ$ SGG data using Tikhonov regularization (based on L-curve and GCV) with Gaussian noise of 1 cE. Unit: 1 mGal

	L-curve				GCV			
	min	mean	max	std	min	mean	max	std
$T_{xx} \rightarrow \Delta g^*$	-29.02	-0.11	29.55	7.90	-26.75	-0.11	27.70	7.89
$T_{yy} \rightarrow \Delta g^*$	-21.89	-0.11	28.80	7.37	-23.88	-0.11	28.37	7.29
$T_{zz} \rightarrow \Delta g^*$	-20.69	0.07	21.57	6.76	-22.94	0.07	24.32	6.13
$T_{xy} \rightarrow \Delta g^*$	-28.04	-0.56	31.26	10.08	-28.60	-0.59	31.33	9.97
$T_{xz} \rightarrow \Delta g^*$	-26.30	-0.03	21.26	7.67	-27.43	-0.04	22.39	7.40
$T_{yz} \rightarrow \Delta g^*$	-27.99	-0.04	38.61	8.68	-28.54	-0.03	35.92	7.93

Table 5.3 clearly shows that both methods of selecting the regularization parameter in the Tikhonov regularization yield more or less the same results. Again Table 5.3 suggests the GCV method for estimating the regularization parameter. Table 5.4 shows the estimated regularization parameters. The table shows that all the regularization parameters are in the order of 10^{-2}. The regularization parameters, which were estimated using the L-curve are smaller than those estimated by the GCV. It means that the bias of the recovered gravity anomalies based on the L-curve are smaller than that of the GCV, but as we assumed in the beginning of this section, our criterion is the closeness of the recovered gravity anomalies to the true ones (simulated one), and since the GCV provided closer results to the true ones we prefer to use the GCV for estimating the regularization parameter, even if it may be more biased than the L-curve solution.

Table 5.4. Values of regularization parameter of the coefficient matrices for recovering $1^\circ \times 1^\circ$ gravity anomaly from $0.5^\circ \times 0.5^\circ$ SGG data derived for Tikhonov regularization using L-curve and GCV, for 1 mE and 1 cE noise on SGG data

	1 mE		1 cE	
	L-curve	GCV	L-curve	GCV
$T_{xx} \rightarrow \Delta g^*$	4.11×10^{-2}	7.01×10^{-2}	5.31×10^{-2}	4.60×10^{-2}
$T_{yy} \rightarrow \Delta g^*$	3.92×10^{-2}	9.72×10^{-2}	5.20×10^{-2}	6.66×10^{-2}
$T_{zz} \rightarrow \Delta g^*$	3.48×10^{-2}	9.24×10^{-2}	4.55×10^{-2}	7.17×10^{-2}
$T_{xy} \rightarrow \Delta g^*$	5.03×10^{-2}	8.74×10^{-2}	5.13×10^{-2}	5.52×10^{-2}
$T_{xz} \rightarrow \Delta g^*$	3.76×10^{-2}	8.26×10^{-2}	3.94×10^{-2}	4.50×10^{-2}
$T_{yz} \rightarrow \Delta g^*$	7.83×10^{-2}	10.97×10^{-2}	4.94×10^{-2}	7.95×10^{-2}

5.5.2 Recovery of $0.5^\circ \times 0.5^\circ$ gravity anomaly from $0.25^\circ \times 0.25^\circ$ SGG data

Xu (1992) stated that the recovery of gravity anomaly with resolution of $0.5^\circ \times 0.5^\circ$ is not easy when the noise of the SGG data are about 0.01 E. However, in this section we are going to test the possibility of recovering a grid of $0.5^\circ \times 0.5^\circ$ gravity anomaly, if the noise level is reduced to 1 mE. In this respect, the gravitational gradients are synthesized at 250 km level with $0.25^\circ \times 0.25^\circ$ resolution to recover the gravity anomalies with $0.5^\circ \times 0.5^\circ$ resolution. Figure 5.4 shows the singular values of the coefficient matrices of the discretized integrals corresponding to each element of the gravitational tensor. Those values of $\mathbf{A}_{zz}$ and $\mathbf{A}_{xz}$ are similar and they are different for $\mathbf{A}_{xx}$ and $\mathbf{A}_{yy}$. The singular values of $\mathbf{A}_{xy}$ and $\mathbf{A}_{yz}$ are again similar to those in the previous section.

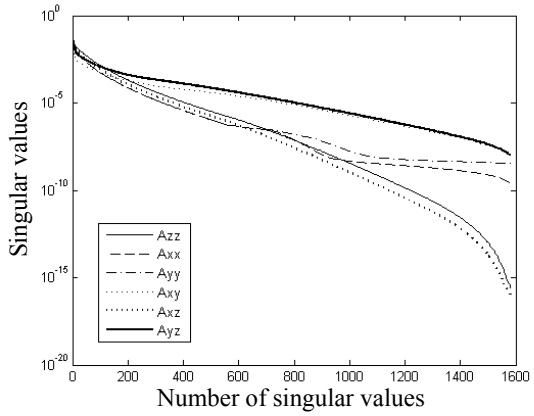

Figure 5.4. Singular values of $\mathbf{A}_{zz}$, $\mathbf{A}_{xx}$, $\mathbf{A}_{yy}$, $\mathbf{A}_{xy}$, $\mathbf{A}_{xz}$ and $\mathbf{A}_{yz}$ matrices, for recovering $0.5^\circ \times 0.5^\circ$ gravity anomaly from $0.25^\circ \times 0.25^\circ$ SGG data

In Table 5.5 the maxima and minima of the singular values and their corresponding condition numbers are presented.

Table 5.5. Maxima and minima of singular values of different system of equations and their corresponding condition numbers κ for recovering $0.5^\circ \times 0.5^\circ$ gravity anomaly from $0.25^\circ \times 0.25^\circ$ SGG data

	$\mathbf{A}_{xx}$	$\mathbf{A}_{yy}$	$\mathbf{A}_{zz}$	$\mathbf{A}_{xy}$	$\mathbf{A}_{xz}$	$\mathbf{A}_{yz}$
$\lambda_{\max}$	5.94×10^{-3}	6.04×10^{-3}	6.20×10^{-3}	3.66×10^{-3}	6.32×10^{-3}	9.55×10^{-3}
$\lambda_{\min}$	5.40×10^{-11}	8.51×10^{-10}	6.41×10^{-17}	3.07×10^{-9}	2.52×10^{-17}	2.63×10^{-9}
κ	1.10×10^{8}	7.10×10^{6}	9.68×10^{13}	1.19×10^{6}	2.51×10^{14}	3.63×10^{6}

In this case, the condition numbers of $\mathbf{A}_{yy}$, $\mathbf{A}_{xy}$ and $\mathbf{A}_{yz}$ are smaller than the other coefficient matrices, and they are expected to be less sensitive to noise vs. for the other coefficient matrices. It should be noted the condition numbers of $\mathbf{A}_{zz}$ and $\mathbf{A}_{xz}$ are considerably large compared with those of other matrices. We will use the Gaussian noise of 1 mE and 1 cE in the inversion process. Figure 5.5 shows the generated noises.

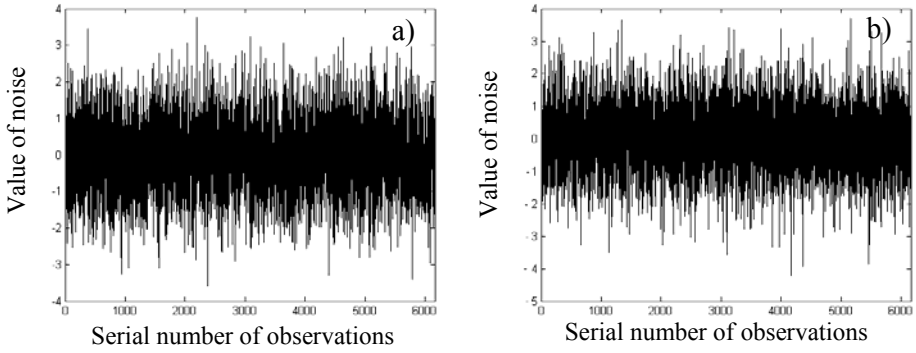

Figure 5.5. Generated Gaussian noise of (a) 1 mE and (b) 1 cE on gravitational gradients.

Table 5.6 presents the statistics of error of the recovered gravity anomalies. In this step we have added 1 mE noise (see Figure 5.5a) for each type of SGG data. One can learn from the table that the L-curve and the GCV methods work well in the presence of 1 mE noise in the data, in spite of having unstable system of equations. The difference between the recovered data based on the L-curve and the GCV is about 1 mGal and may be negligible in practical considerations.

Table 5.6. Statistics of errors of $0.5^\circ \times 0.5^\circ$ recovered gravity anomalies from $0.25^\circ \times 0.25^\circ$ SGG data using Tikhonov regularization (based on L-curve and GCV) with Gaussian noise of 1 mE. Unit: 1 mGal

	L-curve				GCV			
	min	mean	max	std	min	mean	max	std
$T_{xx} \rightarrow \Delta g^*$	-15.38	-0.01	19.89	4.83	-15.49	-0.01	19.55	4.88
$T_{yy} \rightarrow \Delta g^*$	-16.72	-0.00	13.90	4.77	-16.63	-0.00	14.01	4.71
$T_{zz} \rightarrow \Delta g^*$	-13.05	0.00	17.31	3.87	-12.67	-0.00	16.68	3.68
$T_{xy} \rightarrow \Delta g^*$	-19.44	-0.04	19.59	5.94	-16.94	-0.06	17.74	5.13
$T_{xz} \rightarrow \Delta g^*$	-15.33	-0.02	17.46	4.38	-14.83	-0.03	17.50	4.30
$T_{yz} \rightarrow \Delta g^*$	-20.74	-0.00	20.45	5.63	-17.32	-0.00	15.82	4.62

Table 5.7. Statistics of errors of $0.5^\circ \times 0.5^\circ$ recovered gravity anomalies from $0.25^\circ \times 0.25^\circ$ SGG data using Tikhonov regularization (based on L-curve and GCV) with Gaussian noise of 1 cE. Unit: 1 mGal

	L-curve				GCV			
	min	mean	max	std	min	mean	max	std
$T_{xx} \rightarrow \Delta g^*$	-33.69	-0.01	36.20	7.59	-26.51	0.03	29.15	7.32
$T_{yy} \rightarrow \Delta g^*$	-26.39	0.01	22.93	6.71	-23.90	0.01	23.62	6.74
$T_{zz} \rightarrow \Delta g^*$	-21.12	-0.01	25.75	5.68	-19.66	-0.00	26.80	5.71
$T_{xy} \rightarrow \Delta g^*$	-28.88	-0.35	31.08	8.55	-31.34	-0.25	33.28	8.73
$T_{xz} \rightarrow \Delta g^*$	-26.36	-0.20	28.04	6.75	-26.33	-0.17	34.63	6.90
$T_{yz} \rightarrow \Delta g^*$	-21.01	-0.03	29.49	7.08	-23.64	-0.03	27.78	7.20

Table 5.8. Values of regularization parameter of the coefficient matrices for recovering $0.5^\circ \times 0.5^\circ$ gravity anomaly from $0.25^\circ \times 0.25^\circ$ SGG data derived for Tikhonov regularization using L-curve and GCV, for 1 mE and 1 cE noise on SGG data

	1 mE		1 cE	
	L-curve	GCV	L-curve	GCV
$T_{xx} \rightarrow \Delta g^*$	5.05×10^{-2}	4.79×10^{-2}	5.37×10^{-2}	2.59×10^{-2}
$T_{yy} \rightarrow \Delta g^*$	5.19×10^{-2}	5.58×10^{-2}	5.12×10^{-2}	3.47×10^{-2}
$T_{zz} \rightarrow \Delta g^*$	5.40×10^{-2}	7.10×10^{-2}	5.24×10^{-2}	4.39×10^{-2}
$T_{xy} \rightarrow \Delta g^*$	4.88×10^{-2}	6.66×10^{-2}	4.90×10^{-2}	3.21×10^{-2}
$T_{xz} \rightarrow \Delta g^*$	5.25×10^{-2}	5.96×10^{-2}	5.07×10^{-2}	2.92×10^{-2}
$T_{yz} \rightarrow \Delta g^*$	4.71×10^{-2}	8.45×10^{-2}	5.65×10^{-2}	4.69×10^{-2}

In a general view the table shows that the regularization parameter changes slightly when we considered 1 mE vs. 1 cE noise in the SGG data. The regularization parameter related with $T_{yz} \rightarrow \Delta g^*$ differs when the noise level changes. The

regularization parameter estimated by the GCV considerably changes by the noise level. One might interpret this matter in such a way that the estimation process of the regularization parameter by the GCV rely more on the data. However, the consequence of these changes is not important as the standard deviations of the differences do not change considerably.

5.5.3 Recovery of $1^\circ \times 1^\circ$ gravity anomaly from $0.25^\circ \times 0.25^\circ$ SGG data

In this part of the study we present how much over-determination of the SGG data affects recovering of gravity anomalies. In this case, we organize the system of equations in such a way that the resolution of the data are $0.25^\circ \times 0.25^\circ$ and the goal is to estimate a $1^\circ \times 1^\circ$ grid of gravity anomalies. At the first step, we have to analyze the coefficient matrices of the descritized integral equations. Figure 5.6 shows the singular values of the coefficient matrices.

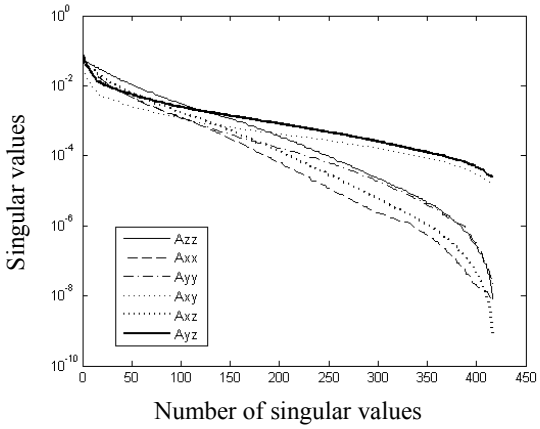

Figure 5.6. Singular values of $\mathbf{A}_{zz}$, $\mathbf{A}_{xx}$, $\mathbf{A}_{yy}$, $\mathbf{A}_{xy}$, $\mathbf{A}_{xz}$ and $\mathbf{A}_{yz}$ matrices, for recovering $1^\circ \times 1^\circ$ gravity anomaly from $0.25^\circ \times 0.25^\circ$ SGG data

Table 5.9 shows the maxima and minima of the singular values of the coefficient matrices as well as their condition numbers. As the table shows the condition numbers of $\mathbf{A}_{xx}$, $\mathbf{A}_{yy}$ and $\mathbf{A}_{zz}$ are all in the order of 10^6, and they are also in the same order for $\mathbf{A}_{xy}$ and $\mathbf{A}_{yz}$ and in order of 10^3. Therefore we can expected that the recovered gravity anomalies from T_{xy} and T_{yz} are less affected by noise in the data.

Table 5.10 confirms our last statement about T_{xy} and T_{yz} components when we use the L-curve method for estimating the regularization parameter. However, as we can see when using the GCV method, we have smallest standard deviation of the differences related with T_{zz} . If we increase the noise to 1 cE level, the result of our inversion is given by Table 5.11.

Table 5.9. Maxima and minima of singular values of different system of equations and their corresponding condition numbers κ for recovering $1^\circ \times 1^\circ$ gravity anomaly from $0.25^\circ \times 0.25^\circ$ SGG data

	$\mathbf{A}_{xx}$	$\mathbf{A}_{yy}$	$\mathbf{A}_{zz}$	$\mathbf{A}_{xy}$	$\mathbf{A}_{xz}$	$\mathbf{A}_{yz}$
$\lambda_{\max}$	4.76×10^{-3}	4.86×10^{-3}	4.97×10^{-3}	2.95×10^{-3}	5.07×10^{-3}	7.70×10^{-3}
$\lambda_{\min}$	8.67×10^{-9}	2.17×10^{-8}	8.11×10^{-9}	1.57×10^{-5}	6.65×10^{-10}	2.49×10^{-5}
κ	5.49×10^{6}	2.24×10^{6}	6.12×10^{6}	1.88×10^{3}	7.61×10^{7}	3.09×10^{3}

Table 5.10. Statistics of errors of $1^\circ \times 1^\circ$ recovered gravity anomalies from $0.25^\circ \times 0.25^\circ$ SGG data using Tikhonov regularization (based on L-curve and GCV) with Gaussian noise of 1 mE. Unit: 1 mGal

	L-curve				GCV			
	min	mean	max	std	min	mean	max	std
$T_{xx} \rightarrow \Delta g^*$	-13.79	-0.01	15.42	5.10	-14.24	-0.01	14.73	4.18
$T_{yy} \rightarrow \Delta g^*$	-18.63	-0.01	19.15	6.36	-12.66	-0.00	10.99	3.74
$T_{zz} \rightarrow \Delta g^*$	-19.76	0.01	14.27	5.50	-7.97	0.00	8.36	2.78
$T_{xy} \rightarrow \Delta g^*$	-12.13	0.01	15.99	4.13	-11.51	0.00	12.61	3.41
$T_{xz} \rightarrow \Delta g^*$	-14.90	-0.00	17.26	4.80	-9.43	-0.00	12.62	3.40
$T_{yz} \rightarrow \Delta g^*$	-9.39	0.00	10.41	2.99	-10.29	0.00	10.05	3.18

Table 5.11. Statistics of errors of $1^\circ \times 1^\circ$ recovered gravity anomalies from $0.25^\circ \times 0.25^\circ$ SGG data using Tikhonov regularization (based on L-curve and GCV) with Gaussian noise of 1 cE. Unit: 1 mGal

	L-curve				GCV			
	min	mean	max	std	min	mean	max	std
$T_{xx} \rightarrow \Delta g^*$	-24.01	0.06	23.72	6.49	-23.60	0.06	23.09	6.55
$T_{yy} \rightarrow \Delta g^*$	-21.16	0.00	21.16	6.85	-22.96	0.01	19.83	6.50
$T_{zz} \rightarrow \Delta g^*$	-17.95	0.01	27.76	5.93	-15.69	-0.00	23.15	5.18
$T_{xy} \rightarrow \Delta g^*$	-23.05	-0.10	30.40	8.72	-22.31	-0.19	29.29	8.31
$T_{xz} \rightarrow \Delta g^*$	-20.81	-0.16	23.25	7.03	-18.77	-0.17	21.86	6.40
$T_{yz} \rightarrow \Delta g^*$	-24.28	-0.01	29.13	9.13	-16.26	-0.02	22.26	6.74

Table 5.12 shows that the regularization parameters estimated by the L-curve and GCV are more or less in the same order. However, as we can see, all the values are larger for the GCV than for the L-curve when the error is about 1 mE, except for T_{yz}. According to Table 5.11 we can see that this magnitude is not significant when inverting T_{yz}. If we increase the noise to 1 cE level, we will obtain smaller values for the regularization parameters. The regularization parameters estimated by the L-curve are very close to each other for each system of equations, while they are very different for the GCV. One may interpret this result as the fact of direct sensitivity of the GCV to the data.

Table 5.12. Values of regularization parameter of the coefficient matrices for recovering $1^\circ \times 1^\circ$ gravity anomaly from $0.25^\circ \times 0.25^\circ$ SGG data derived for Tikhonov regularization using L-curve and GCV, for 1 mE and 1 cE noise on SGG data

	1 mE		1 cE	
	L-curve	GCV	L-curve	GCV
$T_{xx} \rightarrow \Delta g^*$	4.53×10^{-2}	8.13×10^{-2}	4.63×10^{-2}	4.39×10^{-2}
$T_{yy} \rightarrow \Delta g^*$	3.81×10^{-2}	9.86×10^{-2}	5.18×10^{-2}	6.83×10^{-2}
$T_{zz} \rightarrow \Delta g^*$	3.93×10^{-2}	11.69×10^{-2}	4.81×10^{-2}	8.21×10^{-2}
$T_{xy} \rightarrow \Delta g^*$	6.47×10^{-2}	9.81×10^{-2}	4.99×10^{-2}	6.13×10^{-2}
$T_{xz} \rightarrow \Delta g^*$	4.42×10^{-2}	9.44×10^{-2}	4.01×10^{-2}	5.02×10^{-2}
$T_{yz} \rightarrow \Delta g^*$	14.80×10^{-2}	9.36×10^{-2}	3.81×10^{-2}	8.09×10^{-2}

5.6 Inversion of Eötvös type gradients

The previous section showed that the Tikhonov regularization using the GCV method is better than the L-curve method. In this part of our study we want to test downward continuation of the Eötvös type gradients, which are combinations of the HH gradients. In this case we use $T_{xx} - T_{yy}$ and $2T_{xy}$ for recovering the gravity anomaly. In Chapter 4 we have presented their mathematical formulas. Here we concentrate on their inversions. We want to recover the $1^\circ \times 1^\circ$ gravity anomalies from $0.5^\circ \times 0.5^\circ$ and $0.25^\circ \times 0.25^\circ$ grids of the gravitational gradients. The singular values of the coefficient matrices are presented in Figure 5.17.

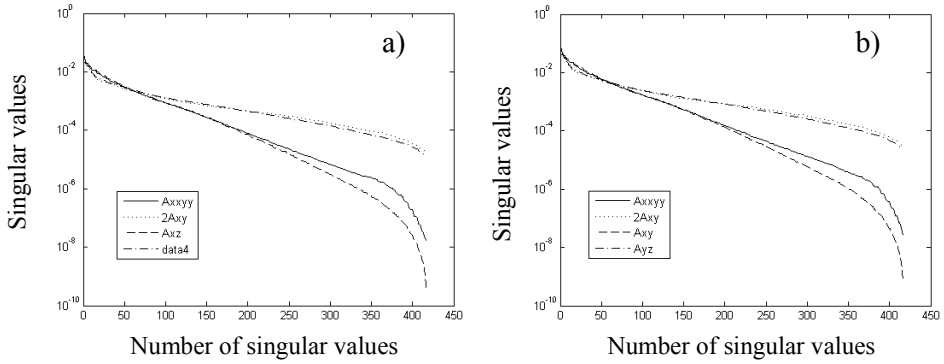

Figure 5.7. Singular values of $\mathbf{A}_{xx}$ - $\mathbf{A}_{yy}$, 2 $\mathbf{A}_{xy}$, $\mathbf{A}_{xz}$ and $\mathbf{A}_{yz}$ for recovering $1^\circ \times 1^\circ$ gravity anomalies from (a) $0.25^\circ \times 0.25^\circ$ and, (b) $0.5^\circ \times 0.5^\circ$ SGG data

The statistics of the inversion are presented in Table 5.13.

Table 5.13. Statistics of errors of $1^\circ \times 1^\circ$ recovered gravity anomalies obtained from inversion of $0.5^\circ \times 0.5^\circ$ and $0.25^\circ \times 0.25^\circ$ Eötvös type gradients. Unit: 1 mGal

		$0.5^\circ \times 0.5^\circ$				$0.25^\circ \times 0.25^\circ$			
		min	mean	max	std	min	mean	max	std
1 mE	$(T_{xx} - T_{yy}, 2T_{xy}) \rightarrow \Delta g*$	-10.39	-0.01	11.15	3.92	-8.91	0.00	9.07	2.98
	$(T_{xz}, T_{yz}) \rightarrow \Delta g*$	-5.85	-0.00	7.89	2.53	-6.97	-0.00	7.62	1.95
1 cE	$(T_{xx} - T_{yy}, 2T_{xy}) \rightarrow \Delta g*$	-21.87	-0.04	29.02	8.20	-15.89	0.06	25.48	6.88
	$(T_{xz}, T_{yz}) \rightarrow \Delta g*$	-25.07	-0.02	22.31	6.19	-15.06	-0.04	14.76	4.92

As we saw in the previous section, over-determination helps the regularization process to suppress the random noise in the data. Table 5.13 shows that the main reason for decreasing the standard error of the differences between the recovered and the true gravity anomalies is related to higher redundancy of the data in joint inversion of T_{xz} and T_{yz} . In this case, there are no changes in the kernel functions of the integrals. The small standard deviation is due to over-determination. The situation is different for inversion of the HH gradients as their kernels change as well. As the table shows considerable improvement is achieved for the HH Eötvös type gradients relative to inversion of each single HH gradient.

5.7 Estimated errors

In the present section, we will study the estimated error of recovered gravity anomalies, assuming that the SGG data only contains random error. A result of the previous numerical studies was that, the GCV method yields better results with respect to those obtained by the L-curve. Here only the propagation of random errors and biases of regularization based on the GCV method will be considered. We start with estimating the propagated random errors. By considering Eq. (5.9b) and using the propagation law of random errors we obtain the covariance matrix of the estimated unknowns:

$$\mathbf{C}_{\mathbf{x}_{\text{reg}}} = \sigma_0^2 \mathbf{N}^{-1} \mathbf{A}^T \mathbf{P} \mathbf{A} \mathbf{N}^{-1}, \tag{5.10}$$

in which σ_0^2 is the variance of unit weight. Figure 5.8 shows the estimated errors of the gravity anomalies from the SGG data contaminated with Gaussian noise of 1 mE. In computing errors we set σ_0^2 to 1 (later on we will show how to estimate the a-posteriori variance factor in such an ill-posed problem). Here, we have presented the propagated errors from $0.5^\circ \times 0.5^\circ$ gravitational gradients at 250 km altitude.

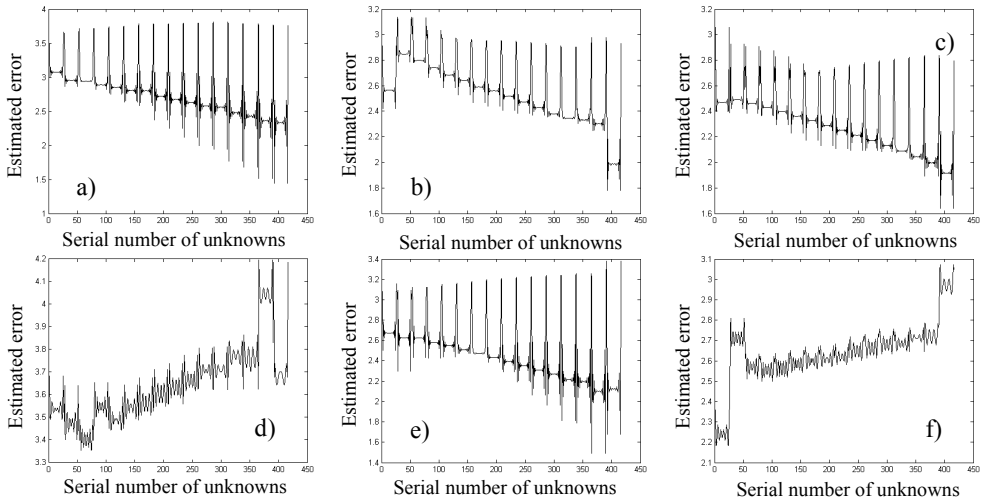

Figure 5.8. Estimated error of $1^\circ \times 1^\circ$ recovered gravity anomalies from $0.5^\circ \times 0.5^\circ$ (a) T_{xx}, (b) T_{yy}, (c) T_{zz}, (d) T_{xy}, (e) T_{xz} and (f) T_{yz} with 1 mE Gaussian noise. Unit: 1 mGal

In the figure "unknowns" stands for recovered gravity anomalies. The horizontal axis of the figures shows the serial number of recovered gravity anomalies from north to south and parallel by parallel in Fennoscandia. The jumps that we see in the figures illustrate that the errors quickly grow up in the end of each parallel of the selected region (Fennoscandia). The figure shows that the largest propagated error are related to inversion of T_{xy} and the smallest one to T_{zz}. The general patterns of the errors are decreasing for inversion of T_{xx}, T_{yy}, T_{zz} and T_{xz} from north to south, but they are increasing for T_{xy} and T_{yz}. The propagated error in inversion of T_{yy} is slightly different with those of T_{xx} and T_{zz}, as we see smaller errors for the first (northern) and last (southern) parallels. Similar error behaviour is seen for T_{xy} as the errors are increasing and larger in the southern part of the region. The propagated error of inverting T_{yz} is small at the most northern parallel. The statistics of the estimated errors for the recovered gravity anomalies are presented in Table 5.14. The table shows that the smallest standard deviation of the propagated errors are related to the gravity anomalies recovered from T_{xy} and T_{yz} and the largest ones are related to T_{xx} and T_{xz}.

In Figure 5.9 we present the propagated errors of $0.5^\circ \times 0.5^\circ$ gravity anomalies from $0.25^\circ \times 0.25^\circ$ grids of the SGG data in order to see how the errors look like. Again we plot the errors by considering 1 mE noise in the SGG data. Again in the figure we see that the errors are decreasing from north to south of the region (Fennoscandia) for all inversion process except that for T_{xy}. The smallest error is related to T_{yz}, and it should be noted that there are two jumps in its plot for the most northern and the least southern parallels, but both jumps are smaller comparing with

the errors of the other gradients. Comparing the errors with the errors of the previous example we see that the magnitudes of these errors are larger.

Table 5.14. Statistics of estimated error of $1^\circ \times 1^\circ$ recovered gravity anomalies from $0.5^\circ \times 0.5^\circ$ SGG data (with 1 mE and 1 cE Gaussian noise). Unit: 1 mGal

	1 mE				1 cE			
	min	mean	max	std	min	mean	max	std
$T_{xx} \rightarrow \Delta g^*$	1.44	2.76	3.81	0.40	3.10	4.51	6.78	0.64
$T_{yy} \rightarrow \Delta g^*$	1.78	2.56	3.13	0.25	2.61	3.34	4.86	0.34
$T_{zz} \rightarrow \Delta g^*$	1.64	2.30	3.05	0.24	2.48	3.27	4.54	0.38
$T_{xy} \rightarrow \Delta g^*$	3.35	3.64	4.20	0.16	4.20	5.61	6.50	0.48
$T_{xz} \rightarrow \Delta g^*$	1.49	2.46	3.38	0.31	3.64	4.86	7.07	0.65
$T_{yz} \rightarrow \Delta g^*$	2.18	2.64	3.07	0.14	3.59	3.95	4.67	0.20

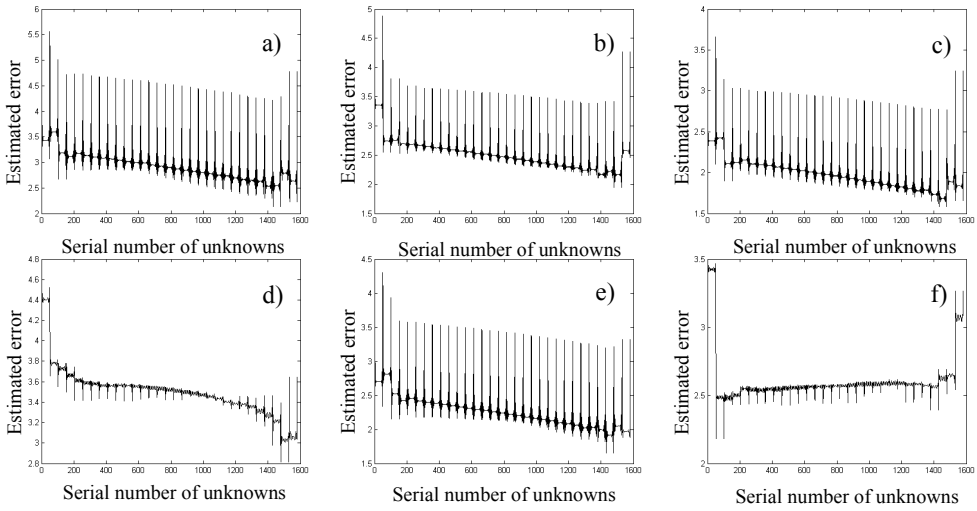

Figure 5.9. Estimated error of $0.5^\circ \times 0.5^\circ$ recovered gravity anomalies from $0.25^\circ \times 0.25^\circ$ (a) T_{xx}, (b) T_{yy}, (c) T_{zz}, (d) T_{xy}, (e) T_{xz} and (f) T_{yz} with 1 mE Gaussian noise. Unit: 1 mGal

The statistics of the estimated errors are presented in Table 5.15. The largest error is related to inversion of T_{xx} and the smallest one to T_{zz} and the least standard deviation is related to T_{yz}. In average point of view we can say that T_{zz} is the best and T_{xy} is the worst gradients for inversion. Now, we consider the case where the $1^\circ \times 1^\circ$ gravity anomalies are recovered from the $0.25^\circ \times 0.25^\circ$ SGG data.

Table 5.15. Statistics of estimated error of $1^\circ \times 1^\circ$ recovered gravity anomalies from $0.5^\circ \times 0.5^\circ$ SGG data (with 1 mE and 1 cE Gaussian noise). Unit: 1 mGal

	1 mE				1 cE			
	min	mean	max	std	min	mean	max	std
$T_{xx} \rightarrow \Delta g^*$	2.02	2.84	5.30	0.39	3.53	4.69	8.86	0.64
$T_{yy} \rightarrow \Delta g^*$	1.84	2.42	4.65	0.30	2.31	3.42	6.55	0.47
$T_{zz} \rightarrow \Delta g^*$	1.59	2.02	3.67	0.25	2.09	2.93	5.59	0.39
$T_{xy} \rightarrow \Delta g^*$	2.95	3.65	4.70	0.24	4.45	5.58	7.67	0.55
$T_{xz} \rightarrow \Delta g^*$	1.67	2.34	4.36	0.32	3.15	4.30	8.24	0.59
$T_{yz} \rightarrow \Delta g^*$	2.26	2.71	3.61	0.19	3.24	4.15	5.67	0.35

Figure 5.10 shows the propagated errors when 1 mE noise are considered in the SGG data.

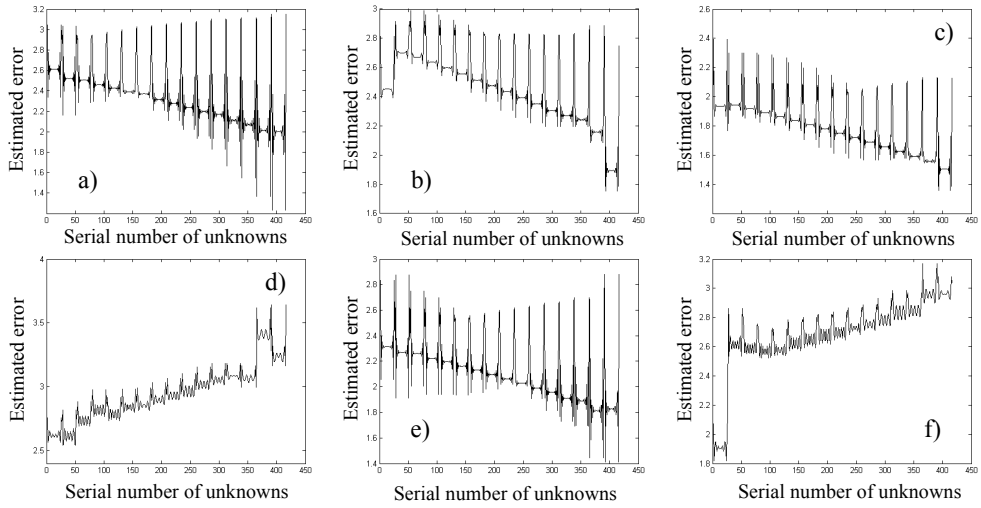

Figure 5.10. Estimated error of $1^\circ \times 1^\circ$ recovered gravity anomalies from $0.25^\circ \times 0.25^\circ$ (a) T_{xx}, (b) T_{yy}, (c) T_{zz}, (d) T_{xy}, (e) T_{xz} and (f) T_{yz} with 1 mE Gaussian noise. Unit: 1 mGal

The patterns of the propagated errors of the $1^\circ \times 1^\circ$ gravity anomalies are very similar with those of Figure 5.9, which means that the distribution of the gravity anomalies (grid resolution) may be related to the propagated error patterns. Again the errors are decreasing from north to south for T_{xx}, T_{yy}, T_{zz} and T_{xz}, while they are increasing for T_{xy} and T_{yz}. Table 5.16 shows that T_{zz} is the best gradients in average.

Table 5.16. Statistics of estimated error of $1^\circ \times 1^\circ$ recovered gravity anomalies from $0.25^\circ \times 0.25^\circ$ SGG data (with 1 mE and 1 cE Gaussian noise). Unit: 1 mGal

	1 mE				1 cE			
	min	mean	max	std	min	mean	max	std
$T_{xx} \rightarrow \Delta g^*$	1.23	2.35	3.15	0.31	3.00	4.57	6.87	0.72
$T_{yy} \rightarrow \Delta g^*$	1.75	2.46	2.99	0.24	2.80	3.43	4.70	0.33
$T_{zz} \rightarrow \Delta g^*$	1.36	1.79	2.39	0.18	2.04	2.80	3.80	0.33
$T_{xy} \rightarrow \Delta g^*$	2.54	2.95	3.64	0.21	4.26	5.38	6.09	0.37
$T_{xz} \rightarrow \Delta g^*$	1.41	2.12	2.88	0.25	3.07	4.24	6.12	0.59
$T_{yz} \rightarrow \Delta g^*$	1.82	2.69	3.17	0.24	3.59	3.93	4.48	0.31

In any adjustment process, when we want to estimate the error of the unknown parameters (in this case the gravity anomalies), we should consider an a-priori variance factor. In our computations, we have assumed that it is equal to 1, and this assumption is not far from reality, because we already know how much noise we have added to the SGG data. However, we can re-scale the variance-covariance matrix of the estimated parameters by the a-posteriori variance factor. Estimation of the variance of unit weight (a-posteriori variance factor) in an ill-posed problem is not as easy as in an ordinary adjustment. In this case, the estimation will not be an unbiased estimation and subsequently the estimated a-posteriori variance factor of an ordinary adjustment is wrong. The scaled variance-covariance matrix of the estimated parameters in an ill-posed problem is:

$$\hat{\mathbf{C}}_{\mathbf{x}_{\text{reg}}} = \hat{\sigma}_0^2 \mathbf{N}^{-1} \mathbf{A}^T \mathbf{P} \mathbf{A} \mathbf{N}^{-1}, \tag{5.11a}$$

where $\hat{\sigma}_0^2$ is the a-posteriori variance factor. The unbiased estimation of this factor has the following from (Xu et al. 2006, Eq. 22, p. 73):

$$\hat{\sigma}_0^2 = \frac{\boldsymbol{\varepsilon}_{\text{reg}}^T \mathbf{P} \boldsymbol{\varepsilon}_{\text{reg}} - \alpha^4 \mathbf{x}^T \left\{ \mathbf{N}^{-1} - \alpha^2 \mathbf{N}^{-2} \right\} \mathbf{x}}{n - r + \alpha^4 \text{trace}\left\{ \mathbf{N}^{-2} \right\}}, \tag{5.11b}$$

where n and r are the number of observables and unknown parameters, respectively. $\boldsymbol{\varepsilon}_{\text{reg}}$ stands for the biased residuals, which are estimated from the regularized solution by

$$\boldsymbol{\varepsilon}_{\text{reg}} = \left(\mathbf{I} - \mathbf{A}_{\text{reg}}^0 \right) \mathbf{L}, \tag{5.11c}$$

where

$$\mathbf{A}_{\text{reg}}^0 = \mathbf{A} \mathbf{A}_{\text{reg}}^- = \mathbf{A} \mathbf{N}^{-1} \mathbf{A}^T \mathbf{P}. \tag{5.11d}$$

In order to perform some numerical studies about estimation of the a-posteriori variance factor, we use the aforementioned system of equations (Eqs. 5.2a-5.2f). We generate again two types of Gaussian noise. The a-posteriori variance factor is estimated using Eq. (5.11b) as well as the bias (Eq. 5.11e). The results of our

computations are presented Tables 5.17 and 5.18. The tables show that the estimated a-posteriori variance factors in such ill-posed problem are close to 1. The differences between $\hat{\sigma}_0^2$ and a-priori variance factor, which we assumed $\sigma_0^2 = 1$, are due to the bias of the regularization. One can also use the standard formula for estimating the a-posteriori variance factor, but the estimate will not be unbiased. In such a case, it is possible to estimate the bias and remove it from the estimated variance factor. A formula for this bias was proposed by Xu et al. (2006), which is given in Eq. (5.11e).

Table 5.17. A-posteriori variance factors and biases due to regularization in recovering $1^\circ \times 1^\circ$ gravity anomalies from $0.5^\circ \times 0.5^\circ$ and $0.25^\circ \times 0.25^\circ$ SGG data

	$0.5^\circ \times 0.5^\circ$				$0.25^\circ \times 0.25^\circ$			
	1 mE		1 cE		1 mE		1 cE	
	$\hat{\sigma}_0^2$	Bias $\hat{\sigma}_0^2$	$\hat{\sigma}_0^2$	Bias $\hat{\sigma}_0^2$	$\hat{\sigma}_0^2$	Bias $\hat{\sigma}_0^2$	$\hat{\sigma}_0^2$	Bias $\hat{\sigma}_0^2$
$T_{xx} \rightarrow \Delta g^*$	1.47	0.20	1.64	0.26	1.04	0.04	1.12	0.05
$T_{yy} \rightarrow \Delta g^*$	1.41	0.20	1.67	0.27	1.03	0.03	1.12	0.05
$T_{zz} \rightarrow \Delta g^*$	1.35	0.16	1.55	0.24	1.02	0.03	1.10	0.04
$T_{xy} \rightarrow \Delta g^*$	1.17	0.10	1.55	0.25	0.99	0.01	1.10	0.04
$T_{xz} \rightarrow \Delta g^*$	1.42	0.19	1.57	0.24	1.04	0.03	1.11	0.04
$T_{yz} \rightarrow \Delta g^*$	1.15	0.09	1.48	0.23	0.98	0.01	1.08	0.04

Table 5.18 A-posteriori variance factors and biases in recovering $0.5^\circ \times 0.5^\circ$ gravity anomalies from $0.25^\circ \times 0.25^\circ$ SGG data

	$\hat{\sigma}_0^2$ (1 mE)	$\hat{\sigma}_0^2$ (1 cE)
$T_{xx} \rightarrow \Delta g^*$	1.76	1.94
$T_{yy} \rightarrow \Delta g^*$	1.76	1.95
$T_{zz} \rightarrow \Delta g^*$	1.72	1.91
$T_{xy} \rightarrow \Delta g^*$	1.58	1.89
$T_{xz} \rightarrow \Delta g^*$	1.75	1.92
$T_{yz} \rightarrow \Delta g^*$	1.54	1.85

The bias in Tables 5.17 and 5.18 is :

$$\text{Bias}\left(\hat{\sigma}_0^2\right) = \frac{\alpha^4 \left\{\text{trace}\left[\mathbf{PAN}^{-1}\mathbf{x}\mathbf{x}^T\mathbf{N}^{-1}\mathbf{A}^T\right] + \sigma_0^2 \text{trace}\left[\mathbf{N}^{-2}\right]\right\}}{n-r}. \qquad (5.11e)$$

Equation (5.11e) is the estimated bias of the a posteriori variance factor which must be removed. We did not present the biases in Table 5.18, because the size of matrices was considerably large and our software was not able to handle them. However, the consequence of the estimated a-posteriori variance factors is similar to that of Table 5.17. In estimating the a-posteriori variance factor using the standard formula (of an

ordinary adjustment) we obtained very close values to 1. Subtracting the biases from such variance factors yields negative values which is meaningless. Consequently, estimation of a-posteriori variance factor using Eq. (5.11b) is good enough for such ill-posed problems.

5.8 Biased-corrected estimation of the gravity anomalies

The Tikhonov regularization is a biased estimation and this bias is the penalty we pay for stabilizing the system of equations. However, the bias can be estimated and removed from the estimated parameter. We call this removal step the bias-correction step, and the corrected unknowns are called biased-corrected parameters. It is not difficult to show that this bias is given by:

$$\text{bias}\left(\mathbf{x}_{\text{reg}}\right) = -\alpha^2 \mathbf{N}^{-1}\mathbf{x}\,, \tag{5.12}$$

where $\mathbf{x}$ is the true value of unknown parameters. $\mathbf{x}_{\text{reg}}$ can be selected as an approximation of $\mathbf{x}$ to estimate the bias. In the following we present the biases of three examples that we considered for the local gravity field determination. We start with the case where a grid of $1^\circ \times 1^\circ$ gravity anomalies are recovered from $0.5^\circ \times 0.5^\circ$ of the SGG data. The following figure shows the estimated biases from the SGG data with 1 mE noise.

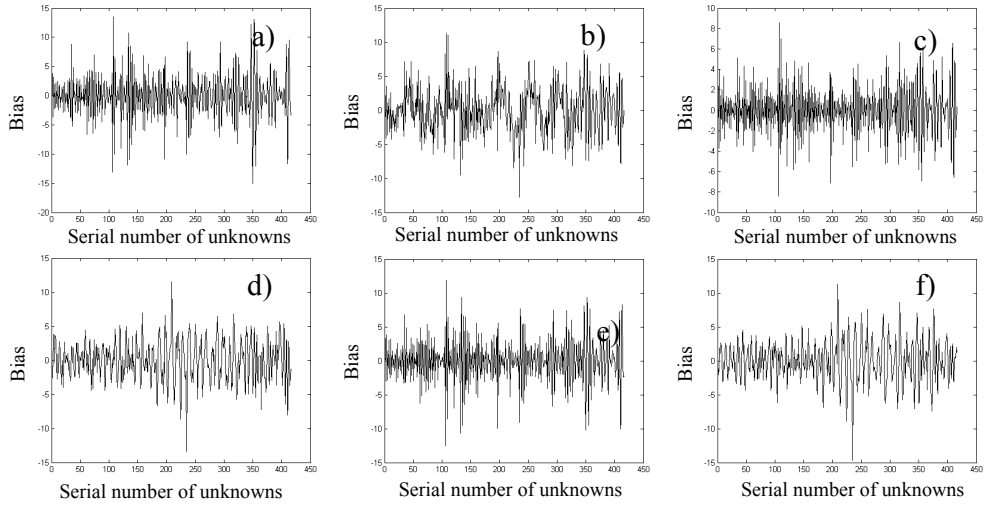

Figure 5.11. Estimated biases of $1^\circ \times 1^\circ$ recovered gravity anomalies from $0.5^\circ \times 0.5^\circ$ (a) T_{xx}, (b) T_{yy}, (c) T_{zz}, (d) T_{xy}, (e) T_{xz} and (f) T_{yz} with 1 mE Gaussian noise. Unit: 1 mGal

In the figure "unknowns" stands for recovered gravity anomalies. Comparing the Figures (5.11a)-(5.11f) we see that the smallest bias is related with T_{zz}, and the other biases are within 15 mGal level. In illustrating these biases we considered 1 mE Gaussian noise in the SGG data, in Table 5.19 we present the statistics of the biased-

corrected recovered gravity anomalies for both 1 mE and 1 cE Gaussian noise in the simulated data.

Table 5.19. Statistics of errors of biased-corrected $1^\circ \times 1^\circ$ recovered gravity anomalies from $0.5^\circ \times 0.5^\circ$ SGG data (contaminated by 1 mE and 1 cE Gaussian noise). Unit: 1 mGal

	1 mE				1 cE			
	min	mean	max	std	min	mean	max	std
$T_{xx} \rightarrow \Delta g^*$	-12.75	-0.01	9.40	2.79	-13.66	-0.12	13.76	4.34
$T_{yy} \rightarrow \Delta g^*$	-7.31	-0.01	7.80	2.65	-7.80	-0.10	7.91	2.90
$T_{zz} \rightarrow \Delta g^*$	-5.51	0.01	7.33	2.31	-9.14	0.07	7.98	3.04
$T_{xy} \rightarrow \Delta g^*$	-9.81	-0.10	12.11	3.53	-14.25	-0.23	14.35	5.12
$T_{xz} \rightarrow \Delta g^*$	-6.43	0.04	6.89	2.43	-14.34	0.04	16.37	4.67
$T_{yz} \rightarrow \Delta g^*$	-6.71	-0.00	7.89	2.48	-11.10	-0.03	12.52	3.66

At first view we see considerable improvements for the recovered gravity anomalies (cf. Table 5.19). The standard deviations in the table show that the recovered parameters from T_{zz} are closer to the true values (simulated values). However, the other gradients can be inverted with more or less the same quality when the noise is in 1 mE level. The largest standard deviation is related to T_{xy} as it was expected. When we increase the noise to 1 cE level, the inversion process behaviour a little bit changes as we can see the closer estimated parameter to the true ones for T_{zz} and T_{yy}. T_{xz} and T_{xx} provide the gravity anomalies with the same order and the largest differences are related with T_{xy}. Let us increase the resolution of the SGG data to $0.5^\circ \times 0.5^\circ$ in order to see how much over-determination improve the biased-corrected recovered gravity anomalies. Figure 5.12 shows the biases of inversions of the simulated SGG data with 1 mE Gaussian noise. The differences between the biased-corrected recovered gravity anomalies are the true ones are presented in Table 5.20.

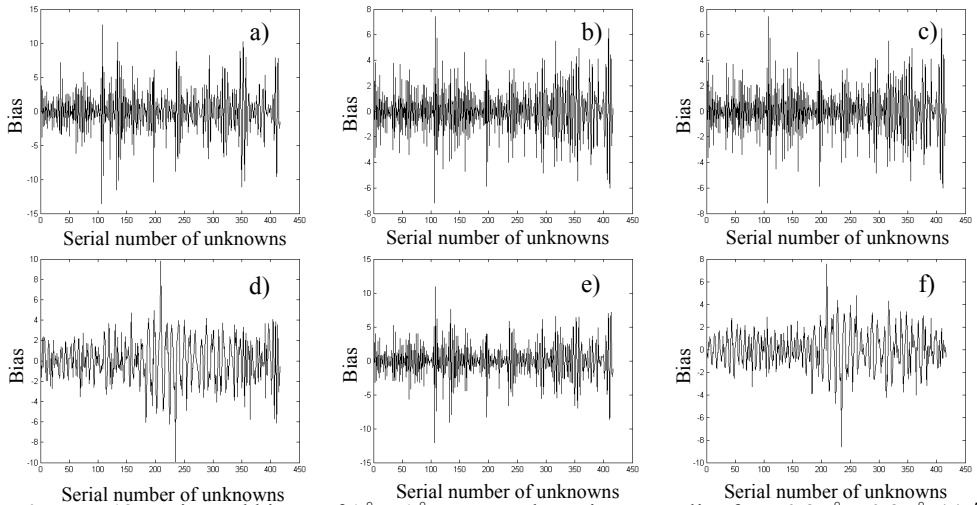

Figure 5.12. Estimated biases of $1^\circ \times 1^\circ$ recovered gravity anomalies from $0.25^\circ \times 0.25^\circ$ (a) T_{xx}, (b) T_{yy}, (c) T_{zz}, (d) T_{xy}, (e) T_{xz} and (f) T_{yz} with 1 mE Gaussian noise. Unit: 1 mGal

Table 5.20. Statistics of errors of biased-corrected recovered $1^\circ \times 1^\circ$ gravity anomalies from $0.25^\circ \times 0.25^\circ$ SGG data contaminated by 1 mE and 1 cE Gaussian noise. Unit: 1 mGal

	1 mE				1 cE			
	min	mean	max	std	min	mean	max	std
$T_{xx} \rightarrow \Delta g^*$	-7.87	-0.01	7.37	2.37	-12.47	0.05	22.12	4.56
$T_{yy} \rightarrow \Delta g^*$	-8.28	-0.00	8.20	2.51	-8.30	0.00	10.71	3.27
$T_{zz} \rightarrow \Delta g^*$	-5.91	0.00	5.28	1.82	-10.44	-0.00	7.92	2.75
$T_{xy} \rightarrow \Delta g^*$	-8.64	0.01	8.79	2.89	-13.77	0.07	17.12	5.28
$T_{xz} \rightarrow \Delta g^*$	-6.47	-0.00	6.04	2.13	-15.12	-0.13	13.18	4.34
$T_{yz} \rightarrow \Delta g^*$	-7.02	-0.00	7.30	2.89	-10.80	-0.01	10.52	3.83

Some improvements are seen in the inversion process although they are at less than 1 mGal level for data with 1 mE noise. Similar conclusion can also be made for the noisy data with 1 cE standard deviation. The last example, in which the resolution of the required gravity anomalies is $0.5^\circ \times 0.5^\circ$ and the resolution of the simulated data is $0.25^\circ \times 0.25^\circ$ is shown in Figure 5.13, which illustrates that the biases are in 15 mGal level except for T_{xx} when the noise is at 1 mE level.

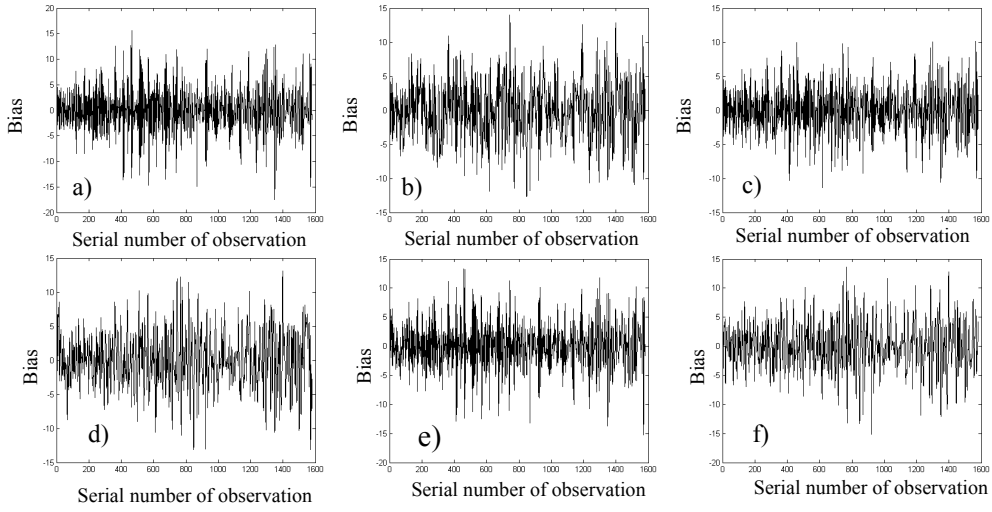

Figure 5.13. Estimated biases of $0.5^\circ \times 0.5^\circ$ recovered gravity anomalies from $0.25^\circ \times 0.25^\circ$ (a) T_{xx}, (b) T_{yy}, (c) T_{zz}, (d) T_{xy}, (e) T_{xz} and (f) T_{yz} with 1 mE Gaussian noise. Unit: 1 mGal

The biased-corrected parameters are presented in Table 5.21, where, again, the Gaussian noise levels of 1 mE and 1 cE are considered.

Table 5.21. Statistics of difference of biased-corrected recovered $0.5^\circ \times 0.5^\circ$ gravity anomalies from $0.25^\circ \times 0.25^\circ$ SGG data (with 1 mE and 1 cE Gaussian noise). Unit: 1 mGal

	1 mE				1 cE			
	min	mean	max	std	min	mean	max	std
$T_{xx} \rightarrow \Delta g^*$	-11.46	-0.01	9.39	2.87	-14.29	0.02	24.93	4.75
$T_{yy} \rightarrow \Delta g^*$	-8.20	-0.00	8.53	2.47	-10.03	0.01	12.23	3.26
$T_{zz} \rightarrow \Delta g^*$	-6.71	0.00	7.00	2.02	-11.67	0.00	8.78	2.86
$T_{xy} \rightarrow \Delta g^*$	-11.66	0.02	12.57	3.58	-17.60	0.00	20.60	5.42
$T_{xz} \rightarrow \Delta g^*$	-8.21	-0.00	7.820	2.30	-17.03	-0.06	15.84	4.23
$T_{yz} \rightarrow \Delta g^*$	-12.66	-0.00	9.09	2.71	-15.72	-0.02	10.72	3.89

5.9 Truncation errors of the integral formulas

Truncating the integrals with isotropic kernels, which means that the kernel function just changes by geocentric angle ψ, are easier than those with non-isotropic kernels. However, isotropy does not hold after differentiation. Here, we present another way for truncating the integral formulas with non-isotropic kernels. The truncation error of the integral formulas generating the gradients can be presented by the following integral:

$$\delta T_{ij}(P) = \frac{R}{4\pi} \iint_{\sigma - \sigma_0} S_{ij}(r, \psi) \Delta g^*(Q) d\sigma, \qquad (5.13)$$

where $i, j = x, y,$ and z. The integration domain $\sigma - \sigma_0$ is related to those part of the integral which are outside of σ_0, which is the inversion area and $\Delta g^*(Q)$ is the gravity anomaly at sea level.

Equation (5.13) can be written as:

$$\delta T_{ij}(P) = \frac{R}{4\pi} \iint_{\sigma} S_{ij}(r, \psi) \Delta g^*(Q) d\sigma - \frac{R}{4\pi} \iint_{\sigma_0} S_{ij}(r, \psi) \Delta g^*(Q) d\sigma, \qquad (5.14)$$

The integration domain of the first integral is all over the globe and this integral, which is the space formulas of the gravitational gradients, can be expressed in terms of spherical harmonics.

The integration domain of the second integral is a specific area for local gravity field determination. In other words, the gravity anomalies inside the integral can be generated with a specific resolution by using an existing EGM and the integration performs to generate the gravitational gradients at satellite level. Subtraction of these

two integrals can be an approximation for the truncation error of the integrals. In the following, these truncation errors are presented and discussed. At the first step of our numerical studies, the gravitational gradients were generated using the EGM96 at 250 km altitude with $0.25^\circ \times 0.25^\circ$ and $0.5^\circ \times 0.5^\circ$ resolutions. A grid of $1^\circ \times 1^\circ$ gravity anomalies at sea level is generated. Figure 5.15 shows the truncation error estimated by Eq. (5.14).

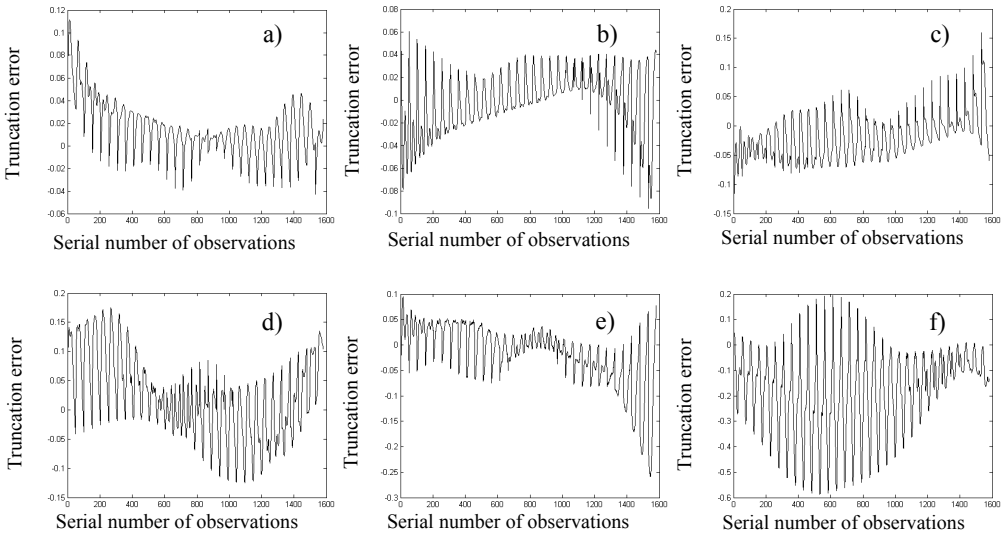

Figure 5.14. Truncation error of $0.5^\circ \times 0.5^\circ$ estimated gravitational gradients (a) δT_{xx}, (b) δT_{yy}, (c) δT_{zz}, (d) δT_{xy}, (e) δT_{xz} and (f) δT_{yz} from $1^\circ \times 1^\circ$ gravity anomalies, respectively. Unit: 1 E

The horizontal axis of the figures presents the serial number of gravitational gradients, which were put in a column vector row by row from the generated grid. The vertical axis shows the truncation error of each gradient. In this study we have 1581 gravitational gradients at the satellite level (250 km) which are estimated from 416 gravity anomalies at sea level. The statistics of these truncation errors are presented in Table 5.22, which shows significant error due to neglecting those portions of gravitational signal in gravitational gradients. The table illustrates the largest truncation error in T_{yz} and the smallest ones are related with T_{xx} and T_{yy}.

We increased the resolution of the gravitational gradients to $0.25^\circ \times 0.25^\circ$ and obtained similar results to Table 5.22.

Let us increase the resolution of the gravity anomalies and gradients to $0.5^\circ \times 0.5^\circ$ and $0.25^\circ \times 0.25^\circ$, respectively. Figure 5.15 shows the result of this investigation.

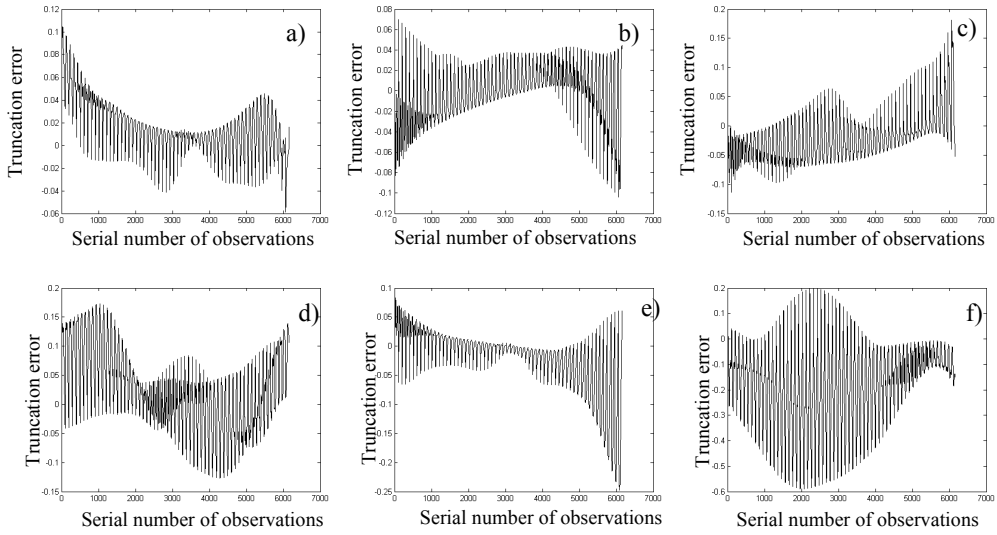

Figure 5.15. Truncation error of $0.25^\circ \times 0.25^\circ$ estimated gravitational gradients (a) δT_{xx}, (b) δT_{yy}, (c) δT_{zz}, (d) δT_{xy}, (e) δT_{xz} and (f) δT_{yz} from $0.5^\circ \times 0.5^\circ$ gravity anomalies. Unit: 1 E

The figure shows that the truncation errors of the integrals follow a very similar pattern independent of resolution of the SGG and terrestrial data. However, the magnitudes of these truncation errors differ.

Table 5.22. Statistics of truncation error of estimated $0.5^\circ \times 0.5^\circ$ gravitational gradients from $1^\circ \times 1^\circ$ gravity anomalies using Eq. (5.14). Unit: 1 E

	min	mean	max	std
δT_{xx}	-0.04	0.01	0.11	$\pm$ 0.02
δT_{yy}	-0.09	-0.00	0.07	$\pm$ 0.02
δT_{zz}	-0.13	-0.02	0.16	$\pm$ 0.04
δT_{xy}	-0.12	0.02	0.17	$\pm$ 0.07
δT_{xz}	-0.24	-0.01	0.08	$\pm$ 0.05
δT_{yz}	-0.59	-0.18	0.19	$\pm$ 0.15

Table 5.23. Statistics of truncation error of $0.25^\circ \times 0.25^\circ$ gravitational gradients from $1^\circ \times 1^\circ$ gravity anomalies using Eq. (5.14). Unit: 1 E

	min	mean	max	std
δT_{xx}	-0.06	0.01	0.10	0.02
δT_{yy}	-0.10	-0.00	0.07	0.03
δT_{zz}	-0.13	-0.02	0.18	0.04
δT_{xy}	-0.13	0.02	0.17	0.07
δT_{xz}	-0.25	-0.02	0.08	0.05
δT_{yz}	-0.59	-0.18	0.20	0.15

At first attention on Tables 5.22-5.23 one might conclude that the truncation errors are very similar. However, it should be kept in mind that the truncation error is categorized as a systematic error and they must be removed from the SGG data prior to downward continuation and inversion even if they are very small. As Tables 5.22 and 5.23 shows the truncation errors are in 1 cE level and considerable.

Chapter 6

Combinations of SGG data

6.1 Introduction

In global geopotential modeling using SGG, three different sets of solutions of the geopotential coefficients are obtained. These solutions are nothing else than the solutions of the VV, VH and HH GBVPs as Martinec (2003) presented. In fact the solution of the Laplace equation is sought using gradiometric boundary values, which are the gradiometric observables. The simple and weighted means are two simple methods of combining the solutions of the GBVPs. This chapter presents some ways for optimal combination of the solution using condition adjustment model and VCE. In local gravity field determination, the simple joint inversion of the SGG data and re-weighting observation using VCE is investigated.

Bjerhammar (1983) was one of the earliest authors suggested using VCE to mix the boundary values problems and called this way of combination stochastic approach with reference to Holota (1983a) and (1983b) and Svensson (1982). In fact he used VCs to update the observation weights in an iterative adjustment problem. The VCE is a well-known topic in geodetic and related sciences. Different methods exist for computing the VCs. One of the most famous methods is the MInimum Norm Quadratic Unbiased Estimator (MINQUE), presented by Rao (1971). Helmert's method is another approach presented by Kelm (1978) and by Grafarend and Schaffrin (1979). The method of LaMotte (1973) and Pukelsheim (1981), which is very popular in statistics, was generalized by Schaffrin (1981) for applications in geodesy. Sjöberg (1985) presented a VC estimator for the adjustment model with a singular covariance matrix. VCE and applications can also be found in Rao and Kleffe (1988). Maximum likelihood estimation of VCs was first presented for geodetic applications by Kubik (1970), Patterson and Thompson (1971) and (1975), Persson (1980) and Koch (1986). Searle et al. (1992) and Koch (1999) provided useful discussions on the concepts of VCs. As an alternative approach a Monte-Carlo algorithm can be used for VC estimation (e.g., Kusche 2003) and Fotopoulous (2003) and (2005). In Grafarend (2006) many details of the Gauss-Markov and Gauss-Helmert models are presented, and VCE is treated both theoretically and numerically.

Xu et al. (2006) presented a method for computing VCs in linear ill-posed models. They have considered a zero-order Tikhonov regularization method (Tikhonov 1963) for estimating the VCs. They also found out that the simultaneous estimation of the regularization parameter and VCs is advantageous. Xu et al. (2007) discussed the estimability of the VCs and proved (as could be expected) that they are not estimable for a fully-unknown variance-covariance matrix. Amiri-Simkooei (2007) and Teunissen and Amiri-Simkooei (2008) explored a new type of least-squares estimator to the VCs.

This chapter starts with the well-known Gauss-Helmert adjustment model. After that some methods of VCE are briefly reviewed and used in combining the SGG data.

6.2 The Gauss-Helmert adjustment model

The Gauss-Helmert model is a generalized model of the Gauss-Markov and the condition adjustment model, i.e. these models are special cases of the Gauss-Helmert model. This model has the following form (Sjöberg 1984c):

$$\mathbf{A}\mathbf{x}+\mathbf{B}\boldsymbol{\varepsilon}=\mathbf{w}\text{, with}\,E\left\{\boldsymbol{\varepsilon}\boldsymbol{\varepsilon}^{T}\right\}=\mathbf{Q}\text{, and }E\left\{\boldsymbol{\varepsilon}\right\}=0\text{,} \tag{6.1}$$

where, $\mathbf{A}$ and $\mathbf{B}$ are the first and second design matrices of dimensions ($k\times m$) and ($k\times n$), respectively with $n\ge k\ge m$, $\mathbf{x}$ is the vector of unknowns, $\boldsymbol{\varepsilon}$ is a stochastic residual vector, $\mathbf{w}$ is the vector of misclosures, $\mathbf{Q}$ is the covariance matrix of observations and $E\left\{\cdot\right\}$ stands for the statistical expectation. We assume that the variance-covariance matrix model is

$$\mathbf{Q}=\sum_{i=1}^{q}\sigma_i^2\mathbf{Q}_i \tag{6.2}$$

where $\mathbf{Q}_i$ are known positive semi-definite sub-matrices of $\mathbf{Q}$, and σ_i^2 are the unknown VCs. The above equation can easily be converted to the condition model as (Sjöberg 1984c)

$$(\mathbf{I}-\mathbf{A}^{0})\mathbf{B}\boldsymbol{\varepsilon}=(\mathbf{I}-\mathbf{A}^{0})\mathbf{w}\text{, or }\bar{\mathbf{B}}\boldsymbol{\varepsilon}=\bar{\mathbf{w}}\text{,} \tag{6.3}$$

where, $\mathbf{A}^{0}=\mathbf{A}\mathbf{A}^{-}=\mathbf{A}\left(\mathbf{A}^{\mathrm{T}}\mathbf{C}^{-}\mathbf{A}\right)^{-}\mathbf{A}^{\mathrm{T}}\mathbf{C}^{-}$. Hence, $\mathbf{A}^{-}$ stands for a specific generalized inverse of $\mathbf{A}$, namely $\mathbf{A}^{-}=\mathbf{A}\left(\mathbf{A}^{\mathrm{T}}\mathbf{C}^{-}\mathbf{A}\right)^{-}\mathbf{A}^{\mathrm{T}}\mathbf{C}^{-}$, where

$$\mathbf{C}=\sum_{i=1}^{q}\sigma_i^2\mathbf{C}_i\ \text{ and }\ \mathbf{C}_i=\mathbf{B}\mathbf{Q}_i\mathbf{B}^{T}\ ,\quad (\text{rank}(\mathbf{C})=k) \tag{6.4}$$

Alternatively, we obtain the condition model by designing **A**=0 in Eq. (6.1). (This implies also that **B** will be different.) Similarly, the method of adjustment by elements (or Gauss-Markov model) is obtained by selecting **B=I** and **w=L** in Eq. (6.1), where **L** is the vector of observations.

6.3 The BQUE of a VC

Now, suppose that we want to estimate a linear combination $\mathbf{p}^T\boldsymbol{\sigma} = \sum_{i=1}^{q} p_i \sigma_i^2$ of the VCs related with Eq. (6.1), where p_i are arbitrary coefficients. A sufficient condition for unbiasedness of the estimator $\bar{\mathbf{w}}^T\mathbf{M}\bar{\mathbf{w}}$ of $\mathbf{p}^T\boldsymbol{\sigma}$ is that (Rao 1971; Sjöberg 1983, Rao and Kleffe 1988)

$$p_i = \text{trace}(\mathbf{M}\mathbf{K}_i), \tag{6.5a}$$

where

$$\mathbf{K}_i = \left(\mathbf{I} - \mathbf{A}^0\right)\mathbf{C}_i\left(\mathbf{I} - \mathbf{A}^0\right)^T, \tag{6.5b}$$

and, in case of normally distributed observation errors, the BQUE, and, in the general case, the MInimum Norm Quadratic Unbiased Estimator of $\mathbf{p}^T\boldsymbol{\sigma}$ is provided by $\mathbf{p}^T\mathbf{S}^-\mathbf{u}$, where $\mathbf{S}^-$ is any generalized inverse of *S* and (Sjöberg 1984c)

$$s_{ij} = \text{trace}\left(\mathbf{R}\mathbf{C}_i\mathbf{R}\mathbf{C}_j\right) \qquad ;i, j=1, 2,\ldots, q \tag{6.6a}$$

$$u_i = \bar{\mathbf{w}}^T\mathbf{R}\mathbf{C}_i\mathbf{R}\bar{\mathbf{w}} \qquad ; \qquad i=1, 2,\ldots, q \tag{6.6b}$$

$$\mathbf{R} = \mathbf{C}^{-1}\left(\mathbf{I} - \mathbf{A}^0\right) = \left(\mathbf{I} - \mathbf{A}^0\right)^T\mathbf{C}^{-1}. \tag{6.6c}$$

6.4 The BQUNE of a VC

Suppose that $\bar{\mathbf{w}}^T\mathbf{M}\bar{\mathbf{w}}$, where **M** is a symmetric matrix, is an unbiased estimator of $\mathbf{p}^T\boldsymbol{\sigma}$. The estimator is not necessarily positive, but if we restrict **M** to the class of matrices $\mathbf{M} = \mathbf{G}\mathbf{G}^T$, where **G** is an arbitrary matrix of compatible dimensions, the quadratic form of $\bar{\mathbf{w}}^T\mathbf{M}\bar{\mathbf{w}}$ will be non-negative. A sufficient condition for the estimator to be unbiased in this case is (Sjöberg 1984c)

$$p_i = \text{trace}\left\{\mathbf{G}^T\left(\mathbf{I} - \mathbf{A}^0\right)\mathbf{C}_i\left(\mathbf{I} - \mathbf{A}^0\right)^T\mathbf{G}\right\}. \tag{6.7}$$

As pointed out by LaMotte (1973) unbiased, non-negative estimators satisfying this relation exist only in special cases. We will restrict the discussion to the unbiased estimation of individual VCs. First we transform $\bar{\mathbf{w}}$ into

$$\boldsymbol{\gamma}_i = \mathbf{F}_i\bar{\mathbf{w}}, \tag{6.8}$$

where we have chosen the projection $\mathbf{F}_i$ as

$$\mathbf{F}_i = \mathbf{I} - \mathbf{C}_{0i}\mathbf{C}_{0i}^{-} \text{ and } \mathbf{C}_{0i} = \mathbf{C} - \sigma_i^2\mathbf{C}_i\,, \tag{6.9a}$$

with

$$\mathbf{C} = \bar{\mathbf{B}}\mathbf{Q}\bar{\mathbf{B}}^T \text{ and } \mathbf{C}_i = \bar{\mathbf{B}}\mathbf{Q}_i\bar{\mathbf{B}}^T\,. \tag{6.9b}$$

Let us introduce $\mathbf{P}_i = \mathbf{F}_i\mathbf{C}_i\left(\mathbf{I} - \mathbf{A}^0\right)^T\mathbf{F}_i$. It can be shown (Sjöberg 1984c) that for $\mathbf{HP}_i \neq 0$ the quadratic form

$$\tilde{\sigma}_i^2 = \boldsymbol{\gamma}_i^T\mathbf{H}\boldsymbol{\gamma}_i \,/\, \text{trace}(\mathbf{HP}_i) \tag{6.10}$$

is a general quadratic unbiased non-negative estimator of σ_i^2 for any non-negative definite matrix $\mathbf{H}$, and for normally distributed observations the variance of $\tilde{\sigma}_i^2$ is given by

$$\text{Var}\left\{\tilde{\sigma}_i^2\right\} = 2\sigma_i^4\text{trace}(\mathbf{HP}_i\mathbf{HP}_i) \,/\, \left\{\text{trace}(\mathbf{HP}_i)\right\}^2\,. \tag{6.11}$$

where σ_i^2 is the true VC (see Eshagh and Sjöberg 2008 for a proof). Sjöberg (1984c) proved that the following estimator is the BQUNE (in the sense of having the smallest variance) among all candidates of Eq. (6.10):

$$\hat{\sigma}_i^2 = \boldsymbol{\gamma}_i^T\mathbf{P}_i^{-}\boldsymbol{\gamma}_i \,/\, \text{rank}(\mathbf{P}_i)\,, \tag{6.12}$$

where $\mathbf{P}_i^{-}$ is any generalized inverse of $\mathbf{P}_i$.

6.5 The MBQUNE of a VC

We will now introduce the MBQUNE. In the Gauss-Markov model of adjustment the MBQUNE and BQUNE are the same. The difference only appears in the condition adjustment and Gauss-Helmert models. As we saw in Eq. (6.1), the Gauss-Helmert model can be converted to the condition adjustment model. However, in these cases $\mathbf{C}_{0i}$ of Eq. (6.9a) is frequently regular, implying that $\mathbf{F}_i$ = 0, and the BQUNE will not exist, but so will MBQUNE, as we will show. Hence, this is the main and important difference between the two estimators. This method was proposed by Eshagh and Sjöberg (2008b) and implemented by Kiamehr and Eshagh (2008) in order to combine the geometric and gravimetric geoid models in Iran. It should be mentioned that $\mathbf{F}_i$ = 0 occurs when we want to combine the solutions of a GBVPs too and this is why we have to consider the MBQUNE for estimating the VCs in our solution.

When deriving the BQUNE, $\boldsymbol{\gamma}_i$ of Eq. (6.8) was set to $\mathbf{F}_i\bar{\mathbf{w}}$, but, as stated above, $\mathbf{F}_i$ vanishes for a regular $\mathbf{C}_{0i}$. In deriving the MBQUNE we define

$$\boldsymbol{\gamma}_i = \mathbf{F}_i\hat{\boldsymbol{\varepsilon}}, \tag{6.13}$$

where $\mathbf{F}_i = \mathbf{I} - \mathbf{Q}_{0i}\mathbf{Q}_{0i}^{-}$ and $\mathbf{Q}_{0i} = \mathbf{Q} - \sigma_i^2\mathbf{Q}_i$, also $\hat{\varepsilon}$ is the minimum norm solution to the matrix system $\bar{\mathbf{B}}\boldsymbol{\varepsilon} = \bar{\mathbf{w}}$, i.e.

$$\hat{\boldsymbol{\varepsilon}} = \mathbf{Q}\bar{\mathbf{B}}^T\mathbf{C}^{-}\bar{\mathbf{w}}. \tag{6.14}$$

This residual vector is thus related to $\boldsymbol{\gamma}_i$ by the equation

$$\boldsymbol{\gamma}_i = \mathbf{F}_i\mathbf{Q}\bar{\mathbf{B}}^T\mathbf{C}^{-}\bar{\mathbf{w}} = \mathbf{F}_i\hat{\boldsymbol{\varepsilon}}. \tag{6.15}$$

In this case, $\mathbf{F}_i$ is defined as it is used in the Gauss-Markov model. Based on normally distribution observations with zero expectation of errors, this holds also for $\boldsymbol{\gamma}_i$, yielding (Eshagh and Sjöberg 2008b):

$$\tilde{\mathbf{P}}_i = \mathbf{F}_i\mathbf{Q}\bar{\mathbf{B}}^T\mathbf{C}^{-}\bar{\mathbf{B}}\mathbf{Q}\mathbf{F}_i. \tag{6.16}$$

Here $\mathbf{F}_i$ separates the residuals (and produces a matrix $\tilde{\mathbf{P}}_i$, that plays the role of a variance-covariance matrix for the i-th group) for each group of observations.

6.6 Optimal combination of integral solution of GBVPs

The gravitational tensor has five impendent elements, which are measured at satellite level. By using combinations of these observables one can obtain three sets of geopotential coefficients. The main reason of obtaining different solutions could be due to discretization error of the integrals and noise in real data. In practice, one cannot obtain the same solutions by these integrals. Usually, the least-squares approach is used to compute an EGM and five independent elements of the gravitational tensor will increase the redundancy in the solution. As was mentioned in the previous chapter, noise is amplified in the inversion process therefore over-determination should be beneficial. However, this chapter emphasizes on the integral formulas, which are solutions of the GBVPs, to determine the geopotential coefficients. Such solutions are not optimal but we want to obtain an optimal solution by combining them. At the first step, the simple and weighted means are studied and after that a condition model is constructed so that VCE can be used to re-weight the observation.

6.6.1 Simple mean versus weighted mean

Rummel et al. (1993) and Gelderen and Rummel (2001) and (2002) investigated the least-squares solutions of the VV, VH and HH GBVPs. However, the simple and weighted mean can be two simple combinations for the integral solutions.

In order to test the simple and weighted mean, equivalent errors is considered for all types of the SGG data, namely $\sigma_{\mathbf{t}_{zz}} = \sigma_{\mathbf{t}_{xz}} = \sigma_{\mathbf{t}_{yz}} = \sigma_{\mathbf{t}_{xx}} = \sigma_{\mathbf{t}_{yy}} = \sigma_{\mathbf{t}_{xy}} = 0.01\,\mathrm{E}$ as well as $30' \times 30'$ resolution for the data at 250 km level. The EGM96 is used to synthesize the data at satellite level and analyze the gravitational field using descretized integrals of Eqs. (2.67a)-(2.67c). Also the EGM96 is supposed as the true solution in this investigation. The degree of resolution for the grid of the SGG data with $30' \times 30'$ resolution at 250 km level is about 198, 199 and 230 for HH, VH and VV solutions, respectively. Figure 6.1a and 6.1b show the combinations based on the simple and weighted mean of the solutions of the GBVPs (VV, VH and HH solutions).

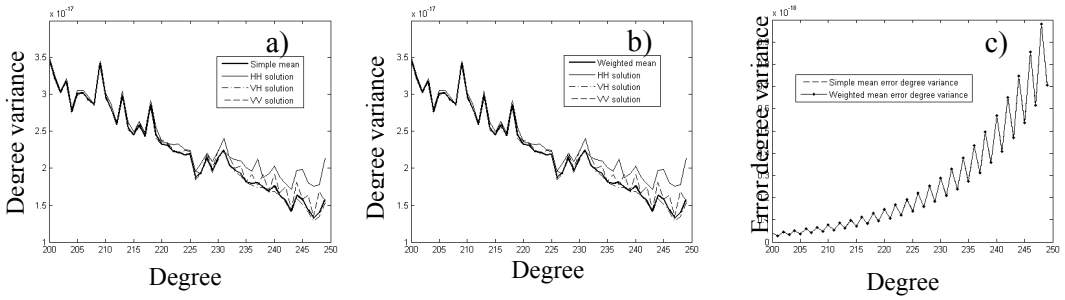

Figure 6.1. (a) Simple mean, (b) weighted mean, (c) error degree variance of simple and weighted mean

As can be seen, both solutions yield more or less the same results. Their spectral differences are visualized in Figure 6.1c. Even the error degree variances of these solutions are more or less the same and this is natural in the presence of the same noise for all SGG data. In the following another way of the combination of the GBVPs is presented. We want to use VCE, as a weighting scheme for the observations, to update the observation weights and obtain an optimal solution. The simple and weighted mean are not suitable tools in this respect, therefore we construct condition equations for the discrete integrals in such a way that we can take advantage of the VCE. In the following subsection, the adjustment of condition model is briefly reviewed.

6.6.2 Adjustment by condition model

The condition adjustment model is:

$$\mathbf{B}\left(\mathbf{L}-\boldsymbol{\varepsilon}\right)=\mathbf{w}=\mathbf{c}'-\mathbf{B}\mathbf{L} \quad \text{and} \quad E\left\{\boldsymbol{\varepsilon}\boldsymbol{\varepsilon}^{T}\right\}=\sigma_0^2\mathbf{Q}\ , \tag{6.17}$$

where $\mathbf{B}$ is the coefficient matrix of observations, $\boldsymbol{\varepsilon}$ stands for the vector of observation noise and $\mathbf{w}$ is the misclosure vector, $\mathbf{Q}$ is the variance-covariance matrix of the observations, $\mathbf{c}'$ is the constant vector of the condition model, $\mathbf{L}$ is the observation vector and, finally, σ_0^2 is the a-priori variance factor. The least-squares solution of the above model will be:

$$\hat{\boldsymbol{\varepsilon}} = \mathbf{B}_{\mathbf{QO}}^{-}\mathbf{w} \ , \tag{6.18}$$

where $\mathbf{B}_{\mathbf{QO}}^{-} = \mathbf{Q}\mathbf{B}^T\left(\mathbf{B}\mathbf{Q}\mathbf{B}^T\right)^{-}$ is a left (normal) inverse of the matrix $\mathbf{B}$; and minus sign superscripted over the parenthesis stands for generalized inverse (Bjerhammar 1973).

Considering Eqs. (2.67a)-(2.67c), two independent condition models can be constructed:

$$\mathbf{B}^{nm}\left(\mathbf{l}-\boldsymbol{\varepsilon}\right) = 0 \, , \tag{6.19}$$

where

$$\mathbf{L} = \begin{bmatrix} \mathbf{t}_{zz} & \mathbf{t}_{xx} & \mathbf{t}_{yy} & \mathbf{t}_{xy} & \mathbf{t}_{xz} & \mathbf{t}_{yz} \end{bmatrix}^T \tag{6.20a}$$

and

$$\mathbf{B}^{nm} = \begin{bmatrix} \mathbf{b}_{zz}^{nm} & -\mathbf{b}_{xx}^{nm} & -\mathbf{b}_{yy}^{nm} & -\mathbf{b}_{xy}^{nm} & 0 & 0 \\ \mathbf{b}_{zz}^{nm} & 0 & 0 & 0 & -\mathbf{b}_{xz}^{nm} & -\mathbf{b}_{yz}^{nm} \end{bmatrix} . \tag{6.20b}$$

Also if we assume that the observations are not correlated, we will have a block-diagonal variance-covariance matrix:

$$\mathbf{Q} = \mathrm{diag}\begin{bmatrix} \mathbf{Q}_{zz} & \mathbf{Q}_{xx} & \mathbf{Q}_{yy} & \mathbf{Q}_{xy} & \mathbf{Q}_{xz} & \mathbf{Q}_{yz} \end{bmatrix}, \tag{6.20c}$$

where $\mathbf{Q}_{zz}$, $\mathbf{Q}_{xx}$, $\mathbf{Q}_{yy}$, $\mathbf{Q}_{xy}$, $\mathbf{Q}_{xz}$ and $\mathbf{Q}_{yz}$ are the co-factor matrices of $\mathbf{t}_{zz}$, $\mathbf{t}_{xx}$, $\mathbf{t}_{yy}$, $\mathbf{t}_{xy}$, $\mathbf{t}_{xz}$ and $\mathbf{t}_{yz}$, respectively, and $\mathbf{C}^{nm} = \mathbf{B}^{nm}\mathbf{Q}\left(\mathbf{B}^{nm}\right)^T$. Superscripts n and m mean that the element changes by degree n and order m. The number of rows of $\mathbf{B}^{nm}$ is always equal to 2, but the number of columns depends on the resolution of the analysis and descretized integrals. Subsequently, $\mathbf{C}^{nm}$ is a 2 by 2 matrix independent on the SGG data with elements:

$$c_{11}^{nm} = \mathbf{b}_{zz}^{nm}\mathbf{Q}_{zz}\left(\mathbf{b}_{zz}^{nm}\right)^T + \mathbf{b}_{xx}^{nm}\mathbf{Q}_{xx}\left(\mathbf{b}_{xx}^{nm}\right)^T + \mathbf{b}_{yy}^{nm}\mathbf{Q}_{yy}\left(\mathbf{b}_{yy}^{n,m}\right)^T + \mathbf{b}_{xy}^{nm}\mathbf{Q}_{xy}\left(\mathbf{b}_{xy}^{nm}\right)^T \tag{6.21a}$$

$$c_{22}^{nm} = \mathbf{b}_{zz}^{nm}\mathbf{Q}_{zz}\left(\mathbf{b}_{zz}^{nm}\right)^T + \mathbf{b}_{xz}^{nm}\mathbf{Q}_{xz}\left(\mathbf{b}_{xz}^{nm}\right)^T + \mathbf{b}_{yz}^{nm}\mathbf{Q}_{yz}\left(\mathbf{b}_{yz}^{nm}\right)^T \tag{6.21b}$$

and

$$c_{21}^{nm} = c_{12}^{nm} = \mathbf{b}_{zz}^{nm}\mathbf{Q}_{zz}\left(\mathbf{b}_{zz}^{nm}\right)^{T}. \tag{6.21c}$$

Similarly, the misclosure vector is a 1 by 2 vector with elements:

$$\mathbf{w} = \begin{bmatrix} w_{1}^{nm} \\ w_{2}^{nm} \end{bmatrix} = \begin{bmatrix} -\left(\mathbf{b}_{zz}^{nm}\right)^{T}\mathbf{t}_{zz} + \left(\mathbf{b}_{xx}^{nm}\right)^{T}\mathbf{t}_{xx} + \left(\mathbf{b}_{yy}^{nm}\right)^{T}\mathbf{t}_{yy} + \left(\mathbf{b}_{xy}^{nm}\right)^{T}\mathbf{t}_{xy} \\ -\left(\mathbf{b}_{zz}^{nm}\right)^{T}\mathbf{t}_{zz} + \left(\mathbf{b}_{xz}^{nm}\right)^{T}\mathbf{t}_{xz} + \left(\mathbf{b}_{yz}^{nm}\right)^{T}\mathbf{t}_{yz} \end{bmatrix}. \tag{6.22}$$

Substituting Eqs. (6.21a)-(6.21c) and (6.22) into Eq. (6.18) and after further simplification, the explicit adjusted error vector is obtained:

$$\begin{bmatrix} \hat{\boldsymbol{\varepsilon}}_{zz}^{nm} \\ \hat{\boldsymbol{\varepsilon}}_{xx}^{nm} \\ \hat{\boldsymbol{\varepsilon}}_{yy}^{nm} \\ \hat{\boldsymbol{\varepsilon}}_{xy}^{nm} \\ \hat{\boldsymbol{\varepsilon}}_{xz}^{nm} \\ \hat{\boldsymbol{\varepsilon}}_{yz}^{nm} \end{bmatrix} = \frac{1}{\left|\mathbf{C}^{nm}\right|} \begin{bmatrix} \mathbf{Q}_{zz}\left(\mathbf{b}_{zz}^{nm}\right)^{T}\left(c_{22}^{nm}w_{1}^{nm} - c_{12}^{nm}w_{2}^{nm}\right) + \mathbf{Q}_{zz}\left(\mathbf{b}_{zz}^{nm}\right)^{T}\left(c_{11}^{nm}w_{2}^{nm} - c_{21}^{nm}w_{1}^{nm}\right) \\ -\mathbf{Q}_{xx}\left(\mathbf{b}_{xx}^{nm}\right)^{T}\left(c_{22}^{nm}w_{1}^{nm} - c_{12}^{nm}w_{2}^{nm}\right) \\ -\mathbf{Q}_{yy}\left(\mathbf{b}_{yy}^{nm}\right)^{T}\left(c_{22}^{nm}w_{1}^{nm} - c_{12}^{nm}w_{2}^{nm}\right) \\ -\mathbf{Q}_{xy}\left(\mathbf{b}_{xy}^{nm}\right)^{T}\left(c_{22}^{nm}w_{1}^{nm} - c_{12}^{nm}w_{2}^{nm}\right) \\ -\mathbf{Q}_{xz}\left(\mathbf{b}_{xz}^{nm}\right)^{T}\left(c_{11}^{nm}w_{2}^{nm} - c_{21}^{nm}w_{1}^{nm}\right) \\ -\mathbf{Q}_{yz}\left(\mathbf{b}_{yz}^{nm}\right)^{T}\left(c_{11}^{nm}w_{2}^{nm} - c_{21}^{nm}w_{1}^{nm}\right) \end{bmatrix} \tag{6.23}$$

where $\left|\cdot\right|$ is the determinant operation.

In the adjustment with condition models, the residual vector is estimated and subtracted from the observations. The results will be the adjusted observations; see E.q (6.24a). In such a case, one can use one condition equation to obtain the unknown parameters. In the case of GBVPs, it does not matter which integral is used to compute the coefficients, one can use the simplest integral, or in other words, the VV solution of the GBVPs (Eq. 2.67a is preferred)

$$\hat{\mathbf{L}} = \mathbf{L} - \hat{\boldsymbol{\varepsilon}}. \tag{6.24a}$$

By using the well-known error propagation laws, the variance-covariance matrix of the corrected observations can be estimated:

$$\mathbf{Q}_{\hat{\mathbf{L}}} = \mathbf{Q}_{\mathbf{L}} + \mathbf{Q}_{\hat{\boldsymbol{\varepsilon}}} = \mathbf{b}^{nm}\mathbf{Q}\left(\mathbf{b}^{nm}\right)^{T} + \mathbf{Q}\left(\mathbf{b}^{nm}\right)^{T}\left[\mathbf{b}^{nm}\mathbf{Q}\left(\mathbf{b}^{nm}\right)^{T}\right]^{-}\mathbf{b}^{nm}\mathbf{Q}. \tag{6.24b}$$

where, $\mathbf{Q}_{\mathbf{L}}$ is the variance-covariance matrix of the observations and $\mathbf{Q}_{\hat{\boldsymbol{\varepsilon}}}$ is for the estimated residuals (the corrections).

Figure 6.2 shows the condition adjustment solution of three GBVPs.

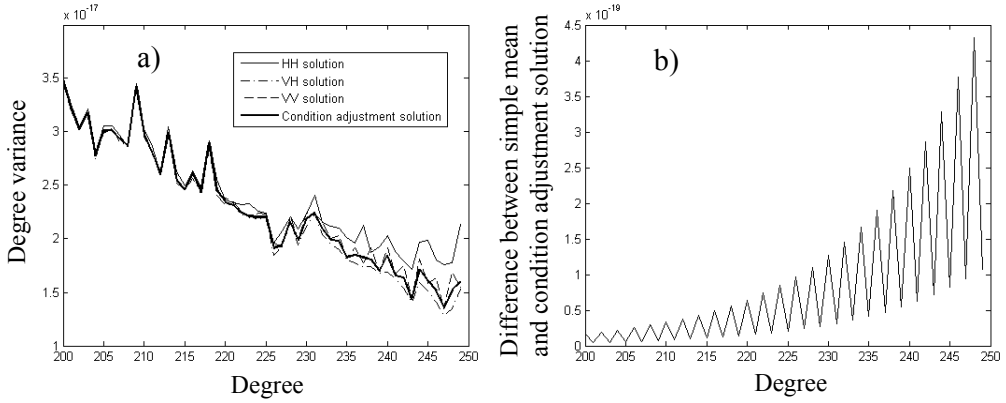

Figure 6.2 (a) Condition adjustment solution. (b) Difference between condition adjustment solution and simple mean

Comparing this figure with Figure 6.1a and 6.1b we can say that the solutions are very similar as expected. The differences between the two solutions are provided in Figure 6.2b. The differences are very small compared to the signal itself (see Fig. 6.2a) and in the order of the numerical error. The question is: why should the complicated solution of the condition model be used, while the simple mean practically provides the same results and it is extremely simple? The idea is not just to use the condition model in combination, but we are seeking a way to re-weight the observations to get better solution. The condition model provides this by considering the VCE technique. In the following section the concept of the VCE is briefly reviewed and expressed how to use the VCE in spectral combination of the GBVPs solutions.

6.6.3 VCE and re-weighting solution

As mentioned in the previous subsection, the idea of constructing the condition models is to use VCE to update the observation weights and obtain an optimal solution. Each condition equation has a misclosure vector which can be used to determine the VCs (according to a pre-described stochastic model for the observations error). The observation weights are re-scaled in order to get better match between the residuals and misclosures. In the following sections the well-known methods of the VCE, namely the BQUE and BQUNE (Sjöberg 1984c) and the MBQUNE (Eshagh and Sjöberg, 2008) are presented. The discussion is continued by the Gauss-Helmert model, which is more general than the condition and the Gauss-Markov models and after that we come to the special case of the condition adjustment. The degree-order VCs (DOVC) as a VC which is estimated according to the stochastic model and the degree and order of solution is defined.

Proposition 6.1 *The BQUE of DOVC based on Eq. (6.19) and stochastic model 1*

$$\mathbf{Q} = \sigma_{\mathrm{VV}}^2 \mathbf{Q}'_{\mathrm{VV}} + \sigma_{\mathrm{HH}}^2 \mathbf{Q}'_{\mathrm{HH}} + \sigma_{\mathrm{HV}}^2 \mathbf{Q}'_{\mathrm{VH}} \quad \textit{(stochastic model 1)}$$

where

$$\mathbf{Q}'_{\mathrm{VV}} = \mathrm{diag}\begin{pmatrix}\mathbf{Q}_{zz} & 0 & 0 & 0 & 0 & 0\end{pmatrix}$$
$$\mathbf{Q}'_{\mathrm{HH}} = \mathrm{diag}\begin{pmatrix}0 & \mathbf{Q}_{xx} & \mathbf{Q}_{yy} & \mathbf{Q}_{zz} & 0 & 0\end{pmatrix}$$
$$\mathbf{Q}'_{\mathrm{VH}} = \mathrm{diag}\begin{pmatrix}0 & 0 & 0 & 0 & \mathbf{Q}_{xz} & \mathbf{Q}_{yz}\end{pmatrix}$$

is (Eshagh 2009f):

$$\left(\hat{\sigma}_j^2\right)^{nm} = \frac{\left[\left(w_1^{nm}\right)^2 + \left(w_2^{nm}\right)^2\right]\left[\left(c_{22}^{nm}\right)^2 + \left(c_{12}^{nm}\right)^2\right] - 2w_1^{nm} w_2^{nm}\left(c_{22}^{nm} + c_{11}^{nm}\right)c_{12}^{nm}}{k_j^{nm}\left[\left(c_{22}^{nm}\right)^2 + 2\left(c_{12}^{nm}\right)^2 + \left(c_{11}^{nm}\right)^2\right]}.$$

Proof. The VCs are determined by $\mathbf{p}^T \mathbf{S}^{-}\mathbf{u}$, the elements of the coefficients matrix $\mathbf{S}$ are:

$$s_{ij} = \mathrm{trace}\left[\left(\mathbf{K}^{nm}\right)^{-1}\mathbf{K}_i^{nm}\left(\mathbf{K}^{nm}\right)^{-1}\mathbf{K}_j^{nm}\right] \tag{6.25}$$

and the right-hand side vector elements are:

$$u_i = \left(\mathbf{w}^{nm}\right)^T\left(\mathbf{K}^{nm}\right)^{-1}k_i^{nm}\left(\mathbf{K}^{nm}\right)^{-1}\mathbf{w}^{nm}, \tag{6.26}$$

where

$$k_{\mathrm{VV}}^{nm} = \mathbf{b}_{zz}^{nm}\mathbf{Q}_{zz}\left(\mathbf{b}_{zz}^{nm}\right)^T, \tag{6.27}$$

$$k_{\mathrm{HH}}^{nm} = \mathbf{b}_{xx}^{nm}\mathbf{Q}_{xx}\left(\mathbf{b}_{xx}^{nm}\right)^T + \mathbf{b}_{yy}^{nm}\mathbf{Q}_{yy}\left(\mathbf{b}_{yy}^{nm}\right)^T + \mathbf{b}_{xy}^{nm}\mathbf{Q}_{xy}\left(\mathbf{b}_{xy}^{nm}\right)^T, \tag{6.28}$$

and

$$k_{\mathrm{VH}}^{nm} = \mathbf{b}_{xz}^{nm}\mathbf{Q}_{xz}\left(\mathbf{b}_{xz}^{nm}\right)^T + \mathbf{b}_{yz}^{nm}\mathbf{Q}_{yz}\left(\mathbf{b}_{yz}^{nm}\right)^T. \tag{6.29}$$

Substituting Eqs. (6.27)-(6.29) into Eq. (6.25) we have

$$s_{ij} = \frac{k_i^{nm}k_j^{nm}\left[\left(c_{22}^{nm}\right)^2 + 2\left(c_{12}^{nm}\right)^2 + \left(c_{11}^{nm}\right)^2\right]}{\left|\mathbf{C}^{nm}\right|^2}. \tag{6.30}$$

Also by substituting Eqs. (6.27a)-(6.29c) into Eq. (6.26) we obtain

$$u_i = \frac{k_i^{nm}}{\left|\mathbf{C}^{nm}\right|^2}\left\{\left(w_1^{nm}\right)^2\left[\left(c_{22}^{nm}\right)^2+\left(c_{12}^{nm}\right)^2\right]-2w_1^{nm}w_2^{nm}c_{21}^{nm}\left(c_{22}^{nm}+c_{11}^{nm}\right)+\left(w_2^{nm}\right)^2\left[\left(c_{11}^{nm}\right)^2+\left(c_{12}^{nm}\right)^2\right]\right\} \tag{6.31}$$

By inserting Eq. (6.31) and Eq. (6.30) into $\mathbf{p}^T\mathbf{S}^{-}\mathbf{u}$ and after simplification the proposition is proven.

The DOVCs of the gravitational gradients can easily be estimated using Proposition 6.1 based on stochastic model 1. As the proposition shows the numerator of this estimator is independent of the form of the stochastic model. The only parameter which depends on the stochastic model is k_j corresponding to each $\left(\hat{\sigma}_j^2\right)^{nm}$ (DOVC). In this combination approach for estimating each geopotential coefficient with degree *n* and order *m*, three DOVCs are estimated which differ by degrees and orders.

According to Proposition 6.1 the denominator of the proposition is always positive as it is a quadratic form. Here, the only possible way of the DOVC to come out negative is to have negative numerator. The first term of the numerator is always positive too, thus the following condition can be written to get negative DOVCs:

$$\frac{\left[\left(w_1^{nm}\right)^2+\left(w_2^{nm}\right)^2\right]\left[\left(c_{22}^{nm}\right)^2+\left(c_{12}^{nm}\right)^2\right]}{2\left(c_{22}^{nm}+c_{11}^{nm}\right)c_{12}^{nm}} < w_1^{nm}w_2^{nm} \tag{6.32}$$

The left hand side of this inequality is always positive but the right hand side will be positive if either $w_1, w_2 < 0$ or $w_1, w_2 > 0$. The problem is when the positive value $w_1 w_2$ is larger than the left hand side of Eq. (6.32), we will get negative DOVCs. In the case where w_1 and w_2 have opposite signs we will also get positive DOVCs as this negative number is always smaller than the positive number in left hand side.

Corollary 2.1 *The BQUE of DOVCs based on Eq. (6.19) and stochastic model 2*

$$\mathbf{Q} = \sigma_{zz}^2\mathbf{Q}'_{zz} + \sigma_{xx}^2\mathbf{Q}'_{xx} + \sigma_{yy}^2\mathbf{Q}'_{yy} + \sigma_{xy}^2\mathbf{Q}'_{xy} + \sigma_{xz}^2\mathbf{Q}'_{xz} + \sigma_{yz}^2\mathbf{Q}'_{yz}$$

(stochastic model 2)

where

$$\begin{aligned}
\mathbf{Q}'_{zz} &= \mathrm{diag}\left(\mathbf{Q}_{zz} \quad 0 \quad 0 \quad 0 \quad 0 \quad 0\right)\\
\mathbf{Q}'_{xx} &= \mathrm{diag}\left(0 \quad \mathbf{Q}_{xx} \quad 0 \quad 0 \quad 0 \quad 0\right)\\
\mathbf{Q}'_{yy} &= \mathrm{diag}\left(0 \quad 0 \quad \mathbf{Q}_{yy} \quad 0 \quad 0 \quad 0\right)\\
\mathbf{Q}'_{xy} &= \mathrm{diag}\left(0 \quad 0 \quad 0 \quad \mathbf{Q}_{xy} \quad 0 \quad 0\right)\\
\mathbf{Q}'_{xz} &= \mathrm{diag}\left(0 \quad 0 \quad 0 \quad 0 \quad \mathbf{Q}_{xz} \quad 0\right)\\
\mathbf{Q}'_{yz} &= \mathrm{diag}\left(0 \quad 0 \quad 0 \quad 0 \quad 0 \quad \mathbf{Q}_{yz}\right)
\end{aligned}$$

is the same as in Proposition 6.1.

Proof. The corollary follows as the only parameter depending on the stochastic model is k_j^{nm} and the estimator presented in Proposition 6.1 does not change by the stochastic model.

Proposition 6.2 *The MBQUNE of DOVCs in the condition model based on stochastic model 1 for VV solution is:*

$$\left(\hat{\sigma}_{VV}^2\right)^{nm} = \left(\hat{\sigma}_{zz}^2\right)^{nm} = \frac{\left(c_{22}^{nm} - 2c_{12}^{nm} + c_{11}^{nm}\right)\left(\hat{\boldsymbol{\varepsilon}}_{zz}^{nm}\right)^T \left(\mathbf{Q}_{zz}\left(\mathbf{b}_{zz}^{nm}\right)^T \mathbf{b}_{zz}^{nm}\mathbf{Q}_{zz}\right)^{-} \hat{\boldsymbol{\varepsilon}}_{zz}^{nm}}{\left|\mathbf{C}^{nm}\right| \operatorname{rank}\left(\mathbf{Q}_{zz}\left(\mathbf{b}_{zz}^{nm}\right)^T \mathbf{b}_{zz}^{nm}\mathbf{Q}_{zz}\right)}, \quad \left|\mathbf{C}^{nm}\right| \neq 0.$$

Proof. Proof of this proposition will be presented with the proof of the next proposition, because of having very similar structure.

Proposition 6.3 *The MBQUNE of DOVCs based on stochastic model 1 for HH and VH solution is (Eshagh 2009f):*

$$\left(\hat{\sigma}_i^2\right)^{nm} = \frac{c_{k'k'}^{nm}\left(\hat{\boldsymbol{\varepsilon}}_i^{nm}\right)^T \left(\mathbf{P}_i^{nm}\right)^{-} \hat{\boldsymbol{\varepsilon}}_i^{nm}}{\left|\mathbf{C}^{nm}\right| \operatorname{rank}\left(\mathbf{P}_i^{nm}\right)} \quad where\ i = \begin{cases} HH & k'=2 \\ VH & k'=1 \end{cases} \ and\ \left|\mathbf{C}^{nm}\right| \neq 0$$

where $\left(\hat{\boldsymbol{\varepsilon}}_{HH}^{nm}\right)^T = \left[\hat{\boldsymbol{\varepsilon}}_{xx}^{nm} \quad \hat{\boldsymbol{\varepsilon}}_{yy}^{nm} \quad \hat{\boldsymbol{\varepsilon}}_{xy}^{nm}\right]^T$, $\left(\hat{\boldsymbol{\varepsilon}}_{VH}^{nm}\right)^T = \left[\hat{\boldsymbol{\varepsilon}}_{xz}^{nm} \quad \hat{\boldsymbol{\varepsilon}}_{yz}^{nm}\right]^T$,

$$\mathbf{P}_{HH}^{nm} = \begin{bmatrix} \mathbf{Q}_{xx}\left(\mathbf{b}_{xx}^{nm}\right)^T \mathbf{b}_{xx}^{nm}\mathbf{Q}_{xx} & \mathbf{Q}_{xx}\left(\mathbf{b}_{xx}^{nm}\right)^T \mathbf{b}_{yy}^{nm}\mathbf{Q}_{yy} & \mathbf{Q}_{xx}\left(\mathbf{b}_{xx}^{nm}\right)^T \mathbf{b}_{xy}^{nm}\mathbf{Q}_{xy} \\ \mathbf{Q}_{yy}\left(\mathbf{b}_{yy}^{nm}\right)^T \mathbf{b}_{xx}^{nm}\mathbf{Q}_{xx} & \mathbf{Q}_{yy}\left(\mathbf{b}_{yy}^{nm}\right)^T \mathbf{b}_{yy}^{nm}\mathbf{Q}_{yy} & \mathbf{Q}_{yy}\left(\mathbf{b}_{yy}^{nm}\right)^T \mathbf{b}_{xy}\mathbf{Q}_{xy} \\ \mathbf{Q}_{xy}\left(\mathbf{b}_{xy}^{nm}\right)^T \mathbf{b}_{xx}^{nm}\mathbf{Q}_{xx} & \mathbf{Q}_{xy}\left(\mathbf{b}_{xy}^{nm}\right)^T \mathbf{b}_{yy}^{nm}\mathbf{Q}_{yy} & \mathbf{Q}_{xy}\left(\mathbf{b}_{xy}^{nm}\right)^T \mathbf{b}_{xy}\mathbf{Q}_{xy} \end{bmatrix}$$

and

$$\mathbf{P}_{VH}^{nm} = \begin{bmatrix} \mathbf{Q}_{xz}\left(\mathbf{b}_{xz}^{nm}\right)^T \mathbf{b}_{xz}^{nm}\mathbf{Q}_{xz} & \mathbf{Q}_{xz}\left(\mathbf{b}_{xz}^{nm}\right)^T \mathbf{b}_{yz}^{nm}\mathbf{Q}_{yz} \\ \mathbf{Q}_{yz}\left(\mathbf{b}_{yz}^{nm}\right)^T \mathbf{b}_{xz}^{nm}\mathbf{Q}_{xz} & \mathbf{Q}_{yz}\left(\mathbf{b}_{yz}^{nm}\right)^T \mathbf{b}_{yz}^{nm}\mathbf{Q}_{yz} \end{bmatrix}.$$

Proof. The adjustment model which is used in our derivation is the condition model; by putting **A**=0 in Eq. (6.16) we obtain

$$\tilde{\mathbf{P}}_i = \mathbf{F}_i\mathbf{Q}\mathbf{B}^T\mathbf{C}^{-1}\mathbf{B}\mathbf{Q}\mathbf{F}_i, \tag{6.33}$$

where *i*=VV, HH, and VH, respectively, and according to the stochastic model 1 we obtain

$$\mathbf{F}_{\mathrm{VV}} = \mathrm{diag}\left(\begin{bmatrix} I & 0 & 0 & 0 & 0 & 0 \end{bmatrix}\right), \tag{6.34a}$$

$$\mathbf{F}_{\mathrm{HH}} = \mathrm{diag}\left(\begin{bmatrix} 0 & I & I & I & 0 & 0 \end{bmatrix}\right), \tag{6.34b}$$

$$\mathbf{F}_{\mathrm{VH}} = \mathrm{diag}\left(\begin{bmatrix} 0 & 0 & 0 & 0 & I & I \end{bmatrix}\right), \tag{6.34c}$$

and finally by using Eqs. (6.34a)-(6.34c), we have

$$\mathbf{P}_{\mathrm{VV}}^{nm} = \left(c_{12}^{nm} - 2c_{12}^{nm} + c_{12}^{nm}\right)\left|\mathbf{C}^{nm}\right|^{-1}\mathbf{Q}_{zz}\left(\mathbf{b}_{zz}^{nm}\right)^{T}\mathbf{b}_{zz}^{nm}\mathbf{Q}_{zz}, \tag{6.35a}$$

$$\mathbf{P}_{\mathrm{HH}}^{nm} = \frac{c_{22}^{nm}}{\left|\mathbf{C}^{nm}\right|}\begin{bmatrix} \mathbf{Q}_{xx}\left(\mathbf{b}_{xx}^{nm}\right)^{T}\mathbf{b}_{xx}^{nm}\mathbf{Q}_{xx} & \mathbf{Q}_{xx}\left(\mathbf{b}_{xx}^{nm}\right)^{T}\mathbf{b}_{yy}^{nm}\mathbf{Q}_{yy} & \mathbf{Q}_{xx}\left(\mathbf{b}_{xx}^{nm}\right)^{T}\mathbf{b}_{xy}^{nm}\mathbf{Q}_{xy} \\ \mathbf{Q}_{yy}\left(\mathbf{b}_{yy}^{nm}\right)^{T}\mathbf{b}_{xx}^{nm}\mathbf{Q}_{xx} & \mathbf{Q}_{yy}\left(\mathbf{b}_{yy}^{nm}\right)^{T}\mathbf{b}_{yy}^{nm}\mathbf{Q}_{yy} & \mathbf{Q}_{yy}\left(\mathbf{b}_{yy}^{nm}\right)^{T}\mathbf{b}_{xy}^{nm}\mathbf{Q}_{xy} \\ \mathbf{Q}_{xy}\left(\mathbf{b}_{xy}^{nm}\right)^{T}\mathbf{b}_{xx}^{nm}\mathbf{Q}_{xx} & \mathbf{Q}_{xy}\left(\mathbf{b}_{xy}^{nm}\right)^{T}\mathbf{b}_{yy}^{nm}\mathbf{Q}_{yy} & \mathbf{Q}_{xy}\left(\mathbf{b}_{xy}^{nm}\right)^{T}\mathbf{b}_{xy}^{nm}\mathbf{Q}_{xy} \end{bmatrix}, \tag{6.35b}$$

and

$$\mathbf{P}_{\mathrm{VH}}^{nm} = \frac{c_{11}^{nm}}{\left|\mathbf{C}^{nm}\right|}\begin{bmatrix} \mathbf{Q}_{xz}\left(\mathbf{b}_{xz}^{nm}\right)^{T}\mathbf{b}_{xz}^{nm}\mathbf{Q}_{xz} & \mathbf{Q}_{xz}\left(\mathbf{b}_{xz}^{nm}\right)^{T}\mathbf{b}_{yz}^{nm}\mathbf{Q}_{yz} \\ \mathbf{Q}_{yz}\left(\mathbf{b}_{yz}^{nm}\right)^{T}\mathbf{b}_{xz}^{nm}\mathbf{Q}_{xz} & \mathbf{Q}_{yz}\left(\mathbf{b}_{yz}^{nm}\right)^{T}\mathbf{b}_{yz}^{nm}\mathbf{Q}_{yz} \end{bmatrix}. \tag{6.35c}$$

Propositions 6.2 and 6.3 follow by inserting Eqs. (6.35a)-(6.35c) into Eq. (6.33).

Proposition 6.4 *The MBQUNE of DOVCs based on stochastic model 2 for HH and VH solution is (Eshagh 2009f):*

$$\left(\hat{\sigma}_i^2\right)^{nm} = \frac{\left[\mathbf{b}_i^{nm}\mathbf{Q}_i\left(\mathbf{b}_i^{nm}\right)^{T}\right]c_{kk}^{nm}\left(\hat{\boldsymbol{\varepsilon}}_i^{nm}\right)^{T}\left(\mathbf{Q}_i\left(\mathbf{b}_i^{nm}\right)^{T}\mathbf{b}_i^{nm}\mathbf{Q}_i\right)^{-}\hat{\boldsymbol{\varepsilon}}_i^{nm}}{\left|\mathbf{C}^{nm}\right|\mathrm{rank}\left(\mathbf{Q}_i\left(\mathbf{b}_i^{nm}\right)^{T}\mathbf{b}_i^{nm}\mathbf{Q}_i\right)}, \quad \left|\mathbf{C}^{nm}\right| \neq 0$$

where

$$i = \begin{cases} xx, yy, xy & k = 2 \\ xz, yz & k = 1 \end{cases}.$$

Proof. The mathematical proof of the proposition is very similar to that of Proposition 6.3. The differences are just due to projector $\mathbf{F}_i$, *i*=*xx*, *yy*, *xy*, *xz* and *yz* and stochastic model 2.

$$\mathbf{F}_{xx} = \mathrm{diag}\left(\begin{bmatrix} 0 & I & 0 & 0 & 0 & 0 \end{bmatrix}\right), \tag{6.36a}$$

$$\mathbf{F}_{yy} = \mathrm{diag}\left(\begin{bmatrix} 0 & 0 & I & 0 & 0 & 0 \end{bmatrix}\right), \tag{6.36b}$$

$$\mathbf{F}_{xy} = \mathrm{diag}\left(\begin{bmatrix} 0 & 0 & 0 & I & 0 & 0 \end{bmatrix}\right), \tag{6.36c}$$

$$\mathbf{F}_{xz} = \mathrm{diag}\left(\begin{bmatrix} 0 & 0 & 0 & 0 & I & 0 \end{bmatrix}\right), \tag{6.36d}$$

$$\mathbf{F}_{yz} = \mathrm{diag}\left(\begin{bmatrix} 0 & 0 & 0 & 0 & 0 & I \end{bmatrix}\right), \tag{6.36e}$$

and

$$\mathbf{C}_i^{nm} = \mathbf{b}_i^{nm}\mathbf{Q}_i\left(\mathbf{b}_i^{nm}\right)^T \begin{bmatrix} 1 & 0 \\ 0 & 0 \end{bmatrix}, \; i=xx,\, yy \text{ and } xy \tag{6.37a}$$

$$\mathbf{C}_j^{nm} = \mathbf{b}_j^{nm}\mathbf{Q}_j\left(\mathbf{b}_j^{nm}\right)^T \begin{bmatrix} 0 & 0 \\ 0 & 1 \end{bmatrix}, \; j=xz \text{ and } yz. \tag{6.37b}$$

The proposition is proved by substituting Eqs. (6.36a)-(6.36e) and Eqs. (6.37a)-(6.37b) into Eq. (6.33) and further simplifications.

6.6.4 Numerical investigation in VCE and re-weighting process

Now we will test the combined solutions using the DOVC estimation. This process is considered in two different cases: first the stochastic model 1 in which one DOCV is estimated for each integral solution is considered and named "combined solution 1". Correspondingly, if the stochastic model 2 with estimation of one DOVC for each type of observation (six DOVCs) is considered and the solution will be called "combined solution 2". Figure 6.3 shows the true and simple mean solution with respect to the combined solution 1. The figure shows that the solution is very close to the simple mean. In some degrees it is superior and in some is inferior with respect to the simple mean. In general one cannot say that the combined solution 1 is better than the simple mean unless their differences are considered. Such differences are presented in Figure 6.6.

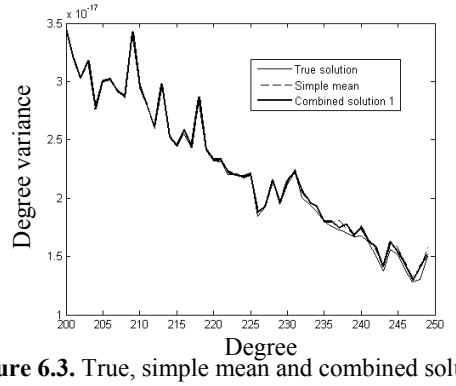

Figure 6.3. True, simple mean and combined solution 1

For some degrees and orders the observables have different weights in the combination. Another important matter is occurrence of the negative DOVC for zonal terms. The BQUNE does not exist for the present problem and we have to use the MBQUNE to estimate the DOVCs. Let us now explain the practical problem to use this estimator. There is the parameter $\mathbf{Q}_{zz}\left(\mathbf{b}_{zz}^{nm}\right)^T \mathbf{b}_{zz}^{nm}\mathbf{Q}_{zz}$ in Proposition 6.3. $\mathbf{b}_{zz}^{nm}$ is a row vector and its dimensions depends directly on the resolution of the data. In the present case, a $30' \times 30'$ grid of the SGG data is considered. Therefore this vector will

have 360×720=259200 column-wise elements. Consequently, $\left(\mathbf{b}_{zz}^{nm}\right)^T \mathbf{b}_{zz}^{nm}$ will be a matrix with dimensions of 259200×259200=67184640000. As Proposition 6.2 shows, $\mathbf{Q}_{zz}\left(\mathbf{b}_{zz}^{nm}\right)^T \mathbf{b}_{zz}^{nm}\mathbf{Q}_{zz}$ should be inverted by a generalized inverse (Bjerhammar 1973). This action is very complicated for ordinary computers, and the situation becomes even worse for estimating the DOVCs of the VV and HH solutions as the dimensions of the matrices are even larger. As a consequence, the MBQUNE is not practical for the time being. It will hopefully be implemental for supercomputers. Considering that the computer technology is being advanced this problem will not be serious in the future.

In order to escape from the negative DOVCs, the simple mean was used for the combination of the corresponding degrees. The investigation shows larger errors for lower orders than higher ones in the three integral solutions of the GBVPs; and after the order 10 the differences are very small or even zero.

In order to present the performance of the DOVC estimation process, the degree n=200 and the order m=2 coefficients (for which the negative DOVC does not happen, are considered) as an instant, but these are not the only coefficient for which the positive DOVC occurs. Figure 6.4 shows the VC ratios of the VV, VH and HH solutions for these degree and order.

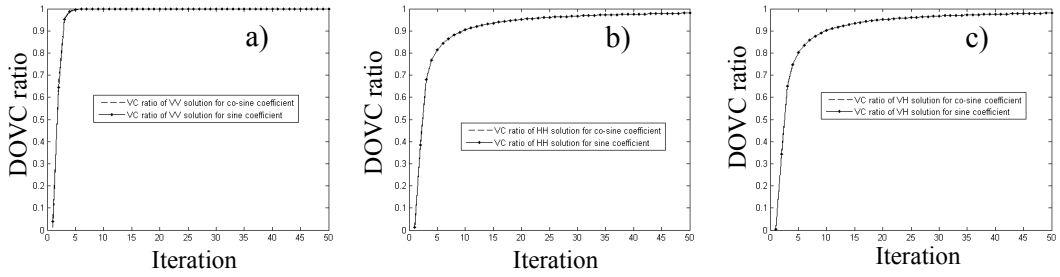

Figure 6.4. VC ratios for (a) VV solution, (b) HH solution and (c) VH solution for n=200 and m=2

The figure presents the speed of convergence of the DOVC ratios to 1. The ratio converges quickly to 1 in the VV solution, but it is very slow for the HH and VH solutions. (The ratios up to 50 iterations are presented). According to the author's investigation the ratios do not converge to 1 even until 500 iterations, but they come closer to 1. Table 6.1 shows the DOVCs of the VV, HH and VH solutions, and it should be stated that the DOVC estimation process is done for cosine and sine coefficients separately. At first view, one can see larger values for the DOVCs for estimating $\hat{S}_{200,2}$ than $\hat{C}_{200,2}$, but it is not important in the re-weighing process. The DOVCs estimation balances the accuracy of the observations and misclosures; and since the latter is very small, it is natural to get small values for the DOVC. Another important matter is to get smallest DOVC for the VH solution. However one see smaller value of the DOVC for the HH solution than the VV solution too. If Proposition 6.1 is considered, the only parameter which depends on the stochastic

model is k_j. This parameter was presented in Eqs. (6.27)-(6.29). One reason to obtain smaller DOVC for the HH solution is that k_{HH} becomes larger, than k_{VV} because of including three quadratic forms (see Eq. 6.27). The ratios of the DOVCs in these solutions show that the relative weights in the solutions of both cosine and sine coefficients are the same.

Table 6.1 shows the DOVCs of the VV, HH and VH solutions. Larger DOVCs are observed for $\hat{S}_{200,2}$ than $\hat{C}_{200,2}$. In Table 6.2 the ratios of the DOVCs are presented for some degrees and orders.

Table 6.1. DOVCs of VV, HH and VH solution for *n*=200 and *m*=2

	$\hat{C}_{200,2}$	$\hat{S}_{200,2}$
$\left(\hat{\sigma}^2_{\mathrm{VV}}\right)^{200,2}$	7.97×10^{-9}	2.41×10^{-6}
$\left(\hat{\sigma}^2_{\mathrm{HH}}\right)^{200,2}$	7.75×10^{-11}	2.34×10^{-8}
$\left(\hat{\sigma}^2_{\mathrm{VH}}\right)^{200,2}$	2.27×10^{-11}	6.87×10^{-9}

Table 6.2. DOVC ratios for VV, HH and VH solutions based on stochastic model 1 for *n*=200, *m*=2, *n*=230, *m*=5, *n*=245, *m*=8

	n=200 *m*=2	*n*=230 *m*=5	*n*=245 *m*=8
$\left(\hat{\sigma}^2_{\mathrm{VH}}\right)^{nm} \Big/ \left(\hat{\sigma}^2_{\mathrm{HH}}\right)^{nm}$	0.29	0.08	0.04
$\left(\hat{\sigma}^2_{\mathrm{VV}}\right)^{nm} \Big/ \left(\hat{\sigma}^2_{\mathrm{HH}}\right)^{nm}$	408.32	404.79	401.04

The stochastic model 2 is considered, or in other words, the combined solution 2, which was presented in Corollary 6.1. Here one DOVC is estimated for each set of observations. The study is confined just to the cases where the positive DOVCs come out. Each time the negative DOVCs are derived the simple mean is selected for combining the coefficients. The negative DOVCs were seen for the zonal coefficients and for some others. According to the author's investigation the negative DOVC frequently occur in the combined solution 2. However they mostly belong to the orders higher than 14 and as it was mentioned before; the author did not observed significant difference among the VV, HH and VH solutions for the higher orders. The result of this combination is visualized in Figure 6.5.

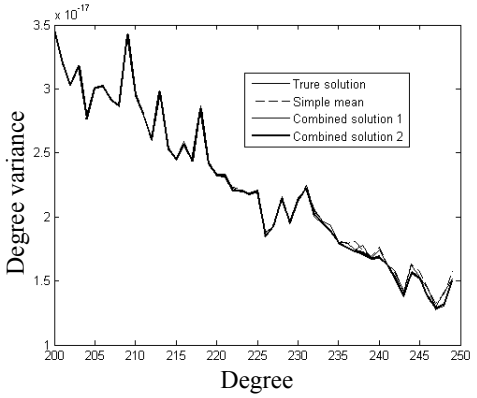

Figure 6.5. True, simple mean, combined solution 1 and 2

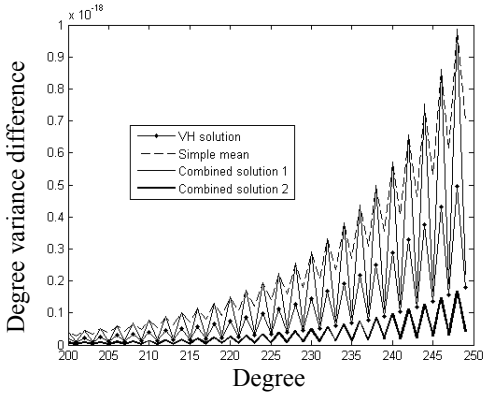

Figure 6.6. Difference between true and simple mean, combined solution 1 and 2

The figure clearly shows that the combined solution 2 is very close to the true solution. For better visualization, we consider the differences between all the solutions and the true solution in Figure 6.6. In the figure the dash line (--), the solid line (-) and the tick solid line (**-**) stand for the differences between the simple mean, combined solution 1 and 2, respectively with the true solution. The figure shows that the even degrees are well estimated in the combined solution 1, but they are at the same as level as the simple mean in odd degrees. Therefore the combine solution 1 is slightly better than the simple mean. Since the VH solution was closer than the VV and HH solutions to the true one, the difference between the true and the VH solution is plotted in Figure 6.6; in order to show that the combined solution 1 is a solution between the simple mean and the VH solution. However, as can be seen, the combined solution 2 is even superior to the VH solution. According to the numerical investigations the DOVCs converge fast in this combined solution. After about 3 iterations all the DOVC ratios converge to 1. Perhaps this is due to the stochastic model which is used. However, the problem of this combination method is to get frequent negative DOVCs for the orders above 14.

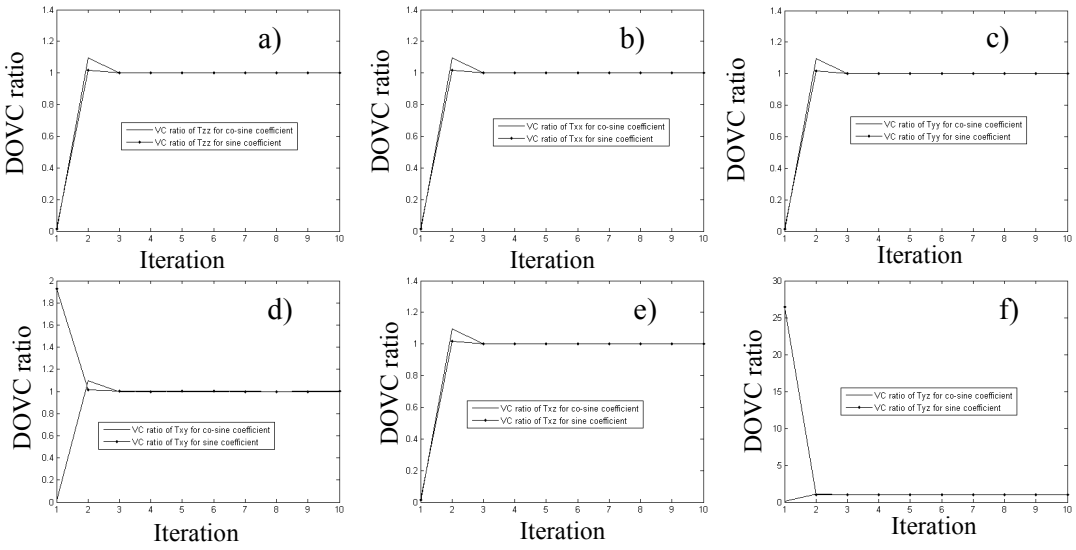

Figure 6.7. VC ratios for T_{zz} ,T_{xx} ,T_{yy} ,T_{xy} ,T_{xz} and T_{yz}

The figure shows that the DOVC ratios for *n*=200 and *m*=2 of T_{zz} ,T_{xx} ,T_{yy} and T_{xz} are very similar and they converge to 1 in 3 iterations. This is not like the combined solution 1 in which the DOVC ratios has uniform convergence. The DOVC ratios of T_{xy} and T_{yz} in the combined solution 2 are very similar as they are decreasing for the cosine coefficients and increasing for sine coefficients.

The DOVCs of these observations in the combined solution 2 are tabulated in Table 6.3. It illustrates the DOVCs of T_{zz} ,T_{xx} ,T_{yy} ,T_{xy} ,T_{xz} and T_{yz} , respectively for *n*=200 and *m*=2. As the table shows $\left(\hat{\sigma}_{xx}^2\right)^{200,2}$ is equal to $\left(\hat{\sigma}_{yy}^2\right)^{200,2}$ in both sine and cosine coefficients. The reason is that the coefficient matrices $\mathbf{b}_{xx}^{nm}$ and $\mathbf{b}_{yy}^{nm}$ are exactly the same in magnitude but they differ in sign. This is why the same DOVCs

for these types of observations are estimated. According to the Laplace equation, the DOVC of T_{zz} should be in order of the DOVCs of T_{yy} and T_{xy} and this is why we obtained $\left(\hat{\sigma}_{zz}^2\right)^{200,2}$ in order of $\left(\hat{\sigma}_{xx}^2\right)^{200,2}$ and $\left(\hat{\sigma}_{yy}^2\right)^{200,2}$. The DOVC of T_{xz} is also in order of $\left(\hat{\sigma}_{zz}^2\right)^{200,2}$, $\left(\hat{\sigma}_{xx}^2\right)^{200,2}$ and $\left(\hat{\sigma}_{yy}^2\right)^{200,2}$; and it is closer to $\left(\hat{\sigma}_{zz}^2\right)^{200,2}$. It seems that there is more or less the same power of the gravitational signal in T_{zz} and T_{xz}. Larger DOVCs are related to T_{xy} and T_{yz} as presented in Table 6.3. The ratios of the VCs are given in Table 6.4 as well.

Table 6.3. DOVCs of $T_{zz}, T_{xx}, T_{yy}, T_{xy}, T_{xz}$ and T_{yz} for n=200 and m=2

	$\hat{C}_{200,2}$	$\hat{S}_{200,2}$
$\left(\hat{\sigma}_{zz}^2\right)^{200,2}$	5.74×10^{-9}	1.6×10^{-6}
$\left(\hat{\sigma}_{xx}^2\right)^{200,2}$	5.64×10^{-9}	1.57×10^{-6}
$\left(\hat{\sigma}_{yy}^2\right)^{200,2}$	5.64×10^{-9}	1.57×10^{-6}
$\left(\hat{\sigma}_{xy}^2\right)^{200,2}$	7.00×10^{-7}	1.96×10^{-4}
$\left(\hat{\sigma}_{xz}^2\right)^{200,2}$	5.72×10^{-9}	1.60×10^{-6}
$\left(\hat{\sigma}_{yz}^2\right)^{200,2}$	9.60×10^{-6}	2.7×10^{-4}

Table 6.4. DOVC ratios of $T_{zz}, T_{xx}, T_{yy}, T_{xy}, T_{xz}$ and T_{yz} based on stochastic model 2 for n=200, m=2, n=230, m=5, n=245, m=8

	n=200 m=2	n=230 m=5	n=245 m=8
$\left(\hat{\sigma}_{xx}^2\right)^{nm} / \left(\hat{\sigma}_{zz}^2\right)^{nm}$	0.98	0.99	1.00
$\left(\hat{\sigma}_{yy}^2\right)^{nm} / \left(\hat{\sigma}_{zz}^2\right)^{nm}$	0.98	0.99	1.00
$\left(\hat{\sigma}_{xy}^2\right)^{nm} / \left(\hat{\sigma}_{zz}^2\right)^{nm}$	122.0	30.92	15.24
$\left(\hat{\sigma}_{xz}^2\right)^{nm} / \left(\hat{\sigma}_{zz}^2\right)^{nm}$	0.99	1.00	1.00
$\left(\hat{\sigma}_{yz}^2\right)^{nm} / \left(\hat{\sigma}_{zz}^2\right)^{nm}$	1671.50	406.13	195.41

This example shows the details of the re-weighting process using the DOVC estimation procedure. However, according to our numerical investigations the general pattern of these DOVCs is more or less the same procedure in other degrees and orders. Table 6.4 shows that T_{xy} and T_{yz} contribute more in the l combination of higher degrees and orders. Also T_{xy} seems to contain more power than T_{yz} even in higher degrees and orders in the combination based one the stochastic model 2.

6.7 Combination of the gravitational gradients in local gravity field determination

In the previous chapter the problem of determining the gravity anomaly at sea level from the SGG data was investigated. Each element of the gravitational tensor was considered separately in local gravity field determination. This section presents the joint inversion of the SGG data or local gravity field determination using full gravitational tensor. In this section, the simple joint inversion by least-squares and after that re-weighting of the observation by VCE is investigated.

6.7.1 Simple joint inversion of the SGG data by least-squares

This section discusses how all the gravitational gradients are merged in one system of equations. We name inversion of such a system of equations simple joint

inversion, because we do not use the VCE in the inversion. Putting the system of equations (Eqs. 5.2a-5.2f) in one system of equations yields:

$$\begin{bmatrix} \mathbf{A}_{zz} \\ \mathbf{A}_{xx} \\ \mathbf{A}_{yy} \\ \mathbf{A}_{xy} \\ \mathbf{A}_{xz} \\ \mathbf{A}_{yz} \end{bmatrix} \mathbf{x} = \begin{bmatrix} \mathbf{t}_{zz} \\ \mathbf{t}_{xx} \\ \mathbf{t}_{yy} \\ \mathbf{t}_{xy} \\ \mathbf{t}_{xz} \\ \mathbf{t}_{yz} \end{bmatrix} + \begin{bmatrix} \boldsymbol{\varepsilon}_{zz} \\ \boldsymbol{\varepsilon}_{xx} \\ \boldsymbol{\varepsilon}_{yy} \\ \boldsymbol{\varepsilon}_{xy} \\ \boldsymbol{\varepsilon}_{xz} \\ \boldsymbol{\varepsilon}_{yz} \end{bmatrix}, \tag{6.38}$$

where the elements of the coefficient matrix were given in Chapter 4. We assume that the stochastic model is the same as of Eq. (6.20c). The least-squares solution of Eq. (6.38) is:

$$\hat{\mathbf{x}} = \mathbf{M}^{-1}\mathbf{L}, \tag{6.39}$$

where $\mathbf{M} = \sum_{i=1}^{6} \mathbf{A}_i^T \mathbf{Q}_i^{-1} \mathbf{A}_i$ and $\mathbf{L}_i = \sum_{i=1}^{6} \mathbf{A}_i^T \mathbf{Q}_i^{-1} \mathbf{t}_i$, and i=1,2,…,5 and 6 correspond to *zz*, *xx*, *yy*, *xy*, *xz* and *yz*, respectively. The solution of Eq. (6.39) is that of an ill-posed problem being very sensitive to the errors of the SGG data. Therefore the system of equations should be regularized. The Tikhonov regularization method is selected with the GCV. In this case, Eq. (6.39) will be converted to

$$\mathbf{x}_{\text{reg}} = \mathbf{N}^{-1}\mathbf{L}, \tag{6.40}$$

where $\mathbf{N}^{-1} = \left(\mathbf{M} + \alpha^2 \mathbf{I}\right)^{-1}$.

In this part, the resolutions of $0.5^\circ \times 0.5^\circ$ and $1^\circ \times 1^\circ$ are considered for the SGG data and the gravity anomaly at sea level, respectively. The singular values of the combined coefficients matrix are presented in Figure 6.8.

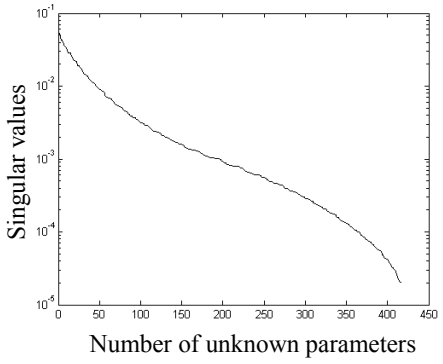

Figure 6.8. Singular values of the coefficients matrix of joint inversion problem Eq. (6.38), when resolution of SGG data is $0.5^\circ \times 0.5^\circ$ and required gravity anomalies is $1^\circ \times 1^\circ$.

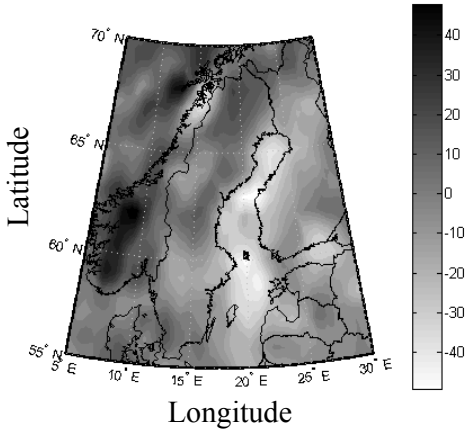

Figure 6.9. Recovered gravity anomalies from joint inversion of SGG data contaminated with 1 mE noise. Unit: 1 mGal

The maximum and minimum singular values are 5.37×10^{-2} and 2.02×10^{-5}, respectively. The condition number is 2.66×10^{3} which means that the joint inversion of the SGG data is more stable than the inversion of each elements of gravitational tensor separately. Two types of Gaussian noise with 1 mE and 1 cE standard deviations are added to the synthesized SGG data. Figure 6.9 shows the recovered gravity anomalies from the joint inversion of SGG data containing 1 mE noise. The error of the estimated gravity anomalies can be estimate using Eq. (5. 10) are presented in Figure 6.10, which shows the estimated errors of the recovered gravity anomalies when the SGG data are contaminated with 1 mE noise and Figure 6.10b for 1 cE. The horizontal axis is number of gravity anomalies from north to south and the jumps are the north-south boundaries of the area. The figure shows considerable changes in error at the highest and lowest parallels of the area (Fennoscandia). The errors of the recovered data are about 2 and 3 mGal when the noise is 1 mE and 1 cE, respectively.

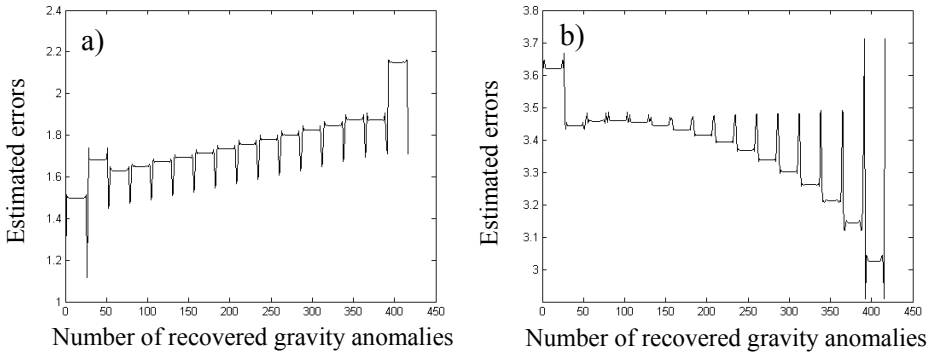

Figure 6.10. Estimated error of recovered gravity anomalies in joint inversion of SGG data with (a) 1 mE and (b) 1 cE noise. Unit: 1 mGal

Equation (5.12) can be used to estimate the bias of the estimated parameters in the numerical example. The biases are presented in Figure 6.11. It is not surprising that the biases will be small when the noise is small. The figure shows that the biases are within 5 mGal and 20 mGal when the noise is 1 mE and 1 cE, respectively. The corresponding regularization parameters, which were estimated using the GCV method, are 0.15 and 0.09, respectively.

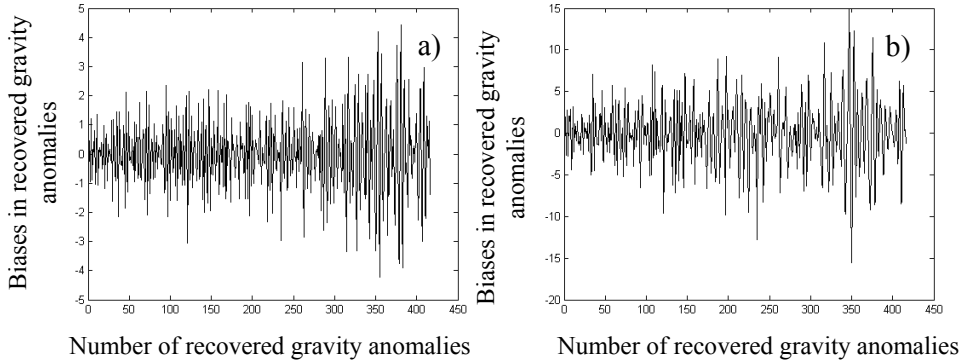

Figure 6.11. Biases of recovered gravity anomalies from SGG data with (a) 1 mE and (b) 1 cE noise. Unit: 1 mGal

In Table 6.5 the statistics of the difference between the recovered and the true gravity anomalies are presented. The table illustrates that the gravity anomalies can very well recovered from joint inversion of the SGG data if the noise of the data is in 1 mE level. The standard deviation is 2.10 mGal which shows that how much the recovered quantities are close to the reality if the noise level is 1 mE. It is 5.15 mGal if the noise of the SGG data is 1 cE. Table 6.6 shows the errors of the biased-corrected estimation of the gravity anomalies and some improvements in the recovery. The improvements for the estimate parameter is not considerable when the noise of the data is about 1 mE, but it is important to reduce the biases for the case where the noise is in 1 cE level.

Table 6.5. Statistics of errors of recovered gravity anomalies from SGG data with 1 mE and 1 cE noise levels. Unit: 1 mGal

	min	mean	max	std
1 mE	-5.74	-0.00	6.70	2.10
1 cE	-19.11	-0.04	16.83	5.15

Table 6.6. Statistics of errors of bias-corrected recovered gravity anomalies from SGG data with 1 mE and 1 cE noise levels. Unit: 1 mGal

	min	mean	max	std
1 mE	-3.89	-0.00	4.52	1.57
1 cE	-9.08	-0.03	8.01	2.91

6.7.2 Joint inversion of SGG data and VCE

In the simple joint inversion of SGG data, which was studied in the previous subsection, the same weights were considered for all the data. We already know that there are different types of gravitational gradients in the gravitational tensor and quality of the gradients is not the same. Here, we will use VCE in such an ill-posed problem to see if the re-weighting process improves the solution. In local gravity field determination, the VCE is not the same as it is in an ordinary least-squares problem. Here, we will investigate how the VCE is performed in such an ill-posed problem.

6.7.2.1 VCE in ill-posed problems

VCE in ill-posed problems has been considered by some authors, for example Koch and Kusche (2002). However, they regularized the ill-posed problem iteratively, and during the iteration process they estimated the VCs as well. Xu et al. (2006) presented a method for estimating the VCs in an ill-posed problem of gravitational field determination from orbital perturbations. They considered the BQUE and introduced a new VC estimator, which was called biased-corrected estimator. In the following, the BQUE of the VC is investigated, and after that the Sjöberg (1984c) VC estimator (BQUNE). However, first the biases (due to regularization) of the estimated VCs will be analyzed in a linear ill-posed problem.

6.7.2.2 Bias analysis of the BQUE

The VCE process in local gravity field determination using the SGG data is an example of VCE in linear ill-posed problems. To do this, it is assumed that the variance-covariance matrix of the data has a block-diagonal structure. The six elements of the gravitational tensor should be inverted in one system of equations to estimate the gravity anomaly. Two different stochastic models were already introduced for the data. In the stochastic model 1, in which for each solution of the VV, VH and HH GBVPs one VC is estimated. In a very similar manner one VC is estimated for each gradient based on stochastic model 2. Since the combined estimation of local gravity field determination requires working with a large system of equations, the VCE process is not practical. However, since the stochastic model has a block-diagonal structure, simple formula for the system of equations from which the VCs are estimated, can be derived. In this case the size of the matrices is reduced six times. Considering the stochastic model 1 or 2, the elements of the coefficient matrix of the system of equations (from which the VCs are estimated) are presented in the following proposition.

Proposition 6.5 *The elements of the system of equations* $\mathbf{S}\boldsymbol{\sigma} = \mathbf{u}$ *based on a Gauss-Markov model with a block-diagonal structure stochastic model is:*

$$s_{ij} = \operatorname{trace}\left[\sum_i \left(\mathbf{I}_n - \mathbf{Q}_i^{-1}\mathbf{A}_i\mathbf{N}^{-1}\mathbf{A}_i^T\right)^2\right]\delta_{ij} +$$

$$+\operatorname{trace}\left[\sum_i \mathbf{Q}_i^{-1}\mathbf{A}_i\mathbf{N}^{-1}\left(\sum_j \mathbf{A}_j^T\mathbf{Q}_j^{-1}\mathbf{A}_j\right)\mathbf{N}^{-1}\mathbf{A}_i^T\right]\left(1-\delta_{ij}\right),$$

and

$$u_i = \sum_i \boldsymbol{\varepsilon}_i^T\mathbf{Q}^{-1}\mathbf{Q}_i'\,\mathbf{Q}^{-1}\boldsymbol{\varepsilon}_i = \sum_i \boldsymbol{\varepsilon}_i^T\mathbf{Q}_i'^{-}\boldsymbol{\varepsilon}_i\ ,$$

where i and j = 1, 2, 3 stands for VV, VH, and HH (combined solution 1). i and j = 1, 2, 3, 4, 5,6 stands for zz, xx, yy, xy, xz and yz (stochastic model 2), respectively, which are selected based on type of the stochastic model. δ *is the Kronecker delta.*

Proof. The proposition follows by considering stochastic model 1 or 2 based on Eqs. (6.6a)-(6.6c). After a relatively long algebraic derivation the proposition is proved.

The proposition clearly shows that the size of the system of equations is six times smaller than the standard formulas and the formulas of the proposition are efficient in computer programming as the formulation does not contain very big null matrices. This proposition can be used in any application in which the stochastic model has a block diagonal structure.

Until now, the effect of ill-posedness of the system of equations was not considered. The main difference between the VCE in well-posed and ill-posed problems is related to the matrix $\mathbf{N}$ and the residual vector $\boldsymbol{\varepsilon}$, as the former includes a regularization matrix, and the latter is a biased estimation of the residual, because the estimated parameters are biased. If the VCE formulas for an ill-posed

problem are considered as they are for a well-posed one, we should write (Xu et al. 2006)

$$s_{ij} = \text{trace}\left[\mathbf{Q}^{-1}\left(\mathbf{I}-\mathbf{A}_{\text{reg}}^{0}\right)\mathbf{Q}_i'\mathbf{Q}^{-1}\left(\mathbf{I}-\mathbf{A}_{\text{reg}}^{0}\right)\mathbf{Q}_j'\right], \tag{6.41a}$$

and

$$u_i = \boldsymbol{\varepsilon}_{\text{reg}}^{T}\mathbf{Q}_i'^{-}\boldsymbol{\varepsilon}_{\text{reg}}. \tag{6.41b}$$

The definition of $\mathbf{Q}$ is the same as that of Eq. (6.20c). $\boldsymbol{\varepsilon}_{\text{reg}}$ and $\mathbf{A}_{\text{reg}}^{0}$ have already been defined in Eqs. (5.11c) and (5.11d). The biased estimation of the errors can be written in terms of the bias as:

$$\boldsymbol{\varepsilon}_{\text{reg}} = \alpha^2\mathbf{A}\mathbf{N}^{-1}\mathbf{x} + \left(\mathbf{I}-\mathbf{A}_{\text{reg}}^{0}\right)\boldsymbol{\varepsilon}, \tag{6.42}$$

Substituting Eq. (6.44) into Eq. (6.43b) and taking the expectation operator we obtain

$$\begin{aligned} E\left\{u_i\right\} = \sum_{j=1}^{m}\text{trace}\left[\mathbf{Q}^{-1}\left(\mathbf{I}-\mathbf{A}_{\text{reg}}^{0}\right)\mathbf{Q}_i'\mathbf{Q}^{-1}\left(\mathbf{I}-\mathbf{A}_{\text{reg}}^{0}\right)\mathbf{Q}_j'\right]\sigma_j^2 + \\ +\alpha^4\text{trace}\left[\mathbf{Q}_i'^{-}\mathbf{A}\mathbf{N}^{-1}\mathbf{x}\mathbf{x}^{T}\mathbf{N}^{-1}\mathbf{A}^{T}\right], \end{aligned} \tag{6.43}$$

Now if we directly take expectation from $\mathbf{S}\boldsymbol{\sigma} = \mathbf{u}$ we have

$$\mathbf{S}E\left\{\hat{\boldsymbol{\sigma}}\right\} = E\left\{\mathbf{u}\right\}. \tag{6.44}$$

Considering Eq. (6.44) and Eq. (6.43) we obtain

$$E\left\{\hat{\boldsymbol{\sigma}}\right\} = \boldsymbol{\sigma} + \mathbf{S}^{-1}\mathbf{d}\mathbf{u}, \tag{6.45}$$

where the second term of the above equation is the bias of the VCs due to regularization, and the elements of the vector **du** is (Xu et al. 2006, Eq. 10, p. 71):

$$du_i = \sum_i \text{trace}\left(\mathbf{Q}_i^{-1}\mathbf{A}_i\mathbf{N}^{-1}\mathbf{x}\mathbf{x}^{T}\mathbf{N}^{-1}\mathbf{A}_i^{T}\right). \tag{6.46}$$

6.7.2.3 Biased-corrected VCE

As was explained in the previous section, the estimated VCs contain biases due to regularization of the system of equations. It is possible is to estimate and remove the biases from the estimated VCs. However, in some practical applications the VCs may come out negative by this subtraction. It means that the estimated biases are unrealistically large. Therefore this idea does not seem practical. We have to use another way of VCE, which remove the biases before VCE process. This idea

was presented and discussed by Xu et al. (2006) which is briefly presented here. The relation between the true and biased estimates is:

$$\mathbf{x}_{\text{reg}} = \mathbf{x} - \alpha^2 \mathbf{N}^{-1}\mathbf{x}\,, \tag{6.47}$$

Inserting the estimated **x** into Eq. (6.47) yields

$$\mathbf{x}_{\text{reg}} = \mathbf{N}^{-1}\mathbf{A}^T\mathbf{Q}^{-1}\mathbf{L} - \alpha^2 \mathbf{N}^{-2}\mathbf{A}^T\mathbf{Q}^{-1}\mathbf{L}\,, \tag{6.48}$$

and the residuals are

$$\bar{\boldsymbol{\varepsilon}}_{\text{reg}} = \alpha^2 \mathbf{A}\mathbf{N}^{-1}\mathbf{x} + \left(\mathbf{I} - \mathbf{A}^0_{\text{reg}} - \alpha^2 \mathbf{A}\mathbf{N}^{-2}\mathbf{A}^T\mathbf{Q}^{-1}\right)\boldsymbol{\varepsilon}\,, \tag{6.49}$$

The quadratic form of the biased-corrected residual is:

$$\bar{u}_i = \left(\boldsymbol{\varepsilon}_{\text{reg}} - \alpha^2 \mathbf{A}\mathbf{N}^{-1}\mathbf{x}\right)^T \mathbf{Q}_i'^{-}\left(\boldsymbol{\varepsilon}_{\text{reg}} - \alpha^2 \mathbf{A}\mathbf{N}^{-1}\mathbf{x}\right). \tag{6.50}$$

Taking the statistical expectation from Eq. (6.50) yields

$$\begin{aligned} E\left\{\bar{u}_i\right\} = \sum_{j=1}^{m} \text{trace}\Big[& \mathbf{Q}^{-1}\left(\mathbf{I} - \mathbf{A}^0_{\text{reg}} - \alpha^2 \mathbf{A}\mathbf{N}^{-2}\mathbf{A}^T\mathbf{Q}^{-1}\right)\mathbf{Q}'_i \times \\ & \times \mathbf{Q}^{-1}\left(\mathbf{I} - \mathbf{A}^0_{\text{reg}} - \alpha^2 \mathbf{A}\mathbf{N}^{-2}\mathbf{A}^T\mathbf{Q}^{-1}\right)\mathbf{Q}'_j\Big]\sigma_j^2\,, \end{aligned} \tag{6.51}$$

and the biased-corrected VCs are estimated by solving the following system of equations

$$\bar{\mathbf{S}}\boldsymbol{\sigma} = \bar{\mathbf{u}}\,. \tag{6.52}$$

Again the problem of working with very large matrices occurs here. However, as the stochastic model is block-diagonal, the formulas can further be simplified.

Proposition 6.6 *The elements of the matrix* $\bar{\mathbf{S}}$ *for estimating the biased-corrected VCs when the stochastic model is block-diagonal are:*

$$\begin{aligned} s_{ij} = \delta_{ij}\Bigg\{ & \text{trace}\left[\sum_i \left(\mathbf{I}_n - \mathbf{Q}_i^{-1}\mathbf{A}_i\mathbf{N}^{-1}\mathbf{A}_i^T\right)^2\right] - 2\alpha^2 \text{trace}\left[\sum_i \left(\mathbf{I}_n - \mathbf{Q}_i^{-1}\mathbf{A}_i\mathbf{N}^{-1}\mathbf{A}_i^T\right)\times\right. \\ & \left.\times \mathbf{Q}_i^{-1}\mathbf{A}_i\mathbf{N}^{-2}\mathbf{A}_i^T\right]\Bigg\} + \left(1-\delta_{ij}\right)\Bigg\{ \text{trace}\left[\sum_i \mathbf{Q}_i^{-1}\mathbf{A}_i\mathbf{N}^{-1}\left(\sum_j \mathbf{A}_j^T\mathbf{Q}_j^{-1}\mathbf{A}_j\right)\mathbf{N}^{-1}\mathbf{A}_i^T\right] \\ & + \alpha^2 \text{trace}\left[\sum_j \mathbf{Q}_j^{-l}\mathbf{A}_j\mathbf{N}^{-1}\left(\sum_i \mathbf{A}_i^T\mathbf{Q}_i^{-1}\mathbf{A}_i\right)\mathbf{N}^{-2}\mathbf{A}_j^T\right] + \\ & + \alpha^2 \text{trace}\left[\sum_i \mathbf{Q}_i^{-l}\mathbf{A}_i\mathbf{N}^{-1}\left(\sum_j \mathbf{A}_j^T\mathbf{Q}_j^{-1}\mathbf{A}_j\right)\mathbf{N}^{-2}\mathbf{A}_i^T\right] \end{aligned}$$

$$+\alpha^4 \text{trace}\left[\sum_j \mathbf{Q}_j^{-1}\mathbf{A}_j\mathbf{N}^{-2}\left(\sum_i \mathbf{A}_i^T\mathbf{Q}_i^{-1}\mathbf{A}_i\right)\mathbf{N}^{-2}\mathbf{A}_j^T\right]\Bigg\}.$$

and

$$u_i = \sum_i \left(\boldsymbol{\varepsilon}_{\text{reg}i} - \alpha^2\mathbf{A}_i\mathbf{N}^{-1}\mathbf{x}\right)^T \mathbf{Q}_i^{-1}\left(\boldsymbol{\varepsilon}_{\text{reg}i} - \alpha^2\mathbf{A}_i\mathbf{N}^{-1}\mathbf{x}\right).$$

6.7.2.4 Numerical studies on VCE in ill-posed problems

In this section the example presented in Subsection 6.7.1 is considered again. First, we consider the stochastic model 1, in which three VCs for the VV, VH and HH gradients are estimated. The Gaussian noise of 1 mE and 1 cE is considered in this study. The following figures show the VC ratios during the VCE process and based on stochastic model 1.

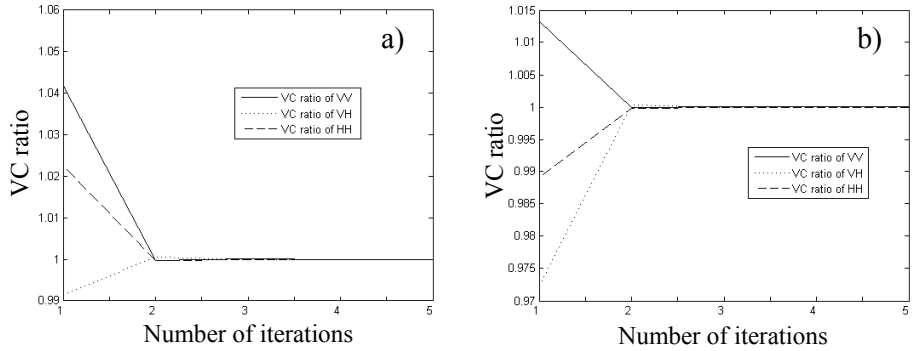

Figure 6.12. VC ratios during VCE process when noise level is (a) 1 mE and (b) 1 cE

Figure 6.12 shows that the ratios of the VCs of the VV and VH components are decreasing and increasing respectively before convergence. The VC ratio of HH components differs by the noise level. It should be stated that equivalents initial VCs are considered and they are equal to 1. Since the noise level is previously known it is expected that the VCs are close to 1. The deviation of the VCs from one could be due to the different structure of the gradient and how they are related to each other in a joint adjustment. The VC ratios presented in Figure 6.12 show clearly these deviations around 1 before convergence. The biased-corrected VC ratios during iterative VCE are presented in Figure 6.13. The figure has very similar pattern as Figure 6.12 but the magnitudes of the VC ratios are slightly different. Since the VCs are very close to their corresponding initial values they cannot considerably change the estimated error of the recovered gravity anomalies.

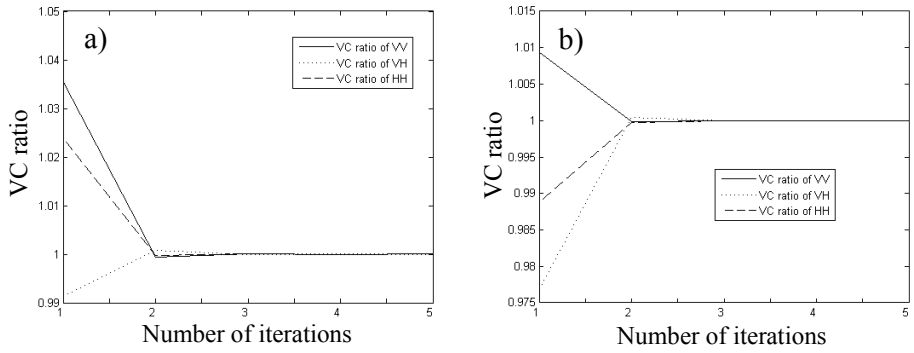

Figure 6.13. VC ratios during biased-corrected VCE process when noise level is (a) 1 mE and (b) 1 cE

The regularization parameter varies during iteration and VCE process. The following figure is provided to illustrate its variations.

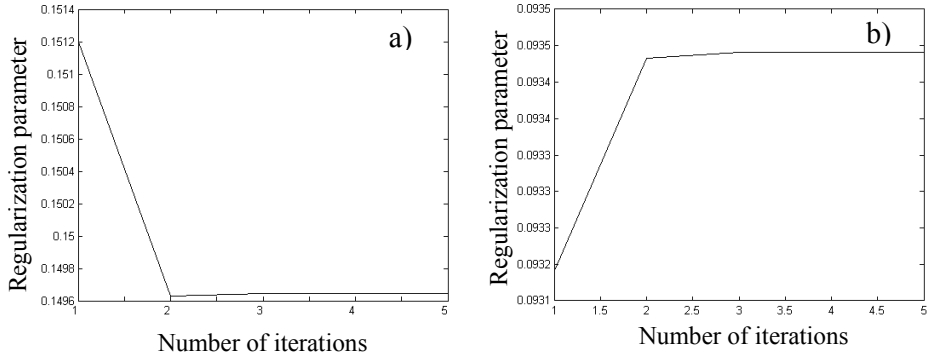

Figure 6.14. Regularization parameter variations during VCE process when noise level is (a) 1 mE and (b) 1 cE

Small changes are seen in the regularization parameter during the VCE and one may say that these changes are not significant. The regularization parameter is decreasing and increasing when the noise level is 1 mE and 1 cE, respectively. However, it converges to a certain value as the VCs do. The variation of this parameter in both biased-corrected VCE and ordinary VCE are more or less the same. Table 6.7 shows the magnitudes of the VCs and their biases and the biased-corrected VCs. The table illustrates the VCs estimated from the VCE process in which the noise level of the SGG data is 1 mE and 1 cE.

Table 6.7. VC, biases due to regularization and biased-corrected VCs

	1 mE		1 cE		1 mE	1 cE
	VC	Bias	VC	Bias	Biased-corrected VC	
$\hat{\sigma}^2_{VV}$	1.04	7.25	1.02	50.37	1.03	1.01
$\hat{\sigma}^2_{VH}$	0.99	3.99	0.97	17.16	0.99	0.98
$\hat{\sigma}^2_{HH}$	1.02	9.33	0.99	49.42	1.02	0.99

It is known the VCE balances the precision of the observables (the SGG data) and the estimated residual. In 1 mE noise level, the VCs of the VV and HH components

are overestimated than the VH. Although these overestimations and underestimations are not significant but they means that the estimated residual for each components do not agree with the initial one. The estimated biases due to regularization are considerable larger than the estimated VCs. Therefore the idea of estimating the biases and removing them form the VCs is not true in this case as the values of the VCs are unrealistically large and negative. One can conclude that the biased estimation of the VCs (bias due to regularization) is more realistic. The biased-corrected VCs are very close to the VCs and they differences may be insignificant.

The statistics of the differences between the true and recovered gravity anomalies after VCE are presented in Table 6.8. No improvements are seen in the recovered gravity anomalies during the VCE according to Table 6.8. The experiments have been repeated and in some cases, some small improvements were seen and in some not. In any case, very small changes were observed which are below 1 mGal level and insignificant.

Table 6.8. Statistics of errors of recovered gravity anomalies considering VCE and biased-corrected VCE. Unit: 1 mGal

		min	mean	max	std
Ordinary VCs	1 mE	-5.71	-0.00	6.74	2.11
	1 cE	-19.14	-0.04	16.87	5.16
Biased-corrected VCs	1 mE	-3.93	-0.00	4.51	1.58
	1 cE	-9.20	-0.03	8.10	2.93

Now, the stochastic model 2 in which one VC is estimated for each set of the gradients is considered. The following figure represents the VC ratios of each gravitational gradient during the VCE process.

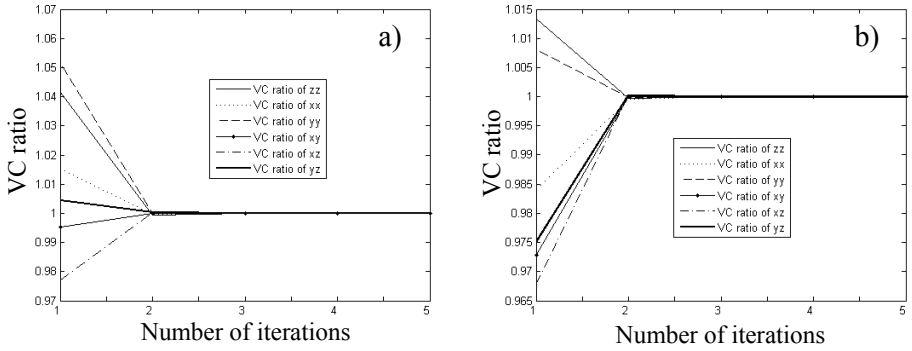

Figure 6.15. VC ratios during VCE process when noise level is (a) 1 mE and (b) 1 cE

Since the initial VCs are close to the true values small changes are seen the VC ratios. As the figure shows, some of the VCs change the behaviour when the noise level changes. The following figure illustrates the biased-corrected VCs ratios in two 1 mE and 1 cE noise levels.

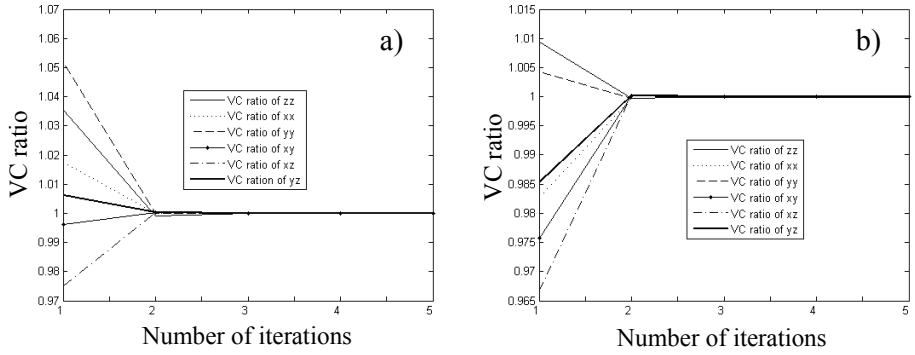

Figure 6.16. Biased-corrected VC ratios during VCE process when noise level is (a) 1 mE and (b) 1 cE

Figure 6.16 can be interpreted as that of Figure 6.15 and the explanation is not repeated here. However, as Figure 6.16 shows the ratios of the biased-corrected VCs are closer to 1 at the first iteration. It means that biased-correction process slightly improves the VCs. The following figure shows the behaviour of the regularization parameter during VCE.

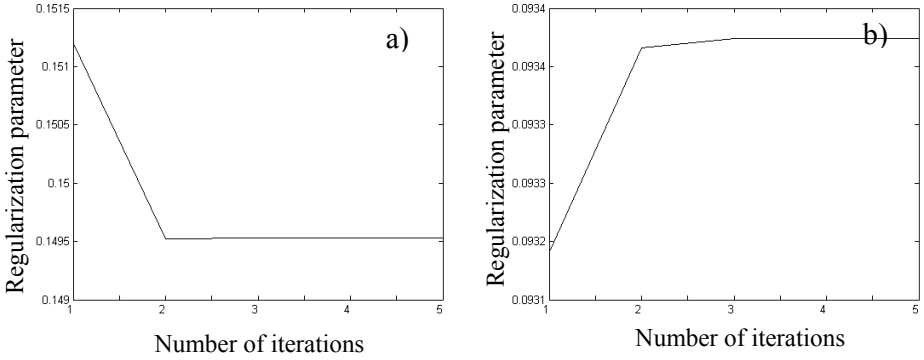

Figure 6.17. Regularization parameter variations during VCE process when noise level is (a) 1 mE and (b) 1 cE

The changes of the regularization parameter are very similar to that of the stochastic model 1. The regularization parameter converges as the VCs converge.

Table 6.9. VCs, biases due to regularization and biased-corrected VCs

	1 mE		1 cE		1 mE	1 cE
	VC	Bias	VC	Bias	Biased-corrected VC	
$\hat{\sigma}^2_{zz}$	1.04	5.29	1.01	50.43	1.03	1.01
$\hat{\sigma}^2_{xx}$	1.01	1.76	0.98	17.49	1.02	0.98
$\hat{\sigma}^2_{yy}$	1.05	1.23	1.01	15.60	1.05	1.00
$\hat{\sigma}^2_{xy}$	0.99	4.59	0.97	18.32	1.00	0.97
$\hat{\sigma}^2_{xz}$	0.98	3.03	0.97	27.82	0.97	0.97
$\hat{\sigma}^2_{yz}$	1.00	9.37	0.97	71.73	1.01	0.98

Again the table shows very small and insignificant difference between the cases where the standard formulas or biased-corrected ones are used to estimate the VCs. One might conclude that the standard formulas of the VCE can be used in solving the ill-posed as well. Table 6.10 shows insignificant improvement of re-weighting least squares solution by VCE.

Table 6.10. Statistics of errors of recovered gravity anomalies. Unit: 1 mGal

		min	mean	max	std
VC	1 mE	-5.75	-0.00	6.71	2.11
	1 cE	-19.14	-0.04	16.89	5.17
Biased-corrected VC	1 mE	-3.95	-0.00	4.58	1.59
	1 cE	-9.18	-0.03	8.10	2.94

6.7.3 Bias analysis of Sjöberg's VC estimator in an ill-posed problem

One reason to establish a biased-corrected VC estimator is to obtain positive values for the VCs. However, if the biased-corrected VCs come out negative, another way of VCE should be sought. It means that a non-negative method should be biased-corrected. One example of these non-negative estimators is the BQUNE which was presented in the beginning of this chapter. This part of thesis concentrates on BQUNE, or the Sjöberg (1984c) VC estimator, which was presented in Eq. (6.12). This estimator is directly involved with the residuals estimated from a least-squares adjustment solution. The beauty of this estimator is its simplicity to use, as Eshagh (2005a) and (2005b) and Eshagh and Sjöberg (2008b) numerically presented the BQUE and BQUNE (Sjöberg estimator) are equivalent if the VCs come out positive. γ_i in this estimator is a projector that separates the residual vectors according to the pre-scribed stochastic model. In the following the bias of Sjöberg's VC estimator is presented.

Proposition 6.7 *The bias of Sjöberg's VC estimator is:*

$$\text{Bias}\left(\sigma_i^2\right)=\frac{\alpha^4\mathbf{x}^T\mathbf{A}^T\mathbf{N}^{-1}\mathbf{F}_i\mathbf{H}\mathbf{F}_i^T\mathbf{N}^{-1}\mathbf{A}\mathbf{x}}{\text{trace}\left(\mathbf{H}\mathbf{P}_i\right)}$$

where

$$\mathbf{P}_i=\mathbf{F}_i\left(\mathbf{I}-\mathbf{A}_{\text{reg}}^0\right)\mathbf{Q}_i'\left(\mathbf{I}-\mathbf{A}_{\text{reg}}^0\right)^T\mathbf{F}_i^T$$

Proof. Equation (6.8), which is the main part of Sjöberg's estimator, will have the following form (see Eq. 6.44)**:**

$$\boldsymbol{\gamma}_i=\alpha^2\mathbf{F}_i\mathbf{A}\mathbf{N}^{-1}\mathbf{x}+\mathbf{F}_i\left(\mathbf{I}-\mathbf{A}_{\text{reg}}^0\right)\boldsymbol{\varepsilon}, \tag{6.53}$$

Consider the following general quadratic VC estimator

$$\text{trace}\left(\mathbf{H}\mathbf{P}_i\right)\sigma_i^2=\boldsymbol{\gamma}_i^T\mathbf{H}\boldsymbol{\gamma}_i. \tag{6.54}$$

substituting Eq. (6.53) into the right hand side of Eq. (6.54) becomes:

$$\boldsymbol{\gamma}_i^T \mathbf{H}\boldsymbol{\gamma}_i = \alpha^4 \mathbf{x}^T \mathbf{A}^T \mathbf{N}^{-1}\mathbf{F}_i^T \mathbf{H}\mathbf{F}_i \mathbf{N}^{-1}\mathbf{A}\mathbf{x} + \boldsymbol{\varepsilon}^T \left(\mathbf{I} - \mathbf{A}_{\text{reg}}^0\right)^T \mathbf{F}_i^T \mathbf{H}\mathbf{F}_i \left(\mathbf{I} - \mathbf{A}_{\text{reg}}^0\right)\boldsymbol{\varepsilon}, \quad (6.55a)$$

or

$$\boldsymbol{\gamma}_i^T \mathbf{H}\boldsymbol{\gamma}_i = \alpha^4 \mathbf{x}^T \mathbf{A}^T \mathbf{N}^{-1}\mathbf{F}_i^T \mathbf{H}\mathbf{F}_i \mathbf{N}^{-1}\mathbf{A}\mathbf{x} + \text{trace}\left(\mathbf{H}\mathbf{F}_i \left(\mathbf{I} - \mathbf{A}_{\text{reg}}^0\right)\boldsymbol{\varepsilon}\boldsymbol{\varepsilon}^T \left(\mathbf{I} - \mathbf{A}_{\text{reg}}^0\right)^T \mathbf{F}_i^T\right). \quad (6.55b)$$

Substituting Eq. (6.55b) into Eq. (6.54) and taking statistical expectation from both sides one obtains:

$$E\left\{\sigma_i^2\right\} = \sigma_i^2 + \alpha^4 \frac{\mathbf{x}^T \mathbf{A}^T \mathbf{N}^{-1}\mathbf{F}_i^T \mathbf{H}\mathbf{F}_i \mathbf{N}^{-1}\mathbf{A}\mathbf{x}}{\text{trace}\left(\mathbf{H}\mathbf{P}_i\right)}. \quad (6.56)$$

The second term in right hand side of Eq. (6.56) is nothing else than the bias of the Sjöberg's VC estimator due to regularization. It should be reminded that the estimator is unbiased if $\mathbf{H} = \mathbf{P}_i^-$ and the bias of the estimator is just due to regularization.

Type of the stochastic model is introduced in the formula by the projection operator $\mathbf{F}_i$. It will have the same structure as Eqs. (6.34a)-(6.34c) if the stochastic model 1 is chosen and Eqs. (6.36a)-(6.36e) is the stochastic model 2 is selected.

6.7.4 Biased-corrected Sjöberg's VC estimator

Sjöberg's VC estimator or BQUNE which is a non-negative estimator may yield negative VC if the bias of the regularization is larger than the VCs. In order to solve this numerical problem the biased-corrected version of Sjöberg's VC estimator are proposed. This estimator is:

$$\hat{\sigma}_i^2 = \frac{\boldsymbol{\gamma}_i^T \mathbf{P}_i^- \boldsymbol{\gamma}_i}{\text{trace}(\mathbf{P}_i^- \mathbf{P}_i)}, \quad (6.57a)$$

where

$$\boldsymbol{\gamma}_i = \mathbf{F}_i \left(\boldsymbol{\varepsilon}_{\text{reg}} - \alpha^2 \mathbf{A}\ \mathbf{N}^{-1}\mathbf{x}\right), \quad (6.57b)$$

$$\mathbf{P}_i = \mathbf{F}_i \left(\mathbf{I} - \mathbf{A}_{\text{reg}}^0 - \alpha^2 \mathbf{A}\mathbf{N}^{-2}\mathbf{A}^T \mathbf{Q}^{-1}\right)\mathbf{Q}_i' \left(\mathbf{I} - \mathbf{A}_{\text{reg}}^0 - \alpha^2 \mathbf{A}\mathbf{N}^{-2}\mathbf{A}^T \mathbf{Q}^{-1}\right)^T \mathbf{F}_i^T. \quad (6.57c)$$

Using Eq. (6.57a)-(6.57c) one can make sure to obtain positive values for the biased-corrected VCs.

Chapter 7

The polar gaps

7.1 Introduction

Polar orbits are suitable orbits for applications of dynamic satellite geodesy because of observing geodetic data with a global coverage. However, the sun-synchronized orbits are preferred for low Earth orbiting satellites. If the inclination of low orbiters is not equal to 90°, then the polar areas are not covered with satellite observations. If a quadrature integral formula is used to compute the geopotential coefficients, a global coverage of SGG data is required. However, the solution of the geopotential coefficients is biased due to the polar gaps.

The polar gaps problem was described by Rummel et al. (1993) and Koop (1993) with concentration on determining the spherical harmonic coefficients (SHCs) using the least-squares method. Sneeuw and van Gelderen (1997) also studied this problem and explained why the near-zonal harmonics are weakly determined in geopotential modeling. They have considered both space-wise and time-wise approaches in their discussions. Tscherning et al. (2000) investigated the polar gaps problem using least-squares collocation. They concluded that the inclusion of gravity data in the gaps will improve the estimates of the geopotential coefficients, for which the quality depends on the availability of global data. Tscherning (2001b) mentioned that the near-zonal harmonics were typically two times larger than the other harmonics when the poles were not covered. He found that if ground gravity data is used to fill-in the gaps, the data should have a resolution twice the one of T_{zz} also concluded that the available airborne and sub-marine gravimetry data would not improve GOCE solution if data from CHAMP and GRACE are available. Pail et al. (2001) used an orthonormalization scheme to orthonomalize the base functions with reference to Hwang (1991) and (1993). They recovered the geopotential coefficients without filling-in the gaps. Rudolph et al. (2002) considered the polar gaps filling-in problem from the SGG data, they conclude that $1^\circ \times 1^\circ$ gravity anomaly blocks can be recovered. They also mentioned that the error of the recovered gravity anomalies reduced from 3 to 10-12 mGal from the rim to the centre of gap. They found also the cross-track direction contain the most information. Metzler and Pail (2005) presented a spherical cap regularization method considering an analytical function, which is defined in the polar region using an EGM. Simons and Dahlen (2006) used the

spherical Slepian function for the polar gaps, and they proposed a new method that expands the source field in terms of a truncated basis set of spherical Slepian function and compared it a with least-squares method. Siemes et al. (2007) incorporated three strategies: augmenting data in the gaps, introducing a priori information for regularization and the Slepian approach again.

In this chapter, it is investigated which parts of the gravitational signal are not well estimated in the spectral solutions of the GBVPs, and it will also be studied how to estimate the gravity anomaly in these areas by direct downward continuation of the SGG data.

7.2 Loss of power of gravitational signal due to polar gaps in SGG

In the integral solutions of the GBVPs, combinations of the gravitational gradients are considered. The polar gaps destroy the unbiasedness of the solution, and some parts of the gravitational signal are weakly determined. For better explanation Figure 7.1 shows a schematic shape of a sphere σ with gaps σ_{N} and σ_{S} (the NPG and the SPG, respectively). If this sphere is the mean sphere of the satellite orbit, the polar gaps are those parts of this sphere, which are not covered by satellite passes (and data).

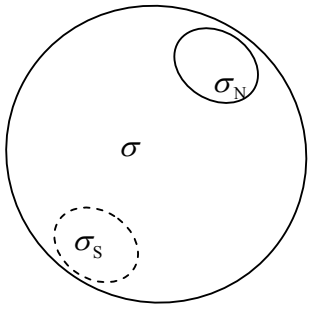

Figure 7.1. Polar gaps

The loss of power of the gravitational signal due to polar gaps was investigated by Sneeuw and Gelderen (1997) by a simple integral approach on the VV gradient (T_{zz}). They found that the zonal and the near zonal geopotential coefficients are weakly estimated because of the polar gaps. Mathematically this idea can be expressed by Eq. (7.1), which is a simple global spherical harmonic analysis of any function *f(Q)* on the sphere σ.

$$t_{nm} = \frac{1}{4\pi} \iint_{\sigma} f(Q) Y_{nm}(Q) d\sigma \ , \tag{7.1}$$

where Q is the integration point and t_{nm} are the SHCs of the function *f(Q)*. The following quadrature estimator of the geopotential coefficients is considered:

$$\hat{t}_{nm} = \frac{1}{4\pi} \iint_{\sigma - \sigma_{\mathrm{N}} - \sigma_{\mathrm{S}}} f(Q) Y_{nm}(Q) d\sigma \ . \tag{7.2}$$

In the case of SGG, the NPG and SPG have the same size σ_0, i.e. $\sigma_{\mathrm{N}} = \sigma_{\mathrm{S}} = \sigma_0$. According to Eq. (7.2) the spectral solutions of the GBVPs can be written:

$$\hat{t}_{nm} = \frac{R^3}{4\pi GM\,(n+1)(n+2)}\left(\frac{r}{R}\right)^{n+3} \iint_{\sigma-2\sigma_0} T_{zz}(Q)\,Y_{nm}(Q)\,d\sigma\,, \tag{7.3a}$$

$$\hat{t}_{nm} = \frac{R^3}{4\pi GM(n+1)(n+2)}\left(\frac{r}{R}\right)^{n+3} \iint_{\sigma-2\sigma_0} \left[T_{xz}(Q)E_{nm}(Q)+T_{yz}(Q)F_{nm}(Q)\right]d\sigma\,, \tag{7.3b}$$

and

$$\hat{t}_{nm} = \frac{R^3}{4\pi GM\,(n-1)n(n+1)(n+2)}\left(\frac{r}{R}\right)^{n+3} \iint_{\sigma-2\sigma_0} \Big[\left(T_{xx}(Q)-T_{yy}(Q)\right)G_{nm}(Q)+$$
$$+2T_{xy}(Q)\,H_{nm}(Q)\Big]d\sigma\,. \tag{7.3c}$$

The relative error in the geopotential coefficients is $\varepsilon_{nm} = \left(\hat{t}_{nm} - t_{nm}\right)\big/ t_{nm}$.

In order to study the loss of power of the gravitational signal numerically, the EGM96 is used to generate the gradients at satellite level (250 km) with $0.5^\circ \times 0.5^\circ$ resolution. Equations (7.3a)-(7.3c) are used to estimate the geopotential coefficients considering 7° polar gaps in the coverage of SGG data. The NPG and SPG are the regions at latitudes above 83° and below -83°, respectively.

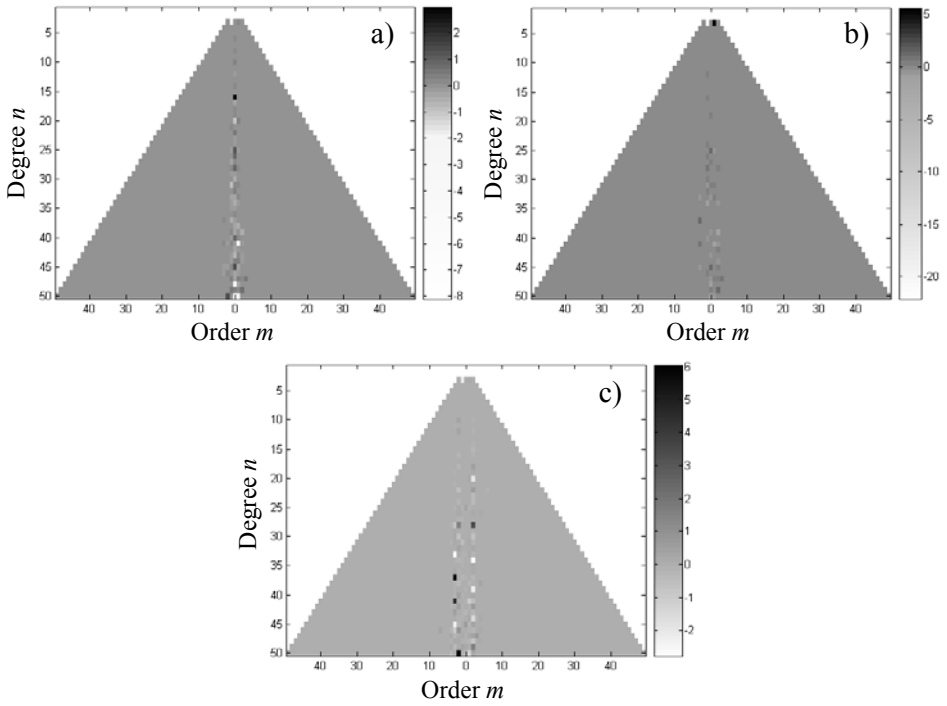

Figure 7.2. Relative error of geopotential coefficients obtained from (a) VV, (b) VH and (c) HH GBVPs

Figure 7.2 shows the triangle spectra of the sine and cosine coefficients below degree and order 50. The left part of each triangle shows the cosine and the right one the sine

geopotential coefficients. The figure shows that the near zonal coefficients are influenced by the polar gaps. It can be seen that the VH gradients are the most influenced gradients. The wedge shape power loss revealed for the VV and HH solutions is the narrowest and widest, respectively. It means that in the VV solution the closer coefficients to the zonal coefficients are weakly determined with respect to that in the HH solution.

7.3 The gravitational gradients around polar gaps

In order to see the significant gradients around the gaps, the gravity anomalies are generated in the NPG and SPG (using the EGM96 to degree and order 360) and Eq. (7.4) is used to generate the gradients at 250 km level. The gradients are computed in the local north oriented frame with $1^\circ \times 1^\circ$ resolution. Figure 7.3 illustrates the produced gravity anomalies in the gaps. The maximum, minimum, mean and standard deviation of the gravity anomaly is 58.80, -79.44, -8.59 and 20.68 mGal, respectively in the SPG, and 46.86, -25.06, 8.95 and 11.14 mGal in the NPG. The figure and the presented statistics show smoother pattern of the gravity anomaly in the NPG than the SPG.

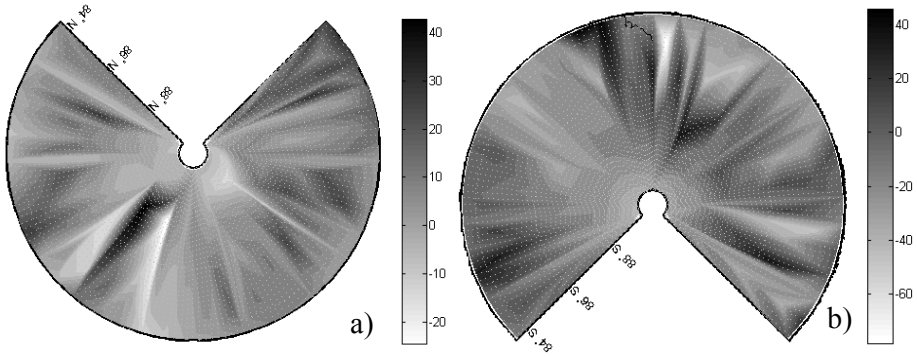

Figure 7.3. Generated gravity anomalies in (a) NPG and (b) SPG. Unit: 1 mGal

Here, we take advantage of the compartment gridding scheme (Heiskanen and Moritz 1967, p. 127, Section 3-2) for recovering the gravity anomaly in the polar gaps. First, we have to investigate up to which limited area around the polar gaps the SGG data is significant. In order to determine this area, the following gradient estimator is used:

$$\tilde{T}_{ij}(P) = \frac{R}{4\pi} \iint_{\sigma_0} S_{ij}(r,\psi) \Delta g^*(Q) d\sigma, \quad P \subset \sigma - \sigma_0 \; ; \; Q \subset \sigma_0 \; , \quad (7.4)$$

where $i, j = x, y, z$ are the derivative symbols and $\Delta g^*(Q)$ is the gravity anomaly at seal level and the integration point Q.

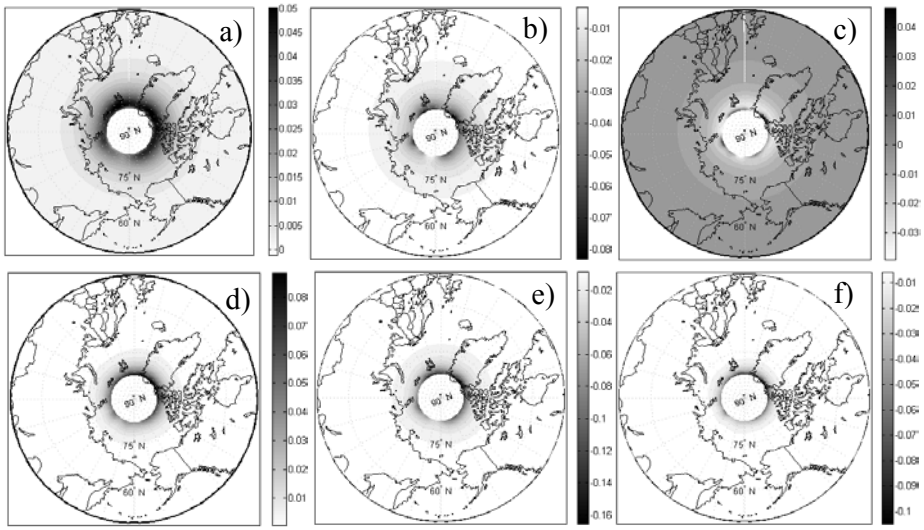

Figure 7.4. Generated gravitational gradients (a) T_{xx}, (b) T_{yy}, (c) T_{zz}, (d) T_{xy}, (e) T_{xz} and (f) T_{yz} at 250 km level from gravity anomalies in NPG. Unit: 1 E

Figures (7.4a)-(7.4c) demonstrate that T_{xx}, T_{yy} and T_{zz} are insignificant at latitudes below 70° around the NPG. T_{xy} and T_{xz} are insignificant at latitudes below 75° and T_{yz} is negligible at latitudes below 80°. Figure 7.5 shows that T_{xx}, T_{yy} and T_{zz} are considerably small at latitudes above -70° around the SPG. The gradients T_{xy}, T_{xz} and T_{yz} at latitudes above 75° are insignificant.

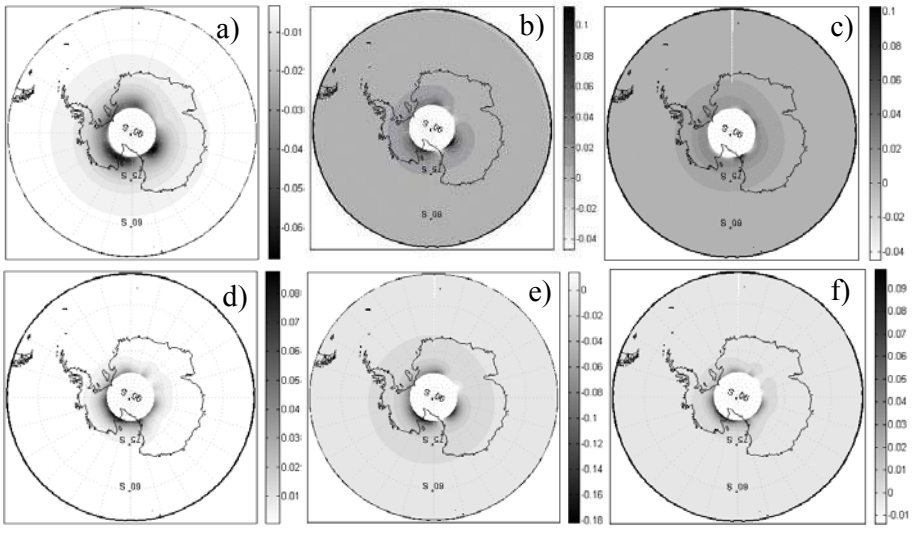

Figure 7.5. Generated gravitational gradients (a) T_{xx}, (b) T_{yy}, (c) T_{zz}, (d) T_{xy}, (e) T_{xz} and (f) T_{yz} at 250 km level from gravity anomalies in SPG. Unit: 1 E

7.4 Gravity field recovery in the polar gaps

In order to determine gravity anomaly in the polar gaps from the SGG data, Eq. (7.4) can be solved reversely. It is assumed that the truncation error (from region $\sigma - \sigma_0$) of Eq. (7.4) has been removed. The solution of such an inversion process will be sensitive to the noise contaminated with the gradients. Here a Gaussian noise level of 1 mE is generated (see Figure 7.6) and added to each gradient to compare the recovery processes of the gravity anomaly. The system of equations related to the inversion of each gradient is stabilized and solved by the Tikhonov regularization method and the GCV is used to estimate its regularization parameter. The recovered gravity anomalies are compared with those computed from the EGM96 (the true values). The errors of the recovered gravity anomalies can be a criterion for testing the quality of inversion.

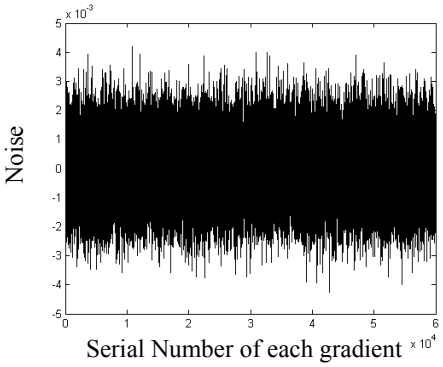

Figure 7.6. Generated Gaussian noise of 1 mE. Unit: 1 E

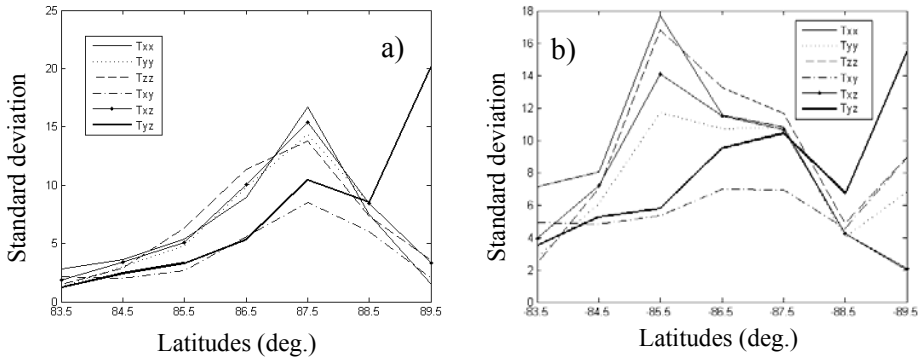

Figure 7.7. Errors of recovered gravity anomalies in (a) NPG and (b) SPG. Unit: 1 mGal

Figure 7.7 represents errors of the recovered gravity anomalies from the rim to the centre of the NPG and the SPG. The figure shows that the errors at latitudes below 84.5° are within 5 mGal. The errors of recovery from T_{xx}, T_{yy}, T_{zz} and T_{xz} are more or less in the same level. In the NPG, the errors are increasing to the latitude 87.5° and decreasing after 87.5°. Figure 7.7a shows that T_{yz} is better than T_{xx}, T_{yy}, T_{zz} and T_{xz} at latitudes below 87.5° and it is the worst at 89.5°. T_{xy} seems to be the best gradient in the NPG. According to Figure 7.7b, the errors considerably differ in the SPG. The errors are similar and more or less in the same level for the recovered gravity anomalies from T_{xx}, T_{yy}, T_{zz} and T_{xz}. T_{xz} and T_{xx} seem to be better than the

others at the latitude -89.5°. T_{yz} is the worst gradient at -89.5°, but it is better than the others at latitudes below -78.5° except for T_{xy} which is the best at latitudes between -84.5° and -88.5°. Figure 7.7 cannot give a general conclusion about the quality of the inversions and suitability of the gradients. Table 7.1 presents conclusive statistics of the total errors of each gradient. The table shows that T_{xx}, T_{zz} and T_{xz} have more or less the same capability in both NPG and SPG. T_{yz} is better than T_{yy}, and T_{xy} is the best gradient.

Table 7.1. Statistics of total errors of recovered gravity anomalies in polar gaps. Unit: 1 mGal

	NPG				SPG			
	Min	mean	max	std	min	mean	max	std
$T_{xx} \rightarrow \Delta g^*$	-31.63	0.03	25.92	7.14	-33.36	0.01	38.26	10.70
$T_{yy} \rightarrow \Delta g^*$	-34.71	-0.06	27.38	6.60	-28.96	0.00	28.41	7.95
$T_{zz} \rightarrow \Delta g^*$	-39.00	-0.03	31.64	6.98	-32.29	-0.01	28.23	10.14
$T_{xy} \rightarrow \Delta g^*$	-17.96	0.15	18.62	4.12	-15.09	0.09	16.00	5.50
$T_{xz} \rightarrow \Delta g^*$	-36.00	-0.04	28.45	6.98	-30.58	0.01	28.14	9.02
$T_{yz} \rightarrow \Delta g^*$	-22.25	-0.37	18.19	5.35	-16.82	0.17	23.41	6.63

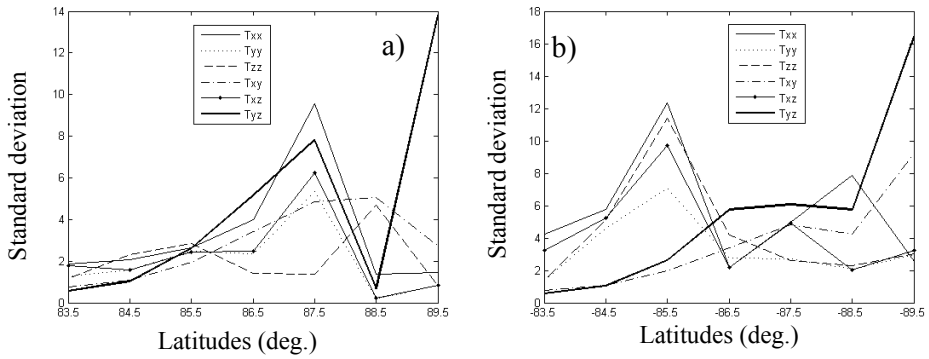

Figure 7.8. Estimated error of recovered gravity anomalies in (a) NPG and (b) SPG. Unit: 1 mGal

Figure 7.8 shows the estimated error (propagated random error) of recovered gravity anomalies in the gaps. The general pattern of the figure is similar to that of Figure 7.7. In the NPG, the estimated errors are smaller than the others at latitudes below 85.5° except for T_{zz}. The errors are increasing to the latitude 87.5° and they are decreasing after 87.5° except for T_{xy} and T_{zz}. T_{yz} is the worst gradient at the latitude 89.5°. Figure 7.9b can be interpreted in a similar way. It shows that the errors of the recovery, from T_{zz}, T_{xx}, T_{yy} and T_{xz}, have similar pattern for the latitudes above -86.5° and larger than those from T_{xy} and T_{yz}. T_{zz} and T_{yy} seem to be better than the others in propagating the random errors. In average, the errors are 3.29, 2.01, 2.09, 2.83, 2.22, 4.53 mGal for the recovered gravity anomalies from T_{xx}, T_{yy}, T_{zz}, T_{xy},

T_{xz} and T_{yz} , respectively in the NPG, and 5.70, 3.36, 4.28, 3.64, 4.37, 5.45 mGal in the SPG.

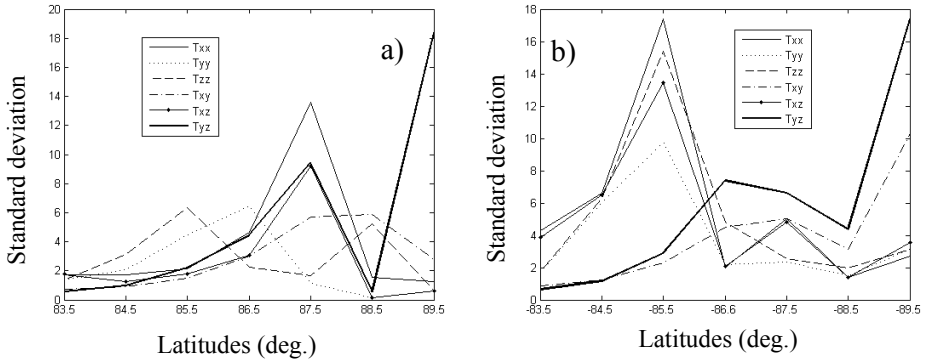

Figure 7.9. Errors of biased-corrected recovered gravity anomalies in (a) NPG and (b) SPG. Unit: 1 mGal

The bias of the regularization can be estimated and removed from the recovered gravity anomalies and the result will be the biased-corrected gravity anomalies. Figure 7.9 shows the errors of the biased-corrected gravity anomalies and some improvements in the recovered quantities. Table 7.2 shows the statistics of errors of the biased-corrected gravity anomalies. It shows that the bias-correction improves the result about 2 mGal in inversion of T_{xy} . In general, it can be stated that the bias-correction process improves the results of inversion of all the SGG data about 3 mGal.

Table 7.2. Statistics of total errors of biased-corrected recovered gravity anomalies in polar gaps. Unit: 1 mGal

	NPG				SPG			
	Min	mean	max	std	min	mean	max	std
$T_{xx} \rightarrow \Delta g^*$	-19.46	0.03	23.91	4.80	-33.54	0.01	39.44	8.48
$T_{yy} \rightarrow \Delta g^*$	-14.19	-0.05	9.95	3.30	-21.02	-0.00	19.07	5.22
$T_{zz} \rightarrow \Delta g^*$	-11.58	-0.03	15.44	3.51	-32.23	-0.01	29.48	7.50
$T_{xy} \rightarrow \Delta g^*$	-9.56	0.13	10.91	2.69	-8.28	-0.00	11.65	2.91
$T_{xz} \rightarrow \Delta g^*$	-16.45	-0.04	17.24	3.35	-26.24	0.00	28.62	6.98
$T_{yz} \rightarrow \Delta g^*$	-23.35	-0.32	16.73	4.31	-13.07	-0.00	19.71	4.27

7.5 Joint inversion of SGG data for recovering gravity anomaly in polar gaps

Increasing the number of observations or over-determination suppresses noise of data. In this section, we use all types of SGG data and construct one system of equations for the inversion. The system is regularized using the Tikhonov regularization by assuming that the data are contaminated with 1 mE noise.

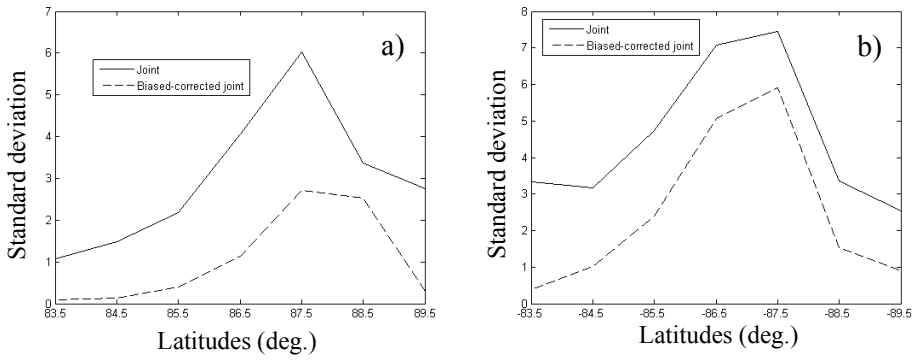

Figure 7.10. Errors of recovered gravity anomalies by joint and biased-corrected joint inversion in (a) NPG and (b) SPG. Unit: 1 mGal

Figure 7.10 shows the errors of the recovered and biased-corrected recovered gravity anomalies. In the figure "Joint" means the errors of recovered gravity anomalies from simple joint inversion and "biased-corrected joint" means errors of those recovered from the biased-corrected joint inversion. By comparing Figure 7.8 with Figure 7.10 one may conclude that the joint inversion of the SGG data performs better than inversion of each single gradient. Figure 7.10 shows that the joint inversion is even better than the biased-corrected recovery from the inversion of each single gradient; see Figure 7.9. Figure 7.10 presents that the errors of biased-corrected gravity anomalies are smaller than those of the simple joint inversion. One may conclude that the joint inversion performs well in rim of the gaps. The statistics of the errors of the joint inversions are presented in Table 7.3. The total error of biased-corrected joint inversion for the NPG and SPG can reach to 1 and 3 mGal, respectively if the noise of the SGG data is 1 mE.

Table 7.3. Statistics of errors of joint recovered and biased-corrected joint recovered gravity anomalies from SGG data in polar gaps. Unit: 1 mGal

	method	min	mean	max	std
NPG	Joint	-14.87	-0.02	12.16	2.84
	Biased-corrected joint	-4.64	-0.01	5.09	1.12
SPG	Joint	-12.51	0.01	15.03	4.70
	Biased-corrected joint	-11.74	0.00	12.04	2.88

Table 7.4 represents that the estimated errors of the recovered gravity anomalies are equal at latitudes below 88.5° in the NPG and above -88.5° in the SPG. The reason could be due to the stable of system of equations in these regions

Table 7.4. Estimated errors of recovered gravity anomalies from joint inversion of SGG data. Unit: 1 mGal

latitude	∓83.5°	∓84.5°	∓85.6°	∓86.5°	∓87.5°	∓88.5°	∓89.5°
SPG	0.27	0.61	1.35	2.61	4.12	1.88	1.63
NPG	0.27	0.61	1.35	2.61	4.11	3.33	0.63

Chapter 8

Conclusions and future works

8.1 Conclusions

In Chapter 2 the simplified version of the geopotential force acting on a satellite was used to study the contribution of orbital perturbations in the satellite gravity gradiometry (SGG) data. It was found that T_{xx} , T_{yy} and T_{xy} are more influenced by the perturbations than the other gradients. In general, the perturbations affect the gradients within 2 E. Perturbation of the satellite track azimuth influences the gradients within 0.2 E. Numerical studies on the new expressions of the gravitational gradients and the tensor spherical harmonics verify the correctness of the formulas. It was illustrated that the vertical-horizontal (VH) solution of the gradiometric boundary value problems (GBVPs) is better than the other solutions in recovering the gravitational field from SGG data. Considering 1 % relative error in degree variances of the solution, an Earth gravitational model (EGM) to degree and order 313 can be computed by solving the VH solution of GBVPs with $5'\times5'$ noise-free SGG data. This number will be 288 and 295 for the VH and the horizontal-horizontal (HH) solutions, respectively. The degree of resolution is 218, 218 and 202 for the vertical-vertical (VV), VH and HH solutions, respectively, if the resolution of the data is $5'\times5'$. According to Institute of Electrical and Electronics Engineers (IEEE), double-precision environment, the maximum degree of achievable EGM is 358 in average (which is very optimistic).

In Chapter 3 we have investigated different ways of formulating the topographic effect (TE) and atmospheric effect (AE) in spherical harmonics. The effects have been computed and presented for an imaginary satellite at 250 km level over Fennoscandia and Iran. Computations show that the TE is quite significant on the SGG data and should be considered in modeling of the gravity field and in the downward continuation process. The maxima of TE are 3 and 1 E in Iran and Fennoscandia based on the spherical harmonic expansion of topography to degree 360. A simple study on the lateral density variation (LDV) of the topographic masses was done, which shows very significant effects on the SGG data. The lateral density variation effect (LDVE) is 116 mE in Iran and 56 mE in Fennoscandia. Different atmospheric density models (ADMs) were investigated, and a new model was proposed as NKTHA, which is better than the other analytical ADMs. Numerical studies show that

the maximum AE is within 5 mE in these regions based on this ADM. The largest effects occurs on V_{zz} , and the least on V_{xy} .

The topographic and atmospheric biases on the gravitational gradients were also formulated in Chapter 3. The important matter in this formulation is the divergence of the spherical harmonic series. If this series is not convergent, the downward continued atmospheric potential is not reliable. The downward continuation using a divergent series is theoretically wrong and definitely the obtained numbers are wrong as well. However, it has been proved by Sjöberg (2007) that the TE until third-order approximation is convergent and can be continued down to sea level without any problem. Based on this philosophy we presented the topographic bias on the downward continued gravitational gradients to sea level. We found simple formulas for the topographic bias on the diagonal elements of the gravitational tensor and we proved that there is no topographic bias on the non-diagonal elements of the tensor. These elements can easily be continued downward to sea level without considering the TE.

Chapter 4 presented the relations between the gravitational gradients and gravity anomaly. The idea is to modify the extended Stokes formula using the least-squares modification (LSM) method. In this respect, a general estimator was presented for the disturbing potential. The elements of the system of equations, from which the modification parameters are estimated, were derived mathematically. For modifying the second-order radial derivative (SOD) of the extended Stokes formula, the coefficient matrix remains the same with that of original extended Stokes' formula (the disturbing potential), if the derivative of modification parameter is estimated directly. In such a case the right hand side of the system of equations will change. In order to generate the truncation coefficients of the SOD of the extended Stokes function (ESF) and the original ESF, the spectral form of the truncation errors is recommended. Numerical studies on estimating the disturbing potential at satellite level show that the resolution of the data is not very significant (below cm level) for all types of the LSM. It will be within 1 mE level for the SOD of the ESF as well. Modification of the VH gravitational gradients is very similar to modification of the Vening-Meinesz formulas. The difference is related to the spectra of their kernel functions. The truncation error of these formulas is very similar to that presented by Hagiwara (1973). In Chapter 4 we presented a general estimator for the VH gradients. The elements of the system of equations for estimating the modification parameters using the LSM methods are derived. The same process was repeated for the HH gradients as well.

According to the general estimators, which were presented for VV, VH and HH gradients, it is easy to validate the diagonal elements of the gravitational tensor. The Laplacian operator yields that $T_{zz}(P)$ is equal to $-T_{xx}(P)-T_{yy}(P)$, and therefore, by estimating $T_{zz}(P)$, the minus of the sum $T_{xx}(P)+T_{yy}(P)$ is validated as well. Also we showed that $T_{xx}(P)-T_{yy}(P)$ can be validated by the LSM of the HH gradients of the extended Stokes formula. Consequently, $T_{xx}(P)$ and $T_{yy}(P)$ can easily be estimated from the previous combination. No problem is observed for validating the VH gradients, as they can be estimated separately.

In Chapter 5 the emphasis was on determining the gravity anomaly from SGG data. The second-order partial derivatives of the extended Stokes formula were inverted in this respect. The singularity analysis of their isotropic kernels was done for the case where the integration and computation points coincide. The analysis showed that the kernel functions $S_{zz}(r,0)$, $S_{xx}(r,0)$ and $S_{yy}(r,0)$ are not singular and $S_{xz}(r,0)$, $S_{yz}(r,0)$, $S_{xy}(r,0)$ are equal to zero. The numerical studies on the inversions (using Tikhonov regularization) show that the GCV is slightly better than the L-curve method of estimating the regularization parameter. The condition numbers of the coefficient matrices of the integrals are in the same level when the resolution of SGG data are $0.5^\circ \times 0.5^\circ$ and $0.25^\circ \times 0.25^\circ$ for recovering a grid of $1^\circ \times 1^\circ$ gravity anomaly in Fennoscandia. The system of equations is considerably unstable for estimating $0.5^\circ \times 0.5^\circ$ gravity anomalies from $0.25^\circ \times 0.25^\circ$ SGG data, but the recovery is possible if the system of equations is well-regularized. The condition number of the coefficient matrices $\mathbf{A}_{xx}$, $\mathbf{A}_{yy}$, $\mathbf{A}_{zz}$ and $\mathbf{A}_{xz}$ are at the same level except for $\mathbf{A}_{xy}$ and $\mathbf{A}_{yz}$, for which the condition numbers are smaller. However, the simulation studies show that the recovered gravity anomaly from these gradients is not as good as those from the others. The small gradient magnitudes might be a reason for this phenomenon, as by adding the noise most part of the gradient is destroyed. In general, one can conclude that for local gravity field determination T_{zz} is the best gradient. After that T_{xx}, T_{yy} and T_{xz} are more suited than the rest. Inversion of the Eötvös type gradients T_{xx} - T_{yy} and $2T_{xy}$ show better performance. One reason of this could be over-determination and another is the change of the integral kernel. However, numerical studies show that the over-determination is more significant than the kernel. The system of equations related with T_{zz} and T_{yz} propagates the noise less than the others. In general, the errors are larger in margins of the area under investigation. The propagated random errors are decreasing from north to south for T_{xx}, T_{yy}, T_{zz} and T_{xz} and increasing for T_{yz}. The numerical study on estimating the a-posteriori variance factor and its bias shows that removing the estimated bias due to the regularization cannot improve the estimates of the a-posteriori variance factor. Bias-correction procedure on the recovered quantity can improve the result about 3 mGal. Since the integral kernels are not isotropic (except for T_{zz}), the direct inversion of each gradient was studied. It is not possible to formulate the truncation error of non-isotropic kernels in spectral form. Therefore it was proposed to transfer the truncation integral formula to space domain instead of spectral domain; although this error will be contaminated with discretization error. Numerical studies on the error, based on the EGM96 to degree and order 360, show that the truncation error is slightly dependent on the resolution of the SGG data. If the grid resolution of unknowns increases as well, the error changes slightly. The truncation error of the integrals is within 1 cE. The numerical studies show that it is not possible to achieve gravity anomaly with 1 mGal accuracy by inverting a single gradient unless the resolution of the grid of gradients increase considerably.

Chapter 6 deals with the optimal combination of the integral solutions of the GBVPs. The variance component estimation (VCE) concept is used in a non-standard way to update the weight of observations. Numerical studies show that estimating one degree-order variance component (DOVC) for each type of observation is better than

the case where the DOVC is estimated for each integral solution. The modified best quadratic unbiased non-negative estimation of the variance components is not practical, as large matrices are involved in the combination. Construction of the condition equations in the simplest way is recommended. The formulas presented in this study are well-suited for the GBVPs. For combining solutions of other boundary value problems, we have to reconstruct the mathematical models.

Fennoscandia (latitudes from 55° to 70°, longitudes between 5° and 30°) was used as a test area for the joint inversion study. A $1^\circ \times 1^\circ$ grid of gravity anomalies was recovered from $0.5^\circ \times 0.5^\circ$ SGG data. The coefficient matrix of the simple joint inversion of the SGG data has larger condition number than the inversion of each gradient (except for T_{xy} and T_{yz}, which have condition number in the same level). The estimated error of the recovered gravity anomalies are increasing and decreasing from the northern to southern part of Fennoscandia for noise of 1 mE and 1 cE, respectively. This study shows that the gravity anomaly can be recovered within 2 and 5 mGal at 1 mE and 1 cE noise level, respectively. The bias-correction procedure improves these numbers to 2 and 3 mGal, respectively. It is expected to reach to 1 mGal accuracy, if the resolution of the SGG data increases.

A large system of equations is constructed for the joint inversion of five independent gradients of the gravitational tensor. It is not easy to use the standard formulas of VCE, as their matrices are relatively big. Assuming that the variance-covariance matrix of the SGG data has a block-diagonal structure, the VCE formulas can be simplified. The bias due to regularization has been formulated as well as the biased-corrected VCE. Numerical studies show that the biases are mostly larger than the VCs and the removal of them usually leads to negative VCs. The biased-corrected VCE may yield better result than the biased VCE, but in the numerical studies insignificant differences were found.

The polar gaps, due to the inclined orbit of satellite, were the main subject of Chapter 7. A numerical study on the spectral solutions of the GBVPs shows that the near zonal spherical harmonic coefficients are very much influenced by the polar gaps. This influence is even more for the VH solution vs. the others by these regions. One may conclude that the VH gradients are more suited for determining the gravity field in polar gaps. For determining the gravity anomaly a special gridding scheme should be used. The compartment gridding algorithm presents a good capability in this respect. Numerical studies show that only the data which is around the gaps and close to the rim is significant. The gradients T_{zz}, T_{xx}, T_{yy} and T_{xz} need more data around the polar gaps than T_{xy} and T_{yz}. T_{xy} and T_{yz} show better capability than the other in polar gaps gravity anomaly recovery. The ring by ring inversion shows that T_{zz}, T_{xx}, T_{yy} and T_{xz} are suited for the gaps rim. The joint inversion of SGG data shows a recovery in the north polar gap within 3 mGal error, and it is 5 within mGal in the south polar gap. These numbers will change to 1 and 3 mGal after bias-correction. The recovery of the gravity field in the north polar gap is simpler than that in the south polar gap, as there is no topography in the former and the gravitational signal is smoother.

8.2 Future works

This dissertation investigated a number of issues related with SGG and the obtained results are promising for future works. The following subjects can be considered for further investigations in the future.

1. In the numerical studies presented in Chapter 2, noise-free SGG data was used to recover the geopotential coefficients. The next step of the study could be to include noise to the data. The solutions of the GBVPs are sensitive to the noise of SGG data. Over-determination helps the solution to suppress the noise, but in the solutions of GBVPs there is no redundancy. This subject is considered for further works. The semi-vectorization numerical algorithm is an efficient technique in synthesis and analysis in SGG developed by Eshagh and Abdollahzadeh (2009a).

2. Considering a numerical atmospheric density model (ADM) is also in our research plan and we are going to find a way to formulate it analytically. The presented formulation could be the first approximation of the AE. Another study can be done on the topographic and atmospheric biases, some part of this investigation has been considered by Sjöberg and Eshagh (in preparation), but it needs more works before coming to a good conclusion. The presented formulas can easily be used to investigate the topographic and atmospheric biases on the geopotential coefficients and even direct downward continuation of the gravitational gradients.

3. The truncation error of the VH and HH integrals were derived in Chapter 4 as well as the elements of the system of equations from which the biased LSM, unbiased LSM and optimum LSM are obtained. Numerical studies on the LSM of these integrals are left for future. The zero- and first-order Paul coefficients $\mathrm{e}_{rk}^{0}(\psi_0)$ and $\mathrm{e}_{rk}^{1}(\psi_0)$ are well-known, and we have derived a relation between the second-order Paul coefficient $\mathrm{e}_{rk}^{2}(\psi_0)$ and $\mathrm{e}_{rk}^{1}(\psi_0)$. Numerical studies on this subject are considered for future works. The relations between the VH truncation coefficients $Q_n^{\mathrm{HH}}(r,\psi_0)$, $Q_n^{\mathrm{VH}}(r,\psi_0)$ and $Q_n^{\mathrm{VV}}(r,\psi_0)$ can be constructed as well. The theory of modification with a spherical ring which was originally presented by Sjöberg and Eshagh (2009) were developed to SGG. This numerical study is restricted to the biased type of the LSM and the VV gradients. The numerical studies on the unbiased and optimum LSMs and the other gradients are left for future works.

4. In Chapter 5 the truncation error of the integral formulas were estimated in spatial domain. However combination of the VH and/or HH gravitational gradients opens another way to formulate the truncation error in spectral domain before downward continuation.

5. In the presented numerical study on combining the gravitational gradients, no negative VCs came out. If the biased-corrected VCE yields negative VCs, Sjöberg's non-negative VC estimator should be used. The bias due to the

regularization was formulated for this estimator, and its biased-corrected version was formulated as well. Numerical studies and practical comparison of this VC estimator and the standard method of best quadratic unbiased estimation are left for future work.

6. All the carried out numerical studies were based on simulations, as no real GOCE data is available. Working with real SGG data of GOCE is in our research plan for the future.

References

Albertella A, F. Migliaccio, F. Sansò (2002). GOCE: The Earth Field by Space Gradiometry, Celestial Mechanics and Dynamical Astronomy 83:1-15.

Amiri-Simkooei A. (2007) Least-Squares estimation of variance components, theory and GPS applications, Doctoral dissertation, Delft University of Technology, Netherlands

Anderson EG. and Mather R. (1975) Atmospheric effects in physical geodesy. Unisurv G23:23-41, University of NSW, Sydney, Australia

Arabelos D. and Tscherning C.C. (1990) Simulation of regional gravity field recovery from satellite gravity gradiometer data using collocation and FFT, Bull. Geod. 64:363-382.

Arabelos D. and Tscherning C.C. (1995) Regional recovery of the gravity field from satellite gradiometer and gravity vector data using collocation, J. Geophys. Res. 100:No. B11:22009-22015.

Arabelos D. and Tscherning C.C. (2007) On a strategy for the use of GOCE gradiometer data for the development of a geopotential model by LSC, 3rd Int. GOCE user workshop, ESRIN, 6-8 Nov. 2006, ESA, SP-627, pp. 69-75.

Balmino G. Barriot J. P. and Vales N. (1990) Non-singular formulation of the gravity vector and gravity gradient tensor in spherical harmonics, Manus. Geod. 15:11-16.

Balmino G. Barriot J. P. Koop R. Middle B. Thong N. C. and Vermeer M. (1991) Simulation of gravity gradients: a comparison study, Bull. Geod. 65:218-229.

Balmino G., F. Perosanz, R. Rummel, N. Sneeuw, H. Sünkel, P. Woodworth (1998). European Views on Dedicated Gravity Field Missions: GRACE and GOCE, An Earth Sciences Division Consultation Document, ESA, ESD-MAG-REP-CON-001.

Balmino G., F. Perosanz, R. Rummel, N. Sneeuw and H. Suenkel (2001). CHAMP, GRACE and GOCE: Mission Concepts and Simulations. Bollettino di Geofisica Teoricae Applicata, 40, 3-4, 309-320.

Baran L. Kuhn M. Claessens S. J. Featherstone W. E. Holmes S.A. and Vanicek P. (2006) A synthetic Earth gravity model designed specifically for testing regional gravimetric geoid determination algorithms, J Geod, 80:1-16.

Bassin, C., Laske, G. and Masters, G. (2000) The Current Limits of Resolution for Surface Wave Tomography in North America, EOS Trans AGU, 81, F897.

Bettadpur S. V. Schutz B. E. and Lundberg J. B. (1992) Spherical harmonic synthesis and least-squares computations in satellite gravity gradiometry, Bulletin Geodesique, 66: 261-271.

Bethencourt A. Wang J. Rizos C. and Kearsley A. H. W. (2005) Using personal computers in spherical harmonic synthesis of high degree Earth geopotential models, Dynamic Planet 2005, Cairns, Australia, 22-26 August.

Bjerhammar A. (1973) Theory of errors and generalized matrix inverses, Elsevier Scientific Publ Co., Amsterdam.

Bjerhammar A. (1983) A stochastic approach to the mixed boundary value problem in physical geodesy, Geodesy in transition, A volume dedicated to Helmut Moritz on the occasion of his 50th birthday, Edited by Schwarz K.P. and Lachapelle G. Division of Surveying engineering, p.25-42, The University of Calgary, Canada

Bouman J. and Koop R. (2003) Error assessment of GOCE SGG data using along track interpolation, Adv. Geosc. 1:27-32.

Bouman J., Koop R., Haagmans R., Muller J., Sneeuw N. Tscherning C.C., and Visser P.(2003) Calibration and validation of GOCE gravity gradienrts, Paper presented at IUGG meeting, pp. 1-6

Bouman J., Koop R., Tscherning C. C. and Visser P. (2004) Calibration of GOCE SGG data using high-low STT, terrestrial gravity data and global gravity field models, J Geod. 78:124-137.

Bölling K. and Grafarend E.W. (2005) Ellipsoidal spectral properties of the Earth's gravitational potential and its first and second derivatives, J Geod 79:300-330.

Chen J. Y. (1982) Methods for computing deflections of the vertical by modifying Vening-Meinesz' function, Bull. Geod. 56:9-26.

Claessens S. J. (2005) New relations among associated Legendre functions and spherical harmonics, J Geod, 79:398-406.

Clenshaw C.W. (1955) A note on the summation of Chebychev series. MTAC. 9:118-120.

Denker H. (2002) Computation of gravity gradients for Europe for calibration/validation of GOCE data, In Proc. IAG International symposium "Gravity and Geoid" Tziavos I.N. (ed.) Aug. 26-30, 2002, Thessaloniki, Greece, p.287-292.

Ditmar P. Kusche J. and Klees R. (2003a) Computation of spherical harmonics coefficients from gravity gradiometry data to be acquired by the GOCE satellite: regularization issues, J Geod. 77:465-477.

Ditmar P. Klees R. and Kostenko F. (2003b) Fast and accurate computation of spherical harmonic coefficients from satellite gravity gradiometry data, J Geod 76:690-705.

Ecker E. and Mittermayer E. (1969) Gravity corrections for the influence of the atmosphere. Bollettino di Geofisica Teorica ed Applicata, 11:70-80

Ellmann A. (2004) The geoid for the Baltic countries determined by the least squares modification of Stokes' formula, Doctoral thesis in Geodesy, Royal Institute of Technology, Stockholm, Sweden.

Ellmann A. (2005) Computation of three stochastic modification of Stokes' formula for regional geoid determination, Comp. & Geos. 31:742-755.

ESA (1999) Gravity Field and Steady-State Ocean Circulation Mission, ESA SP-1233(1), Report for mission selection of the four candidate earth explorer missions, ESA Publications Division, pp. 217, July 1999.

Eshagh M. (2003a) Precise orbit determination of low Earth orbiting satellites, Msc. Thesis, Dept. Geodesy and Geomatics, K.N.Toosi University of Technology, Tehran, Iran.

Eshagh M. (2003b) Consideration of the effect of Gravitational and non-gravitational forces acting on a low Earth orbiting satellite, paper to be presented in 11-th National Iranian Geophysical Conference, 1-3 December, National Geological Center, Tehran, Iran.

Eshagh M. (2005a) Step-variable numerical orbit integration of a low Earth orbiting satellite. J. Earth & Space Phys. (31):1-12.

Eshagh M. (2005b) Variance covariance component estimation and outlier detection, PhD study report, Royal Institute of Technology, Stockholm, Sweden.

Eshagh M. (2005c). On the BQUE and BQUNE methods of variance components estimation. Proceedings Geomatics 84, National Cartographic Center, Tehran, Iran.

Eshagh M. (2008) Non-singular expression for the vector and gradient tensor in a geocentric spherical frame, Comp. & Geosci. 32:1762-1768.

Eshagh M. (2009a) Impact of vectorization on global synthesis and analysis in gradiometry, Accepted for publication in Acta Geod. Geophys. Hun.

Eshagh M. (2009b) Orbit integration in non-inertial frames, Accepted for publication in J. Earth & Space Phys.

Eshagh M. (2009c) Alternative expressions for gravitational gradients in local north oriented frame and tensor spherical harmonics (Submitted).

Eshagh M. (2009d) Effect of lateral density variation of crustal and topographic masses on GOCE gradiometric data: a study in Iran and Fennoscandia. Submitted to Acta. Geod. Geophys. Hung.

Eshagh M. (2009e) Spherical harmonic expansion of the atmospheric gravitational potential based on exponential and power models of atmosphere, Art. Sat. 43(1): 25-43.

Eshagh M. (2009f) Optimal combination of integral solutions of gradiometric boundary value problems with variance components estimation, (Submitted)

Eshagh M. and Abdollahzadeh M. (2009a) A MATLAB software to synthesis and analysis of gradiometric data based on semi-vectorization method (in preparation)

Eshagh M. and Abdollahzadeh M. (2009b) Effect of geopotential perturbations of GOCE on its observations, A numerical study. Submitted to Acta. Geod. Geophys. Hun.

Eshagh M., Abdollahzadeh M. and Najafi-Alamdari M. (2009) Simplification of geopotential perturbing force acting on a satellite, Art. Sat. (Accepted)

Eshagh M. and Najafi-Alamdari, M. (2005a), Investigation of orbital perturbations of a low Earth orbiting (LEO) satellite, paper to be presented in NATM June 27-29, Institute of Navigation ION 61 St. Cambridge, Massachusetts, United States of America.

Eshagh M. and Najafi-Alamdari, M. (2005b), Numerical orbit integration of a low Earth orbiting satellite, paper to be presented in European navigation conference, GNSS 2005, German Institute of Navigation, Muenchen, Germany.

Eshagh M. and Najafi-Alamdari M. (2006) Comparison of numerical Integration methods in orbit determination of low earth orbiting satellites, J Earth & Space Phys. 32(3): 41-57.

Eshagh M. and Najafi-Alamdari, M. (2007) Perturbations in orbital elements of a low Earth orbiting satellite, J. Earth & Space Phys. 33(1):1-12.

Eshagh M. and Sjöberg L.E. (2008a) Impact of topographic and atmospheric masses over Iran on validation and inversion of GOCE gradiometric data, J. Earth. & Space. Phys. 34(3): 15-30.

Eshagh M. and Sjöberg L.E. (2008b) The modified best quadratic unbiased non-negative estimator (MBQUNE) of variance components, Stud. Geophys. Geod. 52:305-320.

Eshagh M. and Sjöberg L.E. (2009a) Topographic and atmospheric effects on GOCE gradiometric data in a local north-oriented frame: A case study in Fennoscandia and Iran, Stud. Geophys. Geod. 53:61-80.

Eshagh M. and Sjöberg L.E. (2009b) Atmospheric effect on satellite gravity gradiometry data, J Geodyn. 47:9-19.

Fotopoulos G. (2003) An analysis on the calibration of geoid, orthometric and ellipsoidal height data. UCGE Report No. 20183.

Fotopoulos G. (2005) Calibration of geoid error models via a combined adjustment of ellipsoidal, orthometric and gravimetrical geoid height data. Journal of Geodesy, vol 79: 111-123.

Freeden W., Gervens T. and Schreiner M. (1994) Tensor spherical harmonics and tensor spherical splines, Manus. Geod. 19: 70-100.

Gelderen M. and Rummel R. (2001) The solution of the general boundary value problem by least-squares, J Geod. 75:1-11.

Gelderen M, Rummel R (2002) Corrections to ‘‘The solution of the general geodetic boundary value problem by least squares”. J Geod 76: 121–122.

Grafarend E. (2006) Linear and non-linear models, fixed effects, random effects, and mixed models. Springer Verlag, 752 p.

Grafarend E. and Schaffrin B. (1979) Variance covariance components estimation of Helmert type, Invited paper, ASP-ASCM- convention, Washington D.C.

Haagmans R. Prijatna K. and Omang O. (2002) An alternative concept for validation of GOCE gradiometry results based on regional gravity, In Proc. Gravity and Geoid 2002, GG2002, August 26-30, Thessaloniki, Greece.

Hagiwara Y. (1972) Truncation error formulas for the geoidal height and the deflection of the vertical, Bull. Geod. 106:453-466.

Hansen P.C. (1998) Rank-deficient and discrete ill-posed problems: numerical aspects of linear inversion. SIAM, Philadelphia.

Heck, B. (2003) On Helmert's Methods of Condensation. J Geod. 77:155-170.

Heiskanen W. and Moritz H. (1967) Physical Geodesy. W.H Freeman and company, San Fransisco and London.

Holmes S.A. and Featherstone W.E. (2002a) A unified approach to the Clenshaw summation and the recursive computation of very high degree and order normalized associated Legende functions. J Geod. 76: 279-299.

Holmes S.A. and Featherstone W.E. (2002b) SHORT NOTES: Extending simplified high-degree synthesis methods to second latitudinal derivatives of geopotential. J Geod 76: 447-450.

Holota P. (1983a) The altimetry-gravimetry boundary-value problem I: linearization, Friedrichs' inequality. Boll. Geod. Sci. Aff. 1:13-32.

Holota P. (1983b) The altimetry-gravimetry boundary-value problem II: weak solution, V-ellipticity. Boll. Geod. Sci. Aff., 1:69-84.

Hsu H.T. (1984) Kernel function approximation of Stokes' integral, In Proc. Local gravity field approximation (Ed. Schwarz P.K.), Aug. 21-Sep. 4, 1984, Beijing, China.

Huang J., Vanicek, P., Pagiatakis S. Brink W. (2001) Effect of topographical mass density variation on gravity and geoid on the Canadian Rocky Mountains, J Geodyn., 74, 805-815.

Hwang C. (1991) Orthogonal functions over the oceans and applications to the determination of orbit error, geoid and sea surface topography from satellite altimetry, PhD dissertation, 229 pp.

Hwang C. (1993) Fast algorithm for the formulation of normal equations in a least-squares spherical harmonic analysis by FFT, Manusc. Geod. 62:46-52.

Hwang C. (1995) A method for computing the coefficients in the product-sum formula of associated Legendre functions, J Geod 70:110-116.

Hwang C. (1998) Inverse Vening Meinesz formula and deflection-geoid formula: application to the prediction of gravity and geoid over the South China Sea, J Geod. 72:304-312.

Hwang C. and Lin J.M. (1998) Fast integration of low orbiter's trajectory perturbed by the earth's non-sphericity, J Geod, 72:578-585.

Ilk K.H. (1983) Ein eitrag zur Dynamik ausgedehnter Körper-Gravitationswechselwirkung. Deutsche Geodätische Kommission, Reihe C, Heft Nr. 288, München

Kaula W. (1963) The investigation of the gravitational fields of the Moon and the planets with artificial satellites. Adv. Space Sci. and Tech, 5:210-226.

Keller W. (1997) Application of boundary value techniques to satellite gradiometry, In Lecture notes in Earth sciences, geodetic boundary value problems in view of the one centimeter geoid, edited by Sanso F and Rummel R, p. 542-558.

Keller W. and Sharifi M.A. (2005) Satellite gradiometry using a satellite pair. J Geod, 78(9): 544-557

Kelm R. (1978) Ist die Variantzshätzung nach Helmert MINQUE? AVN 85(2):49-54.

Kern M. and Haagmans R. (2004) Determination of gravity gradients from terrestrial gravity data for calibration and validation of gradiometric GOCE data, In Proc. Gravity, Geoid and Space missions, GGSM 2004, IAG International symposium, portugal, August 30- September 3, pp. 95-100.

Kern M., Preimesberger T., Allesch M., Pail. R., Bouman J. and Koop R. (2005) Outlier detection algorithms and their performance in GOCE gravity field processing, J Geod. 78:509-519.

Kiamehr R. (2006a) Precise gravimetric geoid model for Iran based on GRACE and SRTM data and the least-squares modification of Stokes' formula with some geodynamic interpretations, Doctoral thesis in Geodesy, Division of Geodesy, Royal Institute of Technology, Stockholm, Sweden

Kiamehr R. (2006b) the impact of lateral density variation model in the determination of precise gravimetric geoid mountainous areas: as case study of Iran, Geophys. J. Int. 167, 521-527.

Kiamehr R. and Eshagh M. (2008) Estimating variance components of ellipsoidal, orthometrc and geoidal heights through the GPS/leveling network in Iran, J. Earth.& Space Phys. 34 (3): 1-13.

Kiamehr R., Eshagh M. and Sjöberg L.E. (2008) Interpretation of general geophysical patterns in Iran based on GRACE gradient component analysis, Acta. Geophys. 56: 440-454.

Klees R., Koop R., Visser P. and Van den IJssel J. (2000) Efficient gravity field recovery from GOCE gravity gradient observations, J Geod. 74:561-571.

Koch K.R. (1986) Maximum Likelihood estimate of variance components. Bull. Geod. pp. 329-338.

Koch K.R. (1999) Parameters estimation and hypothesis testing in linear models. Springer verlag, Heidelberg, Germany.

Koch K.R. and Kusche J. (2002) Regularization of geopotential determination from satellite data by variance components, J Geod., 76:259-268.

Koop R. (1993) Global gravity field modeling using satellite gravity gradiometry. Publ Geodesy, New series, No. 38. Netherland Geodetic Commission, Delft.

Kotsakis C. (2007) A covariance0adaptive approach for regularized inversion in linear models, Geophys. J. Int. 171:509-522.

Krarup T. and Tscherning C.C. (1984) Evaluation of isotropic covariance functions of torsion balance observations, Bull. Geod. 58:180-192.

Kubik K. (1970) The estimation of the weights of measured quantities within the method of least squares. Bull. Geod., 44:21-40.

Kuhtreiber N. (1998) Precise geoid determination using a density variation model, Phys. and Chem. Earth, 23(1), 59-63(5).

Kusche J. (2003) A Monte-Carlo technique for weight estimation in satellite geodesy. J Geod, 76 (11-12):641-652.

Lambeck K. (1988) Geophysical geodesy, the slow deformations of the Earth. Clarendon, Oxford University Press, New York.

LaMotte LR. (1973) On non-negative Quadratic unbiased estimation of variance components. J Am Stat Assoc 68 (343): 728-730.

Lemoine F.G., Kenyon S.C., Factor J.K., Trimmer R.G., Pavlis N.K., Chinn D., Cox CM., Klosko S.M., Luthcke S.B., Torrence M.H., Wang Y.M., Williamson R.G., Pavlis E.C., Rapp R.H. and Olson T.R. (1998) Geopotential model EGM96. NASA/TP-1998-206861. Goddard Space Flight Center, Greenbelt

Li X. (2001a) Vertical resolution: Gravity versus vertical gravity gradient. The Leading Edge, 20: 901-904.

Li Y. (2001b) Processing gravity gradiometer data using an equivalent source technique. Publications in center fro gravity, Electrical and Magnetic studies, Dept. Geophysics, Colorado school of mines.

Li Y. (2001c) 3-D Inversion of gravity gradiometer data. Publications in center fro gravity, Electrical and Magnetic studies, Dept. Geophysics, Colorado school of mines.

Mainville A. (1986) The altimetry-gravimetry problem using orthonormal base functions, Department of geodetic science and surveying, Report No. 373, 203 pp. The Ohio State University, Columbus.

Makhloof A. (2007) The use of topographic-isostatic mass information in geodetic applications, Doctoral dissertation, Dept. of Theoretical and Physical Geodesy, Bonn, Germany.

Makhloof A. and Ilk K.H. (2005) Far-zone topography effects on gravity and geoid heights according to Helmert's methods of condensation and based on Airy-Heiskanen model, proceedings the 3rd minia International conference for advanced trends in Engineering, El-Minia, April 3-5, 2005.

Makhloof A. and Ilk K. H. (2006) Band-limited topography effects in airborne gravimetry using space localizing base functions, EGU conference, 3 April, 2006.

Martinec Z. (1993) Effect of lateral density variations of topographical masses in view of improving geoid model accuracy over Canada. Contract report for Geodetic Survey of Canada, Ottawa, Canada.

Martinec Z. (2003) Green's function solution to spherical gradiometric boundary-value problems, J Geod. 77:41-49.

Martinec Z., Matyska C., Grafarend E.W. and Vaníček P. (1993) On Helmert's 2nd condensation method, Manus. Geod. 18:417-421.

Martinec Z. and Vaníček P. (1994) Direct topographical effect of Helmert's condensation for a spherical geoid. Manus. Geod. 19: 257-268.

Martinec Z., Vanicek P., Mainville A. and Veronneau M. (1995) The effect of lake water on geoidal height, Manus. Geod, 20, 193-203.

Metzler B. and Pail R. (2005), GOCE data processing: the spherical cap regularization approach, Stud. Geophys. Geod. 49: 441−462.

Mickus K.L. and Hinojosa J.H. (2001) The complete gravity gradient tensor derived from the vertical component of gravity: a Fourier transform technique. Journal of Applied Geophysics, 46: 159-274.

Molodensky M.S., Eremeev V.F. and Yurkina M.I. (1962) Methods for study of the external gravity field and figure of the Earth. Trans. From Russian (1960), Israel program for scientific translation, Jerusalem.

Mooney W.D., Laske G. and Masters G.T., (1998) Crust5.1; a global model at 5 by 5 degrees, J. Geophys. Res., 103, 727-747.

Moritz H. (1980) Advanced physical geodesy. Herbert Wichman, Karlsruhe.

Muller J., Denker H., Jarecki F. and Wolf K.I. (2004) Computation of calibration gradients and methods for in-orbit validation of gradiometric GOCE data, In Proc. Second international GOCE user workshop "Goce, The Geoid and Oceanography", ESA-ESRIN, Frascati, Italy, 8-10 March 2004.

Nahavandchi H. (2004) A new strategy for the atmospheric gravity effect in gravimetric geoid determination, J Geod., 77:823-828.

Neyman Yu. M. Li J. and Liu Q. (1996) Modification of Stokes and Vening-Meinesz formulas for the inner zone of arbitrary shape by minimization of upper bound truncation errors, J Geod. 70:410-418.

Novák P. (2000) Evaluation of gravity data for the Stokes-Helmert solution to the the geodetic boundary-value problem. Technical Report 207, Department of Geodesy and Geomatics Engineering, University of New Brunswick, Fredericton, Canada.

Novák P. and Grafarend E.W. (2006) The effect of topographical and atmospherical masses on spaceborne gravimetric and gradiomtric data, Stud. Geophys. Geod., 50:549-582.

Pagiatakis S.D. and Armenakis C. (1999) Gravimetric geoid modeling with GIS, International Geoid Service Bulletin, 8:105-112.

Pail R. (2003) Local gravity field continuation for the purpose of in-orbit calibration of GOCE SGG observations, Adv. Geosc. 1: 11–18

Pail R., Plank G. and Schuh W.D. (2001) Spatially restricted data distributions on the sphere: the method of orthonormalized functions and applications, J Geod. 75:44-56.

Patterson HD. and Thompson R. (1971) Recovery of the inter-block information when block sizes are unequal. Biometrika 58:545-554.

Patterson HD. and Thompson R. (1975) Maximum likelihood estimation of components of variance. In: Proceedings of the 8-th international biometric conference, pp. 197-207.

Paul M.K. (1973) A method of evaluating the truncation error coefficients for geoidal height, Bull. Geod. 110:413-425.

Paul M.K. (1978) Recurrence relations for integrals of associated Legendre functions, Bull. Geod. 52:177-190.

Pawlowski B. (1998): Gravity gradiometry in resource exploration. The Leading Edge, 17: 51-52.

Pawlowski R. and C. Prieto (1997): Gravity gradiometry in natural resource exploration. IGC Footnote Series, Volume 4, Number 1.

Persson C.G. (1980) MINQUE and related estimators for variance components in linear models. PhD thesis, Royal Institute of Technology, Stockholm, Sweden.

Petrovskaya M.S. (1996) Optimal approach to the recovery of the Earth's gravitational field from satellite gradiometry, Art. Sat. 1-23.

Petrovskaya M.S. and Vershkov A.N. (2002) Potential coefficients recovery from the spectra of the full spaceborne gravity gradient tensor. Presented at V Hotine-Marussi symposium on Mathematical geodesy, Matera, Italy, June 17-21.

Petrovskaya M.S. and Vershkov A.N. (2006) Non-singular expressions for the gravity gradients in the local north-oriented and orbital reference frames, J Geod., 80:117-127.

Petrovskaya M. S. and Vershkov A. N. (2007) Local orbital derivatives of the Earth potential expressed in terms of the satellite Cartesian coordinates and velocity, Art. Sat. 42: 17-39.

Petrovskaya M.S. and Vershkov A.N. (2008) Development of the second-order derivatives of the Earth's potential in the local north-oriented reference frame in orthogonal series of modified spherical harmonics, J Geod 82:929–944.

Petrovskaya M.S. Vershkov A.N. and Pavlis N. K. (2001) New analytical and numerical approaches for geopotential modeling, J Geod. 75:661-672.

Petrovskaya M.S. Vershkov A.N. and Zielinski J. B. (2002) Recovering the Earth's potential spectral characteristics from GOCE mission, Adv. Space Res. 30:221-226.

Petrovskaya M.S. and Zielinski J. B. (1997) Determination of the global and regional gravitational fields from satellite and balloon gradiometry missions, Adv. Space Res. 19(11): 1723-1728.

Pukelsheim F. (1981) On the existence of unbiased non-negative estimates of variance covariance components. Annals of Statistics, 9 (2): 293-299.

Rao C.R. (1971) Estimation of variance components-MINQUE theory. J. Multivariate Anal. 1:257-275.

Rao C.R. and Kleffe J. (1988) Estimation of variance components and applications, North-Holand, Amsterdam.

Reed G.B. (1973) Application of kinematical geodesy for determining the shorts wavelength component of the gravity field by satellite gradiometry, Ohio state University, Dept. of Geod Science, Rep. No. 201, Columbus, Ohio.

Reference Atmosphere Committee (1961) Report of the preparatory group for an international reference atmosphere accepted at the COSPAR Meeting in Florance, April 1961. North Holland Publ. Co., Amsterdam.

Reigber, Ch., Jochmann, H., Wünsch, J., Petrovic, S., Schwintzer, P., Barthelmes, F., Neumayer, K.-H., König, R., Förste, Ch., Balmino, G., Biancale, R., Lemoine, J.-M., Loyer, S. and Perosanz, F. (2004), Earth Gravity Field and Seasonal Variability from CHAMP. In: Reigber, Ch., Lühr, H., Schwintzer, P., Wickert, J. (eds.), Earth Observation with CHAMP - Results from Three Years in Orbit, Springer, Berlin, 25-30.

Rizos C. (1979) An efficient computer technique for the evaluation of geopotential from spherical harmonic models, Aust. J. geod. Photo Surv., Vol 31:161-169.

Rudolph S., Kusche J. and Ilk K. H. (2002) Investigations on the polar gap problem in ESA's gravity field and steady-state ocean circulation explorer mission (GOCE), J. Geodyn. 33:65-74.

Rummel R. (1976) A model comparison in least-squares collocation, Bull. Geod. 50:181-192.

Rummel R. (1997) Spherical spectral properties of the Earth's gravitational potential and its first and second derivatives, Geodetic boundary value problems in view of the one centimetre geoid, Lecture notes in Earth sciences Edited by Sanso F. and Rummel R.,p. 359-401.

Rummel R. and Colombo O. (1985) Gravity field determination from satellite gradiometry, Bull. Geod, 59:233-246.

Rummel R., Sanso F., Gelderen M., Koop R., Schrama E., Brovelli M., Migiliaccio F., and Sacerdote F. (1993) Spherical harmonic analysis of satellite gradiometry. Publ Geodesy, New Series, No. 39 Netherlands Geodetic Commission, Delft.

Rummel R., Schwarz K. P. and Gerstl M. (1979) Least squares collocation and regularization, Bull. Geod. 53:343-361.

Rummel R. and van Gelderen M (1992) Spectral analysis of the full gravity tensor. Geophys. J. Int., 111: 159–169.

Rummel R. and van Gelderen M. (1995) Meissl scheme-spectral charachteristics of physical geodesy, Manus. Geod. 20:379-385.

Schaffrin B. (1981) Varianz—Kovarianz—Komponenten—Schätzung bei der Ausgleichung heterogener Wiederholungsmessungen. Dissertation, Bonn 1981.

Searle S.R., Casella G. and McCulloch C.E. (1992) Variance components. Wiley, New York.

Seeber G. (2003) Satellite Geodesy, 2nd completely revised and extended edition, Walter de Gruyter. Berlin. New York.

Seitz K. and Heck B. (2003) Efficient calculation of topographic reductions by the use of tesseroids. Presentation at the joint assembly of the EGS, AGU and EUG, Nice, France, 6–11 April 2003.

Sharifi M.A. (2006) Satellite to satellite tracking in the space-wise approach, PhD dissertation, Geoätisches Institute der Universität Sttutgart, Germany.

Shepperd S. W. (1982) A recursive algorithm for evaluating Molodeski-type truncation error coefficients at altitude, Bull. Geod. 56: 95-105.

Siemes C., Schuh W.D. Cai J., Sneeuw N. and Baur O. (2007) GOCE data processing: the numerical challenge of data gaps, Satus sem., observation of system Earth from space geotechnologien science report 11, p.99-105, Munchen, Germany.

Simons F. J. and Dahlen F. A. (2006) Spherical Slepian functions and the polar gap in geodesy, Geophys. J. Int. 166:1039-1061.

Sjöberg L.E. (1980) Least-squares combination of satellite harmonics and integral formulas in physical geodesy, Gerlands Beitr. Geophysik, Leipzig 89(5):371-377.

Sjöberg L.E. (1981) Least-squares combination of terrestrial and satellite data in physical geodesy, Ann. Geophys., t. 37: 25-30.

Sjöberg L.E. (1982) On the recovery of geopotential coefficients using satellite-to-satellite range-rate data on a sphere, Bull. Geod. 56:27-39.

Sjöberg L.E. (1983) Unbiased estimation of variance-components in condition adjustment with unknowns-a MINQUE approach. ZfV, 108:9.

Sjöberg L.E. (1984a) Least-Squares modification of Stokes' and Vening-Meinez' formula by accounting for truncation and potential coefficients errors. Manus. Geod., 9:209-229.

Sjöberg L.E. (1984b) Least-squares modification of Stokes' and Vening Meinesz' formulas by accounting for errors of truncation, potential coefficients and gravity data, Report No. 27, Department of Geodesy, Uppsala.

Sjöberg L.E., (1984c) Non-negative variance component estimation in the Gauss-Helmert Adjustment model. Manus. Geod., 9: 247-280.

Sjöberg L.E. (1985) Adjustment and variance component estimation with a singular covariance matrix, ZfV 110(4):145-151.

Sjöberg L.E. (1986) Comparisons of some methods of modifying Stokes' formula, Boll. Geod. Sci. Aff. 3:229-248.

Sjöberg L.E. (1991) Refined least-squares modification of Stokes' formula, Manus. Geod. 16:367-375.

Sjöberg L.E. (1993) Terrain effects in the atmospheric gravity and geoid correction. Bull. Geod. 64:178-184.

Sjöberg L.E. (1998a) The ellipsoidal corrections to the topographic geoid effects, J Geod., 77:804-808.

Sjöberg L.E. (1998b) The atmospheric geoid and gravity corrections, Boll. Geod. Sci. Aff. (4):421-435.

Sjöberg L.E. (1999) The IAG approach to the atmospheric geoid correction in Stokes's formula and a new strategy, J Geod., 73:362-366.

Sjöberg L.E. (2000) Topographic effects by the Stokes-Helmert method of geoid and quasi-geoid determinations. J Geod., 74:255-268

Sjöberg L.E. (2001) Topographic and atmospheric corrections of gravimetric geoid determination with special emphasis on the effects of harmonics of degrees zero and one, J Geod. 75:283-290.

Sjöberg L.E. (2003) A general model for modifying Stokes' formula and its least-squares solution, J Geod. 77: 459–464.

Sjöberg L.E. (2004) The effect on the geoid of lateral topographic density variation, J Geod, 78:34-39.

Sjöberg L. E (2006) The effects of Stokes's formula for an ellipsoidal layering of the earth's atmosphere, J Geod., 79:675-681.

Sjöberg L.E. (2007) Topographic bias by analytical continuation in physical geodesy. J Geod 81:345-350.

Sjöberg L.E. and Eshagh M. (2009) Considering data gap in modeling by modified Stokes' formula, (submitted).

Sjöberg L.E. and Nahavandchi. H. (1999) On the indirect effect in the Stokes-Helmert method of geoid determination. J Geod 73:87-93.

Sjöberg L.E. and Nahavandchi H. (2000) The atmospheric geoid effects in Stokes formula, Geophys.J Int., 140:95-100.

Sneeuw N. (1994) Global spherical harmonic analysis by least-squares and numerical quadrature methods in historical perspective, Geophys. J. Int. 118:707-716.

Sneeuw N. (2003) Space-wise, time-wise, torus and Robrough representations in gravity field modeling, Space Sci. Rev., 108:37-46.

Sneeuw N. and van Gelderen M. (1997) The polar gaps, In Lecture notes in Earth sciences, geodetic boundary value problems in view of the one centimeter geoid, edited by Sanso F and Rummel R, p. 559-568.

Sun W. and Sjöberg L.E. (2001) Convergence and optimal truncation of binomial expansions used in isostatic compensations and terrain corrections, J Geod., 74:627-636.

Svensson L. (1982) Pseudodifferential operators. A new approach to the boundary value problem in physical geodesy. Manus. Geod., 8:1–40.

Tapley B., Ries J. Bettadpur S., Chambers D., Cheng M., Condi F., Gunter B., Kang Z., Nagel P., Pastor R., Pekker T., Poole S. and Wang F. (2005), GGM02-An improved Earth gravity field model from GRACE. J Geod, 79:467-478.

Tenzer R., Novák P., Moore P. and Vajda P. (2006) Atmospheric effects in the derivation of geoid-generated gravity anomalies, Stud. Geophys. Geod., 50:583-593.

Tikhonov A.N. (1963) Solution of incorrectly formulated problems and regularization method, Soviet Math. Dokl., 4: 1035-1038, English translation of Dokl. Akad. Nauk. SSSR, 151:501-504.

Toth G. (2003) The Eötvös spherical horizontal gradiometric boundary value problem-gravity anomalies from gravity gradients of the torsion balance, In Gravity and Geoid 2002, 3rd meeting of the IGGC Tziavos (ed.), Gravity and Geoid 2002, pp. 102-107. ziti edition 2003.

Toth G., Foldvary L., Tziavos I. and Adam J. (2004) Upward/downward continuation of gravity gradients for precise geoid determination, Proc. Second International GOCE user workshop "GOCE, The Geoid and Oceanography", ESA-ESRIN, Frascati, Italy, 8-10 March 2004.

Toth G., Foldvary L., Tziavos I. and Adam J. (2006) Upward/downward continuation of gravity gradients for precise geoid determination, Acta Geod. Geoph. Hung. 41:21-30.

Toth G., Forldvary L. and Tziavos I. N. (2007) Practical aspects of upward/downward continuation of gravity gradients, In proc. "The 3rd International GOCE user workshop", ESA-ESRIN, Frascati, Italy, 6-8 Nov. 2006 (ESA SP-627, January 2007).

Tscherning C. C. (1993) Computation of covariances of derivatives of the anomalous gravity potential in a rotated reference frame. Manus. Geod. 18:115-123.

Tscherning C.C. (2001a) Computation of spherical harmonic coefficients and their error estimates using least-squares collocation, J Geod. 75:12-18.

Tscherning C. C. (2001b) Covering the GOCE mission polar data gaps using gradients and ground gravity, In Proc. International GOCE user workshop, ESTEC, 23-24 April 2001, p. 105-110. ESA WPP-188.

Tscherning C.C. (2002) Spherical approximation or no approximation in gravity field modeling, Prepared for the Hotine-Marussi Symposium, Matera, June.

Tschrning C.C., Forsberg R., Albertella A., Migliaccio F. and Sanso F. (2000) The polar gap problem, Space-wise approaches to gravity field determination in Polar areas, Eotvos to mGal, Finsal report, 10 April 2000, Suenkel H. (Ed.), p. 331-336.

Tscherning C.C. and Poder K (1982) Some Geodetic application of Clenshaw summation, Boll. Geod. Sci. Aff. (4).

Tscherning C.C. and Rapp R. (1974) Closed covariance expressions for gravity anomalies, geoid undulations and deflections of the vertical imlied by anomaly degree variance models. Department of Geodetic Science, Report No. 208.

Tscherning C. C., Veicherts M. and Arabelos D. (2006) Calibration of GOCE gravity gradient data using smooth ground gravity, In Proc. GOCINA workshop, Cahiers de center European de Geodynamique et de seismilogie, Vol. 25, pp. 63-67, Luxenburg.

Tsoulis D. (2001) Terrain correction computations for a densely sampled DTM in the Bavarian Alps. J Geod, 75:291-307.

Tuenissen P. and Amiri-Seemkooee A.R. (2008) Least squares variance component estimation, J Geod. 82:65–82.

Tziavos I.N. and Andritsanos V.D. (1998) Improvement in the computation of deflection of the vertical by FFT, 23:71-75.

Tziavos I.N. and Featherstone W.E., (2000). First results of using digital density data in geavietric geoids computation in Australia. IAG Symposia, GGG2000, Springer Verlag Berlin Heidelberg, 123, 335-340.

United State Standard Atmosphere (1976) Joint model of the National Oceanic and Atmospheric administration, national aeronautics and space administration and United states air force, Washington, D.C.

Vermeer M. (1990) Observable quantities in satellite gradiometry, Bull. Geod. 64:347-36l.

Visser P. (1992) the use of satellites in gravity field determination and adjustment, PhD dissertation, University of Delft.

Wallace JM. and Hobbs PV. (1977) Atmospheric Science- An Introductory Survey, Academic press, New York.

Wenzel, H.G. (1981) Zur Geoidbestimmung durch kombination von schwereanomalien und einem kugelfuncationsmodell mit hilfe von integralformeln. ZfV. 106, 3, p.102-111.

Wieczorek M. A. (2007) The gravity and topography of the terrestrial planets, Treatise on Geophysics, in press.

Wild F. and Heck B. (2004a) A comparison of different isostatic models applied to satellite gravity gradiometry, Gravity, Geoid and Space Missions GGSM 2004 IAG International Symposium Porto, Portugal August 30 – September 3, 2004.

Wild, F. and Heck, B. (2004b) Effects of topographic and isostatic masses in satellite gravity gradiometry. Proc. Second International GOCE User Workshop GOCE. The Geoid and Oceanography, ESA-ESRIN, Frascati/Italy, March 8-10, 2004 (ESA SP – 569, June 2004), CD-ROM.

Wolf K. I. (2007) Kombination globaler potentialmodelle mit terresrischen schweredaten fur die berechnung der zweiten ableitungen des gravitationspotentials in satellitenbahnhohe, PhD thesis, University of Hannover, Germany.

Xu P. (1991) Least squares collocation with incorrect prior information, ZfV, 6:266-273.

Xu P. (1992) Determination of surface gravity anomalies using gradiometric observables, Geophys. J. Int., 110: 321-332.

Xu P. (1998) Truncated SVD methods for discrete linear ill-posed problems, Geophys. J. Int., 135: 505-514.

Xu P., Liu Y., Shen Y. and Fukuda Y. (2007) Estimability analysis of variance and covariance components, J Geod. 81:593-602.

Xu P. and Rummel R. (1994) A simulation study of smoothness methods in recovery of regional gravity fields, Geophys. J. Int. 117:472-486.

Xu P., Shen Y., Fukuda Y. and Liu Y. (2006) Variance components estimation in linear inverse ill-posed models. J Geod. 80:69-81.

Zerili F. J. (1970) Tensor harmonics in canonical form for gravitational radiation and other applications. J Math Phys, 11:2203-2208.

Zielinsky J. B. (1975) Solution of the downward continuation problem by collocation, Bull. Geod. 17:267-277.

Zielinsky J.B. and Petrovskaya M.S. (2003) The possibility of the calibration/validation of the GOCE data with the balloon-borne gradiometer, Adv. in Geosci., 1:149-153.

Ågren J. (2004) Regional geoid determination methods for the era of satellite gravimetry, Numerical investigations using synthetic Earth gravity models, Doctoral thesis in Geodesy, Royal Institute of Technology, Stockholm, Sweden